PREDICTION OF WHEEL AND RAIL WEAR USING ARTIFICIAL NEURAL NETWORKS

AMER SHEBANI

A thesis submitted to the University of Huddersfield in partial fulfilment of the requirements for the degree of Doctor of Philosophy

Supervisor Professor Simon Iwnicki

School of Computing and Engineering

Institute of Railway Research

University of Huddersfield

2016

Abstract

The prediction of wheel wear is a significant issue in railway vehicles. It is correlated with safety against derailment, economy, ride comfort, and planning of maintenance interventions, and it can result in delay, and costs if it is not predicted and controlled in an effective way. However, the prediction of wheel and rail wear is still a great challenge for railway systems. Therefore, the main aim of this thesis is to develop a method for predicting wheel wear using artificial neural networks.

Initial tests were carried out using a pin-on-disc machine and this data was used to establish how wear can be measured using an Alicona profilometer.

A new method has been developed for detailed wheel wear and rail wear measurements using 'Replica' material which was applied to the wheel and rail surfaces of the test rig to make a copy of both surfaces. The replica samples were scanned using an optical profilometer and the results were processed to establish wheel wear and rail wear. The effect of load, and yaw angle on wheel wear and rail wear were examined. The effect of dry, wet, lubricated, and sanded conditions on wheel wear and rail wear were also investigated.

A Nonlinear Autoregressive model with eXogenous input neural network (NARXNN) was developed to predict the wheel and rail wear for the twin disc rig experiments. The NARXNN was used to predict wheel wear and rail wear under deferent surface conditions such as dry, wet, lubricated, and sanded conditions.

The neural network model was developed to predict wheel wear in case of changing parameters such as speed and suspension parameters. VAMPIRE vehicle dynamic software was used to produce the vehicle performance data to train, validate, and test the neural network. Three types of neural network were developed to predict the wheel wear: NARXNN, backpropagation neural network (BPNN), and radial basis function neural network (RBFNN). The wheel wear was calculated using an energy dissipation approach and contact position on straight track.

The work is focused on wheel wear and the neural network prediction of rail wear was only carried out in connection with the twin disk wear tests. This thesis examines the effect of neural network parameters such as spread, goal, maximum number of neurons, and number of neurons to add between displays on wheel wear prediction.

The neural network simulation results were implemented using the Matlab program. The percentage error for wheel and rail wear prediction was calculated. Also, the accuracy of wheel and rail wear prediction using the neural network was investigated and assessed in terms of mean absolute percentage error (MAPE). The results reveal that the neural network can be used efficiently to predict wheel and rail wear.

Further work could include rail wear and prediction on a curved track.

Publications

1. A. Shebani, C. Pislaru, “Identification of Nonlinear Systems Using Radial Basis Function Neural Network”, World Academy of Science, Engineering and Technology International Journal of Computer, Information, Systems and Control Engineering, Vol: 8 No: 9, 2014.

2. A. Shebani, C. Pislaru, “Wear Measuring and Wear Modelling Based on Archard, ASTM, and Neural Network Models”, World Academy of Science, Engineering and Technology International Journal of Mechanical, Aerospace, Industrial and Mechatronics Engineering, Vol: 9, No: 1, 2015.

3. A. Shebani, S. Iwnicki, C. Pislaru, “A new method for evaluating wheel and rail wear”, The Third International Conference on Railway Technology: Research, Development and Maintenance Cagliari, Sardinia, Italy 5-8 April 2016.

4. A. Shebani, S. Iwnicki, “The effect of surface conditions on wear of a railway wheel and rail”, presented at ICATES 2016:18th International Conference on Advances in Tribology and Engineering Systems, London, United Kingdom, September, 29-30, 2016.

Table of Contents

List of Figures

List of Tables

Dedications and Acknowledgements

I would like to express my thanks to the following people:

My supervisor Professor Simon Iwnicki for his guidance, encouragement, support, motivation, and immense knowledge.

My co-supervisor Dr Crinela Pislaru for the continuous support, guidance and advice.

Dr Guma Mosbah for his encouragement in understanding the fundamental aspects of artificial neural networks.

The staff at the EPSRC Center for Innovative Manufacturing in Advanced Metrology for their support.

My wife for her unlimited support during the preparation of this work.

My children Ahmed, Moad, Nusiba, Mohamed, and Abdulrahman, and family for their unconditional love and support, and a special thanks goes to my mother.

All the people who I am unable to list but have helped and supported me in one way or another.

Symbols

a, b	Contact ellipse semi-axes
W1	Vertical wear
W2	Horizontal wear
h	Vertical distance
W3	Wear measured at some angle α
X	Longitudinal axis
Y	Lateral axis
Z	Vertical axis
V	Direction of travel
V	Volume of material removed
K_R	Reye's wear constant
W	Work dissipated
V	Volume of material removed
Z	Probability of removal of an atom per atomic encounter
p	Load applied
p_m	Flow pressure
W	Applied load
H	Hardness of a softer material
k	Probability of removing a wear particles
d	Sliding distance
Q	Volume of wear material
w	Wear volume per unit sliding distance
P_n	Normal load
a	Contact spot radius
p_m	Yield pressure of a plastically deformed asperity
$\mathbf{V_n}$	Volume
i_n	Wear rate
I^*	Total wear rate
P	Total normal load on the contact
I	Volume worn per unit sliding distance (wear rate)
P	Normal load
H	Hardness of the softer material
k	Wear coefficient
V	Volume of wear
k	Wear coefficient

S	Sliding distance
H	Hardness of material
N	Normal load
L	Sliding distance
F_N	Normal load
P	Contact pressure
V_{slip}	Sliding velocity
D	Wheel diameter
T	Creep force
γ	Creepage
V	Volume of wear
S	Sliding distance
P	Normal force
K_A	Wear coefficient
$\dot{S}$	Slip velocity
p	Contact pressure
A	Contact area
γ	Slip
K	Wear coefficient
WI	Wear index
K	Constant
T_1	Longitudinal creep force
T_2	Lateral creep force
γ_1	Longitudinal creepage
γ_2	Lateral creepage
d	Pin wear scar diameter
r	Pin radius
h	Height of material removed for pin
R	Disc wear track radius
d	Disc wear track width
$g(z)$	Sigmoid function
z	Constant
$y(t)$	Output of the network
$u(t)$	Input of the network
t	Time
n	Input-memory order

m	Output-memory order
W	Weights matrix
f	Nonlinear function
x	Input
y	Actual output
d	Delay
w_n	Weights
$\hat{y}$	Estimated output
$u(t)$	Input
$y(t)$	Desired output
$\hat{y}_{(t)}$	Estimated output
t_i	Target output
y_i	Estimated output
$W_{ij}(t)$	Old connection weight between node i and node j of the above layer
$W_{ij}(t+1)$	New connection weight between node i and node j of the above layer
η	Learning rate
δ	Error term of the node
O	Actual output of the node.
$X_1, X_{2,} X_3, X_m$	Inputs
$C_1, C_2, \dots, C_m$	Centres
$\emptyset$	Activation function
W	Weights
y	Output of RBFNN
σ	Width of activation function
E_{dist}	Euclidean distance
X_i	Inputs
c_i	Centres
r	Difference between centres and inputs
n	Vector dimension
$W(t+1)$	Updated weights
$W(t)$	Previous weights
$y(t)$	Desired output
$y_m(t)$	Output of the network
$\Phi^T(t)$	Hidden output (Gaussian output)
μ	Learning factor
P	Input vectors

T	Target vectors
MN	Maximum number of neurons
DF	Number of neurons to add between displays
A_i	Actual wear
P_i	Predicted wear
x	actual measurement
y	estimated measurement
i	Time period
N	Number of time periods (number of observed values)
Tγ	Energy dissipated in the wheel–rail contact
T	Total creep force
γ	Creepage

$P_{00}, P_{11}, P_{12}, P_{13}, P_{14}, P_{21}, P_{22}, P_{23}, P_{24}, P_{31}, P_{32}, P_{33}, P_{34}, P_{41}, P_{42}, P_{43}, and\ P_{44}$ Wheel profiles

Abbreviations

ASTM	American Society for Testing and Materials model
3D	Three dimensions
NARXNN	Nonlinear Autoregressive models with eXogenous input neural network
MAPE	Mean absolute percentage error
BPNN	Backpropagation neural network
RBFNN	Radial basis function neural network
ANN	Artificial neural networks
GSR	Global solar radiation
UK	United Kingdom
TOCs	Train Operating Companies
RCF	Rolling contact fatigue
EMU	Electric multiple unit
SEM	Scanning electron microscopy
STM	Scanning tunnelling microscopy
KTH	Royal Institute of Technology Stockholm
USFD	University of Sheffield
BRR	British Rail Research
MBS	Multibody software
GUI	Graphical User Interface
MSE	Mean square error
MLP	Multilayer perceptron neural networks
LMS	Least mean square
TDL	Tapped delay line
MLFF	Multilayer feedforward network
BP	Backpropagation
Newrb	Matlab command to design the RBFNN
LED	Light emitting diode
CCD	Charge coupled device
VHX	Digital microscope
km	Kilometre
mm	Millimetre
μm	Micrometre
nm	Nanometre
s	Second
Ω	Ohm
$\mu\varepsilon$	Micro Strain
N	Newton

Chapter 1 Introduction

1.1 Background

Wear is usually defined as the removal of material from contacting surface by mechanical action [1]. Wheel wear and rail wear are the loss of material from the contacting surface due to rail/wheel interaction. Rail wear is dependant on several parameters such as axle load, train speed , wheel material type, rail material type, curvature, traffic type, lubrication, and environmental conditions [2]. Wheel wear is one of the most significant problems affecting the cost and performance of railway transportation systems [1]. Wheel and rail wear is a significant issue in railway systems. Accurate prediction of this wear can improve economy, ride comfort, prevention of derailment and planning of maintenance interventions. Poor prediction can result in failure and consequent delay and increased costs if it is not controlled in an effective way. However, prediction of wheel and rail wear is still a great challenge for railway engineers and operators.

Artificial neural network is currently used to solve a wide range of complex engineering problems. It has the ability to learn by example, consequently, it is a very useful for simulation of any correlation that is difficult to describe with physical models or other mathematical approaches [3]. Though perfect prediction is seldom possible, neural networks can be used to make reasonably good predictions in a number of cases. In particular, feedforward neural networks have been used frequently in this respect [4].

In this project, artificial neural networks were developed to predict wheel wear and rail wear.

1.2 Research motivation

One of the most critical issues in the railway system is the wheel and rail wear, these issue have a significant impact on the maintenance costs of the railway networks, where the track maintenance is one of the major expenditures for the railways. The wheel and rail wear prediction is therefore a very important issue in railway systems.

Railway spending can be divided into three categories: the cost to maintain the railways, the cost to develop and improve the railways, and the cost to run the railway [5]; As an examples of the cost maintenance:

- From 1980 to 2015, America's freight railroads spent more than $600 billion on maintenance expenses and capital expenditures related to tracks, freight cars , locomotives, bridges, tunnels and other equipment and infrastructure [6].
- In 2014/15, Network Rail Limited in the UK made expenses of £1.5 billion for operating and maintaining the network [7].
- In 2013/14 the Train Operating Companies (TOCs) paid Network Rail a total of £2.4bn in track access charges, of these charges approximately £1bn was used for ongoing maintenance of the infrastructure including track damage maintenance [8].

Wheelsets are one of the most expensive components through the life of a rail vehicle. They require regular maintenance activities such as reprofiling on a wheel lathe, inspection for safety-critical damage to wheel and axle, and renewal of wheelset. There are several reasons for reprofiling such as tread wear, flange wear, and thermal. For example, the tread wear and flange wear are one of the most important reasons for reprofiling for the UK train type "commuter EMU" such as shown in Figure 1.1 [9].

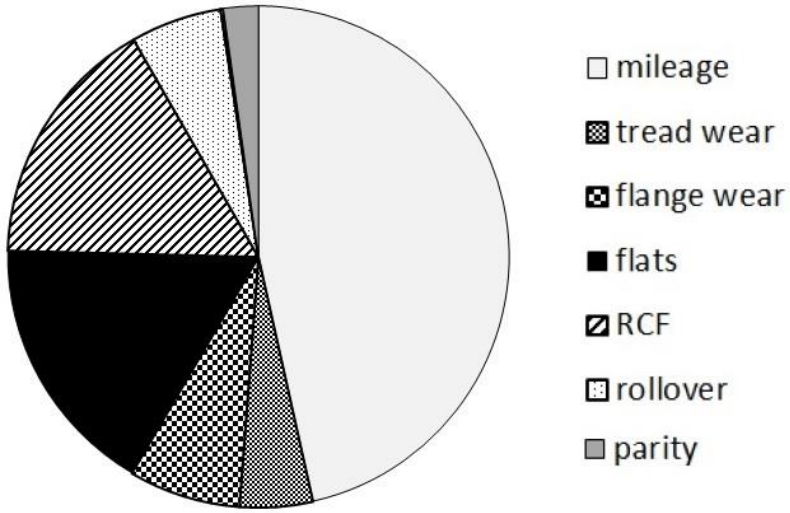

Figure 1. 1 Dominant reasons for reprofiling for UK train type "commuter EMU" [9]

Different types for the UK vehicles are shown in Figure 1.2.

Figure 1. 2 Different types for the UK vehicles

Rail and wheel damage has been a concern in railway systems for several decades [10]. This thesis focuses on the prediction of wheel wear and rail wear using artificial neural networks to help the industry to control its maintenance costs. Several tests were carried out to study the wheel wear and rail wear such as the investigation of load, yaw angle, speed, and surface conditions on wheel wear and rail wear.

1.3 Research Aims and Objectives

The main aim of this research is to assess whether a neural network can predict wear at the railway wheel-rail interface and, if so, to develop a neural network model to predict the wheel wear and rail wear in railway vehicle in order to optimise maintenance and increase the operative life of wheels and rails.

The objectives of this project are defined as follows:

I. Preliminary investigations of the wear process

1. Carry out pin-on-disc tests and measure pin wear and disc wear using 3D optical methods.
2. Investigate the effects of load on pin wear and disc wear for pin-on-disc experiments.

II. Investigation of wheel-rail wear using a twin disc rig

1. Develop a new method for wheel wear and rail wear measurements using replica material, an Alicona profilometer, and a twin disc test rig.
2. Investigate the effects of load, yaw angle, and surface conditions on wheel wear and rail wear using a twin disc test rig.

III. Investigate the use of neural network techniques for prediction of wheel-rail wear

1. Develop a neural network model to predict wheel wear and rail wear for the twin disc rig experiments.
2. Develop a neural network model to predict wheel wear for a railway vehicle.
3. Validate the neural network model using the VAMPIRE vehicle dynamics software including tests such as change of speed, change of longitudinal bush stiffness, change of lateral bush stiffness, change of vertical

bush stiffness, change of longitudinal shear stiffness, change of lateral shear stiffness, and change of vertical shear stiffness.
4. Investigate the effects of neural network parameters on wheel wear prediction.

1.4 Methodology

A pin-on-disc test was carried out in this work to understand the wear behaviour, and to understand how the wear can be measured. Pin wear and disc wear were measured using an Alicona profilometer.

A twin disc tests were carried out to understand wear behaviour for wheel-rail contact. A novel method was developed for wheel and rail wear measurements. Replica material plus an Alicona profilometer were used for wheel wear and rail wear measurements to a twin disc test rig experiments. The University of Huddersfield twin disc test rig was used to establish some realistic conditions for wheel wear and rail wear. This test was used to investigate the effect of some parameters such as load, yaw angle, and surface conditions on wheel wear and rail wear.

Due to the fact that only three parameters: load, yaw angle, and speed can be controlled using the University of Huddersfield twin disc test rig, VAMPIRE vehicle dynamics simulations were used to perform several tests to predict the wheel wear using neural networks. Energy dissipated and the contact position between wheel and rail were used to update the wheel profile after different running distances. Then, wheel wear was calculated using the energy dissipated between wheel and rail.

Neural networks were developed for wheel wear and rail wear prediction and Matlab was used to implement the results. A nonlinear autoregressive model with exogenous input neural network (NARXNN), backpropagation neural network (BPNN), and radial basis function neural network (RBFNN) were developed to predict wheel/rail wear. Series-parallel NARXNN and parallel NARXNN was used to predict he wheel/rail wear for the twin disc rig tests. The inputs of neural network for a twin disc rig tests were load, yaw angle, speed, wheel/rail profile, and first/second derivative for wheel/rail profile; while the output of the neural network was wheel/rail wear. The inputs of neural network for VAMPIRE simulations were speed, running distance, longitudinal bush stiffness, lateral bush stiffness, vertical bush stiffness, longitudinal bush stiffness, lateral bush stiffness, vertical shear stiffness, wheel profile, first derivative of wheel profile, and second derivative of wheel profile; while the output of the neural network was railway wheel wear. The architecture of BPNN for wheel wear prediction was 5-7-2-1; while the RBFNN was designed using newrb command. The effect of neural network parameters on wheel wear prediction was investigated.

The structure of this thesis is illustrated in Figure 1.3.
This thesis is organised as follows:
Chapter 1 presents the background of the topic to be investigated, the motivations which have led to this research, the aims and objectives, methodology, structure of the thesis, introduction to wear, introduction to railway system, wheel wear and rail wear, wear measurement methods and wear testing methods, and multibody dynamics.

Chapter 2 includes a literature review, it reviews the current wear models, the use of computer software in wheel wear estimation, and the use of neural networks for wear prediction and prediction purposes in general.

Chapter 3 describes the materials and devices which were used for pin-on-disc wear experiments such as pin-on-disc machine, and Alicona profilometer, and pin wear and disc wear measurements. The pin-on-disc test is reported in this chapter to show how the wear can be measured using a 3D optical profilometer.

Chapter 4 introduces the twin disc test rig, this test was used to study wheel wear and rail wear. A replica material, Alicona profilometer, and twin disc test rig were used to investigate the effects of load, yaw angle, and surface conditions on wheel wear and rail wear.

Chapter 5 presents an introduction to the neural network, training of the neural network, and the three types of neural networks which were used to predict wheel wear and rail wear in this thesis; Also, this chapter contains the prediction of wheel wear and rail wear using a Nonlinear Autoregressive model with eXogenous input neural network (NARXNN) for the twin disc test experiments.

Chapter 6 contains the prediction of wheel wear using NARXNN for VAMPIRE vehicle dynamic software simulations. The VAMPIRE vehicle dynamics software was used to carry out several tests such as a change of some parameters such as speed, longitudinal bush stiffness, lateral bush stiffness, vertical bush stiffness, longitudinal bush stiffness, lateral bush stiffness, and vertical shear stiffness; the simulation results were then used to train, validate, and test the neural network for wheel wear prediction using the neural network.

Chapter 7 contains the prediction of wheel wear using NARXNN, BPNN, and RBFNN for VAMPIRE vehicle dynamic software simulations, this was done to present that the wheel wear can be predicted using different types of neural networks. In this chapter the effects of the RBFNN parameters on wheel wear prediction were investigated. Also, this chapter includes an investigation of the accuracy of these three types of neural networks for wheel wear prediction.

Chapter 8 contains the discussion, conclusions, and future work.

The major contribution to knowledge of this work is outlined below:

1. The development of a neural network model for wheel and rail wear prediction:
    a. Neural network architecture: a nonlinear autoregressive model with exogenous input neural network (NARXNN) in series-parallel and parallel architecture were developed to predict the wheel and rail wear for a twin disc test rig experiments.
    b. Neural network types: types of neural network such as backpropagation neural network (BPNN), and radial basis function neural network (RBFNN) have been shown to be able to predict railway wheel wear under dynamic conditions.
    c. Neural network inputs: the inputs to the neural network that are required to provide effective prediction of wheel-rail wear have been established. These include load, yaw angle, track speed, running distance, longitudinal bush stiffness, lateral bush stiffness, vertical bush stiffness, longitudinal bush stiffness, lateral bush stiffness, vertical shear stiffness, wheel profile, and first/second derivative of wheel profile.
    d. Neural network parameters: the effect of various key neural network parameters on the ability to predict wheel-rail wear have been established. The effect on the accuracy of wheel/rail wear prediction of the correct selection of neural network parameters has been established.

In this project, a new method was developed for wheel and rail wear measurement using a replica material, Alicona profilometer, and a twin disc test rig. The replica samples were scanned using an optical profilometer and the wheel and rail wear was studied. The new method has been shown to be effective in investigating the effect of load, yaw angle, and surface conditions (dry, wet, lubricated, and sanded conditions) on wheel wear and rail wear.

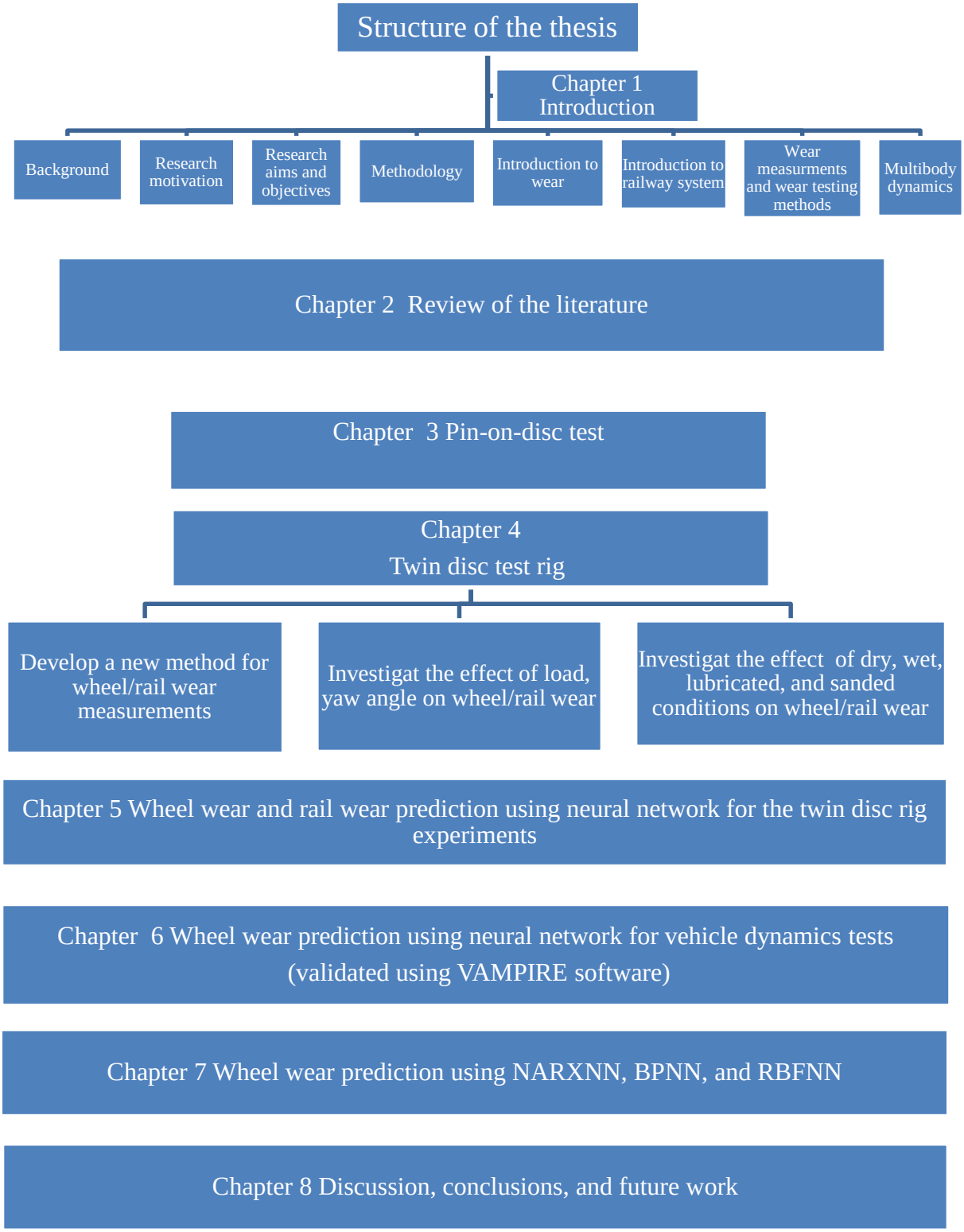

Figure 1. 3 Structure of the thesis

1.5 Introduction to wear

The generally accepted definition of wear is the loss of material which happens as a consequence of relative motion at the surface [11]. Wear may result whenever there is a rolling, sliding, or impact motion between two solid surfaces [12]. The wear rate depends on working conditions such as lubrication, loading, and environment [11]. Wear cannot be eliminated totally, but it can be decreased. Furthermore, there are several methods to reduce the wear such as the selection of material and lubrication [13]. There are many types of wear but the most common types are the abrasive, adhesive, fretting, erosion, fatigue, and chemical wear [11]-[15].

Abrasive wear grows when a solid surface slips on a weaker surface. It involves two possible conditions: two body abrasion and three body abrasion. In the two-body abrasion the solid surface is the more solid of the two rubbing surfaces. In the three-body abrasion the solid surface is a third body, usually pieces of grit trapped between the two other surfaces which are hard enough and able to scratch two surfaces. Abrasive wear is shown in Figure 1.4 [12], [16].

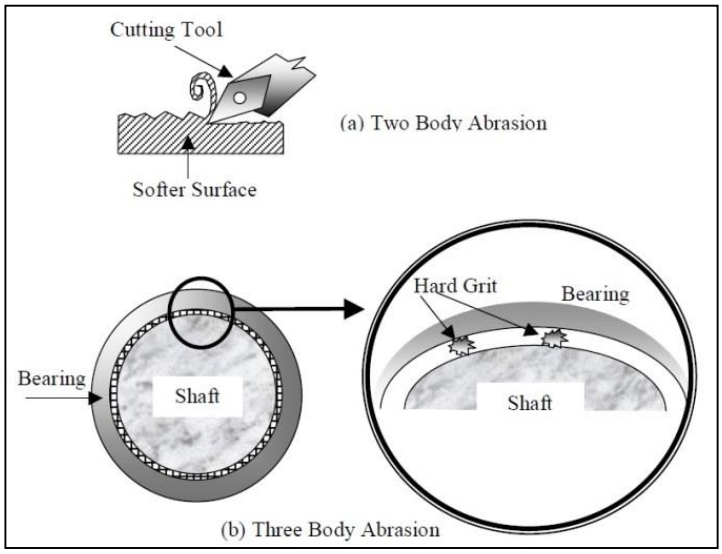

Figure 1. 4 Abrasive wear [16]

Adhesive wear arises when there is a reciprocal transfer of particles through a hard surface and a soft surface. The process involves the transfer of the particles from one surface to the other. The asperities so formed can break in the softer material or in the harder material which leads to a mutual transfer of materials in moving contact. Adhesive wear is shown in Figure 1.5 [14], [17].

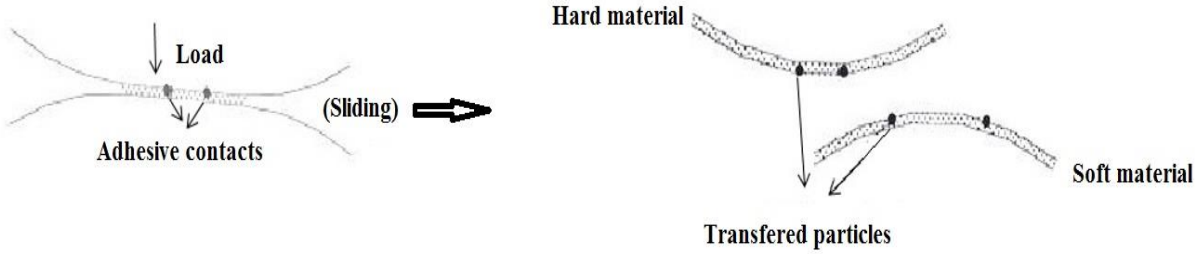

Figure 1. 5 Adhesive wear [14]

Erosion wear can occur by streams of hard particles, and the effect of a liquid. Cavitation erosion is the most common type of erosion wear. The erosion wear phenomenon is shown in Figure 1.6. When the solid particle A is impacted with solid surface B, a part of the surface B is removed. Several factors affect the erosion process such as effect angle, effect velocity, and particle size [16], [18].

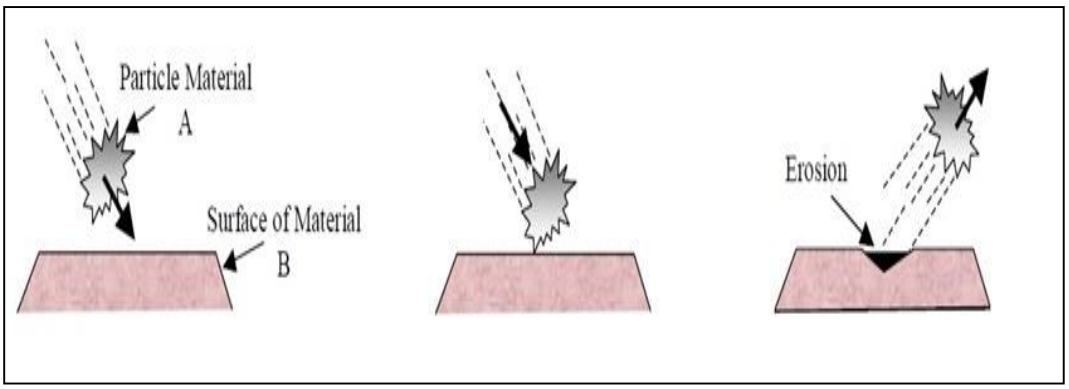

Figure 1. 6 Schematic of erosion wear [16]

Fatigue wear occurs when the surface yields to cyclic loading. At the point where the shear stress is maximum small cracks are initiated, and then, propagate to the surface of material [19], [20]. Fatigue wear can be observed in rolling wear, sliding wear, and impacting wear processes as well. Such as shown in Figure 1.7, a cracks are initially produced, then these cracks grow and propagate through the surface of the material to form cracks under repeated sliding motion. When one surface continues to slide against another surface, the material on the contact surface is broken and wear debris is generated [21].

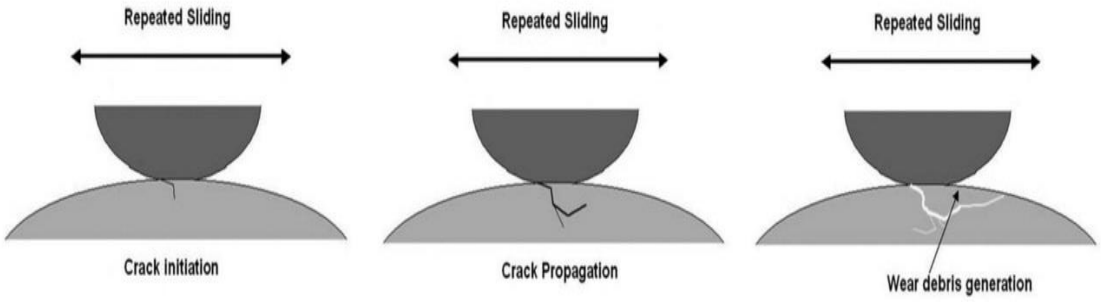

Figure 1. 7 Fatigue wear [21]

Chemical or corrosive wear results from the interaction of the environment with sliding surfaces. The undesired deterioration of a material through chemical or electrochemical interaction with the environment may be defined as the corrosion wear. The sliding motion and chemical reaction are both required for corrosive wear [19], [22]. Corrosion wear is a type of chemical wear [11].

Fretting wear arises if there are slight oscillatory movements between two surfaces. Also, when small relative slipping motion takes place between two surfaces the result is an amount of fine wear debris which is known as fretting wear [11].

Adhesive wear, abrasive wear, fatigue wear, and corrosive wear can be recognized as the major wear types. These four wear types are shown in Figure 1.8 [19].

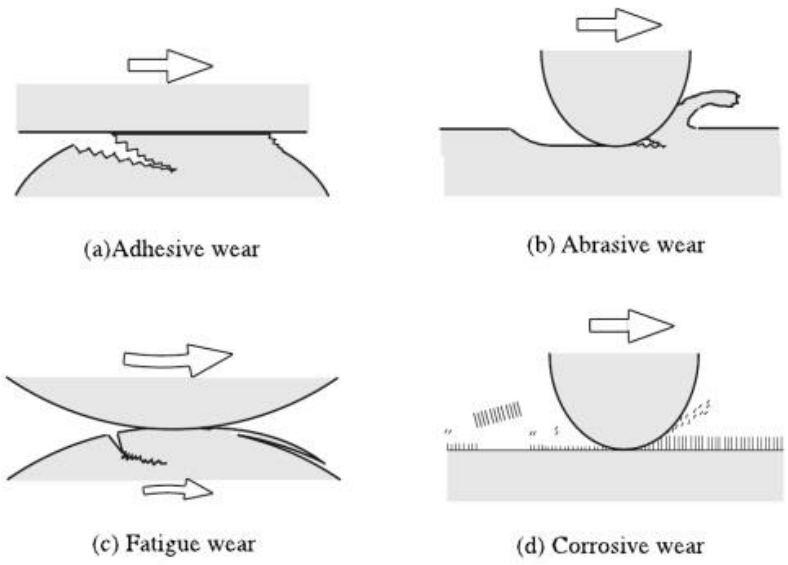

Figure 1. 8 Schematic images of four representative wear modes [19]

1.6 Introduction to railway systems

The railway system is relatively complex. This system consists of several bodies consequently it has many degrees of freedom [23]. Vehicle dynamic behaviour can be defined as the dynamic response of the vehicle to the track. The railway vehicle can move in the following different directions of motion: longitudinal, lateral, vertical, roll, pitch, and yaw. The vehicle/track interface is the combined behaviour of the vehicle and track systems, including the influence of wheel rail contact forces on the system. Effective controlling of the vehicle track interaction will have positive influence on passenger comfort, operational capability, safety, and cost [24].

1.6.1 Railway bogie

A railway bogie consists of several main components such as wheel, primary suspension, secondary suspension, and bogie frame such as shown in Figure 1.9.

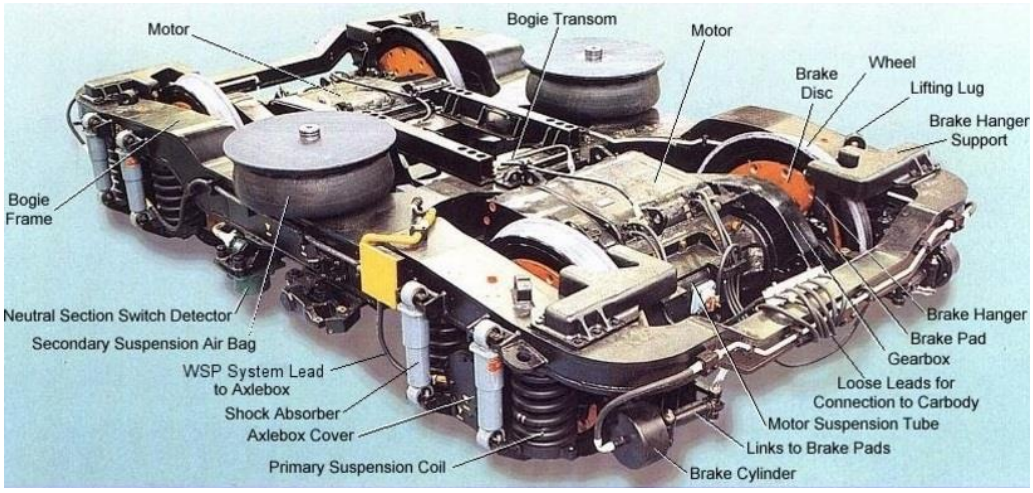

Figure 1. 9 Railway bogie components [25]

1.6.2 Wheelset

A wheelset includes two wheels fixed to an axle. The rail vehicles continue centred on the track because of the tapered profile 'conicity' of the wheel tread, which provides a lateral force on the rail vehicle when it is offset from the track centre. Large conicity is useful to curving performance, but it can create larger lateral forces. The flange of the wheel works to prevent the tread shifting laterally off the rail [26]. A wheelset is shown in Figure 1.10.

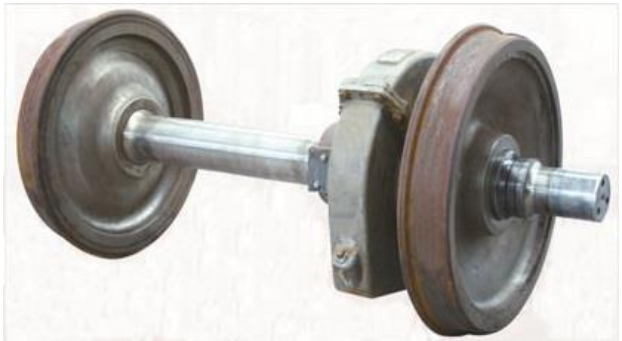

Figure 1. 10 Wheelset

1.6.3 Rail

The most commonly used rail profile is a flat-bottom rail and it is divided into three parts such as shown in Figure 1.11. The top part is the rail head which contacts with the wheel, the middle part is the rail web which supports the rail head, and the bottom part is the rail foot which distributes the load from the web to the underlying superstructure components [27].

The rail is made of straight sections and curves. The increase of the forces acting on train on the curves results in an intensive rail wear, while the changing of the worn rails increases railway maintenance expenses [28].

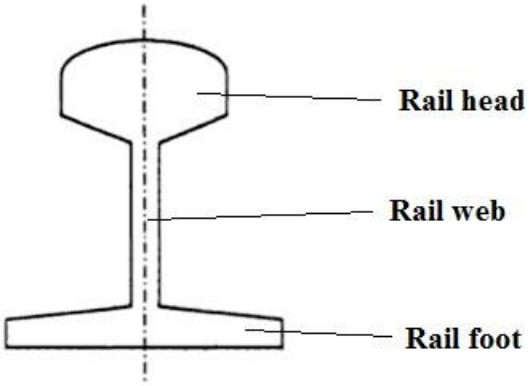

Figure 1. 11 Flat bottom rail [27]

1.6.4 Railway track

A railway track construction consists of rails, sleepers, railpads, fastenings, ballast, subballast, and subgrade such as shown in Figure 1.12. The railway track is consisting of parallel lines of rails to provide a road for the movements of railway vehicles. The function of the track is to lead the train, it carry train safely along the track and through switches to the last stop, and it also carry the weight of the train and distribute the weight over the area that is as large as possible. The distance between the inner edges of the heads of rails in a track called a gauge of the track [23], [29].

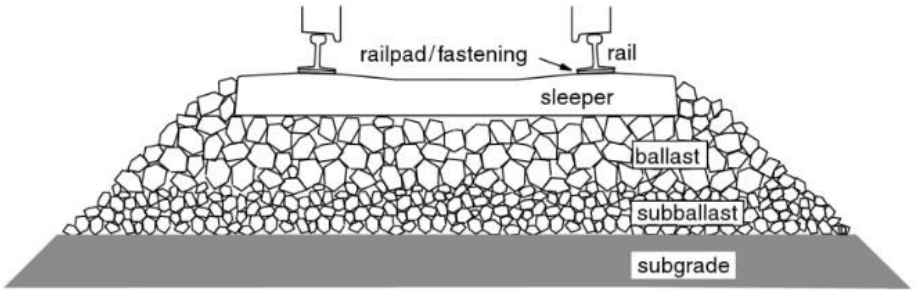

Figure 1. 12 Rail track [23]

1.6.5 Rail-Wheel Interaction

Wheel/rail interaction or interface is the contact between wheel and rail. It can conveniently be categorised as either vertical interaction, or lateral/longitudinal interaction. Vertical interaction deals with the vertical forces between the wheel and the rail. Lateral/longitudinal interaction includes forces that act in either a lateral or longitudinal direction due to wheel/rail creep forces or flange forces [24].

One of the most important factors which has an influence on the railway vehicles dynamics is the contact geometry between wheel and rail. It can be influenced by several parameters such as wheel and rail profiles [30]. The wheel/rail contact interface is shown in Figure 1.13.

Figure 1. 13 Wheel/rail contact interface

The contact patch between wheel and rail is small, typically about 1cm^2 in size. The exact position of contact patch between wheel and rail is affected by the wheel and rail profiles and the degree of curvature of the track. The rail head and wheel tread will be in contact within a straight track, while in the curved track the contact occurs on wheel flange and rail gauge corner. Figure 1.14 shows the contact position and contact stress varies for the two wheels on a right-hand curve [1], [31], [32].

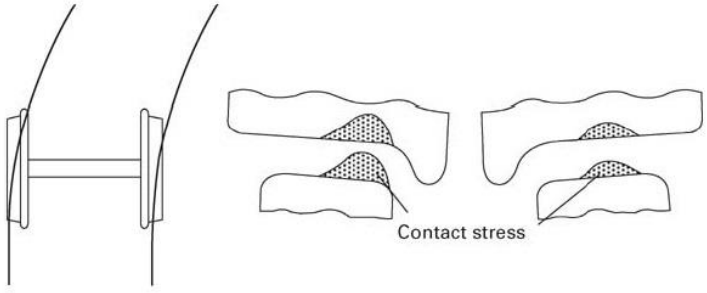

Figure 1. 14 The contact position and contact stress on curve [1]

On a curve, the yaw angle has an effect on wheel and rail wear, the yaw angle in curves is shown in Figure 1.15.

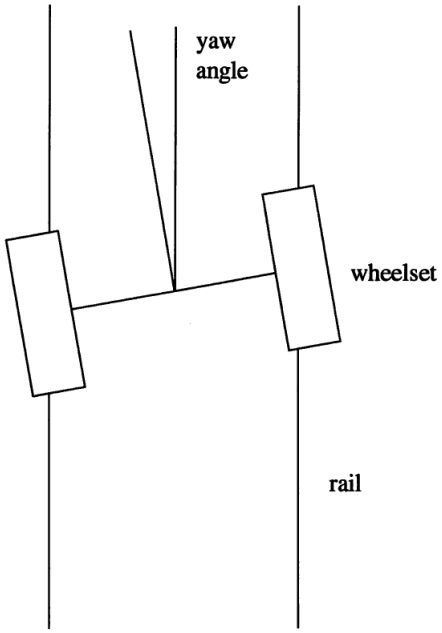

Figure 1. 15 Yaw angle in curves [33]

The wheel/rail contact occurs in three regions such as shown in Figure 1.16 [1]:

1. The contact between wheel tread and rail head occur in region A, this region yields the lowest contact stresses and lateral forces.
2. The contact between wheel flange and rail gauge corner occur in region B, in this region, the wear and contact stresses are much higher.
3. The contact between field sides of wheel and rail occur in region C.

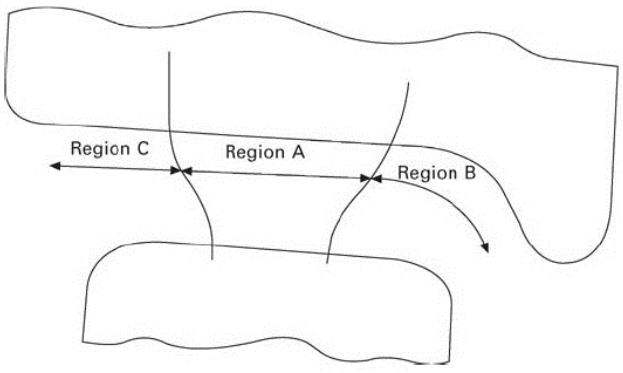

Figure 1. 16 Wheel-rail contact zones [1]

1.6.6 Wheel/rail forces

The dynamic behavior of the railway vehicle is affected by the interaction forces between the wheel and the rail. Several parameters can significantly affect the railway vehicle dynamics such as creep forces, creepage, adhesion, and wear. Hertz's static theory proved that the contact area is elliptical in shape with semiaxes a and b when the two bodies are rolled over each other while being forced against each other. The semiaxes a and b are be influenced by the geometry of the two surfaces and the normal force. The creep and creep forces are shown in Figure 1.17 [34].

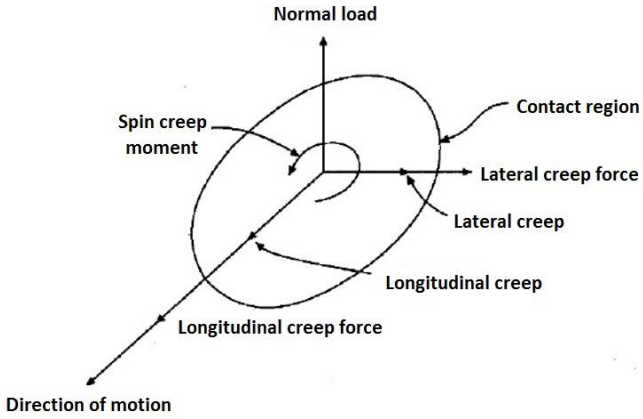

Figure 1. 17 Creep and creep forces [34]

If a wheelset is rolling freely along the track, then there will be no slip between the wheel and rail, so that the rotational velocity is equal to the forward velocity divided by the rolling rdius. If there is no slip, there will be no tangential wheel/rail force. Generally, wheels do not perform a pure rolling motion on the rail, but give rise to creepage (or sliding) and spin in the contact area between rail and wheel. Creepage and spin are in turn the causes of creep forces. The sliding motion is divided into three components; in a longitudinal direction, lateral direction and rotation about an axis perpendicular to the contact [24], [34].

1.7 Wheel wear and rail wear

Wear can be defined as the loss or displacement of material from a contacting surface by mechanical action. The change of wheel profile and rail profile makes a large contribution to track maintenance cost. The wear is the most important factor which can lead to wheel and rail profile change. [23]. An example of form change of wheel and rail profile is shown in Figure 1.18.

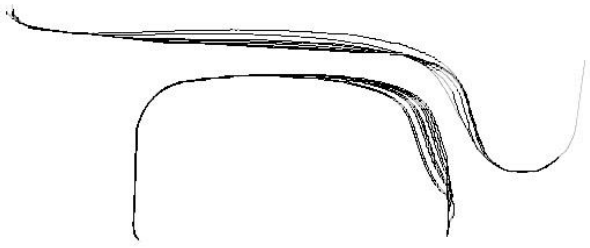

Figure 1. 18 Form change of wheel and rail [23].

The cost of changing damaged rails is much greater than that of changing any other damaged part of track [33]. There are three different positions that can be used for rail wear measurements which are; W1 is the vertical wear, W2 is the horizontal wear at a vertical distance h, and W3 is the wear measured at some angle α such as shown in Figure 1.19 [35].

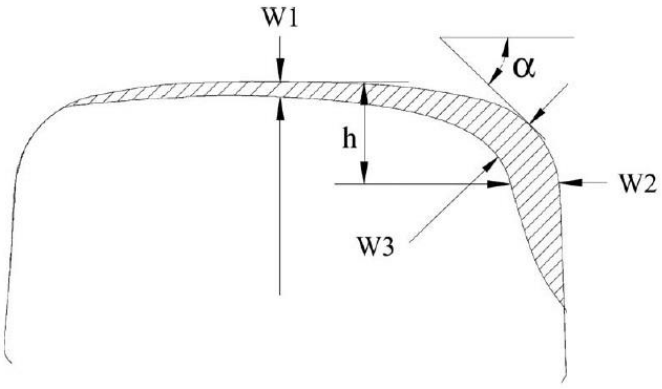

Figure 1. 19 Rail wear [35]

Wear of wheel profiles is one of the most important problems influencing the cost and performance of railway systems. The wheel-rail contact condition is complex, and as a consequence of this complexity, two different wear regions often occur on the wheel profile: one on the tread and the other on the flange [1]. The shape of the wheel profile may vary significantly depending on a large number of factors such as curvature profile, suspension design, and level of traction and braking forces applied. An example of tread wear and flange wear is shown in Figure 1.20 [23].

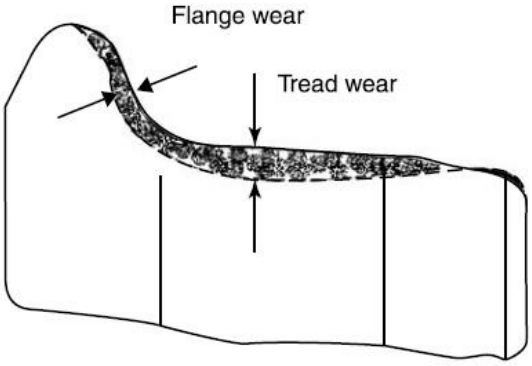

Figure 1. 20 Wheel wear [23].

The wear can be reduced using several factors such as lubricant. Lubricant is generally excellent at reducing wear in severe contact. The benefits of lubrication include the reduction of wheel wear and noise generation [36]. However there are also some disadvantages of lubrication such environmental damage from used lubricants, and reduction in traction and braking [37].

1.8 Wear measurement methods

Wear measurement approaches can be classified into: linear wear dimension, mass difference, wear area, and wear volume. Wear can be expressed by the mass loss "in grams", or the rate of mass loss per unit of usage "grams per mile", but in this case, no information about the distribution of wear over the surface of component is available. Therefore, measuring of wear in term of mass loss can be considered an ineffective method. Another approach for wear measurement is based on linear dimensional measurements, such as wear scar depth or width. This approach is commonly used, but tiny amount of wear are difficult to measure. The same is true of the mass loss method. Material loss can be produces over a restricted area, these area can be measured and are proportional to the amount of wear. Furthermore, the volume can be used as a key approach for wear measurements [38].

A stylus profilometer can used to measure the wear of sample by measuring the change of the linear dimensions of the specimen before and after the test; the wear of sample can also be measured by weighing the sample before and after the test [39].

Common techniques which can be used for wear measurements are weight loss, volume loss, wear scar depth, and geometric measures. Microscopy techniques such as scanning electron microscopy (SEM) and scanning tunnelling microscopy (STM) can be used for wear measurements. A stylus or non-contact optical profiler are an easy technique which can be used to measure the wear depth [17]. An example of wear depth measurement using a stylus is shown in Figure 1.21.

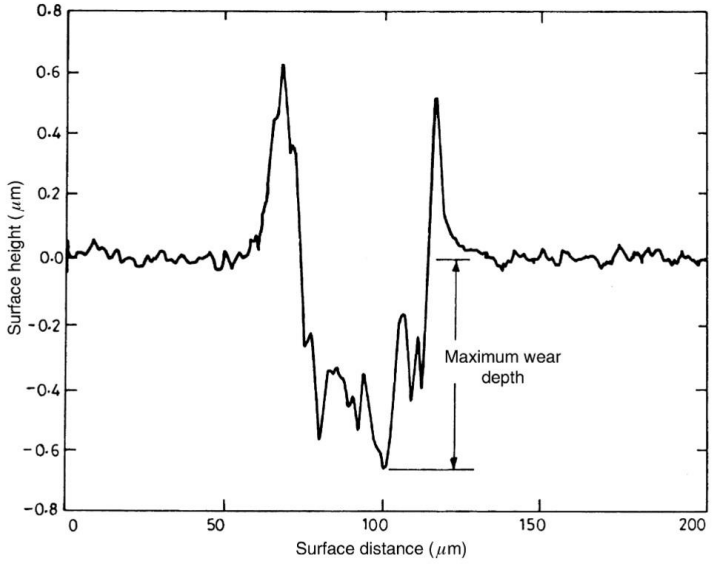

Figure 1. 21 An example of wear depth measurement obtained using stylus [17]

1.9 Wear testing methods

1.9.1 Introduction

There are different techniques which can be used for studying the wear which occurs in the surface contact. The most common and simplest of these techniques are the pin-on-disc test and the twin disc test rig [1].

1.9.2 Pin-on-disc test

The pin-on-disc wear test is one of the most widespread tests which can be used for studying the sliding wear behaviour. The pin-on-disc wear test is shown in Figure 1.22. The pin is pressed against the disc, and relative motion between pin and disc will cause pin wear and disc wear [40].

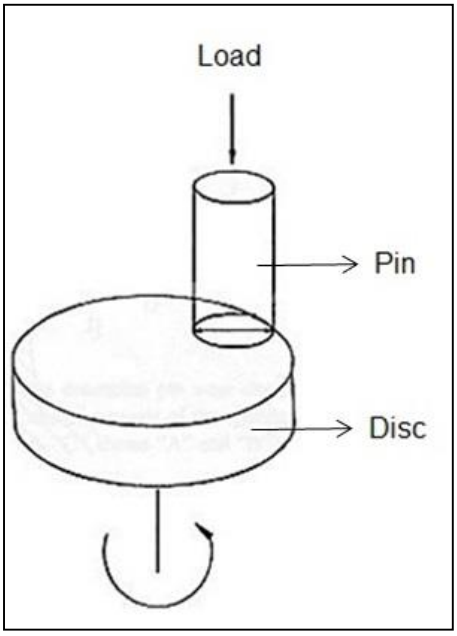

Figure 1. 22 Diagram of the configuration of pin-on-disc test [40]

The cross section of the pin shapes is shown in Figure 1.23.

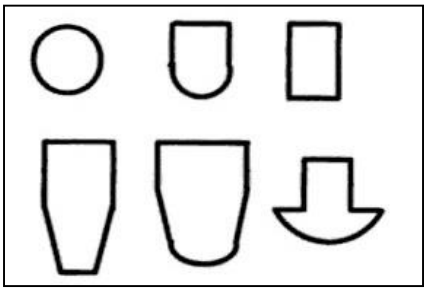

Figure 1. 23 The pin shapes [41]

Profilometer traces before and after wear can be used to determine the depth of worn pin and disc wear scar such as in the Figure 1.24 and Figure 1.25 respectively. After that, the pin wear and disc wear (wear volume) can be determined using proper geometrical relationships or numerical methods [41].

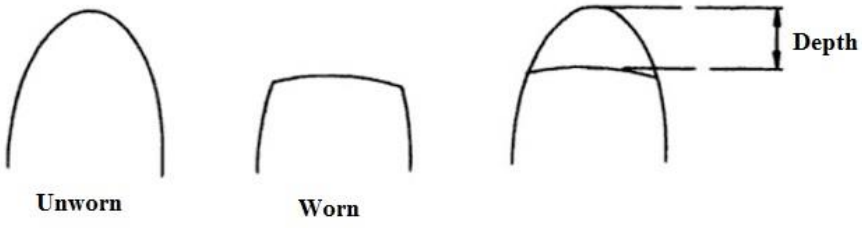

Figure 1. 24 Pin wear depth [41]

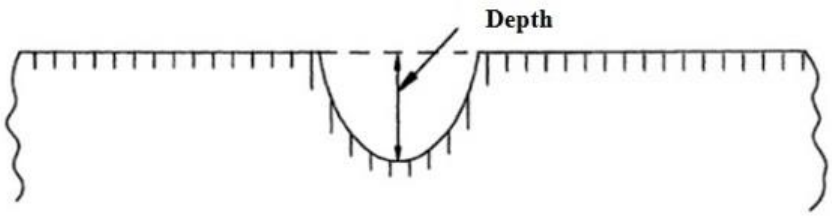

Figure 1. 25 Disc wear scar depth [41]

The pin wear and disc wear can be reported as a volume loss in cubic millimetres, as a change in dimensions of both specimens in millimetres, or as a weight loss in milligram [39].

The pin-on-disc test was used to study the wear by many researchers. An example, the effect of applied load and sliding speed on pin wear and disc wear was investigated [42]-[46].

1.9.3 Twin disc test rig

The twin disc approach has been used widely to study the wheel wear and rail wear [47]. Twin disc tests are frequently used to study wear in railway materials [48]. The twin disc machine is simple and efficient; it consists of two cylindrical rollers pressed into contact and rotating with different peripheral speeds. The variation of the relative velocity and of the contact pressure allows performing the test under different conditions [49]. The twin disc test rig was used by many researches to study the wear at the wheel/rail interface [50], [51]. An example of a twin disc test rig which was used in previous work to study the wheel wear is shown in Figure 1.26 [52].

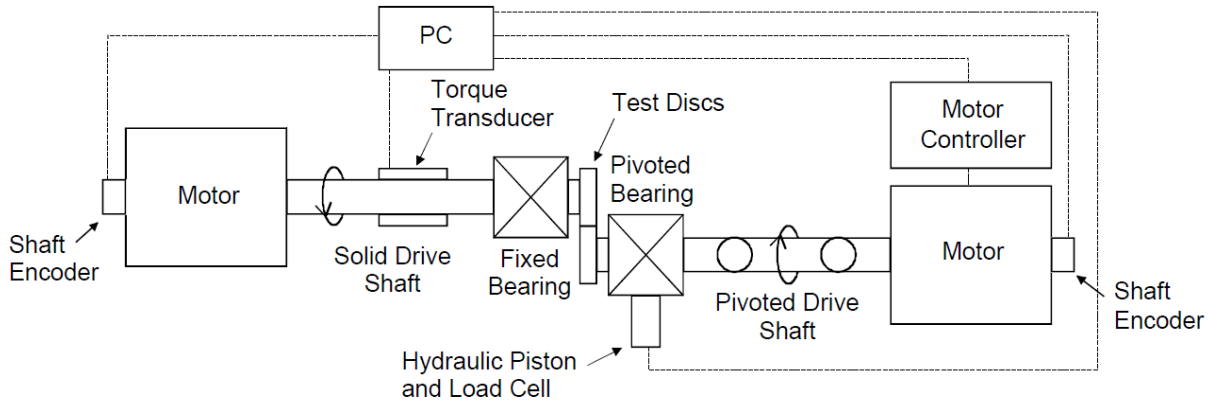

Figure 1. 26 Twin disc test machine [52]

1.10 Multibody dynamics

Multibody dynamics can be used in many fields of engineering research such as railway vehicle systems. A railway vehicle is a complex system consists of various different components. For dynamic behaviour modelling, it is important to simplify this complex system. To design a dynamic model, a multibody approach commonly used. The vehicle will be idealised as a collection of masses representing the bogie frames, body, and wheelsets linked by several suspension elements. Each body is initially considered as having six dynamic degrees of freedom, three translations (lateral, longitudinal and vertical) and three rotations about its axis (roll, pitch and yaw). The vehicle model reqiures an associated axis system as shown in Figure 1.27. Positions of masses, wheelsets and suspension elements are specified in terms of the following positions: The longitudinal axis (X) which is usually fixed at the mid-point of the vehicle; the lateral axis (Y) which is relative to track centreline and height above rail; and the vertical axis (Z) which is relative to the height above the rail. Where (V) is the direction of travel [24], [26], [53].

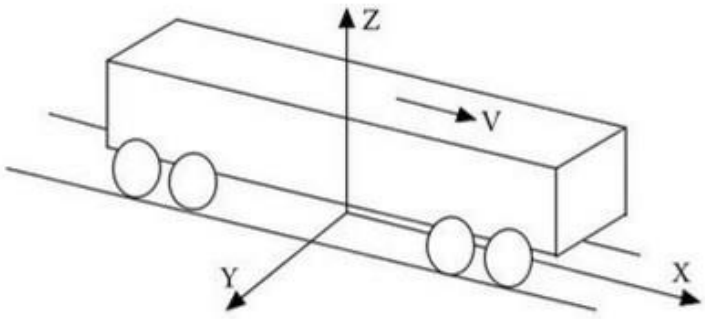

Figure 1. 27 Vehicle modelling axis system [26]

The suspension elements is the main interconnection elements in rail vehicle modelling. The suspension elements include stiffness, bumbstop, damper, friction, pinlink, shear spring, airspring, bush and constraint elements. Dynamic modelling is a means of reperoducing the dynamic behaviour of railway vehicles in a software environment. The use of dynamic simulation tools has many advantages such as the new designs can be tested before they are built, and components adjusted in a less costly way. There are many software packages used to study the vehicle dynamic behaviour such as Simpack (A European package), Gensys (A Swedish package), NUCARS (USA package), VI RAIL (Adams/Rail), and VAMPIRE (UK package). Slightly different results are possible depending on which package is used to perform simulations as they use different approaches for representing wheel/rail contact. There are a number of inputs to any simulation such as vehicle, track, and wheel/rail contact [24], [26].

Chapter 2 Review of the literature

2.1 Wear models

2.1.1 Introduction

The function of wear models is to predict the rate of material removal from the surface. Classical wear theory begins by considering the rate of material removal as a function of some parameters such as load, sliding speed, sliding distance and hardness of material [54]. In sliding wear models there are more than 100 different variables and constants. These models contains between two to twenty six variables in a single equation. Unfortunately, some constants are assigned to represent specific quantitative phenomena which are not readily measurable such as surface strength, and fatigue life of an asperity [55].

Meng and Ludema [55] reported, between 1957 and 1992, that there were 182 wear equations for the several types of wear. The most important issue of the 182 equations is that it include on a great number of variables. Each author combines a different array of variables, often for the same mechanical system.

2.1.2 Review of wear models

Reye in 1860 considered that the volume of material removed from a body was proportional to the energy dissipated into it by the relative motion of the two contacting surfaces such as shown in the following equation [54], [56], [57].

$$V = K_R W \tag{2.1}$$

Where V is the volume of material removed, K_R is Reye's wear constant and W is the work dissipated into the material. Reye's approach was one of the primarily methods to calculate the wear in terms of energy dissipated.

Holm in 1946 considered that the process of wear with regard to the relative motion of surface asperities. He suggested that the individual atoms on opposite asperities were moving towards each other and colliding. His suggestion stated that the wear was a function of the properties of the materials in contact and the load applied over the contact such as shown in the following equation [13], [54], [58], [59].

$$V = Z \frac{p}{p_m} \tag{2.2}$$

In the above equation V is the volume of material removed per unit sliding distance, Z is the probability of removal of an atom per atomic encounter and would depend on the properties of the materials in contact, p is the load applied, and p_m is the flow pressure of a worn surface "hardness of material".

Burwell and Strang suggested that the volume of wear material can be calculated using the following equation [58]:

$$Q = k \frac{W d}{H} \tag{2.3}$$

Where k is the probability of removing wear particles, W is the load, d is the sliding distance, and H is the hardness of material. Thus the wear volume per unit sliding distance w is [58]:

$$w = k \frac{W}{H} \tag{2.4}$$

Archard in 1953 studied the wear process and suggested that there were a number of key considerations that must be included in a wear model. Archard has referenced Holm in his publications and his work could be thought of as an extension or furthering of Holm's wear equation. Archard assumed that two rough surfaces are in discrete contact "The contact consists of individual spots". The area of each spot expands from zero to maximum πa^2, and then shrinks back to zero such as shown in Figure 2.1. Normal load can determined by the following equation [54], [60]-[62]:

$$p_n = \pi a^2 p_m \tag{2.5}$$

Where : p_m is the yield pressure of a plastically deformed asperity, and a is the contact spot radius.

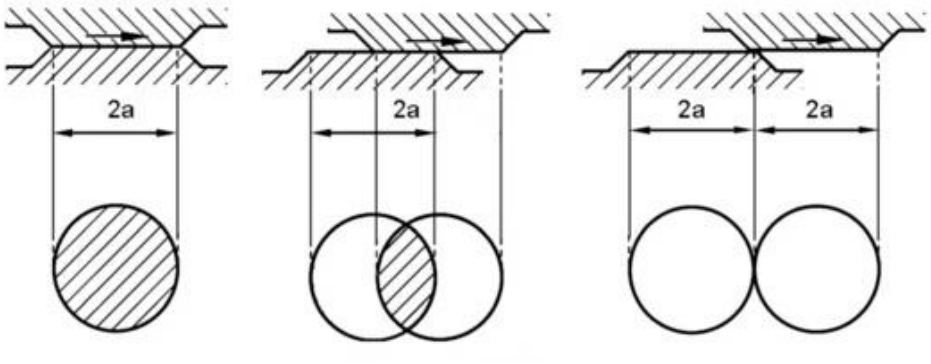

Figure 2. 1 Archard wear model [60], [62]

Assume that this volume consists of a half-sphere of radius a, the volume is given by:

$$V_n = \frac{2}{3} \pi a^3 \tag{2.6}$$

Wear rate (per unit distance of sliding) is given by:

$$i_n = \frac{V_n}{2a} \tag{2.7}$$

Then:

$$i_n = \frac{\pi a^2}{3} \tag{2.8}$$

Therefore:

$$i_n = \frac{P_n}{3 P_m} \tag{2.9}$$

The total wear rate would be equal to the total contribution from all contact spots:

$$I^* = \sum i_n = \frac{P}{3 P_m} \tag{2.10}$$

Where the total normal load on the contact is:

$$P = \sum P_n \tag{2.11}$$

Archard assumed that the wear can be calculated using the following equation:

$$I = k\, I^* \tag{2.12}$$

Where k is constant.

It is written as:

$$I = \frac{k\, P}{3\, P_m} \tag{2.13}$$

It is convenient to designate $K = \frac{k}{3}$ and assume that $P_m = H$.

Then the equation of wear develops in the form:

$$I = \frac{K\, P}{H}\ (mm^3/mm) \tag{2.14}$$

Where: I is the volume worn per unit sliding distance (wear rate), P is the normal load, H is the hardness of the softer material, and K is the wear coefficient.

Then Archard expressed the wear equation such as shown in the following form: [54], [58], [13].

$$V = k\, \frac{N\, S}{H}\ (mm^3) \tag{2.15}$$

Where: V is the volume of wear (mm^3), k is the wear coefficient (-), N is the normal load (N), S is the sliding distance (mm), and H is the hardness of material (N/mm^2).

The wear coefficient (k) can calculated using the following equation [1], [63], [64]:

$$k = \frac{V\, H}{L\, F_N} \tag{2.16}$$

Where: k is the non-dimensional wear coefficient, V is the volume of wear (mm^3), H is the hardness of material (N/mm^2), F_N is the normal load (N) and L is the sliding distance (mm). The wear coefficient k is dimensionless and always less than 1 [60], [65].

The values of wear coefficient k for various materials against steel under dry conditions using pin-on-disc tests are illustrated such as shown in Table 2.1.

Material	k
Mild steel (on mild steel)	7×10^{-3}
α/β brass	6×10^{-4}
PTFE	2.5×10^{-5}
Copper–beryllium	3.7×10^{-5}
Hard tool steel	1.3×10^{-4}
Ferritic stainless steel	1.7×10^{-5}
Polythene	1.3×10^{-7}
PMMA	7×10^{-6}

Table 2. 1 Wear coefficient values [65]

Wear coefficient k for unlubricated surfaces is shown in Table 2.2.

Material combination	k
Low carbon steel on low carbon steel	70×10^{-4}
60/40 Brass on tool steel	6
Teflon® on tool steel	0.25
70/30 Brass on tool steel	1.7
Lucite on tool steel	0.07
Molded bakelite on tool steel	0.024
Silver steel on tool steel	0.6
Beryllium copper on tool steel	0.37
Tool steel on tool steel	1.3
Stellite #1 on tool steel	0.55
Ferritic stainless steel on tool steel	0.17
Laminated bakelite on tool steel	0.0067
Tungsten carbide on low carbon steel	0.04
Polyethylene on tool steel	0.0013
Tungsten carbide on tungsten carbide	0.01

Table 2. 2 Wear coefficient unlubricated surfaces [66]

The wear coefficient depends on several parameters such as a contact pressure, sliding velocity, and temperature and the degree of lubrication in the contact area, therefore, it is a very complex parameter to determine. A wear map can used to describe the wear coefficient as a function of contact pressure and sliding velocity. Each wear map corresponds to a certain rail and wheel material (The rail and wheel are assumed to have similar material properties). Figure 2.2 shows a wear map which is describes four approximate regions, in this chart, the contact pressure limit at 0.8H corresponds to 80% of the hardness, and the wear coefficient depends on the sliding velocity [67].

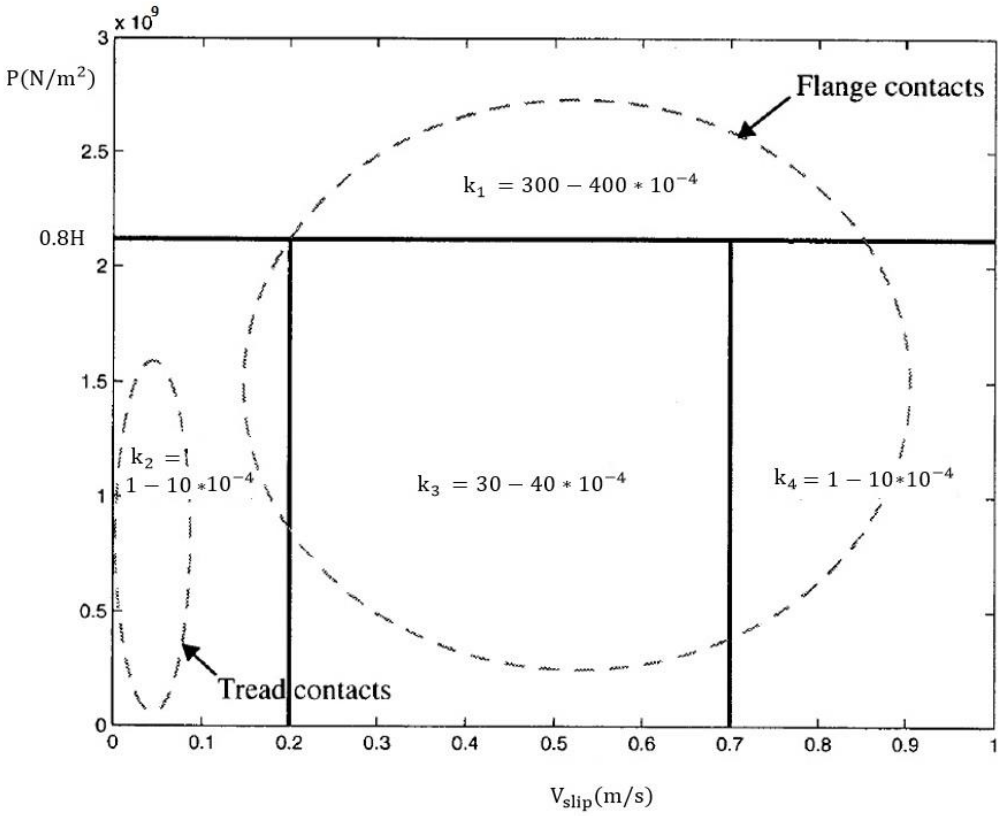

Figure 2. 2 Wear chart for the wear coefficient [67]

Montgomery et al., [54] stated that "there are a number of problems with the assumption that the wear rate is directly proportional to the load, as stated by Archard. The surface characteristics of the materials in contact will be changing as a result of material being removed, they will generally become rougher and therefore a change in the friction coefficient by a factor of two or three could result in a change of the rate of wear by one or more orders of magnitude".

The weakness of using the Archard model for wear modelling is that it depends on the proper calculation of wear coefficient k, where the wear coefficient k is a very complex parameter to determine, if k is not calculated correctly, it will lead to inaccurate results of wear modelling.

The Royal Institute of Technology Stockholm (KTH) developed the following wear model based on the Archard model. The volume of worn material is written as:

$$V = \mathrm{K_A}\ \frac{\mathrm{P\ S}}{\mathrm{H}} \tag{2.17}$$

Where: V is the volume of wear in ($\mathrm{mm^3}$), S is the sliding distance in (mm), P is the normal force in (N), H is the hardness of the softer material in ($\mathrm{N/mm^2}$), and $\mathrm{K_A}$ is wear coefficient. The values of wear coefficient $\mathrm{K_A}$ which shown in Table 2.3 were obtained using a pin-on-disc test, and a twin disc test rig using different materials. Where p is the contact pressure and $\dot{S}$ is the slip velocity [48], [68].

Pressure p[GPa]	Slip velocity ṡ[m/s]	K_A[-]
$p > 2.1$	any ṡ	$300 - 400.10^{-4}$
$p < 2.1$	$\dot{s} \geq 0.2$	$1 - 10.10^{-4}$
$p < 2.1$	$0.2 \leq \dot{s} < 0.7$	$30 - 40.10^{-4}$
$p < 2.1$	$\dot{s} \geq 0.7$	$1 - 10.10^{-4}$

Table 2. 3 Wear coefficient (KTH) [48], [68]

The University of Sheffield (USFD) developed the following wear model. The wear function developed by the USFD relates to the wear rate, which expresses the weight of lost material (μg) per distance rolled (m) per contact area A(mm^2), to the wear index Tγ as follow [68]:

$$\text{Wear rate} = K \frac{T\gamma}{A} \tag{2.18}$$

Where: K is wear coefficient, and T is the creep force, γ is the slip, and A is the contact area.
The wear equations presented by the USFD are shown in Table 2.4. This formulation was developed using twin disc rig experiments. The USFD wear function was developed for wheel (R8T) and rail (UIC60 900A) materials.

Wear regime	Wear range $\frac{T\gamma}{A}$ (N/mm^2)	Wear rate ($\mu g/m/mm^2$)
Mild	$\frac{T\gamma}{A} < 10.4$	$5.3 \frac{T\gamma}{A}$
Severe	$10.4 \leq \frac{T\gamma}{A} < 77.2$	55.0
Catastrophic	$\frac{T\gamma}{A} \geq 77.2$	$61.9 \frac{T\gamma}{A}$

Table 2. 4 The USFD wear function [68]

The Royal Institute of Technology Stockholm model and the University of Sheffield model can be used for wear modelling, but this is also dependent on the correct calculation of the wear coefficient k.

British Rail Research (BRR) developed equations to describe wear behaviour as shown in Table 2.5. Wear is calculated as material loss expressed in mm^2 of lost area from any radial section through the profile per km rolled. Where: T is the creep force (N), γ is the creepage [-], and D is the wheel diameter in (mm) [48], [69]. These equations were obtained from twin disc tests on R8T (wheel) and BS11 (rail) steels.

Friction	Regime	Tγ (N)	Wear Rate (mm2/km rolled)
Dry	Mild	< 100	0.25Tγ/D
Dry	Mild Plateau	> 100 and < 200	25.0/D
Dry	Severe	> 200	(1.19Tγ - 154)/D

Table 2. 5 Equations of the BRR wear function [69]

The British Rail Research model can be used for wear modelling, but the main limitation of the BRR wear model lies in the fact that the equations given in Table 2.5 are only valid for the specific materials considered.

R. Lewis and U. Olofsson [1] presented an approach which can be used for wheel wear modelling (expected wear proportional to wear index WI) as provided bellow:

$$WI = K(T_1 \gamma_1 + T_2 \gamma_2) \tag{2.19}$$

Where K is the constant, T_1, T_2 are the longitudinal and lateral creep forces respectively, and γ_1, γ_2 are the longitudinal and lateral creepages respectively. This relationship between the energy dissipation and material removal can be used to predict wheel/rail wear. This model is one of the most common models which have been used in recent works for wear modelling; accordingly, it has the same drawbacks as most of the classical wear models, which are dependent on the value of certain constants.

The American Society for Testing and Material (ASTM) developed a wear model which can be used to model the pin wear and disc wear for pin-on-disc experiments as shown in the following equations [39], [70], [71]:

$$\text{Pin volume loss} = \frac{\pi h}{6}\left[\frac{3 d^2}{4} + h^2\right] (mm^3) \tag{2.20}$$

The height of material removed for pin (h) is given by:

$$h = r - [\, r^2 - \frac{d^2}{4}\,]^{0.5} \text{ (mm)} \tag{2.21}$$

Where: d is the pin wear scar diameter, and r is the pin radius.

$$\text{Disc volume loss} = 2\pi R\,[\, r^2 \sin^{-1}\left(\frac{d}{2r}\right) - \left(\frac{d}{4}\right)(4r^2 - d^2)^{0.5}] \, (mm^3) \tag{2.22}$$

Where:R is the disc wear track radius, r is the pin radius, and d is the disc wear track width.

The accuracy of pin/disc wear modelling using the ASTM model is dependent on the proper measurements of the pin wear scar dimensions and disc wear scar dimensions, this requires an accurate instrument. The ASTM model has a limitation however, it can only be used to model the pin/disc wear, but it cannot be used for wheel and rail wear modelling.

In the survey of the wear modelling equations, many equations were found for wear modelling; for example, [55] presented 28 equations for erosion wear modelling, and a couple of equations for sliding wear modelling; the problem with these models is that they depend on different variables and constants.

2.2 Computer simulation packages for wear prediction

The modelling of wear can be carried out with mathematical models and computer simulations [13]. The railway wheel wear prediction is a very significant problem in railway systems. In the past, the reprofiling intervals of railway wheels have been planned according to designer's experience. Today, computer simulation tools can be used to predict the wheel wear [72].

This section presents a review of using the computer simulations for wheel/rail wear prediction.

Pearce and Sherratt [73] presented a model which is shown in Figure 2.3 to predict the wheel wear. VAMPIRE software was used to simulate the dynamics of the railway vehicles. The wear algorithm is shown in Table 2.6, the material lost is proportional to the energy dissipated in the contact zone. For wheel wear prediction, two track inputs were selected from VAMPIRE input files, it is a straight track and a curved track. The P8 wheel profile and P11 wheel profile were used in this study. The position of the contact on the wheel, creepage, and creep forces are correlated and summed to calculate the material loss distribution across the wheel profile. The contact patch data were recomputed before each journey and then this step was repeated until a desired mileage was achieved.

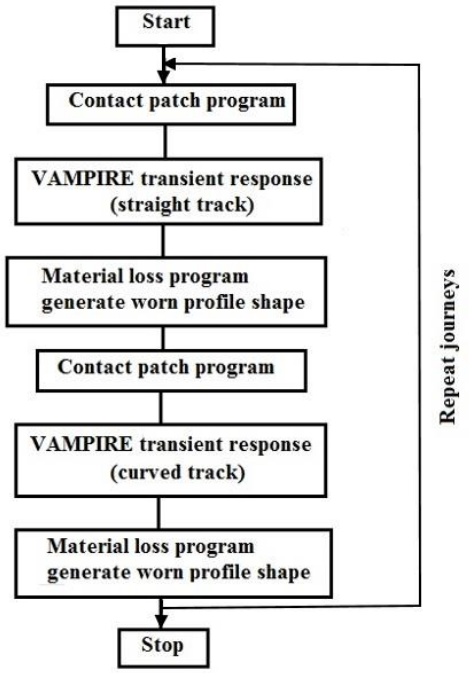

Figure 2. 3 Wheel wear prediction model [73]

$T\gamma < 100N$	material loss $0.25\ T\gamma/D$
$100 \leq T\gamma < 200N$	material loss $25.0/D$
$T\gamma \geq 200N$	material loss $(1.19T\gamma - 154)/D$

Table 2. 6 Wear algorithm [73]

Where T is the creep force (N), and γ is the creepage [-], and D is the wheel diameter in (mm).

Shu et al., [74] used a NUCARS vehicle/track multibody simulation program to estimate the rail wear. The advantage of NUCARS is that the rail profile can be modified online based on wear index (Tγ) and the rail profile is automatically updated for the next run. The rail wear model is shown in Figure 2.4. A wheel database, consisting of new wheel profiles, little worn wheel profiles, and heavy worn wheel profiles. This to reflect the effects of wheel shape on wear. The rail wear predicted using NUCARS model was validated using rail wear test results. The simulation predictions were very close to the test results.

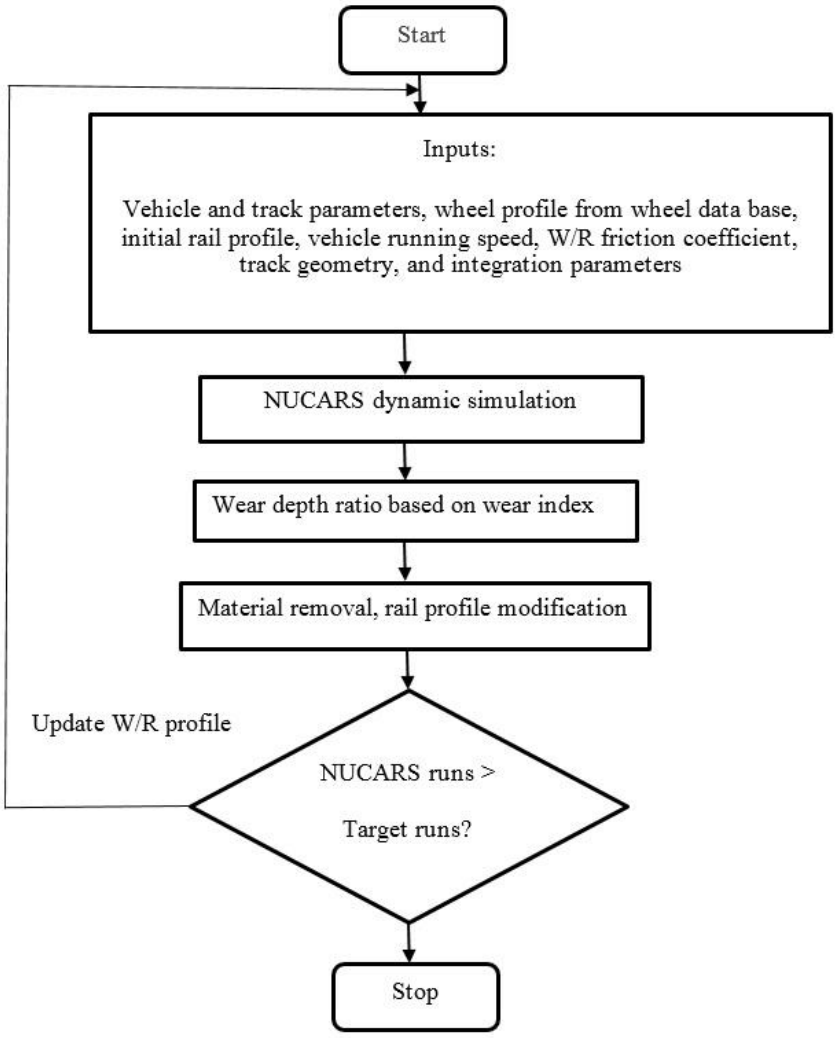

Figure 2. 4 Rail wear simulation procedures in NUCARS [74]

Ward et al., [75] presented a model to predict the wheel wear as shown in Figure 2.5 and Table 2.7. To generate the wear coefficients (k) for the model, a twin disc test was carried out. The approach for wheel wear prediction in this model is based on a wear index. The wear rate was calculated using the following equation:

$$\text{Wear rate} = k\,\frac{T\gamma}{A} \tag{2.23}$$

Where A is the contact area, T is tractive force, and γ is slip at the wheel/rail interface.

Multi-body dynamics simulations of a railway wheelset were carried out using ADAMS/Rail software. The wheel profile was discretised into strips and the wear was determined for each strip. The worn wheel profile is then fed back to the ADAMS/RAIL to update the wheel profile to predict the wheel wear.

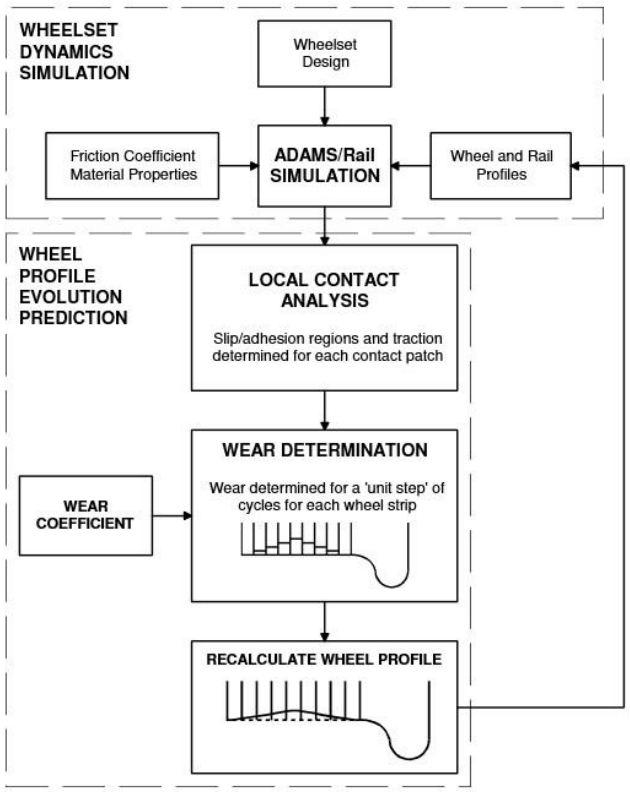

Figure 2. 5 Railway wheel wear modelling scheme [75]

Regime	$\frac{T\gamma}{A}$ (N/mm²)	Wear rate (μg/m/mm²)
k_1	$\frac{T\gamma}{A} < 10.4$	$5.3\,\frac{T\gamma}{A}$
k_2	$10.4 < \frac{T\gamma}{A} < 77.2$	55
k_3	$77.2 < \frac{T\gamma}{A}$	$61.9\,\frac{T\gamma}{A}$

Table 2. 7 Wear regime

Enblom [76] presented a model for wheel wear prediction as shown in Figure 2.6. A commercial Multibody Software (MBS) was used to simulate the dynamics of the railway vehicles. The wheel wear was calculated using the Archard wear model. The wear coefficient was determined using a wear chart, where the value of wear coefficient is a function of contact pressure and sliding velocity. Laboratory tests (twin disc test rig and pin-on-disc rig) were used to determine the wear coefficient. In this paper, the wheel wear was predicted using MBS simulation tool. The wheel wear predicted has been validated by comparing it to wheel wear measured (Stockholm commuter network).

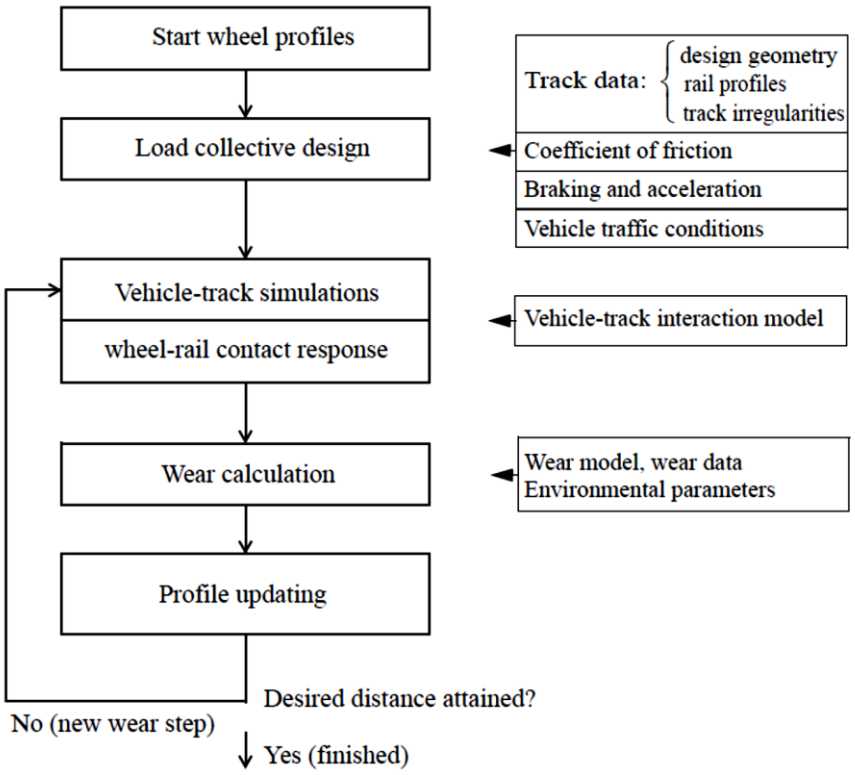

Figure 2. 6 Wheel wear prediction model [76]

Pombo et al., [72] presented a model to predict the wheel wear as shown in Figure 2.7. A commercial Multibody Software (MBS) software was used to simulate the dynamics of the railway vehicles. The MBS tool was applied in this paper in order to assess the effect of primary suspension stiffness, rail cant, traction/braking forces, and vehicle velocity on wheel wear. The wear was calculated using the energy dissipated in the wheel-rail contact.

Pombo et al., [77] presented a model to predict the wheel wear as shown in Figure 2.7. The MBS was used to simulate the dynamics of the railway vehicles. The MBS was applied in this paper in order to show the capabilities of MBS computational tool for wear prediction by evaluating the effect of trainset design, track layout, friction conditions, and wheel flange lubrication on wear. The wheel wear was calculated using the energy dissipated in the wheel-rail contact.

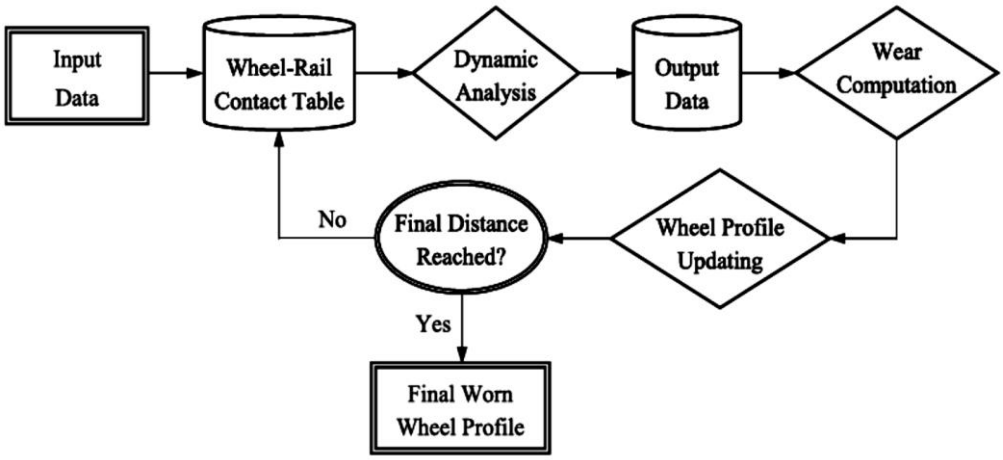

Figure 2. 7 Schematic representation of wear prediction [72], [77]

Bevan et al., [78] provided a model to predict wheel wear. The methodology of wheel wear prediction is shown in Figure 2.8. VAMPIRE vehicle dynamics software was used to simulate the dynamics of the railway vehicles. The VAMPIRE software generated the wheel-rail contact data and forces, these forces and wheel/rail contact data were used as inputs to the model to predict wear. This procedure is used to update the wheel profile, and the volume of material removed was determined using the Archard wear model and energy model. The wear coefficient (k) was determined from a map of wear for wheel/rail steels.

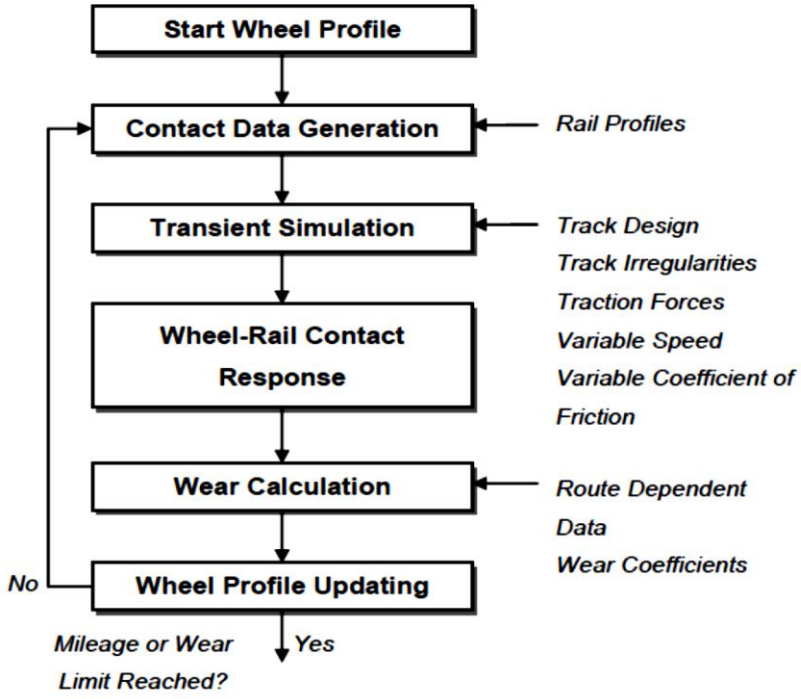

Figure 2. 8 Methodology of wheel wear prediction [78]

Arandojo [79] presented a model for wear prediction as shown in Figure 2.9. The GENSYS software was used in this paper to predict railway wheel wear. The track type, running distance, and type of rail and wheel profiles were loaded to the model as inputs. The vehicle-track interaction is performed in GENSYS software. The wear was calculated based on the Archard law. The GENSYS software is a three-dimensional general multi-body-dynamics program. Several simulations were carried out to predict the railway wheel wear of the first wheelset. A passenger vehicle was used in simulations, it consists of a single carbody with two bogies, four wheelsets and eight wheels.

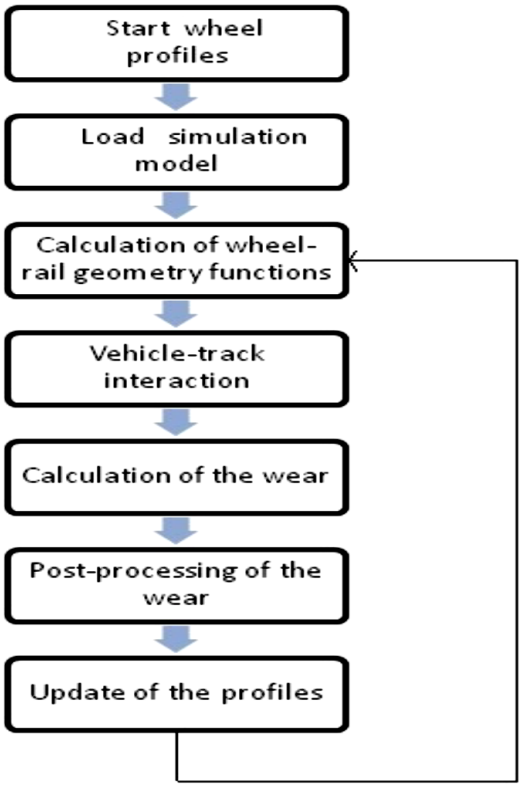

Figure 2. 9 Wheel wear prediction model [79]

Tanifuji [80] used SIMPACK software for wheel wear prediction. The lateral movement of the wheel/rail contact patch and the energy dissipated (Tγ) between wheel and rail were used to estimate the wheel wear as shown in Figure 2.10. Simulation tests were carried out on a straight track and on a curved track to predict the wheel wear. The running distance was 268000 km. Comparisons between wear predicted using SIMPACK software and wear measured were carried out to validate the wheel wear on flange and on tread. The results showed that the wear predicted using SIMPACK software was very close to the wear measured.

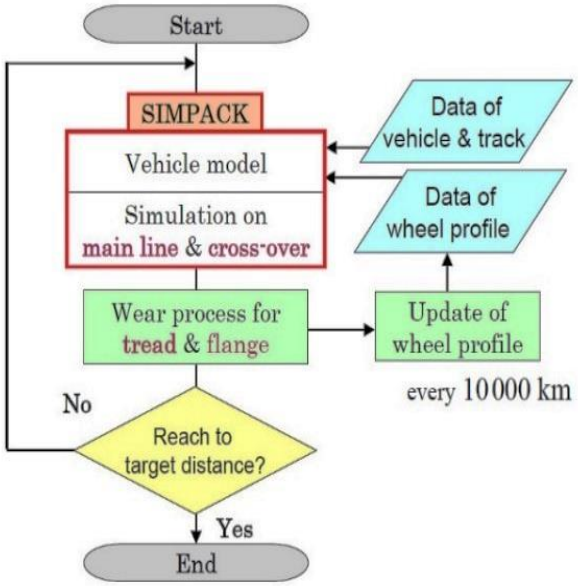

Figure 2. 10 Flow chart for wear prediction [80]

The computer simulation packages such as VAMPIRE, ADAMS/Rail, GENSYS, Multibody Software (MBS), SIMPACK, and NUCARS together with the models which were shown in this review are very useful tools to study railway wheel/rail wear.

The software packages have some advantages, for example, the ADAMS has the advantage of a strong Graphical User Interface (GUI). This means the users can see exactly what they are constructing on the screen in a 3-dimensional form, which can be manipulated around a variety of axis and all the necessary functions can be accessed from the menu system [53].

With respect to this review, it can be noticed that the wear was calculated using either Archard's model or the energy dissipated model. The computer modelling of railway vehicle dynamics can be performed using a number of different commercial software packages.

2.3 Review of use of artificial neural network for prediction

Ramesh and Kumar [81] presented “Many classical wear models can be found in the literature to predict wear but there is no general wear model which can be adopted for all wear problems due to the complex and dynamic nature of the wear phenomenon” [81].

An artificial neural network can be used to solve a wide range of complex engineering problems. This computational tool is very useful to study the systems which are difficult to describe with physical models, the neural network is useful because it has ability to learn by examples [3].

The artificial neural network has been used by many researchers for prediction in different areas. In this review, special attention was given to nonlinear autoregressive network with exogenous inputs (NARXNN), backpropagation neural network (BPNN), and radial basis function neural network (RBFNN) because it were used in this thesis for wheel wear and rail wear prediction.

The following sections present some previous work in which neural networks were used for prediction purposes.

Pit [33], used a neural network for rail wear prediciton. He studied experimentally the wear behaviour of carbide-free bainitic rails. Neural network modelling was carried out on the data received from the British Steel Swinden Technology Center in an attempt to produce a useful empirical model for rail wear prediction. The inputs to the neural network were rail hardness, rail microstructure, wheel hardness, wheel microstructure, Charpy fracture energy, and contact stress. The output of the neural network was the rail wear rate. British Steel Swinden Technology Center provided rail/wheel wear rate, hardness and Charpy fracture energy. A microstructure parameter was used as an input to indicate whether each roller was pearlitic or bainitic; a pearlitic given value of zero and a bainitic given value of one. The author concluded that it is difficult to develop a model for rail wear prediction, the neural network was not successful as there was not enough data for a reliable model to be generated, but a small amount of data showed promising results.

Singh et al., [82] used a back propagation neural network (BPNN) to predict drill wear. The inputs to the neural network were thrust force, torque, feedrate, drill diameter and spindle speed, while the output of the neural network was the flank wear. From the 49 datasets obtained in the experiment, 34 were selected at random for training the network, and the remaining 15 were used for testing the network. The simulation results show that the neural network is able effectively to predict the drill wear.

Huang et al., [83] used a nonlinear autoregressive network with exogenous inputs (NARXNN) based on load prediction to improve scheduling decisions in grid environments. In this paper, the configuration of NARXNN was as follows: input-memory order n=3 and output-memory order m=3, initial weight of each component of W is randomly generated in the scope of (0, 1), while the sigmoid function was used as an activation function. The data set used to train the NARXNN was collected using a number of entities of a grid including resources, users, brokers, information service, network components. The simulation results show that the NARXNN predictor provides good load prediction.

Kumar and Singh [84] used a backpropagation neural network (BPNN) in the prediction of wear loss quantities of A390 aluminium alloy. A pin-on-disc apparatus was used to perform dry sliding wear tests. The inputs to the neural network were the load, sliding speed and time; while the output of the neural network was mass loss. 45 examples were used to train the neural network. The simulation results show that the neural network results was close to experimental results. They concluded that neural network can be used efficiently for wear prediction.

Khudhair and Talib [3] used a backpropagation neural network (BPNN) to predict wear. A pin-on-ring machine was used to study the 13%Cr steel. The inputs of the neural network model were the sliding speed, load, and test time, and the output of the neural network was the wear rate. The simulation results show that the neural network wear was close to actual wear with correlation coefficient of 0.99. The neural network model predictions in this work exhibited good results. They concluded that the neural network can be considered as an excellent tool for wear prediction.

Al Shamisi et al., [85], used a backpropagation neural network (BPNN) and a radial basis function (RBFNN) for predicting global solar radiation (GSR) in Al Ain City. The data between 1995 and 2004 were used for training the BPNN and RBFNN, while the data between 2005 and 2007 were used for testing the models. The obtained results confirmed that the BPNN and RBFNN provided a very good prediction of monthly GSR behavior in Al-Ain city, but the RBFNN was more accurate than BPNN in most of tests. This work was presented in this review because they used the same technique to design the RBFNN which was used in this project, it is “newrb” matlab command, also because they made comparison between the RBFNN and PBNN in prediction, in this thesis a comparison between RBFNN and PBNN in railway wheel wear prediction was carried out as well.

Fathy and Megahed [86] used a backpropagation neural network (BPNN) to predict abrasive wear rate of Cu–Al2O3 nanocomposite. A pin-on-disc machine was used to obtain the wear rate. The inputs to the neural network were the sliding speed, load, and alumina volume fraction; while the output of the neural network was the wear rate. The wear tests were carried out under loads of 2N, 4N, 6N and 8N, at four different alumina volume fractions 0%, 5%, 10%, and 15%, and at four different sliding speeds 0.91m/s, 1.07m/s, 1.21m/s and 1.62m/s. The results obtained show that the backpropagation neural network exhibits a good prediction for wear rate.

Zhang and Li [87] used a radial basis function neural network (RBFNN) to predict the future tourist quantity of Hainan in China. The inputs data set used to train the neural network was related to many factors, for example, geography, environment, culture, government policy, etc. The output of the neural network was the number of tourists after every five years. The "Newrbe" Matlab command was used to design the RBFNN. Matlab results show that the RBFNN can accurately predict the future tourist quantity of Hainan area. This paper was presents in this review because the "Newrbe" Matlab command was used in this project to design the RBFNN for wheel wear prediction.

Nagaraj et al., [88] used a backpropagation neural network (BPNN) to predict wear of Aluminium-silicon alloy. The wear test was performed using a pin-on-disc machine under dry condition. The inputs to the neural network were the load, sliding velocity, time duration, speed, and sliding distance; while the output of the neural network was the wear loss. The wear predicted using neural network was compared with actual wear. The simulation results show that the wear predicted using BPNN was close to actual wear. They concluded that the neural technique can be used for wear prediction.

Kumar et al., [89] used a backpropagation neural network (BPNN) to predict the wear of aluminium–fly ash composites. Wear tests were conducted using a pin-on-disc wear test at different loads and sliding speed. The data obtained from experiments were used for training and testing the neural network model. Neural Network Toolbox of Matlab was used to design the BPNN. The BPNN was trained automatically with the Matlab function 'train'. The data set was divided randomly into training and test data set. Data sets of 98 were used as a training set, while 10 data sets were used for testing the network. Levenberg–Marquard algorithm was used to train the network. The training was terminated when the mean square error (MSE) is equal to 0.001. The major conclusion of the present work is that the neural network predicted the wear rate within an error range of 5%; therefore, the accuracy of neural network was 95%.

Khamis and Abdullah [21] used a nonlinear autoregressive network with exogenous inputs neural network (NARXNN) and backpropagation neural network (BPNN) for wheat price prediction. Past data for the wheat price from 1978 until 2012 was used to train the neural network. 409 samples were used to train, validate, and test the neural networks. 70% of dataset was used for training, 15% for validation and 15% for testing of neural network. A comparison between the NARXNN and BPNN for wheat price prediction was carried out. Matlab neural network toolbox was used to perform the prediction of wheat price. They concluded that the NARXNN is better than BPNN in wheat price prediction. Therefore, the NARXNN model is the suitable model to predict the wheat price. This work was presented in this review because a comparison between railway wheel wear prediction using NARXNN and BPNN was carried out in this project, and the Matlab neural network toolbox was used in this project to perform the prediction of wheel and rail wear prediction.

Cătălina-Lucia and Hakob [90] used a nonlinear autoregressive network with exogenous inputs (NARXNN) to predict the stock market. Backpropagation algorithm was used to train the NARXNN. The samples which were used to train and test the network consisted of historical weekly observations of a set of variables such as the opening, closing, highest and lowest price respectively from Bucharest Stock Exchange between 3/1/2009 and 11/30/2014. 200 sample datasets were used to train the NARXNN, while 100 samples were used to test the NARXNN. The results obtained using the NARXNN model showed good prediction from the point of view of mean square error. Matlab was used to convert the series-parallel NARXNN to the parallel NARXNN in order to perform a multi-step-ahead prediction task (prediction of stock market in the case of a new samples). This work was presented in this review because the NARXNN which was used in this paper to predict the stock market was used in this thesis to predict wheel wear and rail wear.

2.4 Chapter conclusion

Regarding the literature review, two basic types of wear models have been used for wear modelling: sliding models such as Archard wear model, and energy transfer models.

The Archard wear model is the most frequently used for wear modelling in practical engineering applications; once the wear coefficient is obtained, the amount of wear can be simulated.

The American Society for Testing and Material (ASTM) developed a model which can be used for pin wear and disc wear modelling for a pin-on-disc test.

Computer simulations such as VAMPIRE, ADAMS/Rail, GENSYS, SIMPACK, Multibody Software (MBS), and NUCARS software have been used in many previous works to update the wheel profile, then the wheel wear was calculated using either a sliding model (Archard wear model) or energy dissipated model. Therefore, the wheel and rail wear are usually estimated using either Archard wear model or energy dissipated model. The Archard wear model is widely used for modelling wear due to rolling and sliding contact. The energy dissipated and contact position between wheel and rail can be used for wheel wear estimation.

Neural networks were used by many researchers to predict the pin wear and disc wear, the results showed that the neural networks can be used for wear prediction. One of the previous works (Pit) tried to predict rail wear using a neural network; the author concluded that the neural network did not predicted the rail wear very well because there was not enough data to train the network; but the author said “a small amount of data showed promising results”.

The next chapter introduces a pin-on-disc test. This test was carried out in this project to present how the wear can be measured using a 3D optical profilometer.

Chapter 3 Laboratory test (Pin-on-disc test)

(The pin-on-disc chapter has been reduced and the sections on pin and disc wear modelling using ASTM, measurements using microscope and Talysurf have been removed).

3.1 Pin-on-disc test philosophy

The pin-on-disc test has been used extensively to study wear [41]. It is one of the most widespread tests which can be used to study the sliding wear behaviour [40]. This test was carried out in this thesis to present how the wear can be measured using a 3D optical profilometer.

3.2 Pin-on-disc test

A pin-on-disc machine (AEROTECH UNIDEX 11) was used in this project is shown in Figure 3.1.

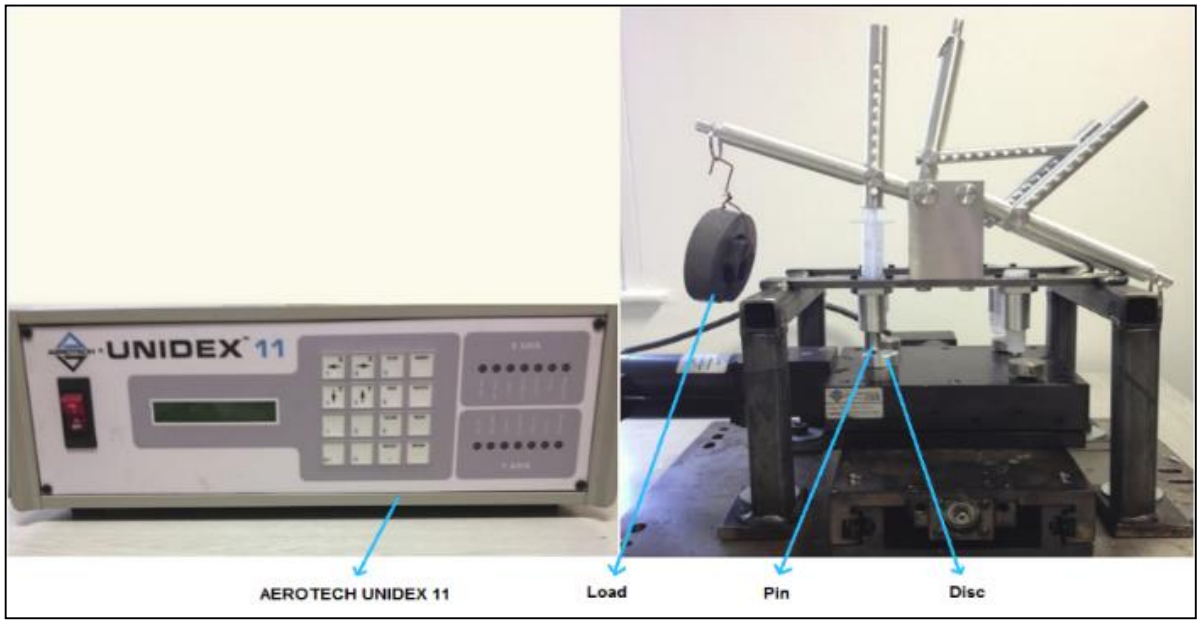

Figure 3. 1 Pin-on-disc machine (AEROTECH UNIDEX 11) - University of Huddersfield

Pin-on-disc experiments were conducted at loads of 6N, 10N, 16N, and 22N, with a test time of one hour for each test, sliding speed of 500mm/min, and sliding distance of 5mm in forward and backward direction. The specimens which were used in this test were as follows: The pin was made of mild carbon steel EN8, while the disc was made of aluminium 6082. The hardness of the pin is 255(HB), while the hardness of the disc is 95(HB). The pin dimensions were 49.49mm height and 11.98mm diameter; and the disc dimensions were 25.73mm in diameter and 9.08mm in thickness.

The pin/disc were put under an Alicona profilometer before and after test, and take image for both surfaces and save it as reference 1 (before test) and reference 2 (after test). The 'Differences' option for Alicona software was selected to calculate the pin wear and disc wear in terms of volume loss per unit area (mm^3/mm^2).

3.3 3D an Alicona profilometer for pin wear and disc wear measurements

The Alicona profilometer (INFINTE FOCUS G4) which is shown in Figure 3.2 was used in this work for pin wear and disc wear measurements.

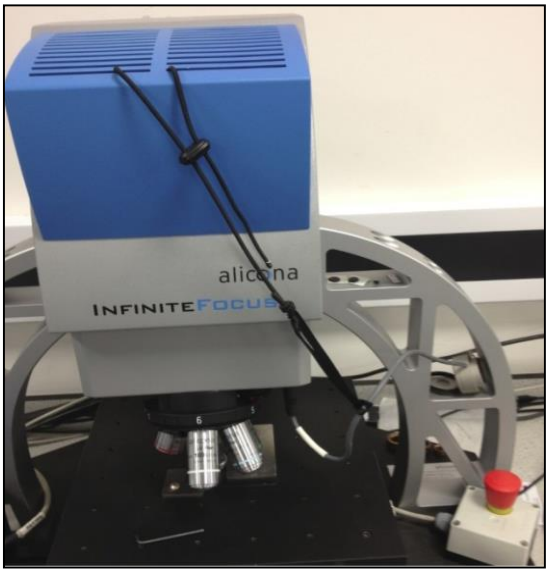

Figure 3. 2 Alicona (INFINTE FOCUS G4) - University of Huddersfield

An Alicona microscope has a motorized stage that moves in the xy direction, while the microscope objectives move in the z direction. It is non-contact microscope. The objectives has range from 2.5x - 100x magnification and has a vertical resolution of up to 10 nm at 100x magnification [91].

Table 3.1 shows the technical specifications of the Alicona profilometer which was used in this project for wear measurement.

Measurement principle	Non-contact, optical.
Travel range X/Y/Z	100 mm x100 mm x100mm
Maximum measurable area	10000mm^2
Maximum measurable profile length	100mm
Min. repeatability	0.001µm - 0.12µm
Vertical resolution	1µm
Maximum measurable slope angle	Up to 87^0

Table 3. 1 Technical specifications of Alicona profilometer [92], [93]

3.3.1 Focus variation instrument

Figure 3.3 shows the schematic diagram of a typical focus variation instrument. White light produced by light emitting diode (LED) is transmitted to the sample through the beam splitter (mirror) and the objective lens. The light is reflected in different directions due to variations in the topography and the reflectivity of the sample. The objective was used to collect the reflected light and projected to charge coupled device (CCD) sensor. The degree of focus changes from low to high and back to low again by moving the sample in the vertical direction in relation to the objective lens. A topographic 3D data model of the surface is produced using continuous vertical scanning. Also, a 3D depth of surface can be obtained using focus variation technique [93]-[95].

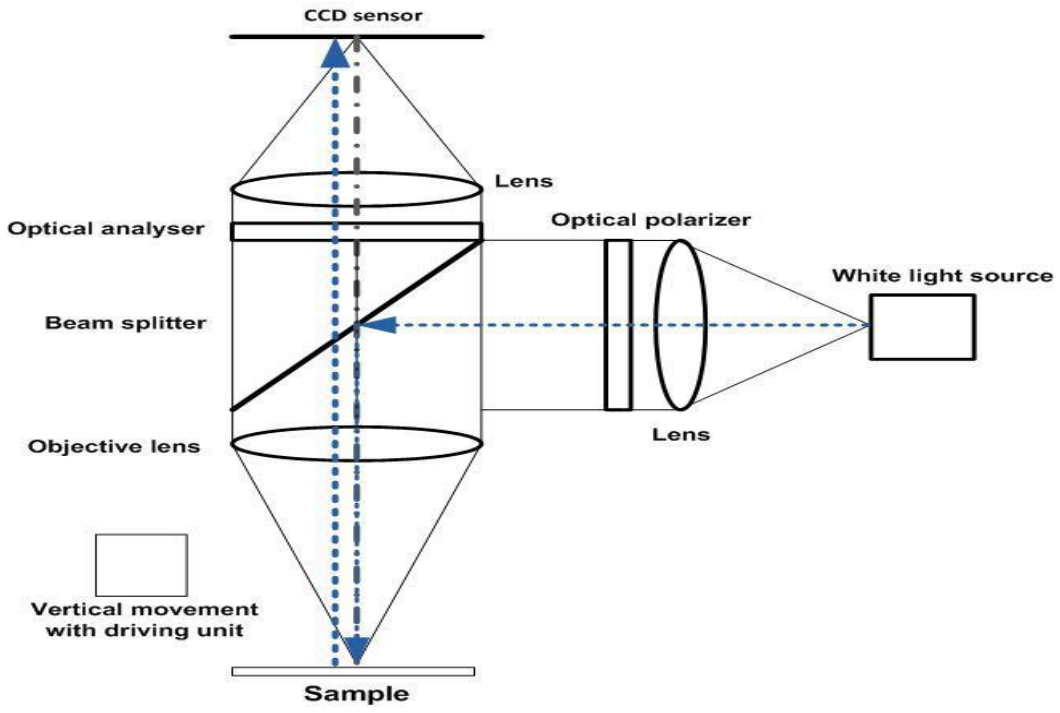

Figure 3. 3 Focus variation instrument [93]

3.4 Pin wear and disc wear measurements using an Alicona profilometer

Table 3.2 shows the pin wear and disc wear measured using the Alicona profilometer after applied loads of 6N, 10N, 16N, and 22N respectively.

Test No	Load (N)	Pin wear (mm^3/mm^2)	Disc wear (mm^3/mm^2)
1	6	$2.5224 . 10^{-3}$	0.0786
2	10	$2.6041 . 10^{-3}$	0.0798
3	16	$2.9062 . 10^{-3}$	0.1226
4	22	$3.1965 . 10^{-3}$	0.2301

Table 3. 2 Pin wear and disc wear measured using Alicona profilometer

Table 3.2 shows the pin wear and disc wear after applied loads of 6N, 10N, 16N, and 22N. The test results show that the pin wear and disc wear was effected by increases in load. The pin wear and disc wear increased with the increase of load; this is due to the fact that, as the load increases a frictional heat is generated at the contact surface and hence the strength of the material decreases, consequently the pin/disc wear was increased. On the other hand, when the applied load increased, the actual area of contact was increased, resulting in increased frictional force and real surface area in contact causing higher wear. Therefore, the pin wear and disc wear is proportional to the load. Test results show also that the disc wear was bigger than pin wear; that because the disc was made of Aluminium and the pin was made of steel; where the hardness of steel is 255HB, while the hardness of Aluminium is 95HB.

Additional measurements were achieved using the Alicona profilometer for pin-on-disc tests; so as to discover more information about wear behaviour. Pin/disc surfaces before and after applied loads of 6N, 10N, 16N, and 22N are shown in Figure 3.4 and Figure 3.5 respectively. The colour bar tells how big the deviation between database 1 (pin/disc surface before test) and database 2 (pin/disc surface after test).

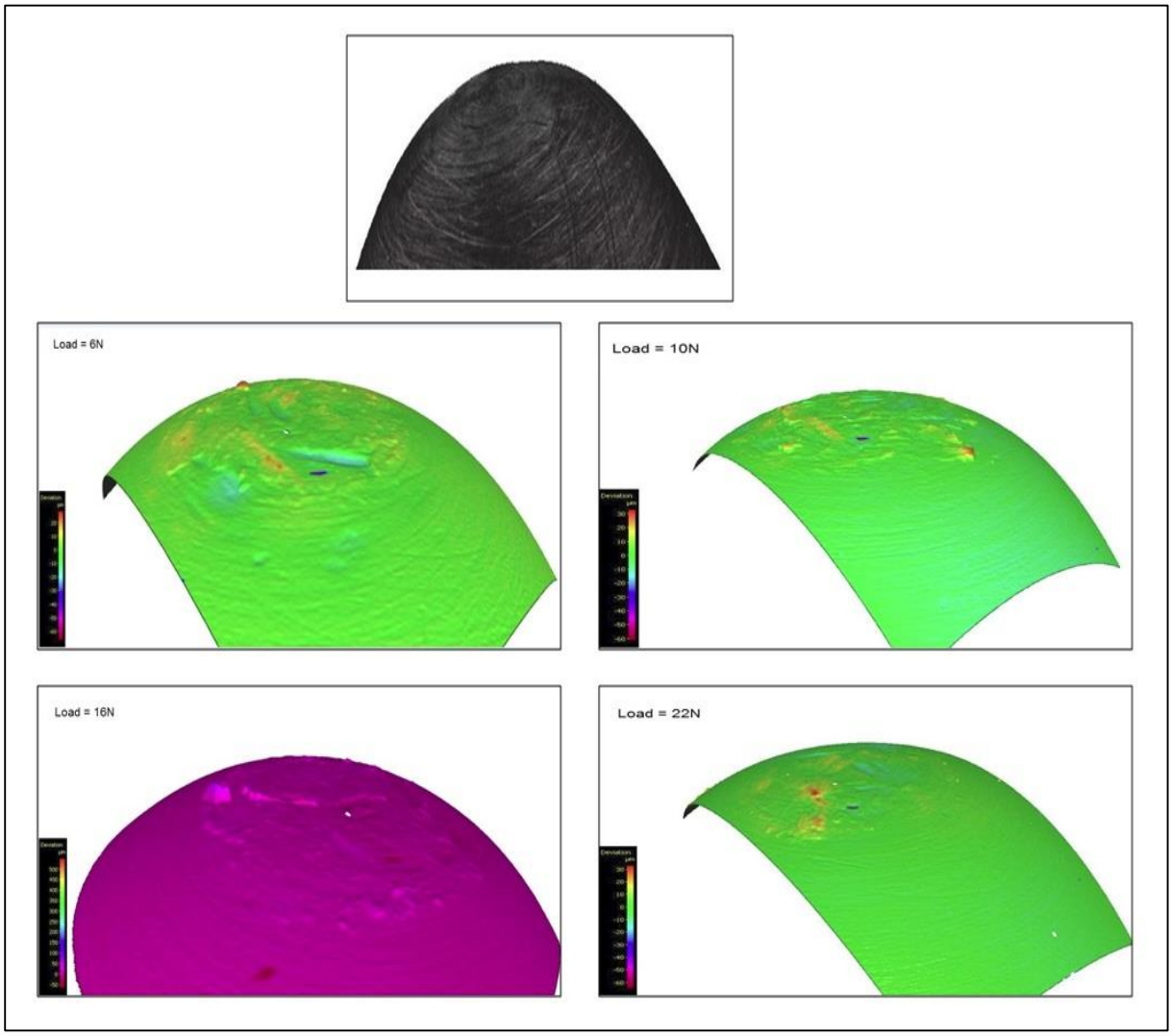

Figure 3. 4 Pin surface before and after tests

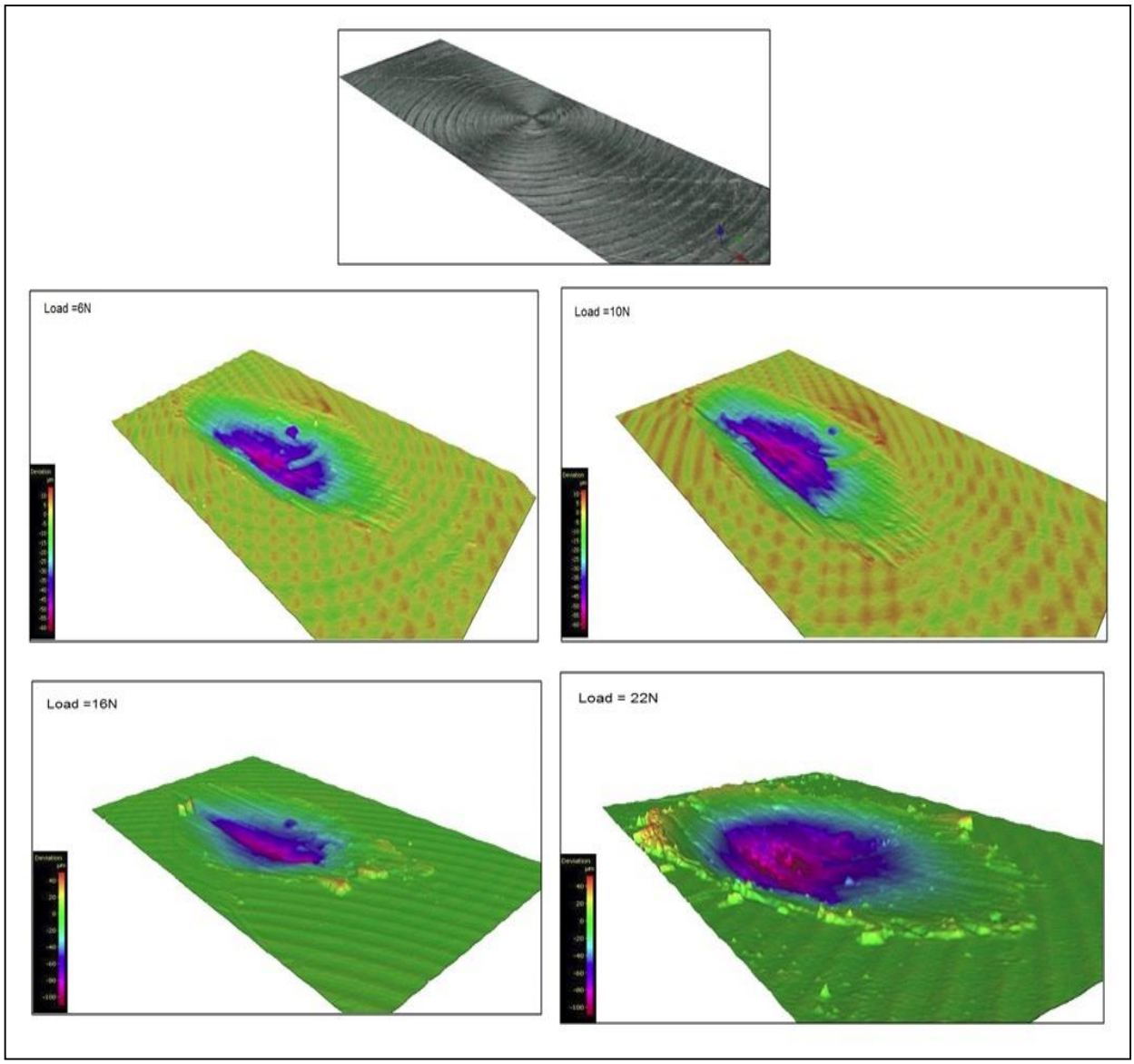

Figure 3. 5 Disc surface before and after tests

3.5 Chapter discussion

Pin wear and disc wear were measured using an Alicona profilometer after applied loads of 6N, 10N, 16N, and 22N respectively. Tests results were shown in Table 3.2. Tests results show that the pin wear and disc wear was effected by increase of load. The pin wear and disc wear increases with the increase of load. Test results show that the disc wear was bigger than pin wear that because the disc was made of Aluminium (95HB) and the pin was made of steel (255HB).

Figure 3.4 and Figure 3.5 show the pin surface and disc surface before and after applied loads of 6N, 10N, 16N, and 22N respectively. It can be seen that the pin surface and disc surface before tests were smooth, and after applied load of 6N both surfaces became worn, then by increase of applied load to 10N, 16N, and 22N the pin/disc surfaces became more worn, consequently the pin/disc wear was increased.

3.6 Chapter conclusion

The main findings of this chapter are summarised in the following points:

- Pin wear and disc wear were increased with increase of applied load.
- The Alicona profilometer can be used for pin wear and disc wear measurements.

The pin-on-disc test was carried out in this project for measuring the pin wear and disc wear using Alicona profilometer. The next chapter presents a twin disc test rig, it was used to reflect some real conditions for a railway vehicle dynamic behaviour. This thesis focuses on studying and predicting the wheel wear and rail wear for twin disc rig experiments under different conditions. The University of Huddersfield twin disc test rig was used to achieve several experiments to study the wheel wear and rail wear.

Chapter 4 Laboratory test (Twin disc test rig)

4.1 Twin disc test rig philosophy

The twin-disc system consists of the use of two rollers pressed into contact, the variation of the relative velocity and of the contact pressure allows performing of the test under different conditions [49]. Twin disc test rig is used widely for wheel and rail wear investigations [96].

A twin disc test rig was carried out in this work to reflect some real conditions of the railway vehicle dynamics. In this project the following tests were carried out using the University of Huddersfield twin disc rig: effect of load on wheel and rail wear test, and effect of yaw angle on wheel wear and rail wear test.
The effect of surface conditions such as dry, wet, lubricated, and sanded conditions on wheel wear and rail were also investigated using the twin disc test rig.

4.2 Introduction to the University of Huddersfield twin disc test rig

The University of Huddersfield twin disc rig consists of an upper steel wheel of 310mm diameter, and a lower steel wheel with a diameter of 290mm. The rollers and shafts are made of EN24T steel. Vertical force of up to 4kN can be applied on the two wheels using a jacking mechanism. The rig consists of a rotary table to allow a relative yaw angle between the wheels. A three phase motor is used to rotate the wheel roller at varying speeds, using a corresponding three phase inverter [97].
The twin disc rig for the University of Huddersfield is shown in Figure 4.1.
The drawing for the two rollers (wheel profile and rail profile) for the University of Huddersfield twin disc rig are shown in appendix 1.

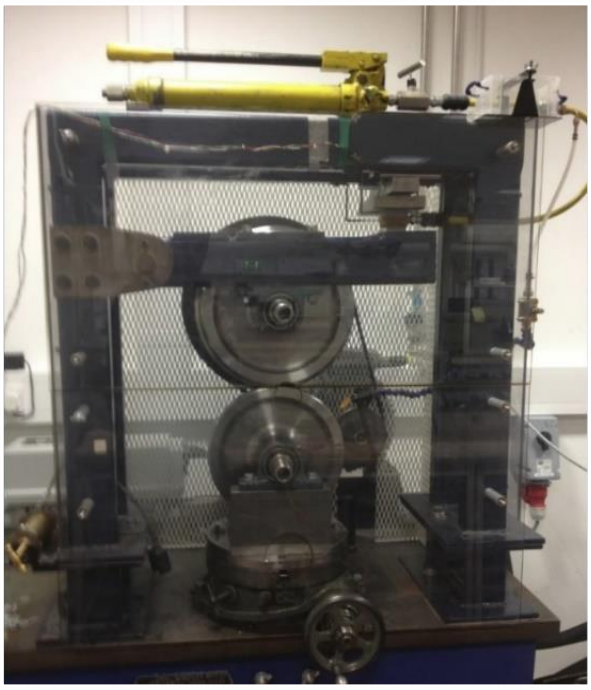

Figure 4. 1 The University of Huddersfield twin disc test rig

Schematic of the University of Huddersfield twin disc rig is shown in Figure 4.2.

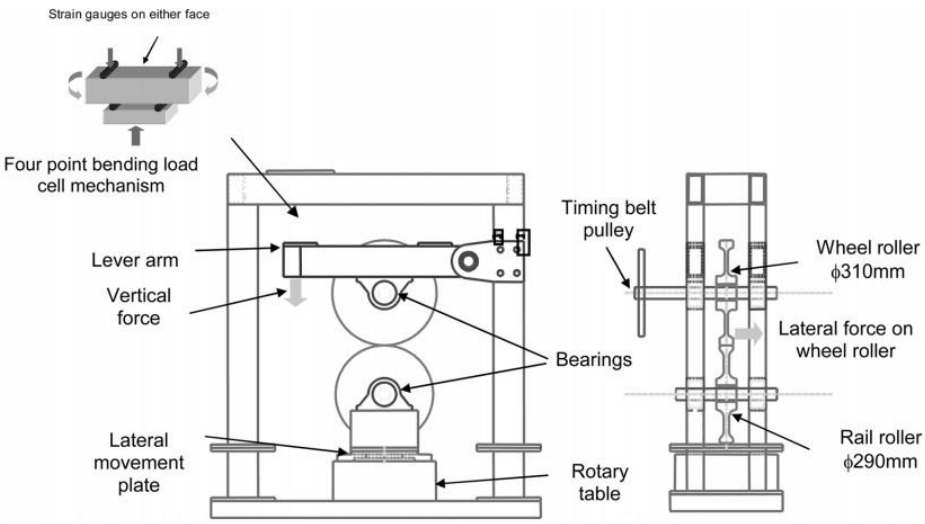

Figure 4. 2 Schematic of the University of Huddersfield twin disc rig [97]

Table 4.1 shows the technical details of the wheel and rail roller for the University of Huddersfield twin disc rig.

Parameters	**Wheel roller**	**Rail roller**
Profile	Standard UK wheel profile P8	BS 113A rail profile
Scale	1/3	1/3
Diameter	310 mm	290 mm
Thickness	50mm	25mm
Material	EN24T steel	EN24T steel

Table 4. 1 Technical details of the wheel and rail roller - University of Huddersfield

4.3 Load calibration using an Instron tensile testing machine and strain indicator

The calibration of the load (four-point bending mechanism) was carried out using the Instron 3369 tensile testing machine which is shown in Figure 4.3, and strain indicator P-3500 which is shown in Figure 4.4.

Figure 4. 3 Instron 3369 tensile testing machine

Figure 4. 4 Strain indicator P-3500

The strain gauge was used to measure the strain exerted on the roller of the twin disc rig using the instron tensile testing machine. Strain gauges are generally comprised of resistive foils arranged in a grid pattern, attached to the test specimen; therefore, the strain on the test specimen is directly transferred to the strain gauge of which the electrical resistance of the foil is proportional to the amount of deformation on a body. The electrical resistance of a conductor varies with change in length; this can be used to extract accurate strain measurements. Figure 4.5 shows the strain gauges which were connected on the test specimen as a bridge connection, it was used for load calibration using instron tensile testing machine.

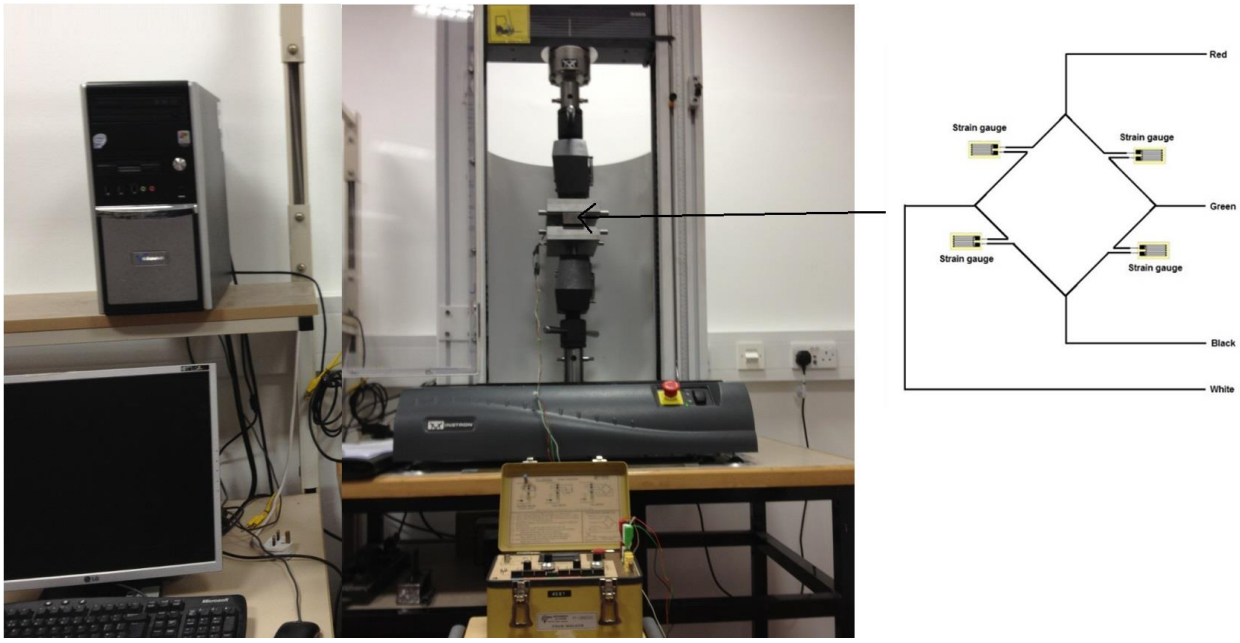

Figure 4. 5 Instron tensile testing machine, strain indictor, and strain gauges for load calibration

The experimental setup described above in conjunction with a strain indicator enables the measurement of the bending strain exerted on the test specimen. The technical details for strain gauges are a resistance of 120Ω and a gauge factor of 2.10.

The instron machine and strain indicator were used to perform load calibration test for the twin disc rig. The load was applied using the instron machine in steps, and the corresponding strain exerted on test specimen is recorded using strain indicator.

During the load calibration, the load was applied gradually through the instron machine; and the corresponding strain values were recorded from the strain indicator P-3500. The load calibration was shown in Figure 4.6. The result shows that the bending force (applied load) is proportional to the bending strain.

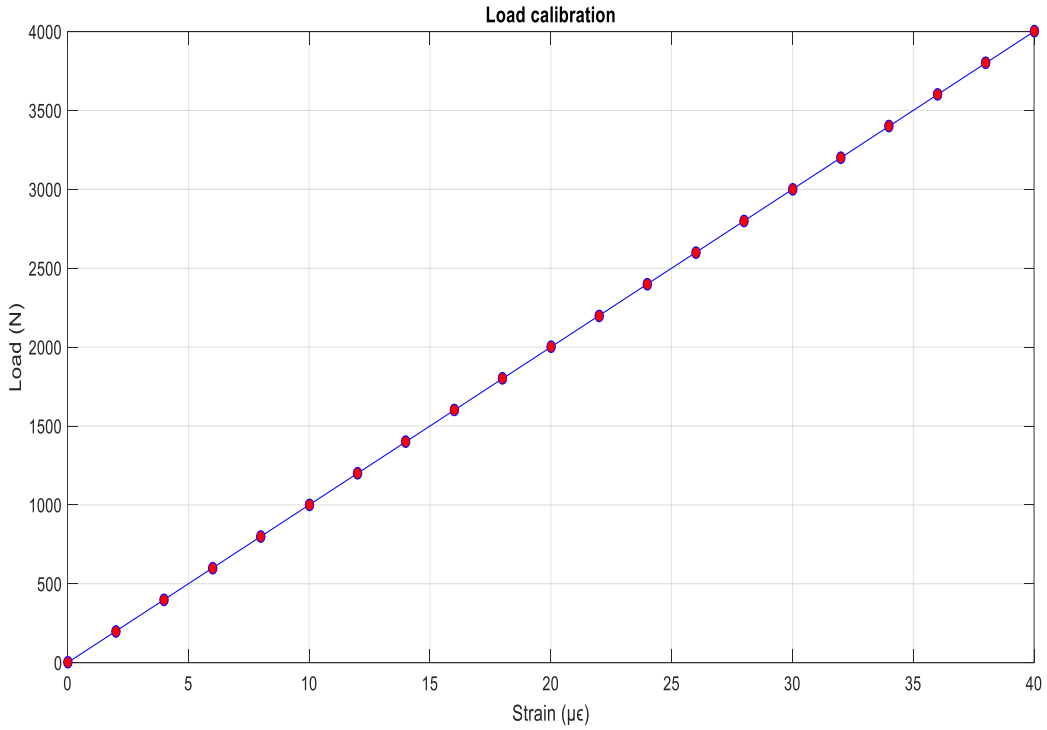

Figure 4. 6 Load calibration curve

4.4 Development of a new method for wheel wear and rail wear measurements

The twin disc rig was used in this project to reflect some conditions of the real wheel/rail interface. Replica material together with an Alicona profilometer were used for wheel and rail wear measurements.

4.4.1 Introduction to replica material

The replica material consists of a compound of two materials (polymer and the curing agent), which were mixed in a nozzle such as shown in Figure 4.7. Replica process: the nozzle of the gun should have pointed close to the surface as possible in order to avoid trapping air in the replica and to force the material into the surface. Then, the replica material was left drying for the drying time suggested by the manufacturer. At the end the replica was removed carefully [98].

Figure 4. 7 Dispensing gun and cartridge of replica material [98]

Replica material (AccuTrans Casting Silicone) was used for producing accurate impressions on smooth or rough surfaces such as shown in Figure 4.8 [98].

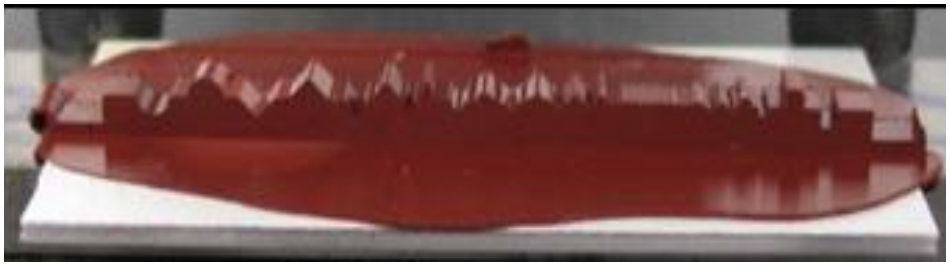

Figure 4. 8 AccuTrans Casting Silicone [98]

4.4.2 Use of replica material for wheel and rail wear measurements

In this project the replica material was used for wear measurements of the twin disc test rig rollers, where the replica material was used to make a copy of the surfaces of two rollers before test and after each test, and then the Alicona profilometer was used to measure the rollers wear. The AccuTrans replica material which was used in this project for wheel and rail wear measurements is shown in Figure 4.9. The Alicona profilometer was shown in Figure 3.2 in chapter 3.

Figure 4. 9 Replica material (AccuTrans)

Tests were carried out in this project using the twin disc test rig to investigate the effect of load, yaw angle, and speed on the wheel and rail wear under dry conditions. The effect of dry, wet, lubricated, and sanded conditions on wheel and rail wear were also investigated. The twin disc rig was used in this project to reflect some conditions of the real wheel/rail interface. Replica material together with an Alicona profilometer were used for wheel and rail wear measurements using the twin disc rig. Figure 4.10 shows a sample of replica material for the wheel and rail surfaces; and after it had been removed.

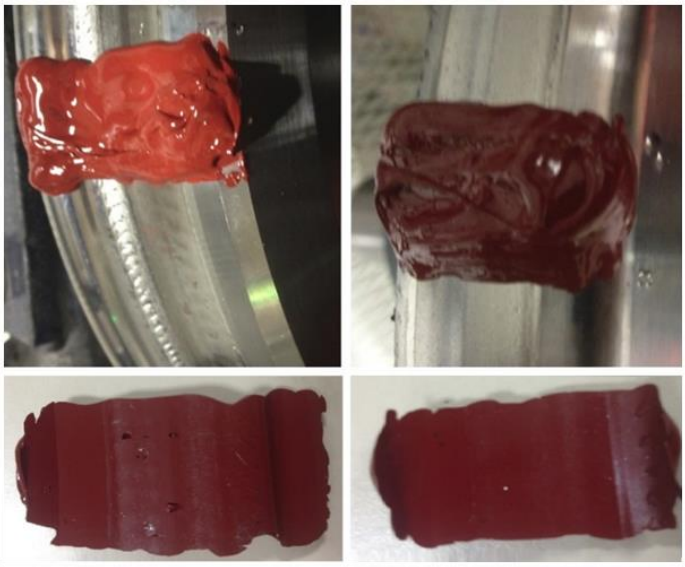

Figure 4. 10 Sample of replica material on the wheel and rail surfaces; and after removed

Figure 4.11 shows a sample of replica surface for twin disc roller under the lens of the Alicona profilometer. The wheel sample dimensions were 5mm width and 35mm length, and the rail sample dimensions were 5mm width and 20mm length.

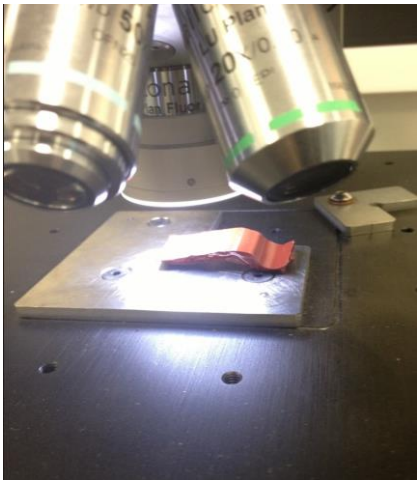

Figure 4. 11 Sample of replica for wheel under Alicona lens

In this project, the wheel and rail wear were measured using the Alicona profilometer using the DifferenceMeasurments Module. The wear was measured by taking a digital image of the wheel and rail surfaces before the test and saving it as a reference 1, and taking another image of the wheel and rail surfaces after the test and saving it as a reference 2; then, the DifferenceMeasurments Module in Alicona software was used to compute the wheel and rail wear in term of volume loss per unit area (mm^3/mm^2). The steps of wheel and rail wear measurements using an Alicona profilometer are shown in appendix 2 [99].

4.5 Twin disc test rig for wheel wear and rail wear measurement

The twin disc machine, replica material, and Alicona profilometer were used in this project to investigate the effect of several parameters, such as load, and yaw angle on wheel and rail wear as shown in the following sections. Replica material and an Alicona profilometer were used for wheel/rail wear measurements during these tests. The wheel sample dimensions were 5mm in width and 35mm in length, while the rail sample dimensions were 5mm in width and 20mm in length.

4.5.1 Effect of load on wheel wear and rail wear

The effect of load on wheel wear and rail wear (volume removed) under dry conditions was investigated. The speed of the rig rollers was 960rpm, the test time for each run was 60 min, the yaw angle was 0.4°, the distance was 112176m, and the load was varied from 1000N to 3400N in 6 steps such, as outlined in Table 4.2.

Test No	Load(N)	Wheel wear(mm^3/mm^2)	Rail wear(mm^3/mm^2)
1	1000	0.0067	0.0071
2	1400	0.0121	0.0132
3	1800	0.0207	0.0236
4	2200	0.0250	0.0348
5	2600	0.0334	0.0487
6	3000	0.0378	0.0538
7	3400	0.0453	0.0659

Table 4. 2 Effect of load on wheel wear and rail wear

Figure 4.12 shows the variation of wheel/rail wear with different values of load.

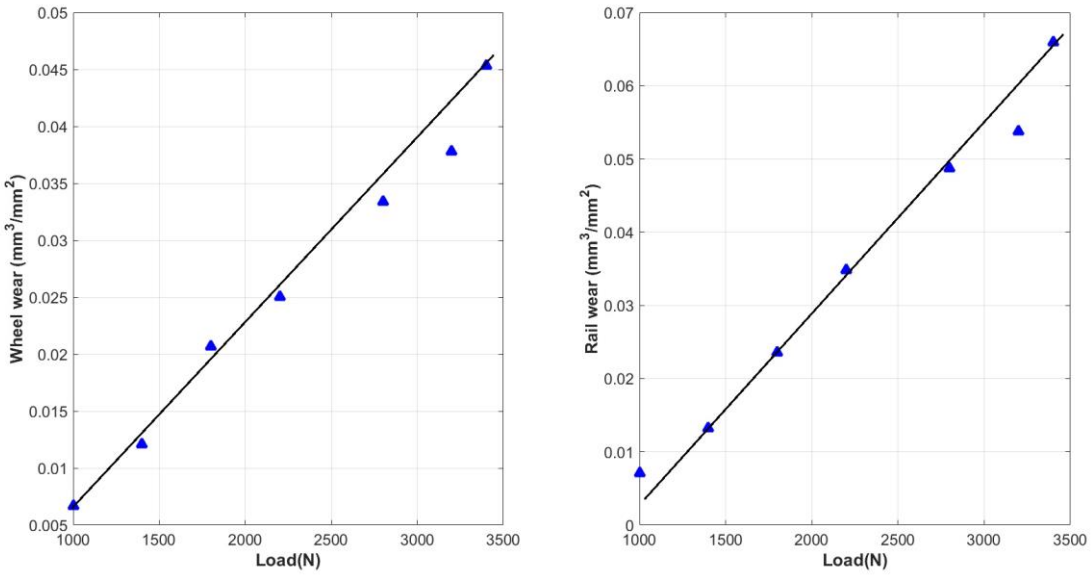

Figure 4. 12 Variation of wheel/rail wear with different values of load

Figure 4.12 and Table 4.2 show the effect of load on wheel wear and rail wear under dry conditions. The test results show that the wheel wear increased approximately linearly from $0.0067 mm^3/mm^2$ at a load of 1000N to $0.0453 mm^3/mm^2$ at load of 3400N. The rail wear increased approximately linearly from $0.0071 mm^3/mm^2$ at a load of 1000N to $0.0659 mm^3/mm^2$ at a load of 3400N. The test results highlight that the applied load has a direct effect on wheel wear and rail wear, where the wheel wear and rail wear were increased by increases of applied load. The test results also show that the relationship between wheel/rail wear and load is approximately linear.

4.5.2 Effect of yaw angle on wheel wear and rail wear

The effect of yaw angle on wheel wear and rail wear (volume removed) under dry condition was investigated. The speed of the rig rollers was 960rpm, the test time for each run was 60 min, the load was 2200N, the distance was 112176m, and the yaw angle was varied from 0.1° to 0.7^{o} in 6 steps, as presented in Table 4.3.

Test No	Yaw angle(degree)	Wheel wear(mm^3/mm^2)	Rail wear(mm^3/mm^2)
1	0.1^{o}	0.0070	0.0117
2	0.2^{o}	0.0095	0.0162
3	0.3^{o}	0.0121	0.0206
4	0.4^{o}	0.0198	0.0325
5	0.5^{o}	0.0332	0.0499
6	0.6^{o}	0.0422	0.0721
7	0.7^{o}	0.0530	0.0877

Table 4. 3 Effect of yaw angle on wheel wear and rail wear

Figure 4.13 shows the variation of wheel/rail wear with different values of yaw angle.

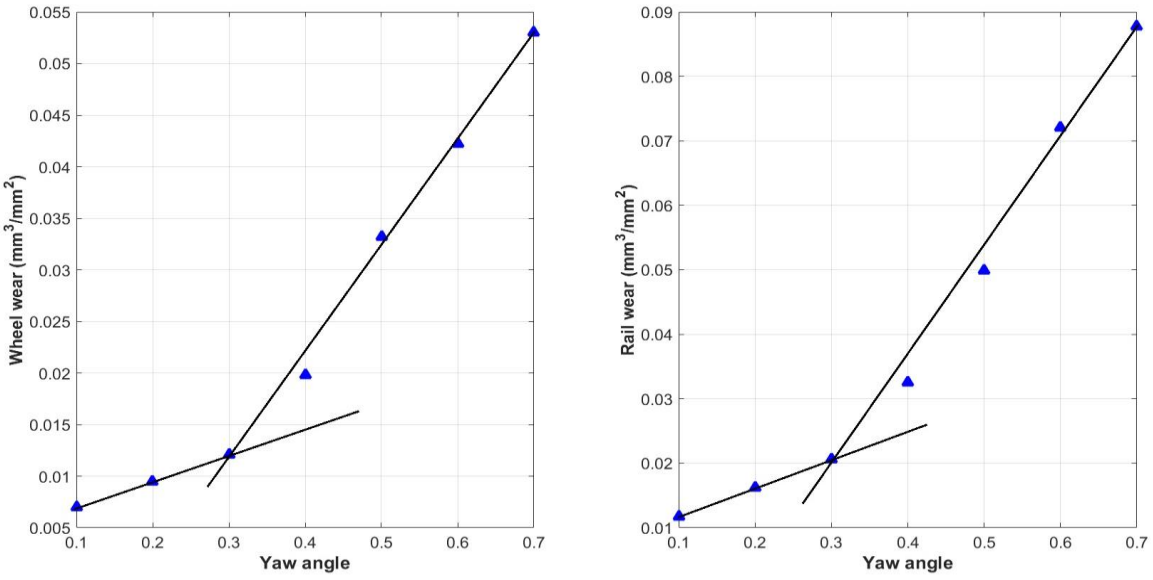

Figure 4. 13 Variation of wheel/rail wear with different values of yaw angle

Figure 4.13 and Table 4.3 show the effect of yaw angle on the wheel wear and rail wear under dry conditions. The test results demonstrate that the wheel wear increased from $0.0070\text{mm}^3/\text{mm}^2$ at a yaw angle of 0.1^o to $0.0530\text{mm}^3/\text{mm}^2$ at yaw angle of 0.7^o. The rail wear increased from $0.0117\text{mm}^3/\text{mm}^2$ at a yaw angle of 0.1^o to $0.0877\text{mm}^3/\text{mm}^2$ at yaw angle of 0.7^o.

The results show that the wheel wear and rail wear were increased by increasing the yaw angle. The test results show that the wheel/rail wear has approximately the same trend at low value of yaw angle (0.1^o to 0.3^o); then when the yaw angle increased between 0.4^o and 0.7^o, the wheel/rail wear was increased rapidly; when the results were plotted such as shown in Figure 4.13 it can be seen that the relationship between wheel/rail wear and yaw angle is non-linear. The increasing of the yaw angle led to increase of lateral creepage and lateral creep force which led at a certain yaw angle (0.4^o) to wear transation from mild to severe wear as shown in Figure 4.13.

The values of yaw angle to be used during these tests were determined by consideration of the lateral creepage and (and consequent lateral creep force) as discussed below. The longitudinal creepage is virtually zero when no longitudinal traction occurs between wheel and rail ($\gamma_1 = 0$). The lateral creepage can determined using the following equation [97]:

$$\gamma_2 = \tan \psi \tag{4.1}$$

Where ψ is the yaw angle between wheel and rail.

In Kalker's linear theory, the lateral creep force can be written as [97]:

$$F_2 = -f_{22}\,\psi \tag{4.2}$$

Where f_{22} is the Kalker's linear creep coefficient (N) [97]:

$$f_{22} = (a.b).G.C22 \tag{4.3}$$

Where, a and b are the contact ellipse semi-axes (m), G the Shear modulus (N/m^2), and C22 the tabulated creep coefficient.

The 'point' contact between the rollers results in a contact patch size, assuming it to be elliptical and Hertzian with a normal load of 2.2 kN, of 1.19mm by 0.97mm, and C22 = 1.55. The resultant contact stress is approximately the same as the full-size case [97].

The value of G for structural steel is 75GN/m^2. Equations 4.1, 4.2, and 4.3 were used to calculate the lateral creep force and lateral creepage as shown in Table 4.4.

Yaw angle (degree)	Lateral creep force (N)	lateral creepage [-]
0.1	234.65	0.0017
0.2	469.31	0.0034
0.3	703.96	0.0052
0.4	938.63	0.0069
0.5	1173.30	0.0087
0.6	1408.00	0.0104
0.7	1642.70	0.0122

Table 4. 4 Yaw angle, lateral creepage, and lateral creep force

The results shown in Table 4.4 show the lateral creep force and lateral creepage with changing of yaw angle, results show how the lateral creep force was increased with increase of yaw angle, which led to increase of wheel and rail wear as shown in Figure 4.13.

During the tests, the range of yaw angle was between 0.1^{o} to 0.7^{o}, and the range of load was between 1000N to 3400N. These values were selected as representative of values seen in operation of typical railway vehicles [100], [101], [102], [103], [104]. In operation of the tests it was found that with yaw angles of greater than 0.7^{o} very heavy flange contact occurred.

4.5.3 Section discussion

In this chapter a new method was developed to study the wheel and rail wear using replica material and an optical profilometer. Copies of the wheel and rail surface were taken, then the samples were put under an Alicona profilometer to investigate the effect of key parameters on wheel wear and rail wear.

This section examines the effect of load, and yaw angle on wheel wear and rail wear using laboratory twin disc tests under dry conditions; the test results can summarized as follows:

The effect of load on wheel wear and rail wear for the twin disc rig experiments was investigated; in this study seven loads were applied (1000N to 3400N in six steps). For this purpose, the replica material and Alicona profilometer were used for wheel wear and rail wear measurements. The twin disc test results show that with increase of applied load the wheel wear and rail wear were increased as follows: When the load was 1000N, the wheel wear measured was $0.0067\text{mm}^3/\text{mm}^2$; and when the load was 3400N, the wheel wear increased to $0.0453\text{mm}^3/\text{mm}^2$. When the load was 1000N, the rail wear measured was $0.0071\text{mm}^3/\text{mm}^2$; and when the load was 3400N, the rail wear increased to $0.0659\text{mm}^3/\text{mm}^2$. The load has observable effect on wheel wear and rail wear.

The effect of yaw angle on wheel wear and rail wear for the twin disc rig experiments was investigated; in this study seven yaw angles were applied (0.1degree 0.7degree in six steps). For this purpose, the replica material and Alicona profilometer were used for wheel wear and rail wear measurements. Wear take place at every wheel and rail interaction but with curves the wear is much higher because of slip. The twin disc test results show that with the increase of yaw angle, a lateral slip was increased which led to increase of lateral creep force, which led to increases of material removed from wheel and rail surfaces. The test results show that the wheel/rail wear were increased with increase of yaw angle. When the yaw angle was 0.1^o, the wheel wear measured was $0.0070\text{mm}^3/\text{mm}^2$; and when the yaw angle was 0.7^o, the wheel wear increased to $0.0530\text{mm}^3/\text{mm}^2$. When the yaw angle was 0.1^o, the rail wear measured was $0.0117\text{mm}^3/\text{mm}^2$; and when the yaw angle was 0.7^o, the rail wear increased to $0.0877\text{mm}^3/\text{mm}^2$. The yaw angle has a significant effect on wheel wear and rail wear. However, some scratches were formed during the process of changing the position of contact which led to increases of wheel/rail wear.

The results have demonstrated that applied load, and yaw angle increase the wheel wear and rail wear. Therefore, it can be concluded that the applied load, and yaw angle all impact on the wheel wear and rail wear. The relationship between wheel/rail wear and load is approximately linear. The relationship between wheel/rail wear and yaw angle is nonlinear.

4.6 Effect of load on wheel wear and rail wear with different sequence of load

The effect of load on wheel wear and rail wear with different sequence was investigated in the following section. This test was carried out to investigate whether the wear was the same when the load was applied in a different sequence.

Test1: Wheel/rail wear with sequence of load (1000N, 1400N, 1800N, and 2200N). Table 4.5 shows the effect of load on wheel wear and rail wear under dry condition; speed =960rpm, test time = 60 min, the distance was 112176m, and yaw angle = 0.4°.

Test No	Load (N)	Wheel wear(mm^3/mm^2)	Rail wear(mm^3/mm^2)
1	1000	0.0067	0.0071
2	1400	0.0121	0.0132
3	1800	0.0207	0.0236
4	2200	0.0250	0.0348

Table 4. 5 Wheel/rail wear with sequence of load

Test2: Wheel/rail wear with different sequence of load (1400N, 1000N, 2200N, and 1800N). Table 4.6 shows the effect of load on the wheel wear and rail wear under dry condition; speed =960rpm, test time = 60 min, the distance was 112176m, and yaw angle = 0.4°. The percentage error between the wheel/rail wear for the two tests was calculated using equation 4.4.

Test No	Load (N)	Wheel wear (mm^3/mm^2)	Error%	Rail wear (mm^3/mm^2)	Error%
1	1400	0.0135	-10.37	0.0148	-12.12%
2	1000	0.0059	13.55	0.0081	-14.08%
3	2200	0.0237	5.48	0.0356	-2.29%
4	1800	0.0213	-2.81	0.0218	7.62%

Table 4. 6 Wheel/rail wear with different sequence of load, and the error

The percentage error between two measurements can be calculated using the following equation [105]:

$$Error = \frac{x-y}{y} * 100\ \% \tag{4.4}$$

Where x is the actual measurement and y is estimated measurement.

The effect of load on wheel wear and rail wear with different sequences of load was carried out. The error between the wheel/rail wear for the two tests was calculated as shown in Table 4.6. The test results show that the wheel/rail wear with sequence of load was close to the wheel/rail wear with a different sequence of load. The percentage error was between 2.29% to 14.08%; this error is due to a change of wheel and rail surfaces; the wheel/rail surfaces became more worn during the tests.

4.7 Effect of dry, wet, lubricated, and sanded conditions on wheel wear and rail wear

The twin disc test rig was used to investigate the effect of several surface conditions on wheel wear and rail wear such as dry, wet, lubricated, and sanded conditions. Replica material and the Alicona profilometer were used for wheel/rail wear measurements during these tests. The wheel sample dimensions were 5mm in width and 35mm in length, while the rail sample dimensions were 5mm in width and 20mm in length. The speed of the rail wheel was 960rpm, the test time was 10 min, the yaw angle was 0.5°, the distance was 18696m, and the load varied from 1000N to 2200N in 6 steps.

4.7.1 Effect of dry conditions on wheel wear and rail wear

The variation of wheel wear and rail wear under dry conditions after a distance of 18696m is shown in Table 4.7.

Test No	Load (N)	Wheel wear(mm^3/mm^2)	Rail wear(mm^3/mm^2)
1	1000	0.0023	0.0031
2	1200	0.0030	0.0045
3	1400	0.0072	0.0097
4	1600	0.0098	0.0126
5	1800	0.0140	0.0168
6	2000	0.0178	0.0245
7	2200	0.0258	0.0333

Table 4. 7 Wheel wear and rail wear under dry conditions

Figure 4.14 shows the variation of wheel wear and rail wear with different values of load under dry conditions.

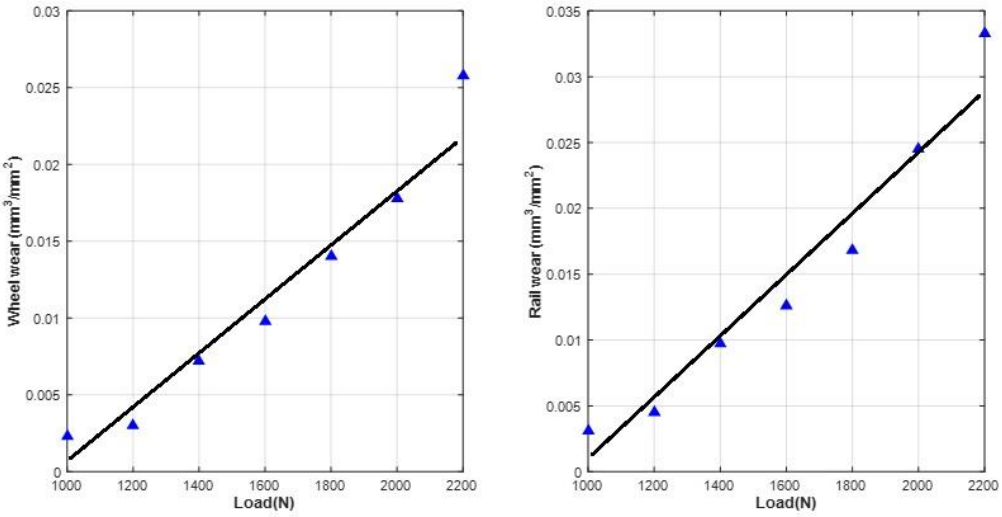

Figure 4. 14 Variation of wheel wear and rail wear under dry conditions

Figure 4.14 shows the variation of wheel wear and rail wear under dry conditions with different loads. The wheel wear increased approximately linearly from $0.0023 mm^3/mm^2$ at load of 1000N to $0.0258 mm^3/mm^2$ at load of 2200N. The rail wear increased approximately linearly from $0.0031 mm^3/mm^2$ at load of 1000N to $0.0333 mm^3/mm^2$ at load of 2200N. The test results show that the wheel wear and rail wear were increased by increasing load under dry conditions. The test results show also that the wheel and rail wear increased approximately linearly under dry conditions.

4.7.2 Effect of wet conditions on wheel wear and rail wear

Water was used in this test to investigate the effect of wet conditions on wheel wear and rail wear. The variation of wheel and rail wear under wet conditions after a distance of 18696m is shown in Table 4.8. The twin disc rig provided with a small water tank fixed on the top of the rig, this tank connected to a tube to provide the water into the wheel-rail contact, the amount of water dropped on the contact during the wet conditions tests was controlled using nozzle and valve.

Test No	Load (N)	Wheel wear(mm^3/mm^2)	Rail wear(mm^3/mm^2)
1	1000	0.0017	0.0025
2	1200	0.0024	0.0038
3	1400	0.0054	0.0084
4	1600	0.0078	0.0102
5	1800	0.0100	0.0142
6	2000	0.0144	0.0204
7	2200	0.0165	0.0257

Table 4. 8 Wheel wear and rail wear under wet conditions

Figure 4.15 shows the effect of wet conditions on wheel wear and rail wear with different values of load.

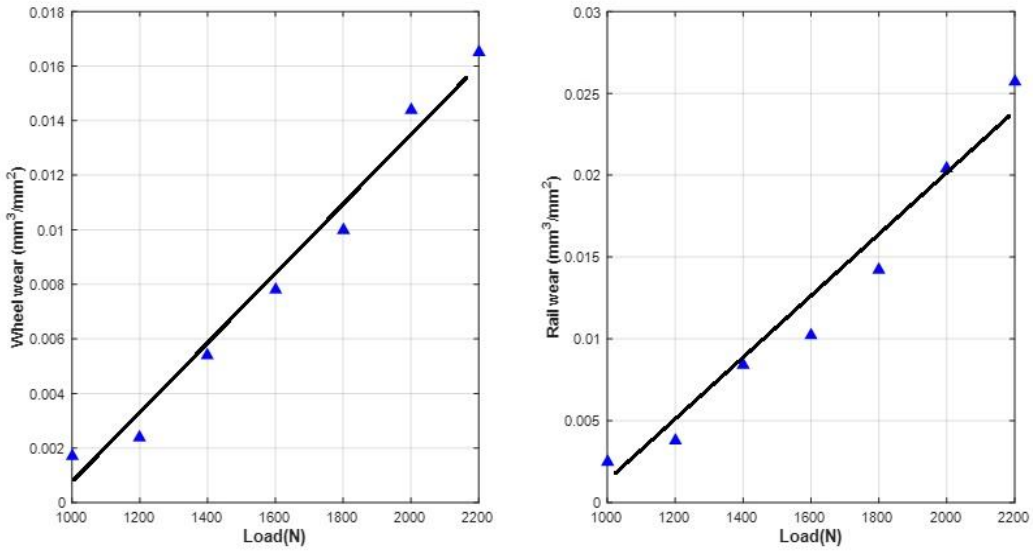

Figure 4. 15 Variation of wheel wear andrail wear under wet conditions

Figure 4.15 shows the variation of wheel wear and rail wear under wet conditions with different loads. The wheel wear increased approximately linearly from $0.0017mm^3/mm^2$ at load of 1000N to $0.0165mm^3/mm^2$ at load of 2200N. The rail wear increased approximately linearly from $0.0025mm^3/mm^2$ at load of 1000N to $0.0257mm^3/mm^2$ at load of 2200N. The test results show that the wheel wear and rail wear were increased by an increase of load under wet conditions. The test results show also that the wheel and rail wear increased approximately linearly under wet conditions. Furthermore, the test results show that the wheel and rail wear decreased under wet conditions in comparison to dry conditions. The results have demonstrated that the water reduced the wheel and rail wear.

4.7.3 Effect of lubricated conditions on wheel wear and rail wear

Millmax 46 oil was used in this test to examine the effect of lubricated conditions on wheel wear and rail wear. The variation of wheel wear and rail wear under lubricated conditions after a distance of 18696m is shown in Table 4.9. For lubricated conditions tests, some drops of oil were put on the wheel and rail surfaces before each test, where the oil was covered all the wheel-rail contact area.

Test No	Load (N)	Wheel wear(mm^3/mm^2)	Rail wear(mm^3/mm^2)
1	1000	0.0012	0.0017
2	1200	0.0018	0.0026
3	1400	0.0041	0.0062
4	1600	0.0057	0.0093
5	1800	0.0071	0.0115
6	2000	0.0093	0.0144
7	2200	0.0130	0.0185

Table 4. 9 Wheel wear and rail wear under lubricated conditions

Figure 4.16 shows the variation of wheel/rail wear with different values of load under lubricated conditions.

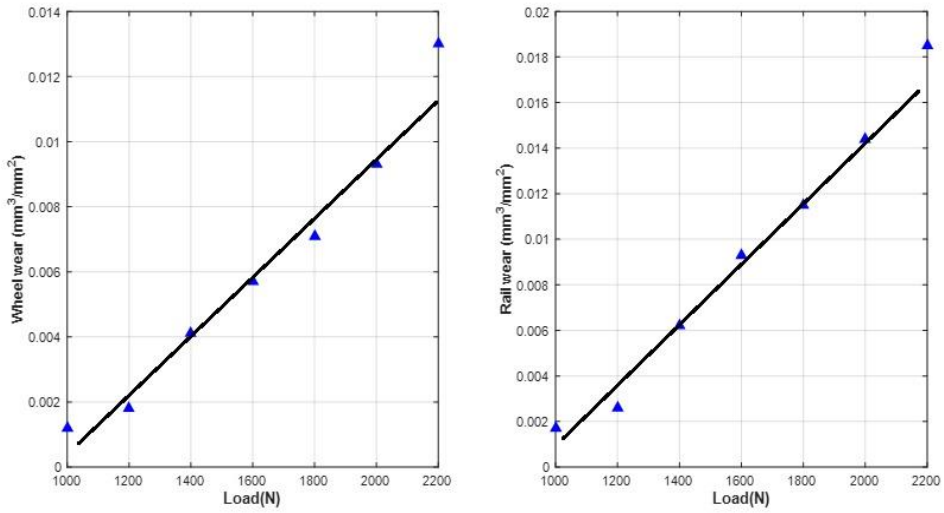

Figure 4. 16 Variation of wheel wear and rail wear under lubricated conditions

Figure 4.16 shows the variation of wheel wear and rail wear under lubricated conditions with different loads. The wheel wear increased approximately linearly from $0.0012mm^3/mm^2$ at load of 1000N to $0.0130mm^3/mm^2$ at load of 2200N. The rail wear increased approximately linearly from $0.0017mm^3/mm^2$ at load of 1000N to $0.0185mm^3/mm^2$ at load of 2200N. The test results show that the wheel wear and rail wear were increased by increase of load under lubricated conditions. The test results also show that the wheel wear and rail wear increased approximately linear under lubricated conditions with different loads. Furthermore, the test results show that the wheel wear and rail wear decreased under lubricated conditions compared to dry conditions; and the wheel wear and rail wear under lubricant conditions was less than in cases of wet conditions. The results have demonstrated that the oil reduced the wheel wear and rail wear.

4.7.4 Effect of sanded conditions on wheel wear and rail wear

Sand was used in this test to investigate the effect of sanded conditions on wheel wear and rail wear. The variation of wheel wear and rail wear under sanded conditions after a distance of 18696m is shown in in Table 4.10. For sanded conditions, a tube was fixed to the rig, and then some sand was provided inside this tube, then the sand was spread on the wheel-rail contact during the sanded conditions tests.

Test No	Load (N)	Wheel wear(mm^3/mm^2)	Rail wear(mm^3/mm^2)
1	1000	0.0032	0.0052
2	1200	0.0041	0.0073
3	1400	0.0088	0.0141
4	1600	0.0112	0.0175
5	1800	0.0169	0.0269
6	2000	0.0236	0.0377
7	2200	0.0341	0.0584

Table 4. 10 Wheel wear and rail wear under sanded conditions

Figure 4.17 shows the variation of wheel wear and rail wear with different values of load under sanded conditions.

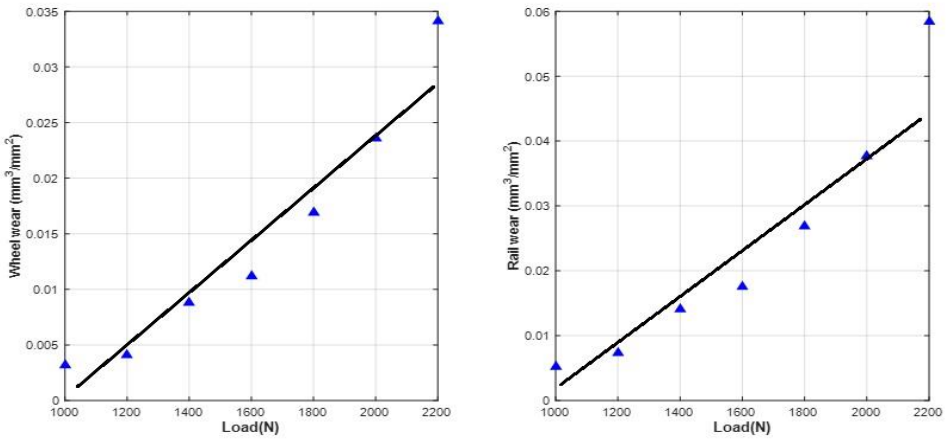

Figure 4. 17 Variation of wheel wear and rail wear under sanded conditions

Figure 4.17 shows the variation of wheel wear and rail wear under sanded conditions with different loads. The wheel wear increased approximately linearly from $0.0032 mm^3/mm^2$ at load of 1000N to $0.0341 mm^3/mm^2$ at load of 2200N. The rail wear increased approximately linearly from $0.0052 mm^3/mm^2$ at load of 1000N to $0.0584 mm^3/mm^2$ at load of 2200N. The test results show that the wheel wear and rail wear were increased by increases of load under sanded conditions. The test results also show that the wheel wear and rail wear increased approximately linear under sanded conditions with different loads. Furthermore, the test results show that the wheel wear and rail wear increased under sanded conditions in comparison to dry conditions. Scratches and other damage were seen on the wheel and rail surfaces after the addition of sand and consequently both wheel wear and rail wear damage rates increased under these conditions.

4.7.5 Comparison between wheel wear and rail wear under dry, wet, lubricated, and sanded conditions

Figure 4.18 shows a comparison between wheel wear and rail wear under dry, wet, lubricated, and sanded conditions.

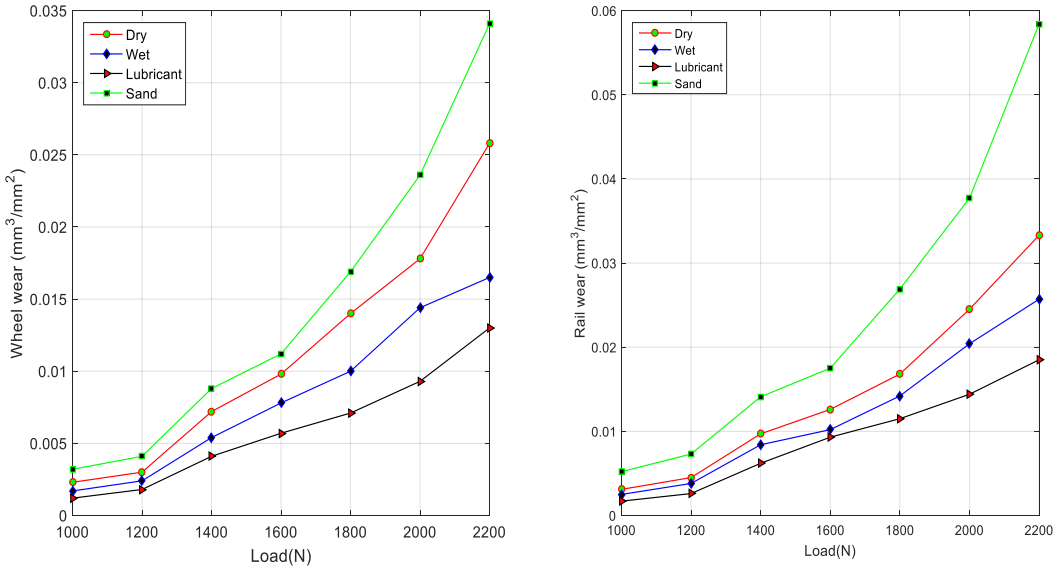

Figure 4. 18 Wheel/rail wear under dry, wet, lubricated, and sanded conditions

Figure 4.18 presented the results of investigating the effect of wheel/rail surface conditions on wheel/rail wear for the twin disc rig experiments. The results shown in Figure 4.18 show that the wheel and rail wear was influenced by wet, lubricated, and sanded conditions. The results have demonstrated that the both water and oil reduce wheel and rail wear, while the sand increased wheel and rail wear.

The results have demonstrated that the wheel wear and rail wear increased under dry, wet, lubricated, and sanded conditions. The relationship between wheel/rail wear and load under dry, wet, lubricated, and sanded conditions is nonlinear; probably due to the wear rate mechanism changing as the other parameters change such as load, and the profile surface after each test. Some relationships between wheel/rail wear and surface conditions are established in the next section.

4.7.6 Section discussion

The effect of surface conditions on wheel wear and rail wear was investigated as follows: Figure 4.14 and Table 4.7 show the test results of wheel wear and rail wear under dry conditions; Figure 4.15 and Table 4.8 show the test results of wheel wear and rail wear under wet conditions; Figure 4.16 and Table 4.9 show the test results of effect of lubricated conditions on the wheel and rail wear; and Figure 4.17 and Table 4.10 show the test results of wheel wear and rail wear under sanded conditions. All these test results were summarized such as shown in Table 4.11 to present the effect of surface conditions on wheel wear and rail wear.

Test No	Load (N)	Wheel wear (mm^3/mm^2) Dry	Rail wear (mm^3/mm^2) Dry	Wheel wear (mm^3/mm^2) Wet	Rail wear (mm^3/mm^2) Wet	Wheel wear (mm^3/mm^2) Lubricated	Rail wear (mm^3/mm^2) Lubricated	Wheel wear (mm^3/mm^2) Sanded	Rail wear (mm^3/mm^2) Sanded
1	1000	0.0023	0.0031	0.0017	0.0025	0.0012	0.0017	0.0032	0.0052
2	1200	0.0030	0.0045	0.0024	0.0038	0.0018	0.0026	0.0041	0.0073
3	1400	0.0072	0.0097	0.0054	0.0084	0.0041	0.0062	0.0088	0.0141
4	1600	0.0098	0.0126	0.0078	0.0102	0.0057	0.0093	0.0112	0.0175
5	1800	0.0140	0.0168	0.0100	0.0142	0.0071	0.0115	0.0169	0.0269
6	2000	0.0178	0.0245	0.0144	0.0204	0.0093	0.0144	0.0236	0.0377
7	2200	0.0258	0.0333	0.0165	0.0257	0.0130	0.0185	0.0341	0.0584

Table 4. 11 Effect of surface conditions on wheel/rail wear

The test results shown in Table 4.11 were used to find the results which are shown in Table 4.12. Table 4.12 shows the effect of wet, lubricated, and sanded conditions on wheel wear and rail wear. As an example: after an applied load of 1000N, the wheel wear decreased by a factor of 1.3 and the rail wear decreased by a factor of 1.2 under wet conditions; the wheel wear decreased by a factor of 1.9 and the rail wear decreased by a factor of 1.8 under lubricated conditions; and the wheel wear increased by a factor of 1.3 and the rail wear increased by a factor of 1.6 under sanded conditions.

Test No	Load (N)	Wheel wear (−) Wet	Rail wear (−) Wet	Wheel wear (−) Lubricated	Rail wear (−) Lubricated	Wheel wear (−) Sanded	Rail wear (−) Sanded
1	1000	↓ 1.3	↓ 1.2	↓ 1.9	↓ 1.8	↑ 1.3	↑ 1.6
2	1200	↓ 1.2	↓ 1.1	↓ 1.6	↓ 1.7	↑ 1.3	↑ 1.6
3	1400	↓ 1.3	↓ 1.1	↓ 1.7	↓ 1.5	↑ 1.2	↑ 1.4
4	1600	↓ 1.2	↓ 1.2	↓ 1.7	↓ 1.4	↑ 1.1	↑ 1.3
5	1800	↓ 1.4	↓ 1.1	↓ 1.9	↓ 1.4	↑ 1.2	↑ 1.6
6	2000	↓ 1.2	↓ 1.2	↓ 1.9	↓ 1.7	↑ 1.3	↑ 1.5
7	2200	↓ 1.5	↓ 1.2	↓ 1.9	↓ 1.8	↑ 1.3	↑ 1.7
Average	--	↓ 1.3	↓ 1.1	↓ 1.8	↓ 1.6	↑ 1.2	↑ 1.5

Table 4. 12 Effect of surface conditions on wheel/rail wear

Figure 4.18 shows the comparison between the effects of the four surface conditions on wheel wear and rail wear. For example, after an applied load of 2200N, the wheel wear was $0.0258 mm^3/mm^2$ under dry conditions, and it decreased $0.0165 mm^3/mm^2$ under wet conditions, and decreased to $0.0130 mm^3/mm^2$ under lubricated conditions, while it was increased to $0.0341 mm^3/mm^2$ under sanded conditions. The rail wear was $0.0333 mm^3/mm^2$ under dry conditions, and it decreased to $0.0257 mm^3/mm^2$ under wet conditions, and decreased to $0.0185 mm^3/mm^2$, while it was increased to $0.0584 mm^3/mm^2$ under sanded conditions. The wet conditions decreased the wheel wear by a factor of 1.5, the lubricated conditions decreased the wheel wear by a factor of 1.9, while the sanded conditions increased the wheel wear by a factor of 1.3. The wet conditions decreased the rail wear by a factor of 1.2, the lubricated conditions decreased the rail wear by a factor of 1.8, while the sanded conditions increased the rail wear by a factor of 1.7.

4.8 Chapter Conclusion

The findings of the investigation of this chapter can be summarised as follows:

The effect of load, yaw angle and wheel/rail surface conditions on wheel wear and rail wear were investigated. Results of analysis of wear tests indicates that there is relationship between increase of load, yaw angle and wheel/rail wear. Tests results show that the applied load, and yaw angle all impact on the wheel/rail wear. The relationship between wheel/rail wear and load is approximately linear. The relationship between wheel/rail wear and yaw angle is nonlinear.

The test results show that the wheel wear and rail were influenced by wet, lubricated, and sanded conditions. The key findings are: The wet conditions decreased the wheel wear by a factor of 1.3, the lubricated conditions decreased the wheel wear by a factor of 1.8, while the sanded conditions increased the wheel wear by a factor of 1.2. The wet conditions decreased the rail wear by a factor of 1.1, the lubricated conditions decreased the rail wear by a factor of 1.6, while the sanded conditions increased the rail wear by a factor of 1.5. The test results show also show that the wheel and rail wear increased nonlinearly under dry, wet, lubricated, and sanded conditions with different loads.

The replica material and Alicona profilometer can be used to study the effect of some parameters such as load, yaw angle, and surface conditions on wheel wear and rail wear. This work introduced the replica material and an optical instrument as effective tools to study the wheel wear and rail wear. Another advantage of the use of the replica material is that it is a permanent record of the wheel and rail surface, while an advantage of the Alicona profilometer is that it can measure the wheel wear and rail wear at high resolution.

Chapter 5 Prediction of wheel wear and rail wear using artificial neural networks for a twin disc rig tests

(Chapter 3 in exam draft has been included in chapter 6 (now chapter 5)).

5.1 Introduction to Neural Networks

In 1943 McCulloch and Pitts [106] presented an introduction to simplified neurons, they introduced these neurons to achieve the computational tasks. In 1969 Minsky and Papert [107] published a neural networks book titled of perceptrons. Backpropagation neural network was presented in 1986 by Rumelhart, Hinton and Williams [108], they presented the delta rule to train multi-layered networks.

Currently most institutes and universities have a neural networks group within their departments. An artificial neural network can be categorised as a computational model which has the ability to learn [109]. A neural network consists of input unit, weights, an activation function, and output unit [110]. The most common activation function is a sigmoid function which is shown in Figure 5.1.

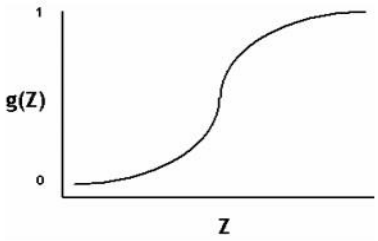

Figure 5. 1 Sigmoid Activation Function [111]

The logistic function is the most common sigmoid activation function that plots within the range of 0 to 1. The sigmoid function is expressed in the following general form [111]:

$$g(z) = \frac{1}{1+e^{-z}} \tag{5.1}$$

Where z is constant that determines how steep the function is.

5.2 Multilayer Perceptron Neural Network (MLP)

The most important class of neural networks is the multilayer perceptron neural network (MLP). Multilayer perceptron neural network consists of an input layer, one or more hidden layers, and an output layer. The architecture of the multilayer perceptron neural network is shown in Figure 5.2 [112], [113].

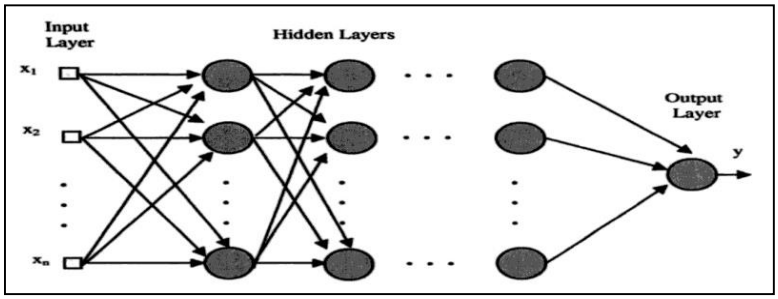

Figure 5. 2 The architecture of the multilayer perceptron neural network [113]

5.3 Training of neural network

The most common training algorithms in neural networks are the supervised training algorithm and the unsupervised training algorithm.

Supervised training method uses a teacher to train the network. In supervised training method, the response is compared with the desired output; if there are difference between the response and the desired output, then, the error is used to make adjustments to the weights until the response matches the desired output. In unsupervised training method no teacher is uses in the training, while the adaption rule generates the error signal which are used to adapt the weights of neural network. The supervised training method, and the unsupervised training method are shown in Figure 5.3 and Figure 5.4 respectively [114].

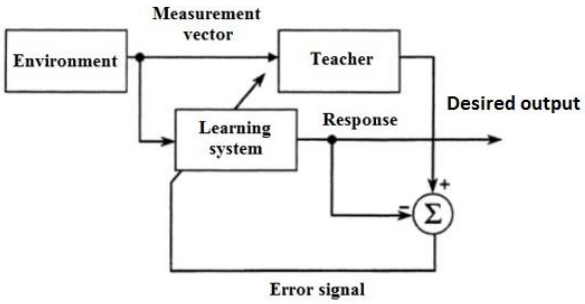

Figure 5. 3 Block diagram of supervised training method [114]

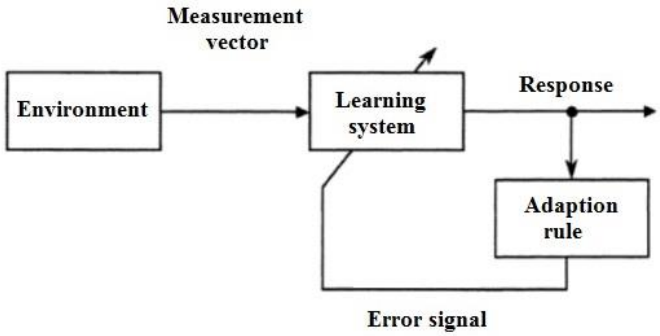

Figure 5. 4 Block diagram of unsupervised training method [114]

The training of neural network uses modified weights to produces more desirable results. There are several algorithms which can be used to train neural networks such as the Hobbs rule, and the delta rule. Hobbs rule is used for unsupervised training, while the delta rule used for supervised training. The delta means reduces the difference between the actual output and desired output. The delta rule is the common neural network learning algorithm. In this rule, the weights are updated to minimize the mean squared error of the network. The delta rule is sometimes referred to as least mean square (LMS) rule or backpropagation rule [115]-[118].

5.4 Neural networks types

The neural networks are divided in terms of their structure into two types: feedforward network and recurrent network [119]. In feedforward neural networks the information flows in one direction without feedback (loops). The information travelled from the inputs to the outputs, and without feedback between output layer and input layer. The feedforward neural network can consists of more than one hidden layer [115], [120]. In recurrent neural network the information can a flow in forward direction and a backward direction (it contain feedback connections), the outputs of neurons can fedback to the same neurons or to neurons in previous layers [121].

Three types of neural network were used in this thesis for prediction of wheel wear and rail wear. The first network is a Nonlinear Autoregressive model with eXogenous input neural network (NARXNN). This is a type of recurrent neural network and the advantages of the NARXNN are that it has fast training and the output of NARXNN is fedback to the input of the feedforward neural network so that the network output is available during the training of the NARXNN and more efficient inputs can be used for training of neural network.

The second network is a backpropagation neural network (BPNN) which is a type of feedforward neural network, the advantage of using this neural network is that the Levenberg-Marquardt algorithm is used to adjust the weights to reduce the error between the actual output and the network output.

The third network is a radial basis function neural network (RBFNN) which is a type of feedforward neural network. The advantage of the RBFNN is that the training is divided into two stages: the first stage is to select the centres of hidden layers, and select the widths of the Gaussian functions; while the second stage is to adapt the weights using least mean squares algorithm; this can lead to more accurate results.

The performance of the RBFNN depends on the proper selection of these three parameters, centres, widths and the weights. The BPNN and the RBFNN were used the supervised training algorithm for training, where the target acts as a ‘teacher’ to reduce the error, while the output of the network is used to adjust the weights.

5.4.1 Nonlinear Autoregressive model with eXogenous input neural network (NARXNN)

A Nonlinear Autoregressive model with eXogenous input neural network (NARXNN) was used in this project for wheel wear and rail wear prediction. The NARXNN can be implemented using a feedforward neural network [122]. Figure 5.5 shows the structure of the NARXNN which are called NARX recurrent neural networks. This network simply uses a TDL-type network (Tapped delay line) with a feedback connection from the output of the network to the input [83]. The function of the delay line (TDL) or taps is to feed the neural network with the past values of inputs.

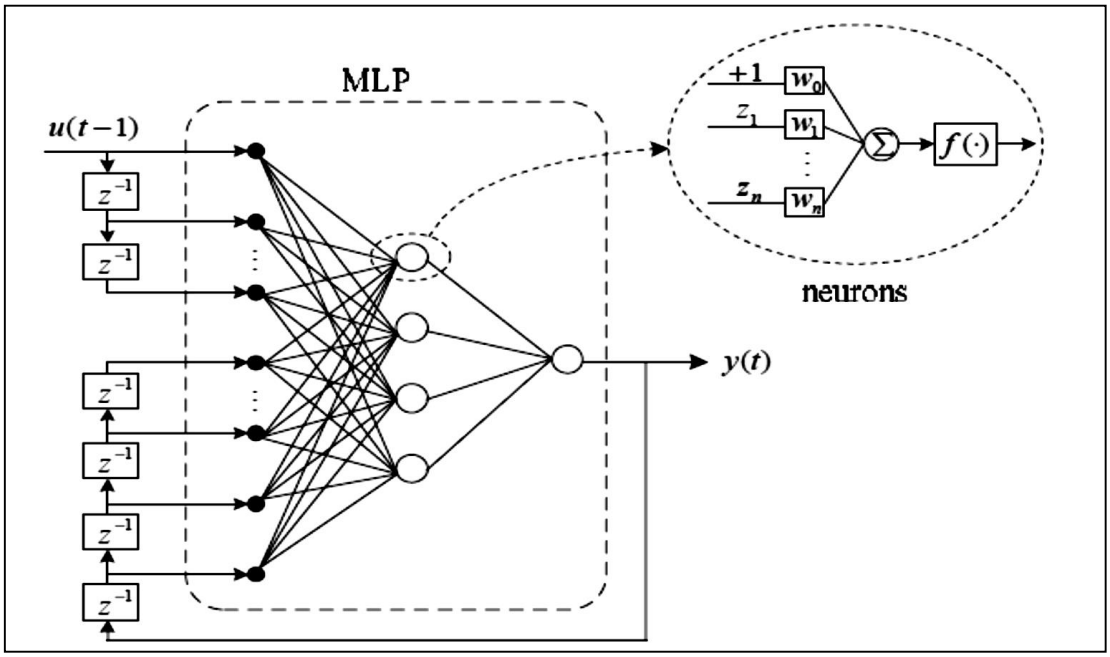

Figure 5. 5 The structure of NARXNN [83], [122]

The output of the NARXNN is represented using the following equation:

$$y(t) = f(u(t-1), u(t-2), \dots, u(t-n), y(t-1), y(t-2), \dots, y(t-m), W) \quad (5.2)$$

Where $u(t)$ is the input and $y(t)$ is the output of the network at time t, n and m are the input-memory and output-memory order, W is a weights matrix, and f is a nonlinear function. The output at time t depends on both its past m values and the past n values of the input as well.

The nonlinear autoregressive network with exogenous inputs neural network (NARXNN) is a recurrent dynamic network, with feedback connections. The scheme of NARXNN is depicted in Figure 5.6. Where x is the input, y is the desired output, d is the delay, w_h is the weights, and $\hat{y}$ is the estimated output. The NARXNN can be used in several applications such as a predictor [90], [123].

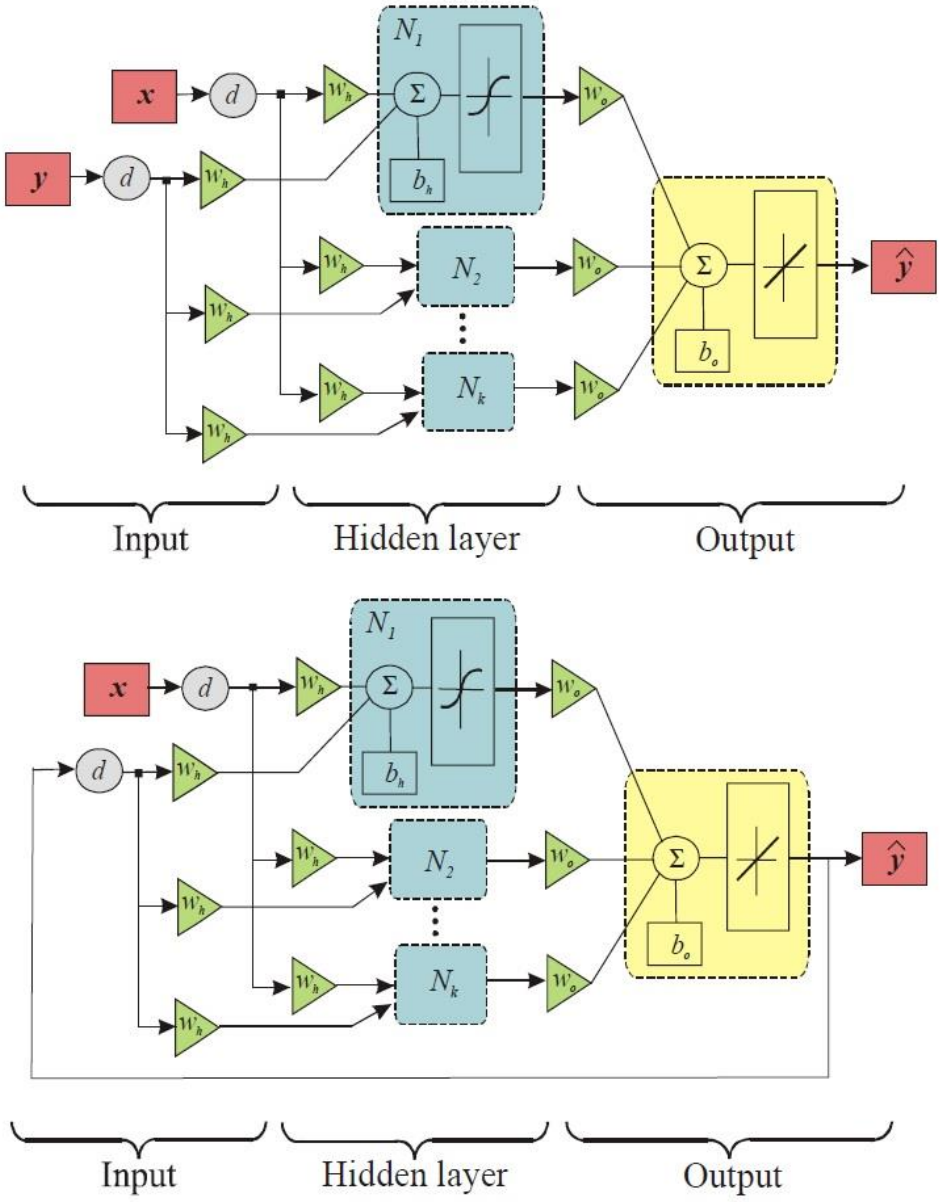

Figure 5. 6 Structure of the NARXNN: series-parallel (up); parallel (down) [124]

Figure 5.7 implements the parallel architecture NARXNN and series-parallel architecture NARXNN. The output of NARXNN is fedback to the input of the feedforward neural network as part of the NARXNN in parallel architecture. This has some advantages such as the input to the feedforward network is more accurate. Where u(t) is the input, y(t) is the desired output, and $\hat{y}_{(t)}$ is the estimated output.

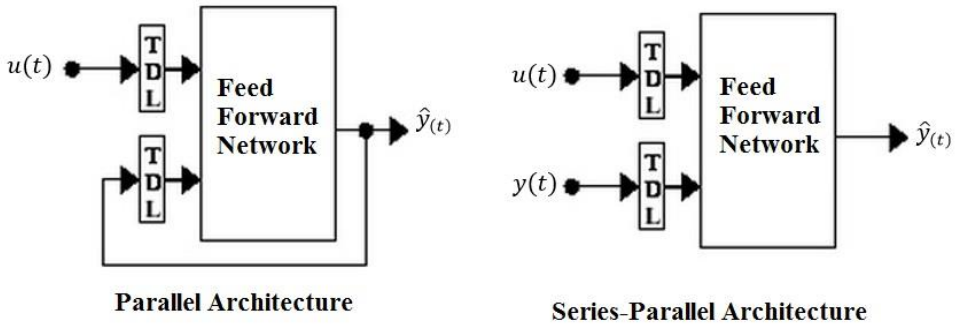

Figure 5. 7 Parallel and series-parallel architecture of NARXNN [123]

A toolbox function (closloop) in Matlab can used to convert the NARXNN from the series-parallel structure (open loop) to the parallel structure (closed loop) which is useful for multi-step-ahead prediction. The training of neural networks can achieve with the open loop which called the series-parallel architecture including the validation and testing. After that, the parallel architecture take place to execute the multistep-ahead prediction [125], [126].

An example of a NARXNN (series-parallel architecture) with 24 hidden layers and 2 delay times designed using Matlab is shown in Figure 5.8.

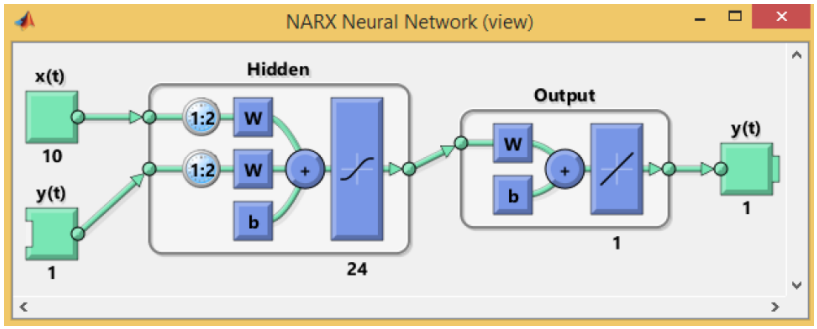

Figure 5. 8 Series-parallel architecture of NARXNN [90]

Matlab can be used to convert the series-parallel NARXNN into the parallel NARXNN, in order to achieve a multi-step-ahead prediction. The parallel NARXNN is shown in Figure 5.9 [90], [123], [125].

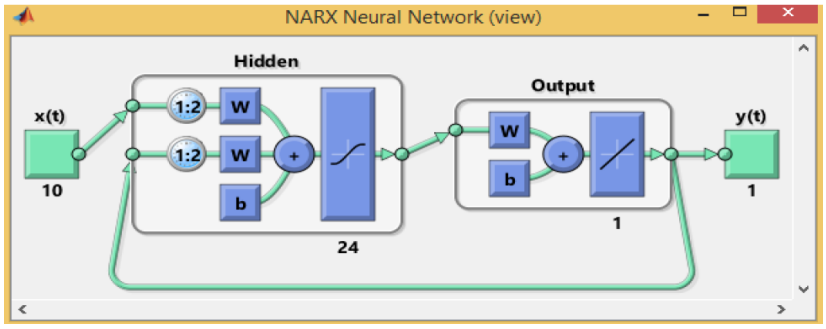

Figure 5. 9 Parallel architecture of NARXNN [90]

NARXNN can be trained using a backpropagation algorithm. The typical performance function used in training (to reduce the error between actual output and estimated output) is the mean square error (MSE).

The MSE is shown in the following equation [90], [122].

$$\mathrm{MSE} = \frac{1}{\mathrm{N}} \sum_{\mathrm{i}=1}^{\mathrm{N}} (\mathrm{e_i})^2 = \frac{1}{\mathrm{N}} \sum_{\mathrm{i}=1}^{\mathrm{N}} (\mathrm{t_i} - \mathrm{y_i})^2 \tag{5.3}$$

Where $\mathrm{t_i}$ the target output and y_i is the estimated output.

The activation functions of the neurons in hidden layers can be defined using the logistic function which was presented in equation 5.1 [90].

The Lavenberg-marquardt backpropagation algorithm is usually used to train the NARXNN. The training of NARXNN automatically stops when the validation error (MSE) begins to increase [21].

The “Performance” option in Matlab windows which is shown in Figure 5.10 can be used to plot the performance training record to check for possible overfitting. Also, the “Regression” option can be used to check the regression coefficient.

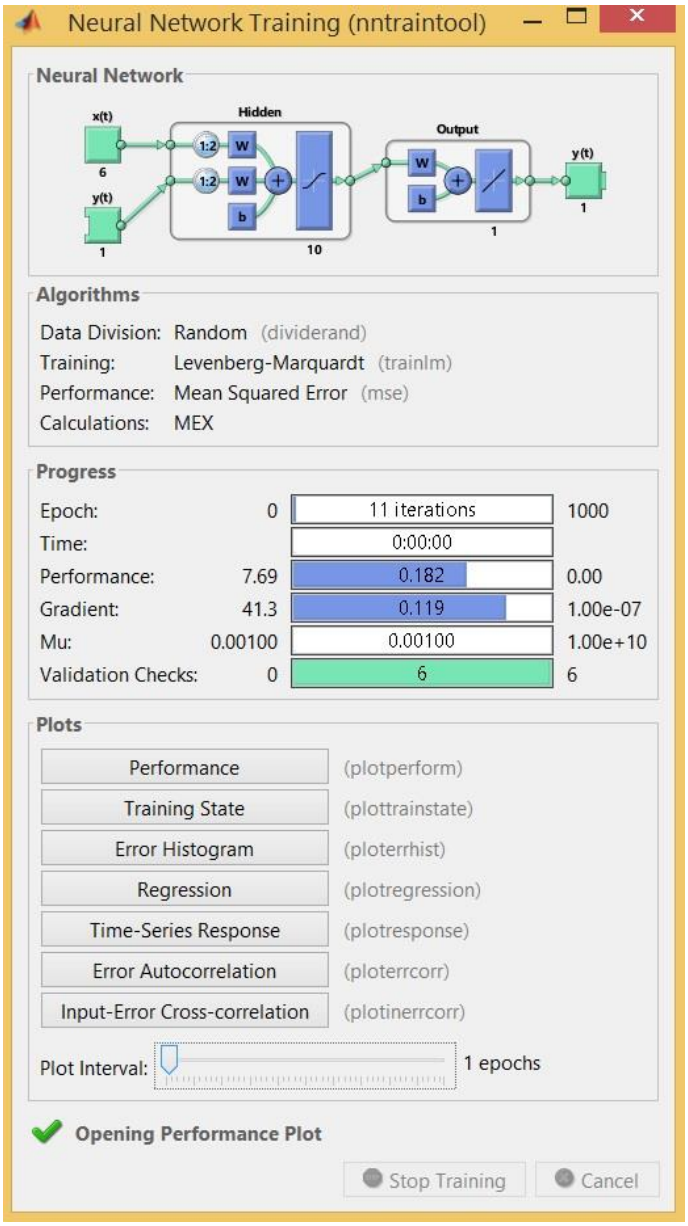

Figure 5. 10 Neural network training windows

Mathworks [127] presented the performance function for training, validation and test error for certain simulations such as shown in Figure 5.11. It shows that better validation performance was at epoch 38. After 44 epochs the training stopped because the validation error increased. These results show a good network performance because the test error and the validation error have similar characteristics, and there is no any significance over fitting has happened.

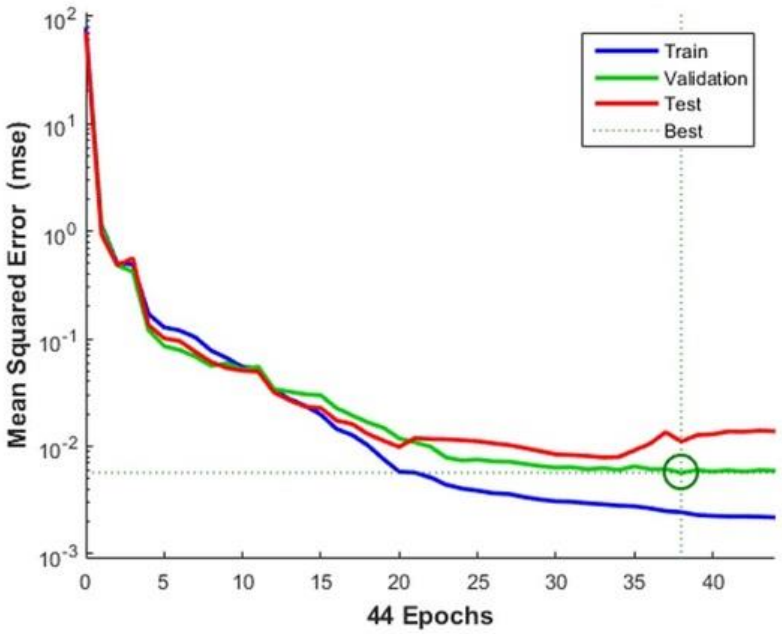

Figure 5. 11 Performance of neural network [127]

The regression plot is used to validate the performance of the network as it shows a regression between network output and network target for each of the data subsets. The R values give some sense of the networks ability to generalise. The R value is an indication of the relationship between the outputs and targets. When R is equal to 1 it is indicative of an exact linear relationship between output and target. If R is tends to zero, then there is no linear relationship between output and target [128].

Khamis and Abdullah [21] presented the regression for the training, validation, and testing of NARXNN for certain simulations such as shown in Figure 5.12; the R value for training, validation, and test results were greater than 0.9; this indicates that there is linear relationship between output and target.

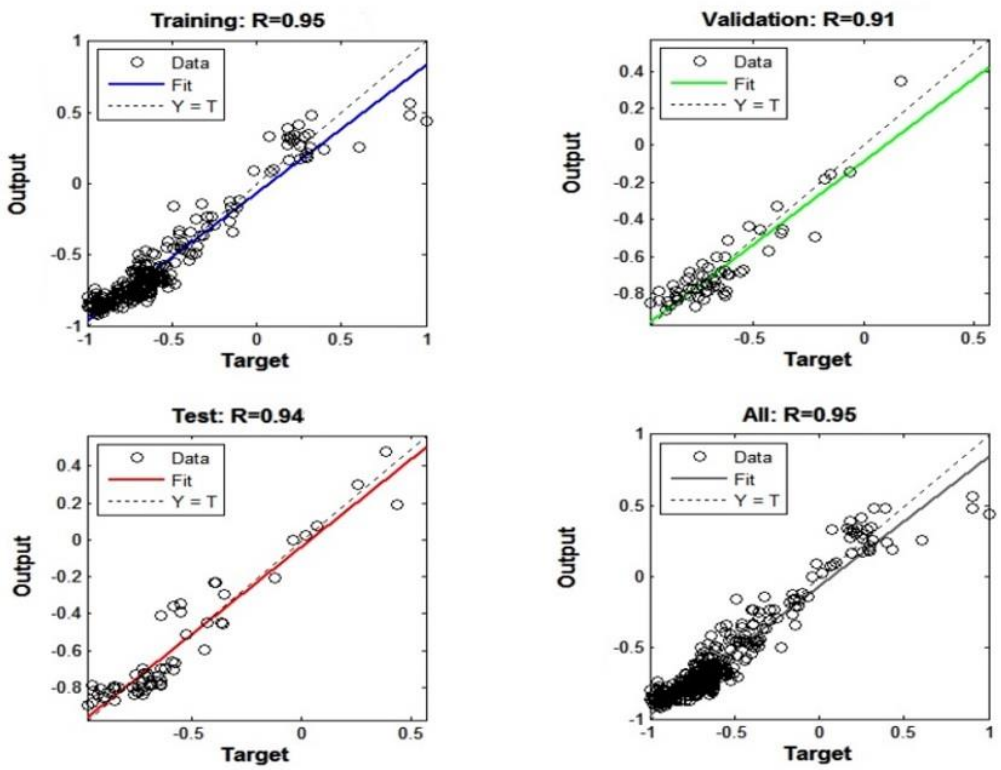

Figure 5. 12 Example of Matlab regression plot [21]

5.4.2 Backpropagation Neural Network (BPNN)

This section describes one of the most common types of artificial neural network. Multilayer feedforward (MLFF) neural network with backpropagation (BP) learning (multilayer perceptron). A general multilayer feedforward (MLFF) network is illustrated in Figure 5.13. The MLFF consists of three layers: Input layer, hidden layers, and output layer. The hidden layer is sometimes called the internal layer because it only receives internal inputs then produces internal outputs. It consists of one or more hidden layers [129].

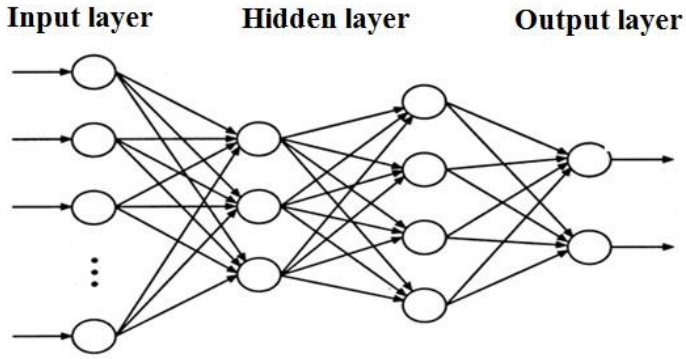

Figure 5. 13 MLFF Backpropagation Neural Network (BPNN) [129]

The backpropagation training process requires an activation function. One of the most common activation functions is the sigmoid function which is shown in equation 5.1 [129].

The most common training algorithm which is used for training of BPNN is a Levenberg-Marquardt algorithm which adjusts the weights to reduce the error. The backpropagation training algorithm is designed to minimize the mean square error (MSE). The MSE is the function which is commonly used to optimize network performance. The mean squared error (MSE) is shown in equation 3.3.

The weights can updated using the following equation [86]:

$$W_{ij}^{m}(t+1) = W_{ij}^{m}(t) + \eta\, \delta_{j}^{m}\, O_{i}^{m-1} \tag{5.4}$$

Where $W_{ij}(t)$ is the old weight; $W_{ij}(t+1)$ is the new weight; η is the learning rate ($\eta = 0 \ldots 1$); δ is the error term; and m indicates the layers except the input layer; and O is the actual output of the node.

For training MLFF, the Levenberg-Marquardt algorithm is the fastest training function. The Matlab command 'trainlm' is a network training function that updates weight and bias values according to Levenberg-Marquardt optimization [130].

Table 5.1 shows the Matlab commands and it is description which can be used to terminate the training of multilayer neural networks. The setting shown in Table (5.1) can be changed, but the result will affects.

net.trainParam.epochs	1000	Maximum Number of Training Epochs (Iterations)
net.trainParam.min_grad	1e-6	Minimum Gradient Magnitude
net.trainParam.max_fail	6	Maximum Number of Validation Increases

Table 5. 1 The Matlab commands to terminate the training of multilayer neural networks [130]

The most common problem facing researchers is the number of hidden layer selection. Until now there is no an accurate method to determine the number of hidden layer of neural network. The number of hidden layer is very important for the training of the neural network. The trial and error method is the most common algorithm which can be used to select the number of hidden layers [131].

When the training and testing of BPNN is complete; the network training windows, performance plot, and regression plot can be obtained as shown in Figure 5.10, 5.11, and 5.12 respectively. “Performance” option can be used to check the overfitting. Also, the “Regression” option can be used to check the regression coefficient.

5.4.3 Radial basis function neural network (RBFNN)

The radial basis function neural network (RBFNN) has an input, hidden, and output layer as shown in Figure 5.14. The hidden layer consists of RBF activation function [86]. The training of RBFNN can be carried out as: select the centres of hidden layers, select the widths of the Gaussian functions, and adapt the weights [132].

The centres of the RBFNN can be selected using different strategies, but the common approaches are fixed centres selected randomly, and K-Means clustering algorithm [133]. The simple algorithm for selecting the centres (C_i) of radial basis function is to set the centres equal to a random subset of the input vectors from the training set, this algorithm is called centre selection using a subset of data points [134].

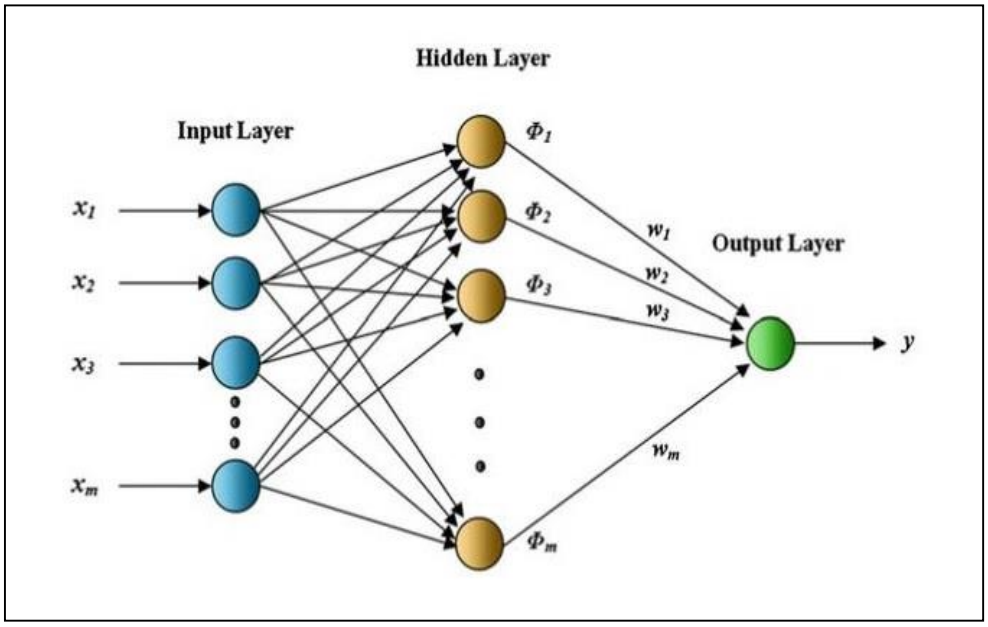

Figure 5. 14 Radial Basis Function Network (RBFNN) Architecture [135]-[137]

Where $X_1, X_2, X_3 \ldots, X_m$ are the inputs, and $C_1, C_2, \ldots, C_m$ are the centres. Here, the dimension of each centre for m input network is $(m \times 1)$ [136], [137].

The output of RBFNN can represented such as shown in the following equation [117], [135], [136]:

$$y = \sum_{j=1}^{m} W_j \, \emptyset_j \tag{5.5}$$

Where $\emptyset$ is the activation function, and W is the weights.

The common activation function of RBFNN is the Gaussian function ($\emptyset$) [135]-[138]:

$$\emptyset(x) = \exp\left(\frac{-r^2}{2\sigma^2}\right) \tag{5.6}$$

$$r = || x - c || \tag{5.7}$$

Where C are the centres, x are the inputs, and σ is the width of activation function.

Euclidean distance method is the most common method which can used to calculate the width of activation function for RBFNN such as shown in the following equation [114], [138], [139]:

$$E_{dist} = \sqrt{\sum_{i=1}^{n} (X_i - c_i)^2} \quad , i = 1,2,3,\ldots,n \tag{5.8}$$

Where: X_i are the inputs, c_i are the centres, and n is the vector dimension.

The least mean square algorithm (LMS) is the most common algorithm which can used for adapting the weights of the output layer for the RBFNN such as shown in the following equation [114], [138]-[140]:

$$W(t+1) = W(t) + \mu\,(y(t) - y_m(t))\Phi^T(t) \tag{5.9}$$

Where $W(t+1)$ is the updated weights, $W(t)$ is the previous weights originally set to zero, $y(t)$ is the desired output, $y_m(t)$ is the output of the network, $\Phi^T(t)$ is the hidden layer output (Gaussian output), and μ is the learning factor of the RBFNN. The learning factor is a positive gain factor term that controls the adaptation rate of the algorithm ($0 < \mu \leq 1$).

The mean square error (MSE) is used for measuring the performance of the RBFNN, it shown equation 3.3 [141].

The RBFNN can be designed using the following Matlab command (newrb) [142]-[144]:

$$net = newrb(P, T, goal, spread, MN, DF) \tag{5.10}$$

Where: P is the input vectors, T is the target vectors, goal is the mean squared error (MSE), spread is the spread of RBF, MN is the maximum number of neurons, and DF is the number of neurons to add between displays.

In matlab, the newrb command can be used to design and train the RBFNN; one neuron created, and then, the neurons are added until stopping criteria such as goal or MN was achieved. The training of the RBFNN will be stopped when the sum-squared error falls less than error goal or a maximum number of neurons has been reached [145].

One of the main functions used to design RBF neural network is the newrb, in this case the Gaussian function used as activation function, and the centres were set equal to a random subset of the input vectors from the training set, while the width of Gaussian function is explicitly set by the user [146].

The RBFNN is faster in training compared to other type of neural network such as backpropagation neural network (PBNN) [147]-[149].

5.5 Section conclusion

An introduction to artificial neural networks was presented in this section. Three types of neural networks were introduced: The nonlinear autoregressive network with exogenous inputs neural network (NARXNN), the backpropagation neural network (BPNN), and the radial basis function neural network (RBFNN).
These three types of neural network were introduced in this chapter because they were developed in this project for wheel/rail wear prediction. Neural networks are usually trained using a supervisor training algorithm, where the target (teacher) is used as a supervisor to achieve the training. The supervised training algorithm was used to train the neural networks in this work to predict the wheel and rail wear.

The NARXNN can be designed in parallel structure and series-parallel structure. NARXNN and BPNN usually trained using Levenberg-Marquardt algorithm which is adjusts the weights to reduce the error. The backpropagation training algorithm designed to minimize the mean square error to optimize network performance.

The radial basis network can be designed using the newrb Matlab command. The training of the radial basis function neural network will be stopped when the sum-squared error falls less than error goal or a maximum number of neurons has been reached.

5.6 Neural network model for wheel wear and rail wear prediction

In this project, the neural network model was developed to predict the wheel wear and rail wear as shown in Figure 5.15.

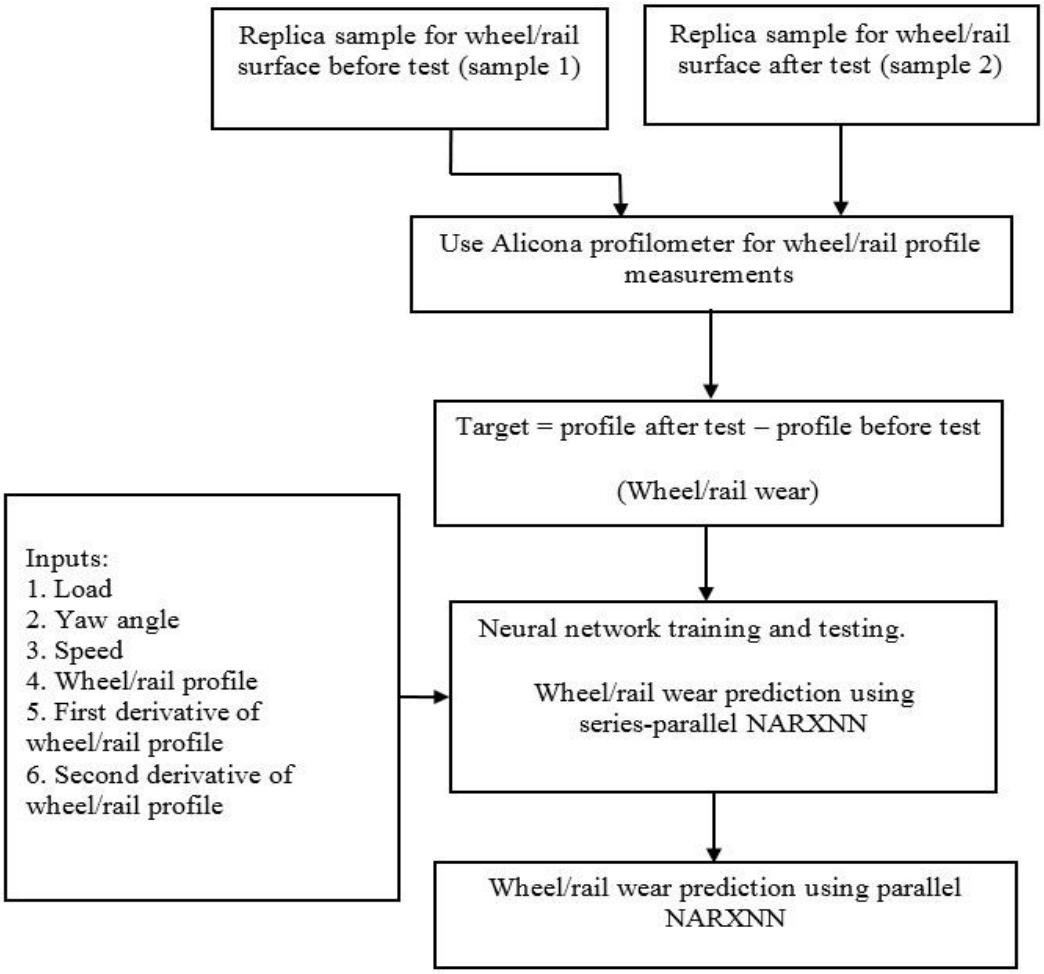

Figure 5. 15 Neural network model for the wheel/rail wear prediction

The series-parallel NARXNN and parallel NARXNN were used to predict the wheel/rail wear for the twin disc rig experiments under dry, wet, lubricated, and sanded conditions as follows:

1. Wheel/rail wear prediction using series-parallel NARXNN: In this test, the following twin disc tests were used to train, validate, and test the NARXNN. The load was 1200N, 1400N, and 1600N; the yaw angle was 0.2 degree, 0.3 degree, and 0.4 degree; and the speed was 420rpm, 540rpm, and 660rpm. 261 samples were used for wheel/rail wear prediction using series-parallel NARXNN. The dataset was divided into 70% for training, 15% for validation, and 15% for testing of NARXNN.
2. Wheel/rail wear prediction using parallel NARXNN: The parallel NARXXNN used to predict wheel/rail wear of the new samples without retraining the network. This in order to perform the multi- step-ahead prediction task (wheel/rail wear prediction in case of new samples). In this test, the following twin disc test was used to test the NARXNN, the load was 1800N, the yaw angle was 0.5 degree, and the speed was 780rpm. 87 samples were used for wheel/rail wear prediction using parallel NARXNN.

The neural network model shown in Figure 5.15 was used for both networks with same architecture (series-parallel NARXNN and parallel NARXNN). In the parallel NARXNN, the output of network is fed back to the input (closed loop); while in the series-parallel NARXNN, there is no connection between output and input (open loop) such as shown in Figure 5.16 and Figure 5.17.

5.7 Wheel wear and rail wear prediction using neural network for the twin disc rig experiments

After the twin disc rig experiments were carried out, a neural network model was developed to predict the wheel wear and rail wear as shown in this chapter. A nonlinear autoregressive network with exogenous inputs neural network (NARXNN) was developed to predict the wheel wear and rail wear for the twin disc rig experiments under several conditions.

The advantages of the NARXNN are that it has fast training, and it can be used as a predictor for nonlinear systems. Modelling using neural networks has emerged as a powerful tool in finding relationships in complex problems and has been used successfully in many fields where the relationship between input and output in a system is very hard to describe. NARXNN has been widely used in the field of system modelling due to its approximation and generalization ability for nonlinear system.

NARXNN was used in railway system modelling, for example, it was used to predict vehicle vibration. The simulation results show that the established NARXNN prediction model can predict the vehicle-body vertical vibration acceleration more accurately [150].

A NARXNN was used in this work for wheel wear and rail wear prediction because the NARXNN has fast coverage, the output of NARXNN is fed back to the input of the feedforward neural network as part of the NARXNN architecture which usually leads to more accurate training, and the NARXNN can be used to predict wear in case of new samples without retraining the network.

The neural network model shown in Figure 5.15 was used for wheel wear and rail wear prediction. The University of Huddersfield twin disc test rig was used to perform several tests such as effect of load, yaw angle, speed and surface conditions such as dry, wet, lubricated, and sanded conditions on wheel and rail wear. The test time for wheel/rail wear measurements was 10min for each test. During these tests, the replica material and Alicona profilometer were used to measure the wheel and rail wear. Then the data collected from the test results were used to train, validate, and test the NARXNN during wheel/rail wear prediction.

The load, the yaw angle, the speed, and the wheel/rail profile were chosen as inputs to the neural network model because they had an effect on wheel and rail wear during tests. The first derivative of wheel/rail profile, and the second derivative of wheel/rail profile presents the rate of change of wheel/rail profile, it was chosen as inputs to the neural network model because it can assist to train the neural network. Useful information about wheel/rail profile can obtained by computing the first derivative of wheel/rail profile and second derivative of wheel/rail profile which were assisted to train the neural network model. Matlab used to calculate the first derivative of wheel/rail profile and second derivative of wheel/rail profile. The output of the neural network was wheel/rail wear.

Series-parallel NARXNN and parallel NARXNN were used to predict the wheel wear and rail wear as shown in the following sections: Wheel/rail wear prediction using series-parallel NARXNN, in this test, the following twin disc tests were used to train, validate, and test the NARXNN. The load was 1200N, 1400N, and 1600N; the yaw angle was 0.2 degree, 0.3 degree, and 0.4 degree; and the speed was 420rpm, 540rpm, and 660rpm. 261 samples were used for wheel wear and rail wear prediction using NARXNN. The dataset was divided into 70% for training, 15% for validation, and 15% for testing of NARXNN. The series-parallel NARXNN was designed with input delays of 1:2, feedback delays of 1:2, 1 hidden layer with 10 neurons were used, and the NARXNN architecture was 6-10-1 as shown in Figure 5.16.

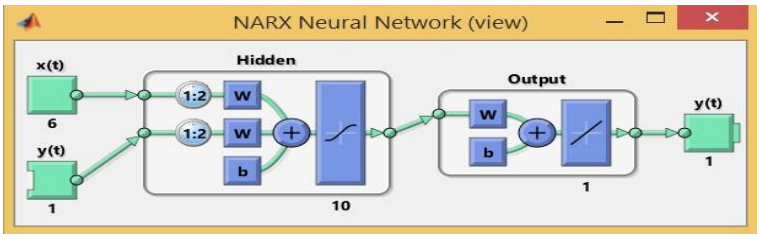

Figure 5. 16 Series-parallel network (NARXNN) [125, 127]

The logistic function was used as an activation function of the neurons in the hidden layers as shown in equation 5.1[90]. The performance function which was used in the training of NARXNN is the mean square error (MSE), it was used to reduce the error between actual output and estimated output such as shown in equation 5.3 [122]. The Levenberg-Marquardt algorithm was used as a network training function that updates the weight and bias values. The Levenberg-Marquardt algorithm has the fastest convergence. This advantage is especially noticeable if very accurate training is required. Levenberg-Marquardt was used to train the NARXNN using the Matlab. The training continues until validation error failed to decrease for six iterations (validation stop). The Levenberg-Marquardt algorithm usually assumes that the performance function is a mean squared errors (mse) [122]. Mean absolute percentage error (MPAE) was used to calculate the NARXNN model accuracy for wheel wear and rail wear prediction. The MPAE was shown in equation 5.11 [151], [152], [154], [155]. The percentage error was calculated using equation 5.12 [105], this equation was used to calculate the percentage error between wheel/rail wear measured and predicted using NARXNN.

Wheel/rail wear prediction using parallel NARXNN: this additional test was performed to present the ability of NARXXNN to predict wheel/rail wear for the case of new samples without retraining the network. Series-parallel network architecture which was shown in Figure 5.16 was converted into a parallel configuration in order to perform the multi- step-ahead prediction task (wheel/rail wear prediction in case of new samples) [125]-[127]. An example of parallel NARXNN architecture was presented in Figure 5.17.

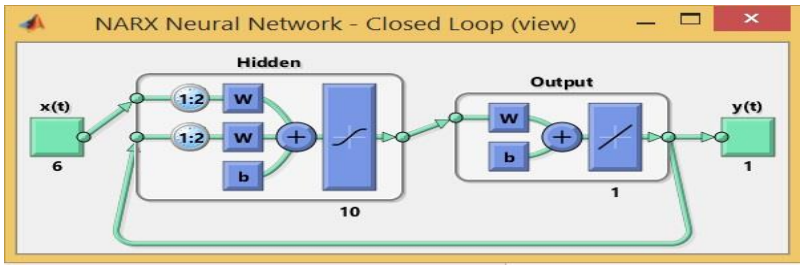

Figure 5. 17 Parallel network (NARXNN)

The function "CLOSELOOP" in the Matlab replaces the feedback input with a direct connection from the output layer, with the feedback loop closed, it can be used to perform multi-step-ahead predictions [127]. In this test, the following twin disc test was used to test the NARXNN, the load was 1800N, the yaw angle was 0.5 degree, and the speed was 780rpm. 87 samples were used for wheel wear and rail wear prediction using NARXNN. The mean absolute percentage error (MPAE) was used to calculate the NARXNN model accuracy, it was calculated using equation 5.11. The percentage error was calculated using equation 5.12.

The following equation was used to calculate the mean absolute percentage error (MAPE) [151], [152]:

$$\text{MAPE} = \frac{1}{N} \sum_{i=1}^{N} \frac{|A_i - P_i|}{Ai} \text{ X } 100 \tag{5.11}$$

Where A_i is the actual wear, P_i is the predicted wear, i is time period, and N is the number of time periods (number of observed values).

The following equation was used to calculate the percentage error [105]:

$$\text{Perecntage error } = \frac{|\text{ wear predicted} - \text{actual wear}|}{\text{actual wear}} \text{ X } 100 \tag{5.12}$$

MATLAB has been recognised as an effective neural network modelling tool and is subsequently used in this project to implement the neural network model for wheel/rail wear prediction. The Matlab code was used to implement the results of wheel wear and rail wear prediction using series-parallel NARXNN and parallel NARXNN was shown in appendix 3 [127]. The Matlab code was used to calculate the mean absolute percentage error (MAPE), and the percentage error such as shown in appendix 4. Appendix 5 presents how the data is used to train, validate, and test the neural network model during prediction of wheel and rail wear using neural network.

The following sections present the wheel wear and rail wear prediction using the series-parallel NARXNN and parallel NARXNN under dry, wet, lubricated, and sanded conditions (All results for unseen data).

5.7.1 Wheel wear and rail wear prediction under dry conditions

The actual wheel wear, and the wheel wear predicted using series-parallel NARXNN are shown in Figure 5.18. Since the tests were performed under loads of 1200N, 1400N, and 1600N; three profiles were obtained; each profile contains 87 sample; therefore, the three profiles together contain 261 samples, these 261 samples were used to train, validate, and test the network. The 261 samples were divided into 70% for training, 15% for validation, and 15% for testing of series-parallel NARXNN. The training data set and validation dataset was not presented in this work, just the test dataset was presented (wear predicted) such as shown in Figure 5.18. The testing dataset shown in Figure 5.18 were 39 samples (15% of 261 samples), it is chosen randomly (no sequence) by the Matlab neural network toolbox.

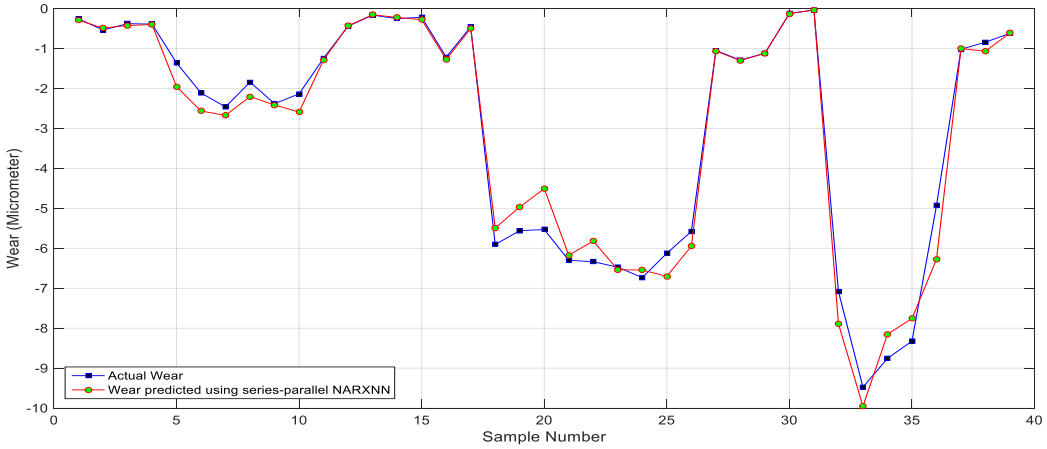

Figure 5. 18 Actual wheel wear and predicted using series-parallel NARXNN under dry conditions

The actual wheel wear and the wheel wear predicted using parallel NARXNN are shown in Figure 5.19. Since the test was performed under load of 1800N was used to test the parallel NARXNN; therefore, a one profile obtained; this profile contains 87 sample; all of these 87 samples were used to test the parallel NARXNN (wear predicted) such as shown in Figure 5.19, it can be notice that the samples were sequences because it implements the full profile.

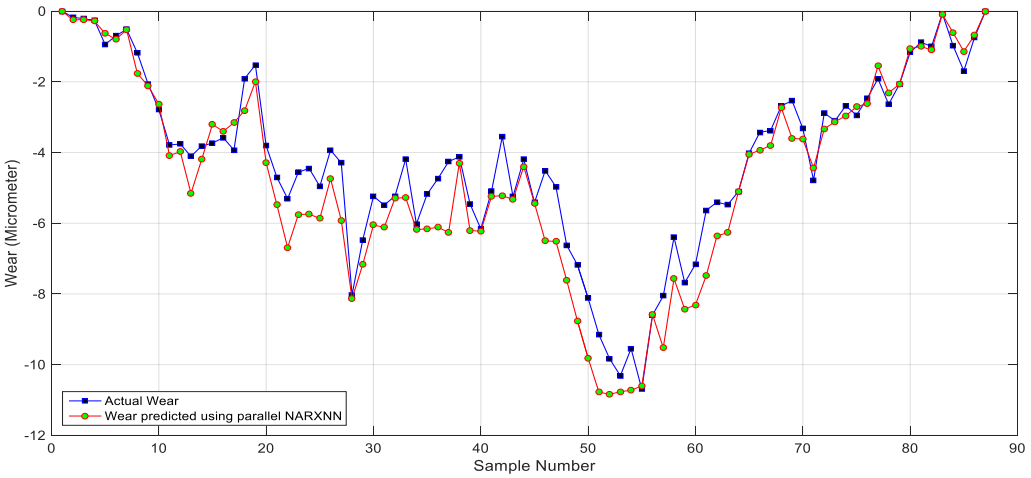

Figure 5. 19 Actual wheel wear and predicted using parallel NARXNN under dry conditions

The actual rail wear and the rail wear predicted using series-parallel NARXNN are shown in Figure 5.20.

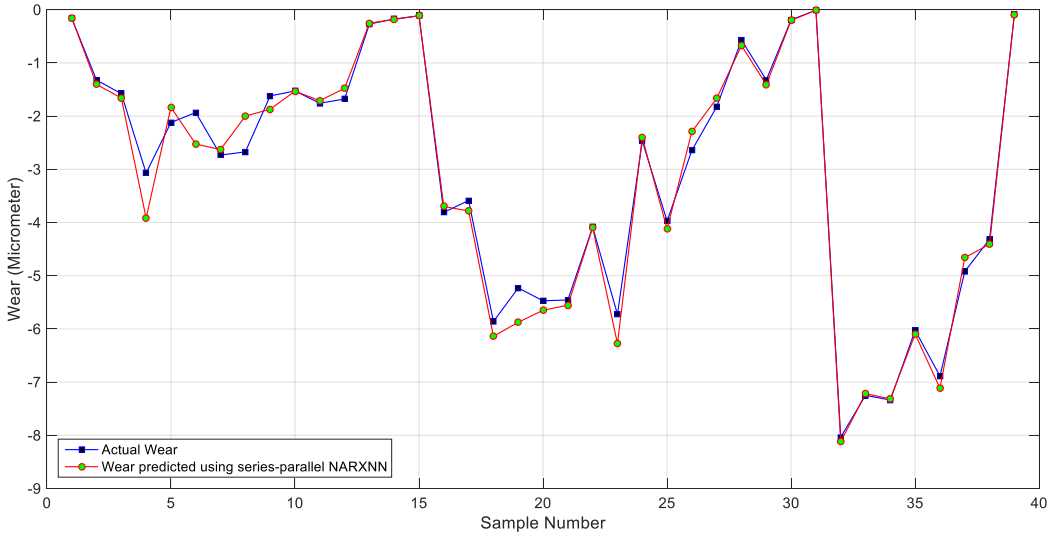

Figure 5. 20 Actual rail wear and predicted using series-parallel NARXNN under dry conditions

The actual rail wear and the rail wear predicted using parallel NARXNN are shown in Figure 5.21.

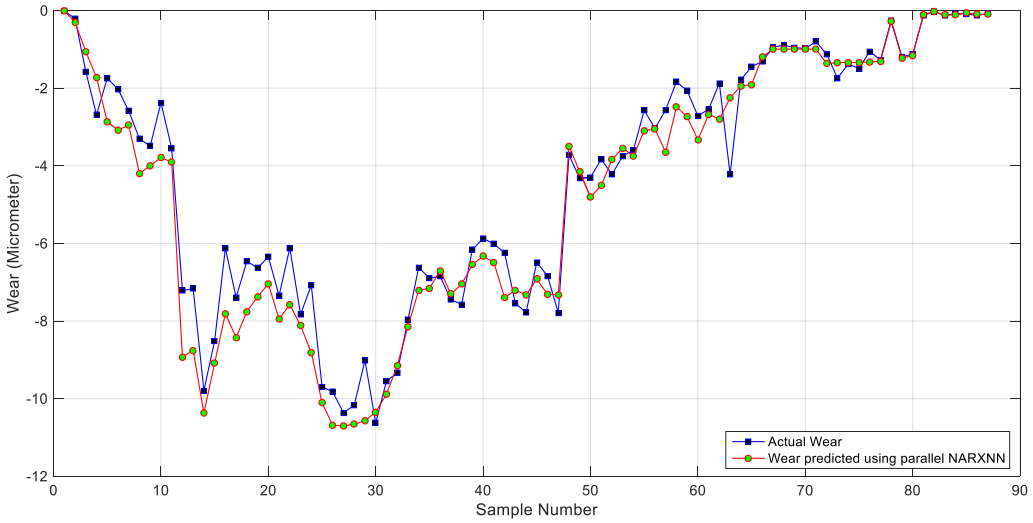

Figure 5. 21 Actual rail wear and predicted using parallel NARXNN under dry conditions

In the following sections, the left graphs show the actual and predicted wheel/rail wear using series-parallel NARXNN; while the right grahps show the actual and predicted wheel/rail wear using parallel NARXNN.

5.7.2 Wheel wear and rail wear under wet conditions

The actual wheel wear and wheel wear predicted using series-parallel and parallel NARXNN are presented in Figure 5.22. The simulation results show that the predicted wheel wear was close to the actual wheel wear.

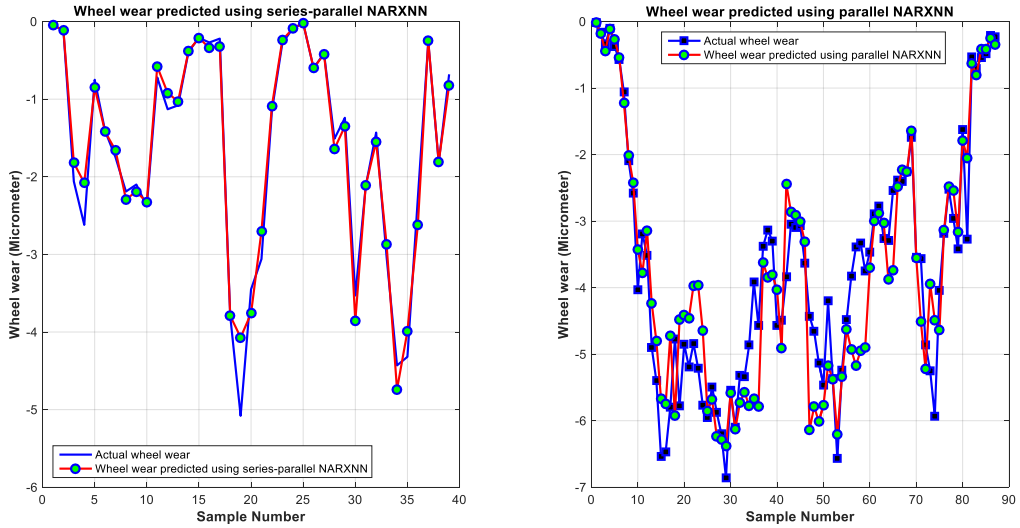

Figure 5. 22 Actual wheel wear and predicated using NARXNN under wet conditions

The actual rail wear and rail wear predicted using series-parallel and parallel NARXNN are presented in Figure 5.23. The simulation results show that the predicted rail wear was close to the actual rail wear.

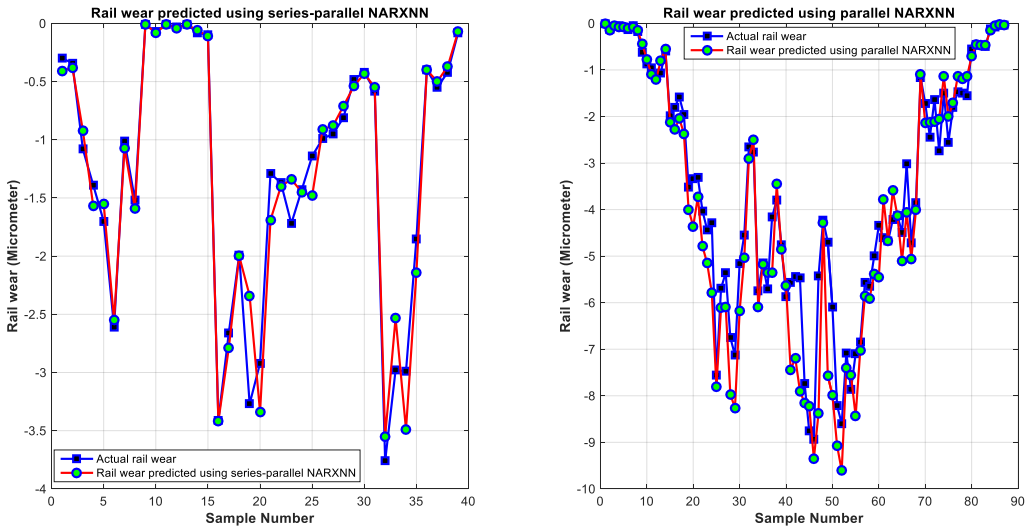

Figure 5. 23 Actual rail wear and predicated using NARXNN under wet conditions

5.7.3 Wheel wear and rail wear under lubricated conditions

The actual wheel wear and wheel wear predicted using series-parallel and parallel NARXNN are presented in Figure 5.24. The simulation results show that the predicted wheel wear was close to the actual wheel wear.

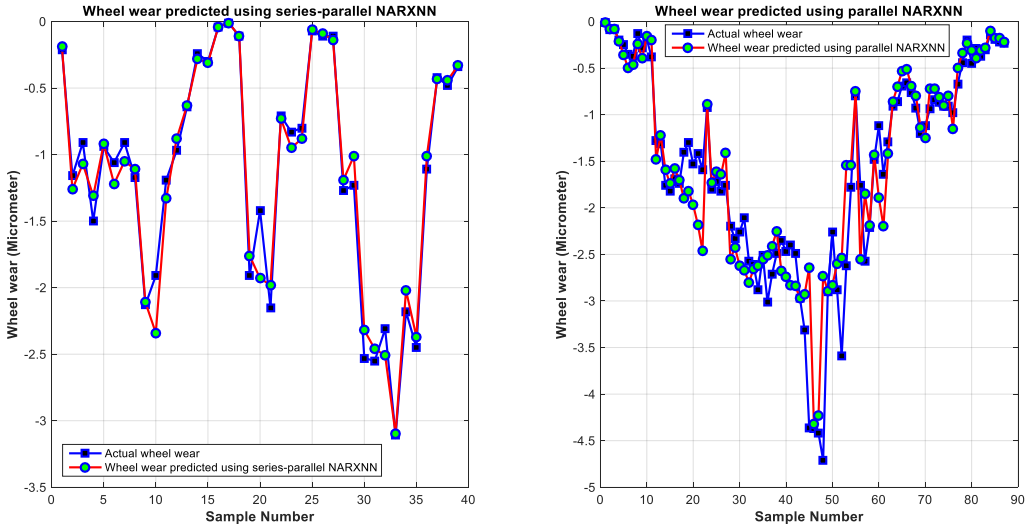

Figure 5. 24 Actual wheel wear and predicated using NARXNN under lubricated conditions

The actual rail wear and rail wear predicted using series-parallel and parallel NARXNN are presented in Figure 5.25. The simulation show that the predicted rail wear was close to the actual rail wear.

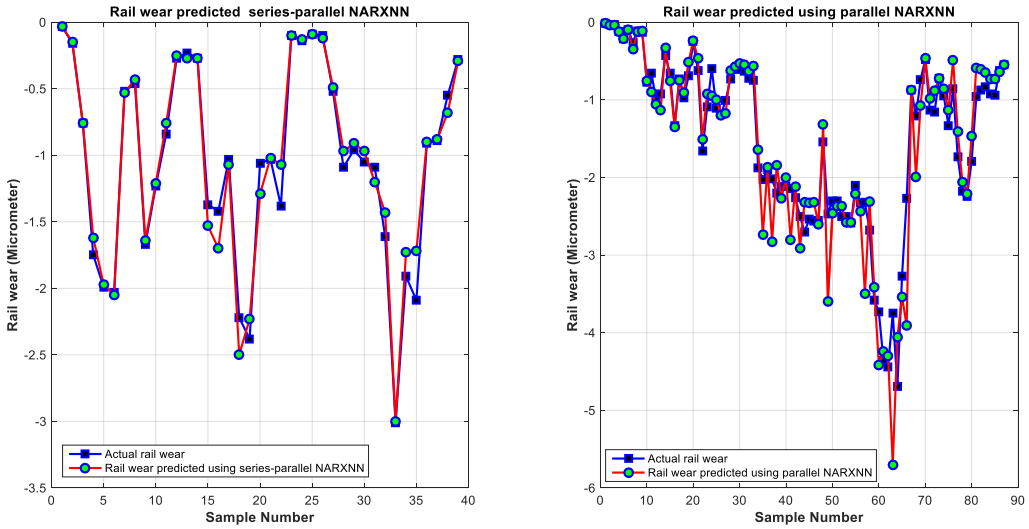

Figure 5. 25 Actual rail wear and predicated using NARXNN under lubricated conditions

5.7.4 Wheel wear and rail wear under sanded conditions

The actual wheel wear and wheel wear predicted using series-parallel and parallel NARXNN are presented in Figure 5.26. The simulation results show that the predicted wheel wear was close to the actual wheel wear.

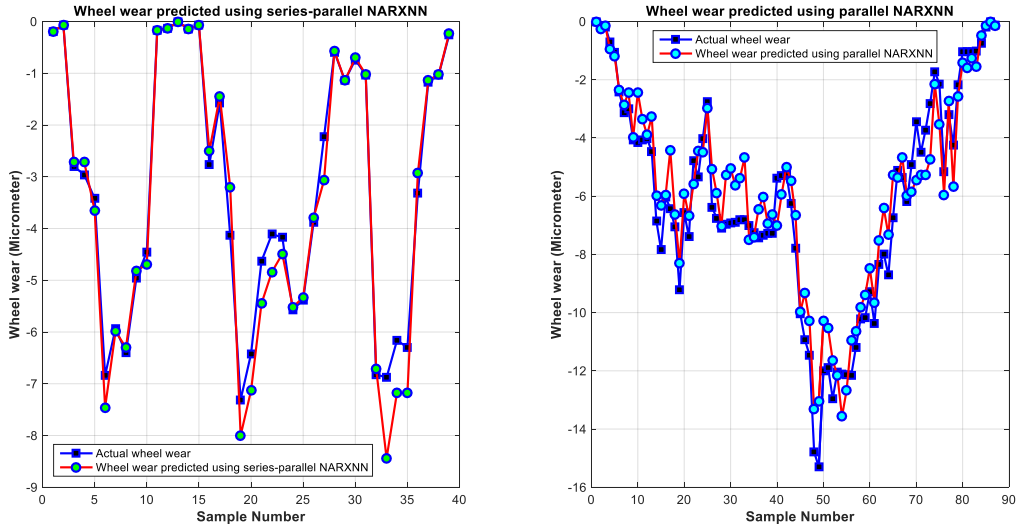

Figure 5. 26 Actual wheel wear and predicated using NARXNN under sanded conditions

The actual rail wear and rail wear predicted using series-parallel and parallel NARXNN are presented in Figure 5.27. The simulation results show that the predicted rail wear was close to the actual rail wear.

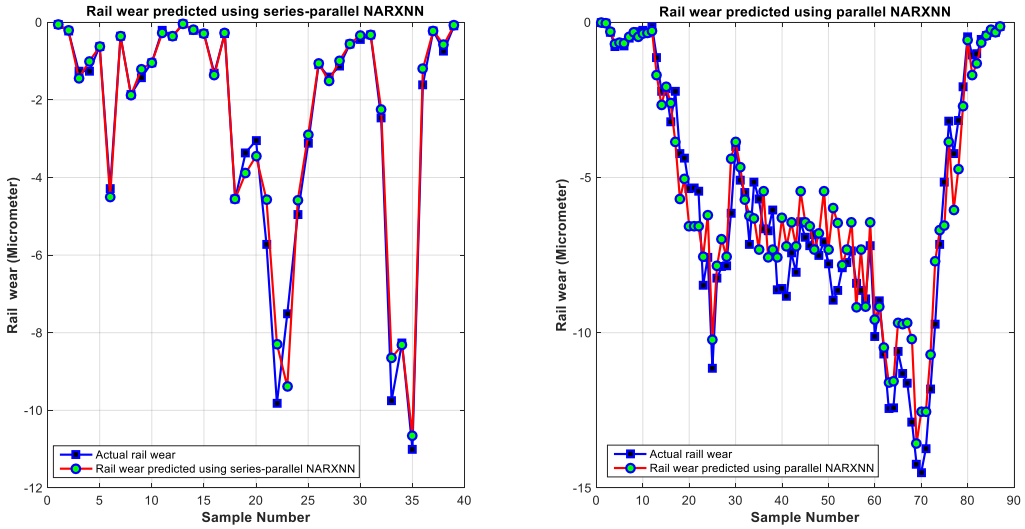

Figure 5. 27 Actual rail wear and predicated using NARXNN under sanded conditions

The actual and predicted wheel/rail wear, percentage error, and mean absolute percentage error under dry, wet, lubricated, and sanded conditions were shown in Tables in appendix 6.

5.7.5 Section discussion

Series-parallel and parallel NARXNN were developed to predict the wheel wear and rail wear for the twin disc test rig under dry, wet, lubricated, and sanded conditons. The accuracy of the wheel wear and rail wear prediction using neural network model under wet, lubricated, and sanded conditions are illustrated in Table 5.2 and Table 5.3 respectively. The accuracy of neural network model was calculated in terms of mean absolute percentage error (MAPE).

	Dry	Wet	Lubricated	Sanded
MAPE% for series-parallel NARXNN	8.58%	8.54%	8.94%	6.63%
MAPE% for parallel NARXNN	16.93%	14.46%	18.63%	17.49%

Table 5. 2 MAPE for wheel wear prediction using series-parallel and parallel NARXNN

	Dry	Wet	Lubricated	Sanded
MAPE% for series-parallel NARXNN	7.17%	11.37%	7.54%	9.54%
MAPE% for parallel NARXNN	16.01%	15.31%	15.87%	15.95%

Table 5. 3 MAPE for rail wear prediction using series-parallel and parallel NARXNN

The percentage error for wheel/rail wear prediction was calculated, and the results show good prediction of wheel and rail wear in term of percentage error, where the wheel wear and rail wear predicted using NARXNN was close to actual wheel wear and rail wear.

The MAPE was between 6.63% and 11.37% for series-parallel NARXNN; then, the accuracy of NARXNN model was between 88.63% and 93.37%. The MAPE was between 14.46% and 18.63% for parallel NARXNN; then, the accuracy of NARXNN model was between 81.37% and 85.54%. Therefore, the accuracy of the NARXNN model was between 81.37% and 93.37%.

- The results shown in Table 5.2 and Table 5.3 show that the wheel/rail wear predicted using the neural network model was close to the measured wheel/rail wear, where the MAPE was between 6.63% and 18.63%.
- The series-parallel NARXNN was more accurate than the parallel NARXNN for wheel/rail wear prediction.
- The difference in the values of MAPE shown in Table 5.2 and Table 5.3 is due to the values of the input parameters used to train the neural network.

5.7.6 Wheel wear and rail wear prediction under dry conditions (with different architecture of neural network)

In this section additional simulations carried out with different neural network architecture are reported on.

The three architectures of NARXNN were:

6-7-1 (6 inputs, 7 hidden layer, and 1 output layer).

6-10-1 (6 inputs, 10 hidden layer, and 1 output layer).

6-13-1 (6 inputs, 13 hidden layer, and 1 output layer).

The range of yaw angle used with the series-parallel NARXNN was 0.2 degree, 0.3 degree, and 0.4 degree, while 0.5 degree was used with parallel NARXNN.

The wheel/rail wear predicted using the three NARXNN architecture were copmared with the actual wheel/rail wear such as shown in the following sections:

The actual wheel wear, and the wheel wear predicted using series-parallel NARXNN are shown in Figure 5.28.

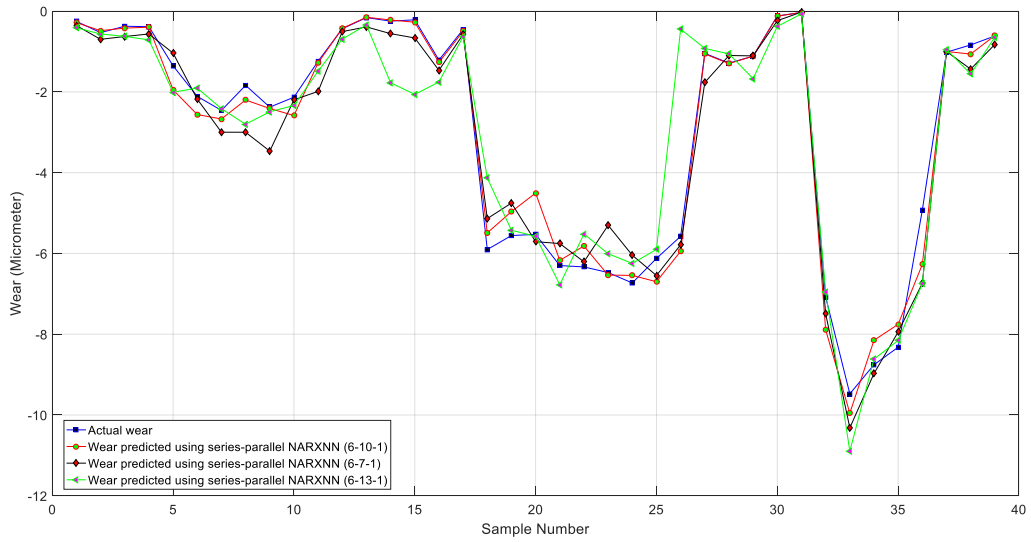

Figure 5. 28 Actual wheel wear and predicted using series-parallel NARXNN under dry conditions

The actual wheel wear and the wheel wear predicted using parallel NARXNN are shown in Figure 5.29.

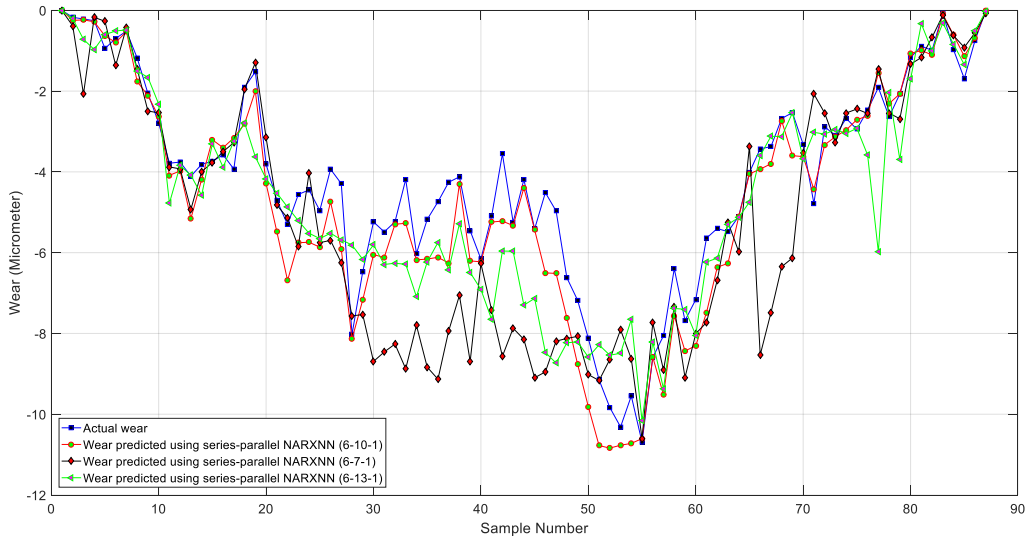

Figure 5. 29 Actual wheel wear and predicted using parallel NARXNN under dry conditions

The actual rail wear and the rail wear predicted using series-parallel NARXNN are shown in Figure 5.30.

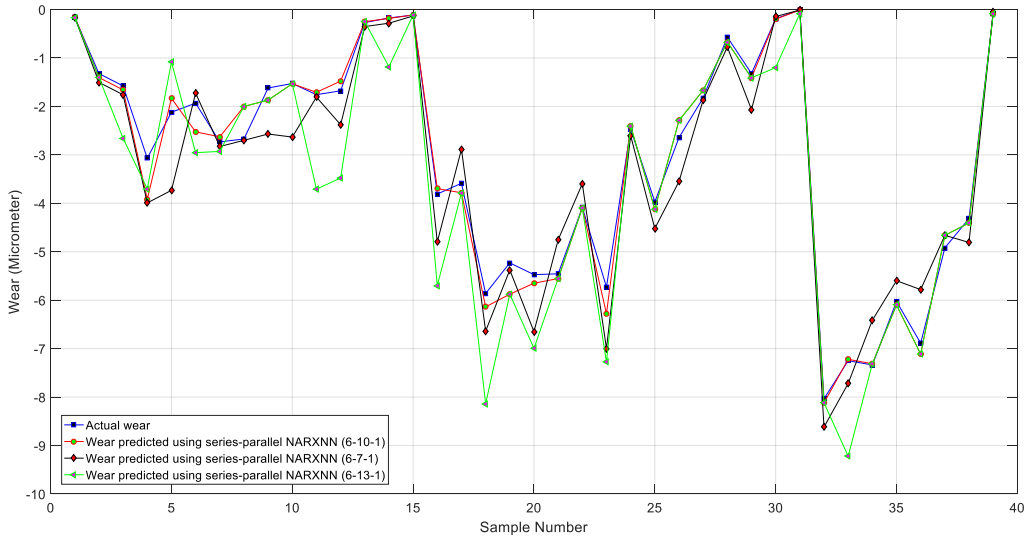

Figure 5. 30 Actual rail wear and predicted using series-parallel NARXNN under dry conditions

The actual rail wear and the rail wear predicted using parallel NARXNN are shown in Figure 5.31.

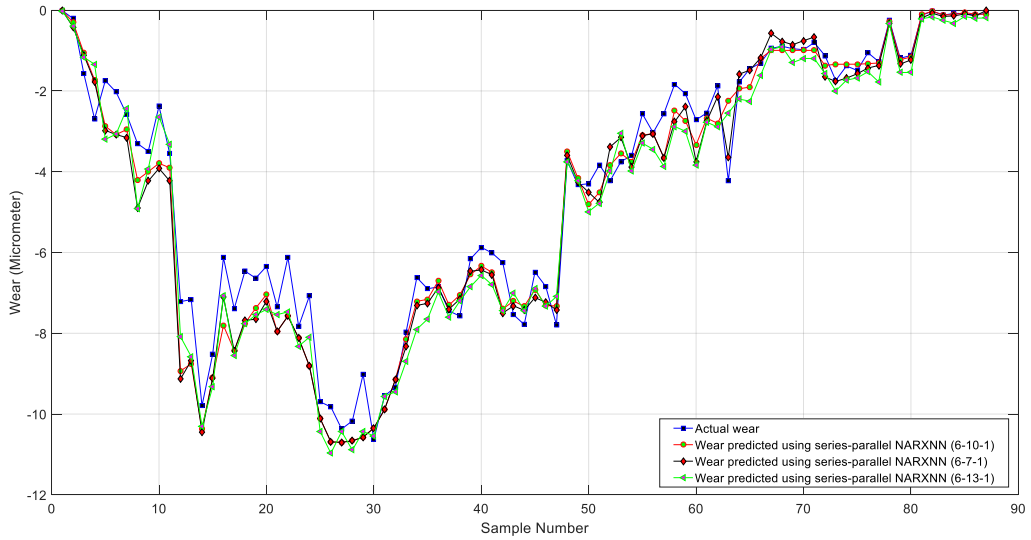

Figure 5. 31 Actual rail wear and predicted using parallel NARXNN under dry conditions

5.8 Section discussion

Series-parallel and parallel NARXNN were developed to predcit the wheel wear and rail wear for the twin disc test rig under dry conditions with different architectures of the neural networks. The accuracy of the wheel wear and rail wear prediction using the neural network models is shown in Table 5.4 and Table 5.5. The accuracy of neural network model was calculated in terms of mean absolute percentage error (MAPE).

Architecture:	6-7-1	6-10-1	6-13-1
MAPE% for series-parallel NARXNN	35.8%	8.58%	72.07%
MAPE% for parallel NARXNN	36.44%	16.93%	55.67%

Table 5. 4 MAPE for wheel wear prediction using series-parallel and parallel NARXNN

Architecture:	6-7-1	6-10-1	6-13-1
MAPE% for series-parallel NARXNN	22.03%	7.17%	69.44%
MAPE% for parallel NARXNN	21.81%	16.01%	34.85%

Table 5. 5 MAPE for rail wear prediction using series-parallel and parallel NARXNN

- For wheel wear the MAPE was 35.8% for series-parallel NARXNN (6-7-1), 8.58% for series-parallel NARXNN (6-10-1), and 72.07% for series-parallel NARXNN (6-13-1).
- For wheel wear the MAPE was 36.44% for parallel NARXNN (6-7-1), 16.93% for parallel NARXNN (6-10-1), and 55.67% for parallel NARXNN (6-13-1).
- For rail wear the MAPE was 22.03% for series-parallel NARXNN (6-7-1), 7.17% for series-parallel NARXNN (6-10-1), and 69.44% for series-parallel NARXNN (6-13-1).
- For rail wear the MAPE was 21.81% for parallel NARXNN (6-7-1), 16.01% for parallel NARXNN (6-10-1), and 34.85% for parallel NARXNN (6-13-1).

- The accuracy of wheel/rail wear prediction using NARXNN was investigated and assessed in term of MAPE such as:

➢ The MAPE for series-parallel NARXNN (6-10-1) was 8.58%, it was smaller than the MAPE for the series-parallel NARXNN (6-7-1) and series-parallel NARXNN (6-13-1). Therefore, the series-parallel NARXNN (6-10-1) was more accurate than the series-parallel NARXNN (6-7-1) and series-parallel NARXNN (6-13-1) for wheel wear prediction.

➢ The MAPE for parallel NARXNN (6-10-1) was 7.17%, it was smaller than the MAPE for the parallel NARXNN (6-7-1) and parallel NARXNN (6-13-1). Therefore, the parallel NARXNN (6-10-1) was more accurate than the parallel NARXNN (6-7-1) and parallel NARXNN (6-13-1) for rail wear prediction.

5.9 Chapter conclusion

The twin disc rig was used in this project to investigate wheel wear and rail wear under dry, wet, lubricated and sanded conditions. Then, a neural network model was developed to predict the wheel wear and rail wear for the twin disc test rig experiments. The inputs of this model were the load, the yaw angle, the speed, the wheel/rail profile, the first derivative of wheel/rail profile, and the second derivative of wheel/rail profile; while the output of neural network model was the wheel/rail wear.

The test data was then collected and used to examine the ability of neural network to predict wheel wear and rail wear. This study has verified the ability of series-parallel NARXNN to make closely accurate predictions. Parallel NARXNN developed to predict the wheel wear and rail wear for the case of new samples.

The simulation results show that the wheel wear and rail wear predicted using NARXNN was close to actual wear for unseen data under dry, wet, lubricated, and sanded conditions. The optimal results during training and testing of the NARXNN obtained with input delays were 1:2, feedback delay 1:2, and 1 hidden layer with 10 neurons.

The findings obtained using the proposed neural approach yielded better results from the perspective of the mean absolute percentage error (MAPE) measure. The accuracy of the NARXNN model was between 81.37% and 93.37%. Therefore, it can be concluded that an artificial neural network can be used efficiently as a predictor of wheel wear and rail wear for a twin disc rig experiments.

The accuracy of wheel/rail wear prediction using neural network was influenced by the architecture of neural network.

Chapter 6 Prediction of railway wheel wear using an artificial neural network for a railway vehicle

In this work, an artificial neural network was developed to predict railway wheel wear in case of changing parameters such as speed, longitudinal bush stiffness, lateral bush stiffness, vertical bush stiffness, longitudinal bush stiffness, lateral bush stiffness, and vertical shear stiffness.

In order to provide the data to train, validate, and test the neural network during wheel wear prediction the VAMPIRE vehicle dynamics software tool was used. Passenger vehicle model, UK wheel profile type of P8, UK rail profile type of BS113a-20, and straight track was set up using VAMPIRE (Appendix 7). The following suspension parameters were used in this work to predict wheel wear using neural networks: primary bush (longitudinal stiffness), and primary spring (longitudinal stiffness).

6.1 Introduction to VAMPIRE vehicle dynamics software

VAMPIRE uses a multi-body modelling method that enables the user to assemble a mathematical model of almost any rail vehicle configuration. The VAMPIRE pro. 6.30 was used in this work to perform the simulations. The VAMPIRE GUI is shown in Figure 6.1. For wheel wear prediction, the transient analysis programme is run and the energy expended per unit distance travelled calculated for each wheel/rail contact. This is the product of creep force and creepage (Tγ), is one of the output types available in the transient programme. Experimental work has demonstrated that the amount of metal removed through wheel is proportional to the energy dissipated in the wheel–rail contact. Therefore, the expected wear of wheel can be studied and predicted by calculating the energy dissipated between wheel and rail (Tγ) [156], [157].

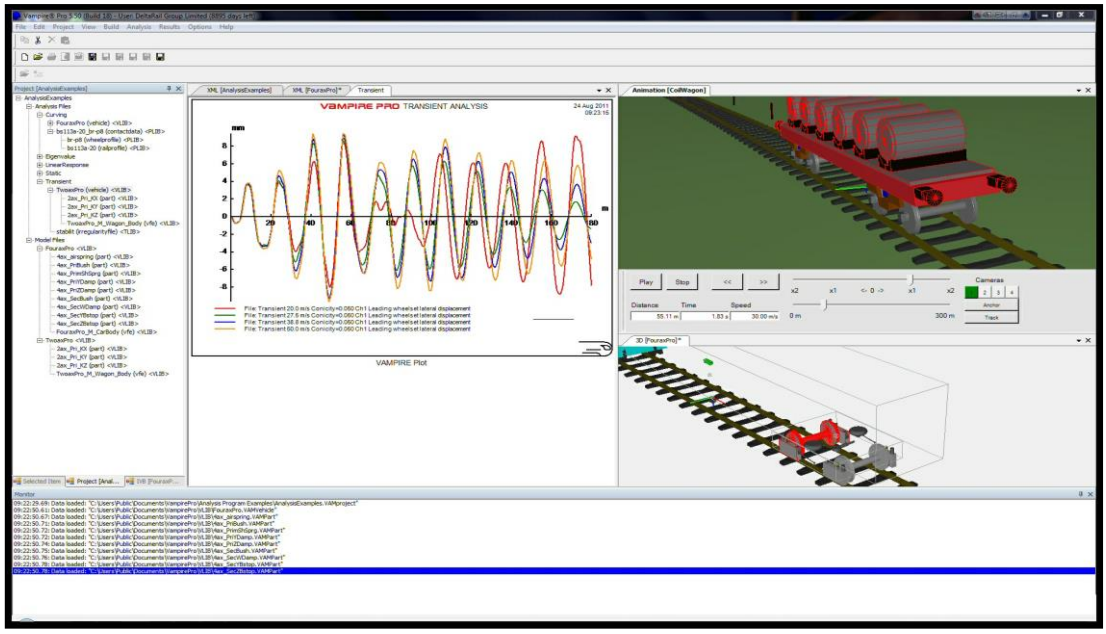

Figure 6. 1 VAMPIRE vehicle dynamics software platform [156], [157]

VAMPIRE Pro contains all the pre-processing and post-processing options required to perform the railway studies and investigations such as vehicle design, track damage, and accident investigation. The pre-processors include tools for wheel rail contact data, and track plotting. The post-processors include extensive plotting facilities for simulation data, statistical analysis, and data filtering. Analysis programs include non-linear transient response analysis, linear eigenvalue analysis, curving analysis, and static analysis [157].

Table 6.1 shows the types of straight track provided by VAMPIRE vehicle dynamics software, it shows the line speed, track length, and standard deviation of lateral and vertical irregularities. All the sections of track are straight but include measured cant and curvature irregularities.

TRACK	Line Speed	Length	Std. Dev.	Std. Dev.
	Km/h		Lateral	Vertical
TRACK110	110	5km	3.04mm	5.12mm
TRACK160	160	5km	2.46mm	2.77mm
TRACK200	200	5km	1.42mm	2.39mm
TRACK225	225	5km	1.36mm	2.00mm
TRACK270	270	4km	1.04mm	1.81mm

Table 6. 1 Track types used by VAMPIRE vehicle dynamics software [156], [157]

The neural network approach in this thesis focussed on straight track to demonstrate the potential of the methods used. Further work would be required to evaluate the applicability on the more complex case with curved track.

6.2 The methodology of wheel wear prediction using VAMPIRE software

The methodology of wheel wear prediction using VAMPIRE is shown in Figure 6.2. The VAMPIRE multibody software was used to carry out vehicle-track simulations to simulate the energy dissipated ($T\gamma$) and the contact position between wheel and rail at each wheel/rail contact .

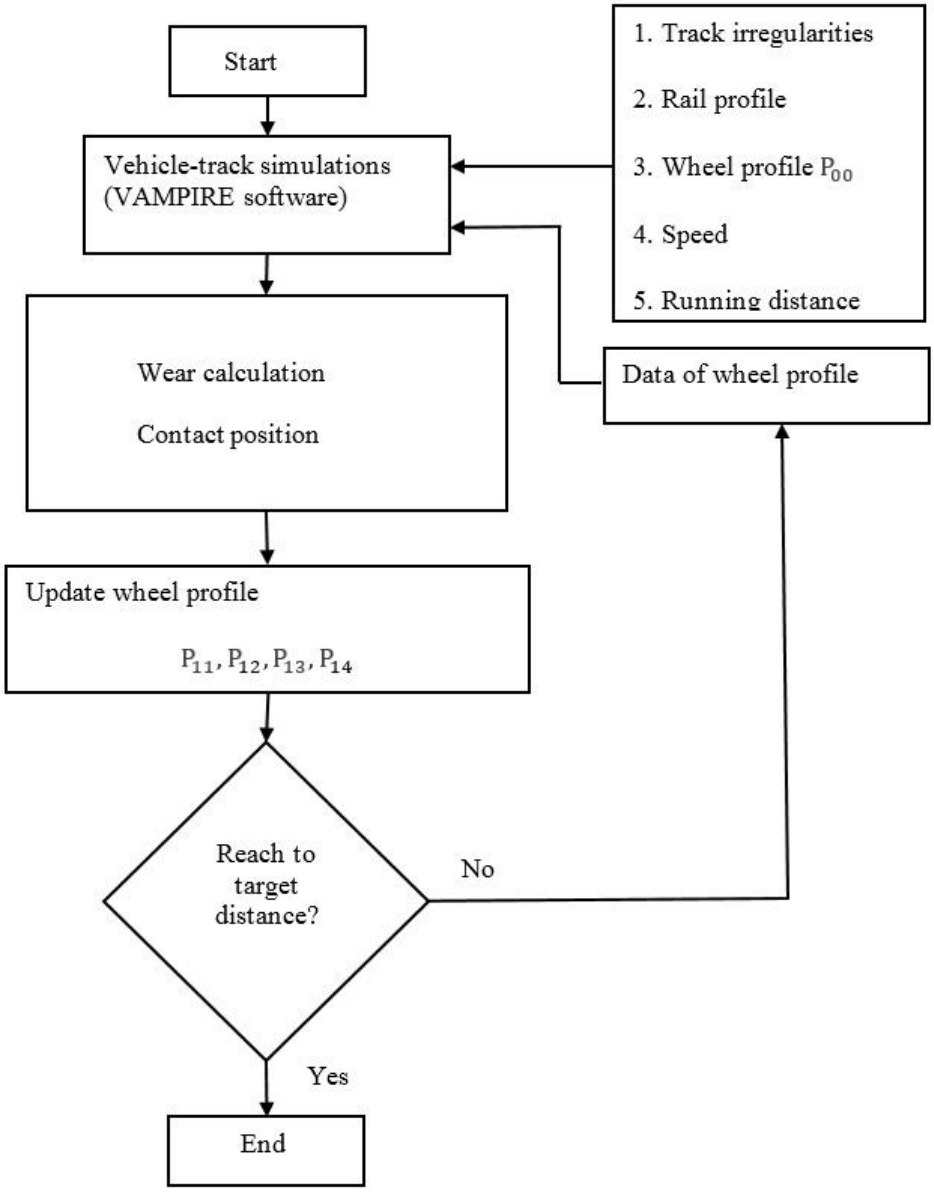

Figure 6. 2 Methodology of wheel wear prediction using VAMPIRE software [76], [77]

In this project, wheel wear was predicted using energy dissipated (Tγ) and contact position between wheel and rail, such as shown in the following steps:

1. An initial new wheel profile (called P_{00}), track with irregularities (track110), rail profile, speed, and running distance were provided to the VAMPIRE software.
2. Tγ at the wheel tread and rail at the location of the contact were defined as outputs in VAMPIRE software.
3. The VAMPIRE dynamic simulation was run.
4. Tγ and the position of wheel on rail were used to calculate the wear index (wheel tread wear) as shown in Figure 6.3; to obtain the worn wheel profile (called P_{11}); the wheel wear at w1 to w18 was estimated using Matlab program as shown in appendix 8 (Wheel wear estimated after different running distances 50000km, 100000km, 150000km, and 200000km).
5. The worn wheel profile P_{11} was used as input to the VAMPIRE software.
6. The steps 2 to 5 were repeated until the wheel profiles P_{12}, P_{13}, and P_{14} were obtained at speed of 5m/s.

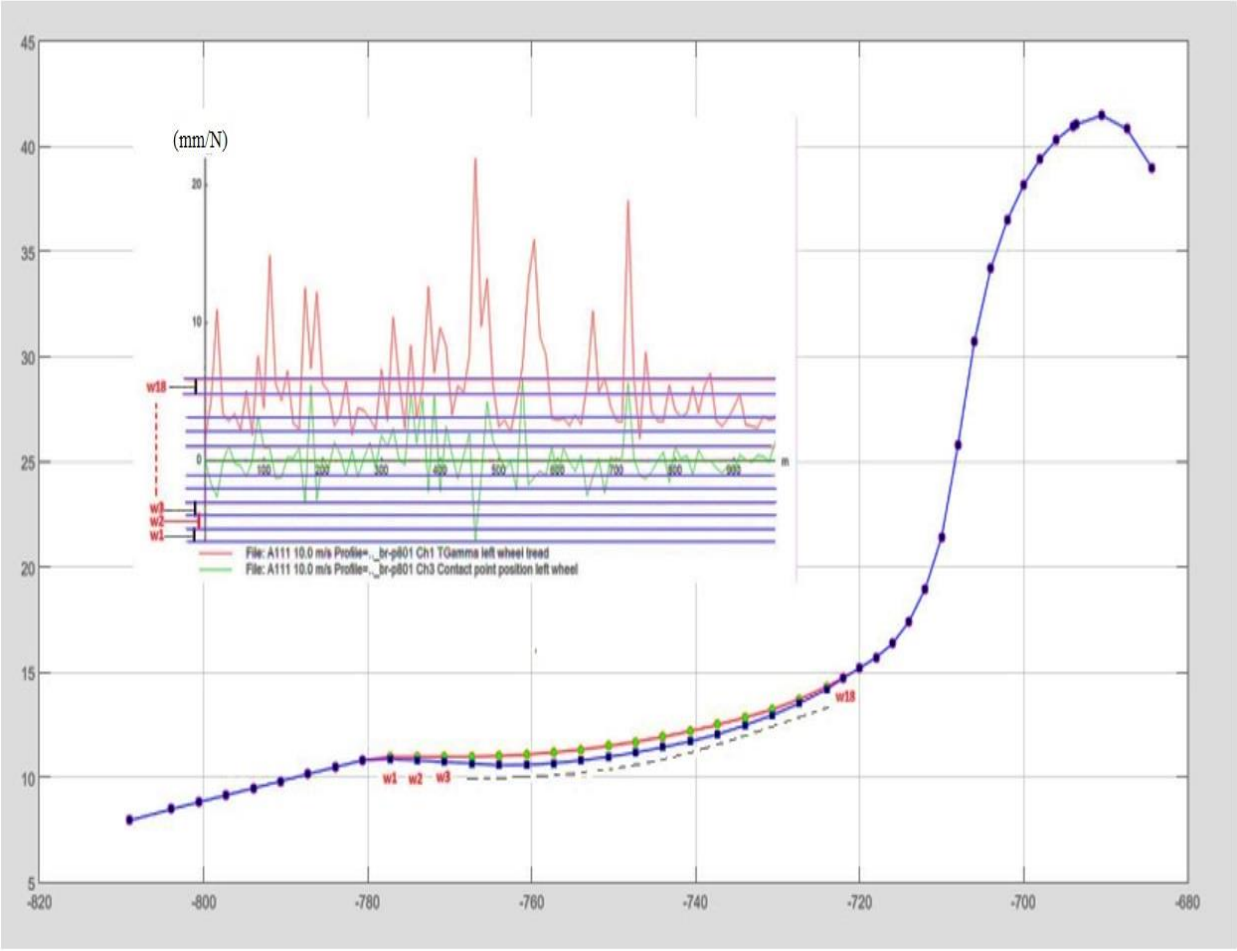

Figure 6. 3 Wheel tread wear estimation using Tγ and contact position

The wear of wheel can be described as a loss in cross-sectional area as a function of energy dissipated between wheel and rail. The wear can be described as a loss in cross-sectional area due to the passage of a known number of vehicle axles ($mm^2/1000$ axles) [158]. The wear can be defined as in the following equations [156], [157]:

1. For mild wear if $T\gamma < 160N$:

$$\text{Wear} = T\gamma * 0.005 \ (mm^2/1000 \text{ axles}). \quad (6.1)$$

2. For severe wear if $T\gamma \geq 160N$:

$$\text{Wear} = T\gamma * 0.025 - 3.2 \ (mm^2/1000 \text{ axles}). \quad (6.2)$$

The $T\gamma$ in all tests in this project was less than 160N; then the wear was calculated using the following equation:

$$\text{Wear} = T\gamma * 0.005 * 10^{-4} \quad (6.3)$$

In the Vampire program, the Wheel Rail Wear program was used for wheel wear prediction.

The following section outlines how the wheel wear was established after different running distances (50000km, 100000km, 150000km, and 200000km) such as shown in Figure 6.2 and Figure 6.3.

The new wheel profile P_{00} was uploaded to Vampire, then the Vampire program was run, after that, the contact position and energy dissipated ($T\gamma$) were obtained.

For the distance of 50000km, and at speed of 5m/s, the wear calculated using the equation 6.3.

Since the track distance was 5000m, and the simulation step in the Vampire was 5, then, 1000 values of the energy dissipated ($T\gamma$) were obtained , then 1000 values of wear calculated.

After the 1000 values of wear were calculated, each values of wear occurring at same location on the profile were summed together, therefore, 18 summed values of wear were obtained (w1 to w18); The Matlab program shown in appendix 8 was used to calculate the w1 to w18 values.

The wear (w1 to w18) subtracted from the new wheel profile to obtain the worn wheel profile after running distance of 50000km.

Then, the worn wheel profile P_{11} (after running distance of 50000km) uploaded to vampire, the vampire program run; and calculate the worn wheel profile P_{12} and the wear after running distance of 100000km using same above steps.

The previous steps are repeated to estimate the worn wheel profile P_{13} and the wear after running distance of 150000km; after that, the previous steps repeated to estimate the worn wheel profile P_{14} and the wear after running distance of 150000km.

Change the speed to 10m/s and estimate the P_{21}, P_{22}, P_{23}, and P_{24}.

Change the speed to 20m/s and estimate the P_{31}, P_{32}, P_{33}, and P_{34}.

Change the speed to 30m/s and estimate the P_{41}, P_{42}, P_{43}, and P_{44}.

Figure 6.4 shows the energy dissipated (TGamma: Tγ) and the contact position at left wheel with track110, which is generated using the VAMPIRE software.

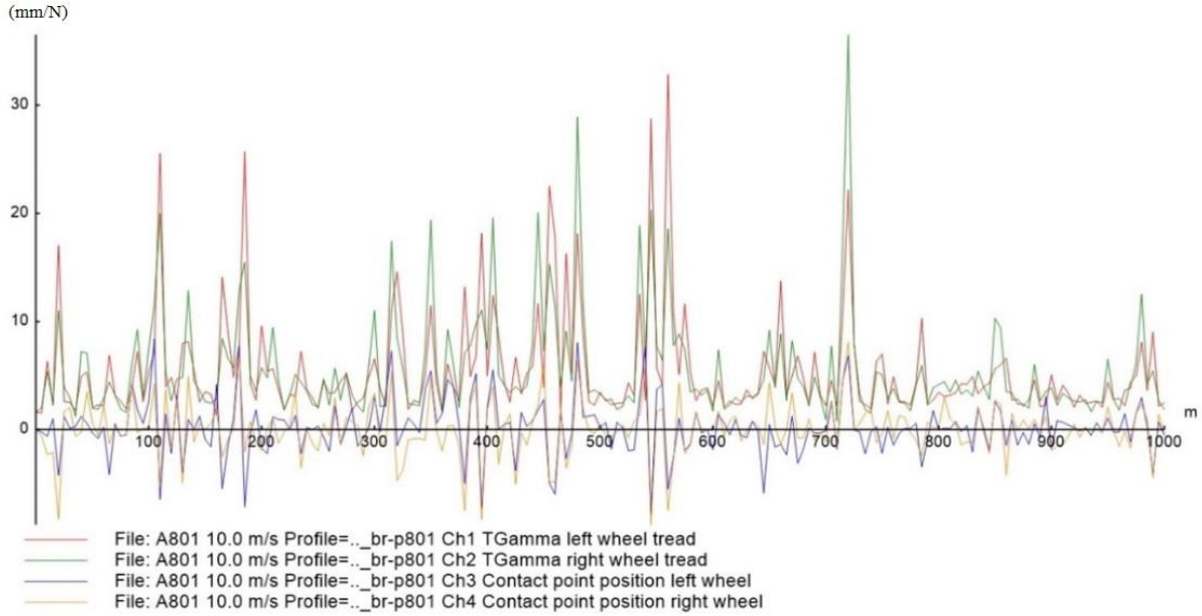

Figure 6. 4 Tγ [N] and contact position [mm] for left/right wheel tread on a straight track

Figure 6.5 illustrates the contact point position on a straight track, which is calculated using the VAMPIRE software, the wheel/rail contact position for zero lateral shift of wheelset relative to the rail was in range of -777mm to -722mm lateral shift.

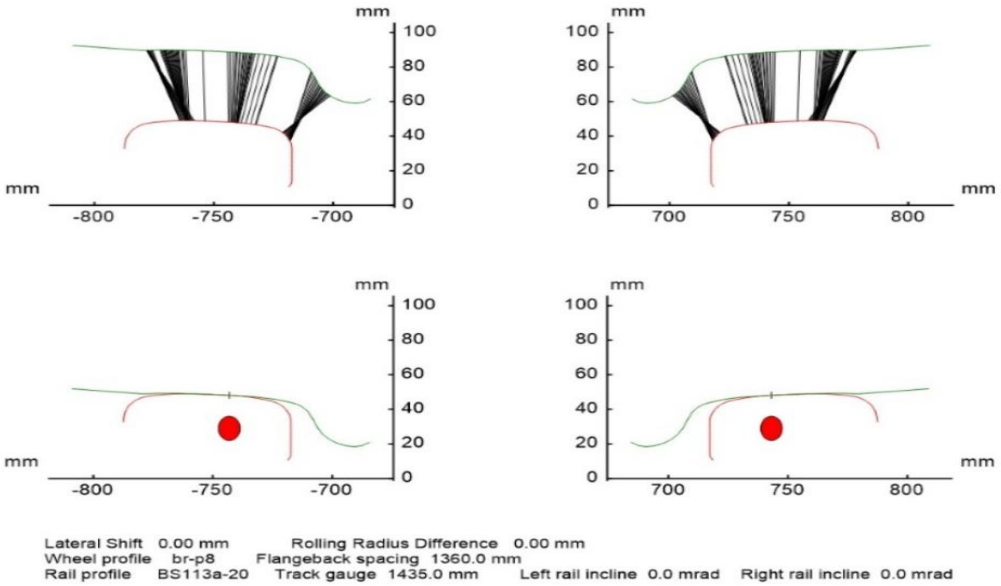

Figure 6. 5 Wheel/rail contact position for zero lateral shift of wheelset on a straight track

The transient response analysis was used in this project for wheel wear prediction. To create a transient analysis run file use the Run File Editor program. The calculation includes all the non–linear features of VAMPIRE vehicle models, and can use the full non–linear wheel/rail contact equations [156], [157].

6.3 Neural network model for the wheel wear prediction

The neural network model was developed to predict wheel wear is illustrated in Figure 6.6. Wheel profile before and after simulations were estimated using VAMPIRE software. A nonlinear autoregressive model with exogenous input neural network (NARXNN) was used in this chapter for wheel wear prediction.

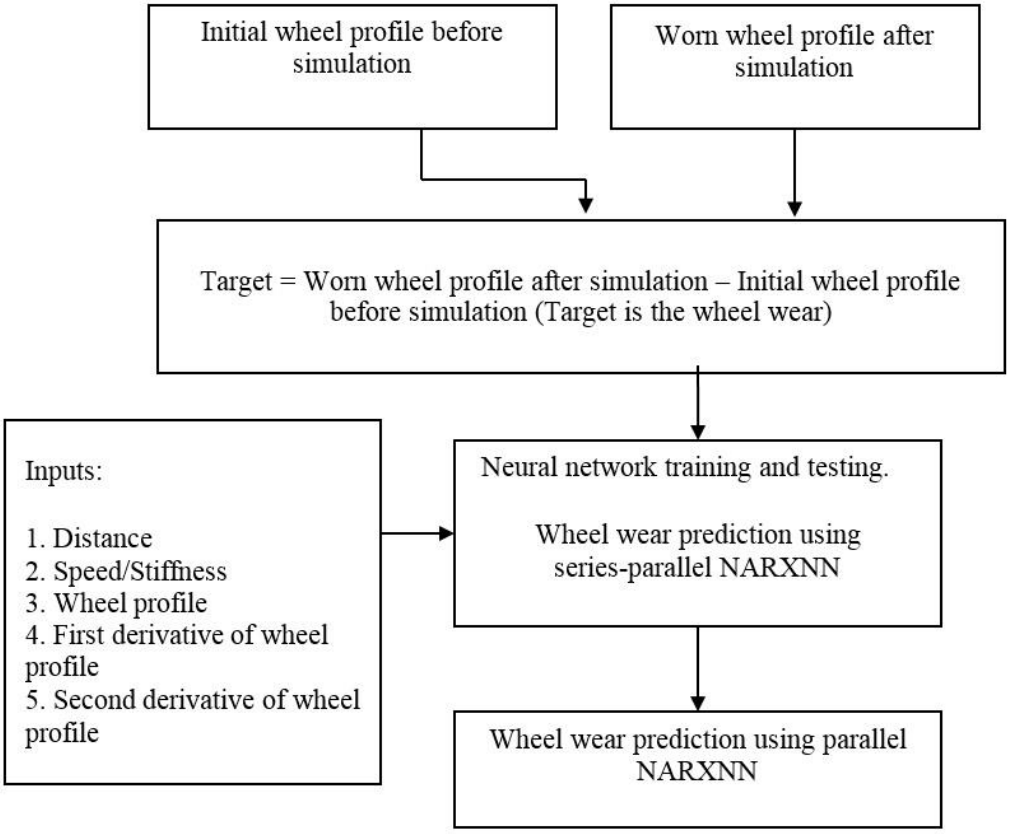

Figure 6. 6 Neural network model for wheel wear prediction

The speed, running distance, longitudinal bush stiffness, lateral bush stiffness, vertical bush stiffness, longitudinal bush stiffness, lateral bush stiffness, vertical shear stiffness, and wheel profile were selected as inputs to the neural network model because they are the parameters which had an effect on railway wheel wear during the simulations; and the first derivative of wheel profile and second derivative of wheel profile were selected as inputs to the neural network model because it presents the rate of change of wheel profile, these derivatives were assisted to train the neural networks. Matlab was used to calculate the first derivative of wheel profile and second derivative of wheel profile. The output of the neural network was the railway wheel wear.

- For wheel wear prediction using series-parallel NARXNN: The data which were obtained using VAMPIRE simulations were divided into three groups: 70% for training, 15% for validation, and 15% for testing of neural network. 216 samples were used to train, validate, and test the network.

- For wheel wear prediction using parallel NARXNN: The data which were obtained using VAMPIRE simulations were used to test the neural network. 18 samples were used to test the network.

The Matlab code which is shown in appendix 3 is to use the NARXNN for wheel wear prediction. The Matlab code which is shown in appendix 4 was used to calculate the mean absolute percentage error (MAPE), and the percentage error. The MAPE was calculated using equation 5.11, while the percentage error was calculated using equation 5.12. The railway wheel wear predicted using VAMPIRE, railway wheel wear predicted using NARXNN, percentage error, and mean absolute percentage error (MAPE) were shown in Tables in appendix 9. All results shown in this chapter are for unseen data.

6.3.1 Change of speed

The wheel profile with speed of 5m/s, 10m/s, 20m/s and 30m/s; running distance of 50000km, 100000km, 150000km, and 200000km are shown in Figure 6.7 respectively.

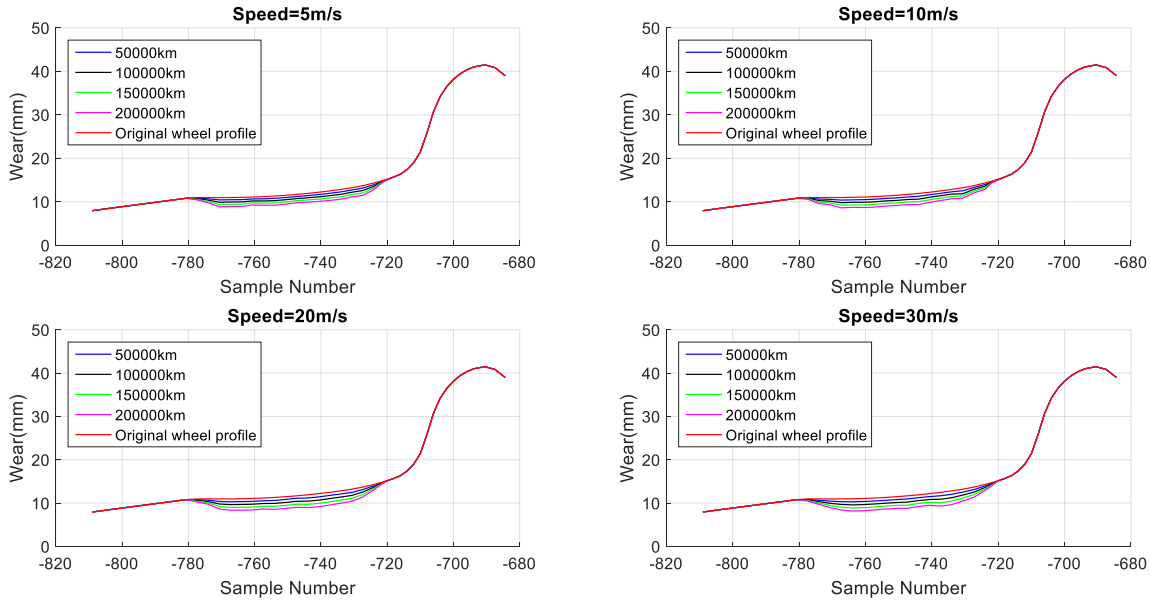

Figure 6. 7 Wheel profile evolution at different speeds

The wheel wear at different speeds are shown in provided in Figure 6.8.

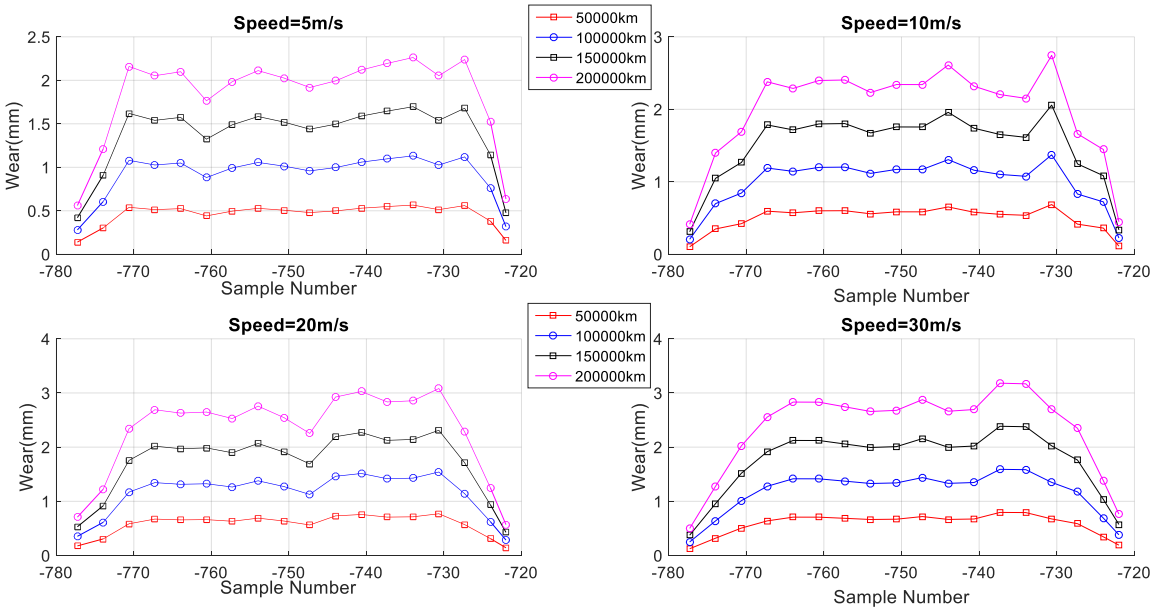

Figure 6. 8 Wheel wear at different speeds

1. Wheel wear prediction using the series-parallel NARXNN: The inputs to the neural network were: speed of 5m/s, 10m/s, and 20m/s; running distance of 50000km, 100000km, and 150000km; wheel profiles $P_{11}, P_{12}, P_{13}, P_{14}, P_{21}, P_{22}, P_{23}, P_{24}, P_{31}, P_{32}, P_{33}$, and P_{34}; first derivative of wheel profiles; and second derivative of wheel profiles; while the output of the neural network was wheel wear. The wheel wear predicted using VAMPIRE and the NARXNN are shown in Figure 6.9.

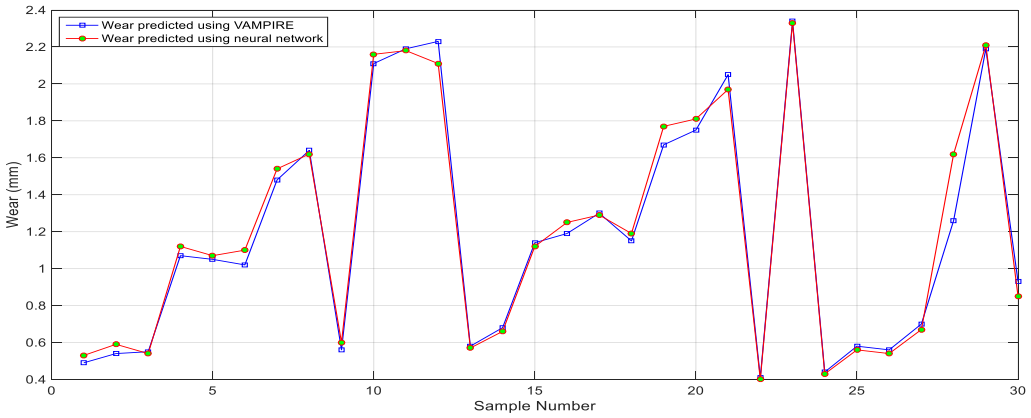

Figure 6. 9 Wheel wear predicted using VAMPIRE and series-parallel NARXNN

The simulation results show that the predicted wheel wear using neural network was close to wheel wear predicted using VAMPIRE. The mean absolute percentage error was 4.32%. Maximum predicted wear using VAMPIRE was 2.34mm.

2. Wheel wear prediction using parallel NARXNN. The inputs to the neural network were: speed of 30m/s; running distance of 200000km; wheel profile P_{44}; first derivative of wheel profile; and second derivative of wheel profile; while the output of the neural network was wheel wear. The wheel wear predicted using VAMPIRE and the NARXNN are shown in Figure 6.10.

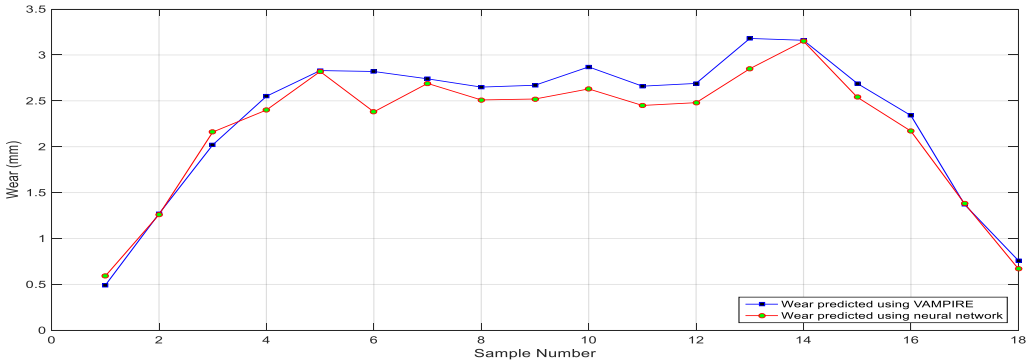

Figure 6. 10 The wheel wear predicted using VAMPIRE and parallel NARXNN

The simulation results show that the predicted wheel using neural network wear was close to wheel wear predicted using VAMPIRE. The mean absolute percentage error was 7.14 %. Maximum predicted wear using VAMPIRE was 3.18mm.

6.3.2 Change of longitudinal bush stiffness

The wheel profile for longitudinal bush stiffness of 30MN/m, 50MN/m, 70MN/m and 80MN/m; running distance of 50000km, 100000km, 150000km, and 200000km such as is shown in Figure 6.11 respectively.

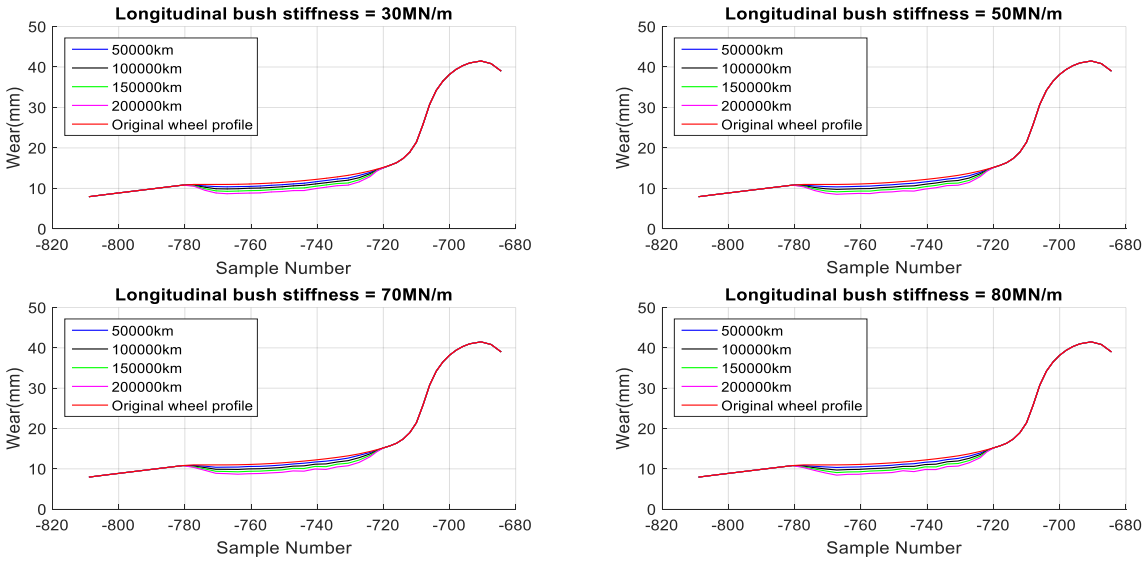

Figure 6. 11 Wheel profile evolution at different longitudinal bush stiffness

The wheel wear at different longitudinal bush stiffness are shown in Figure 6.12 respectively.

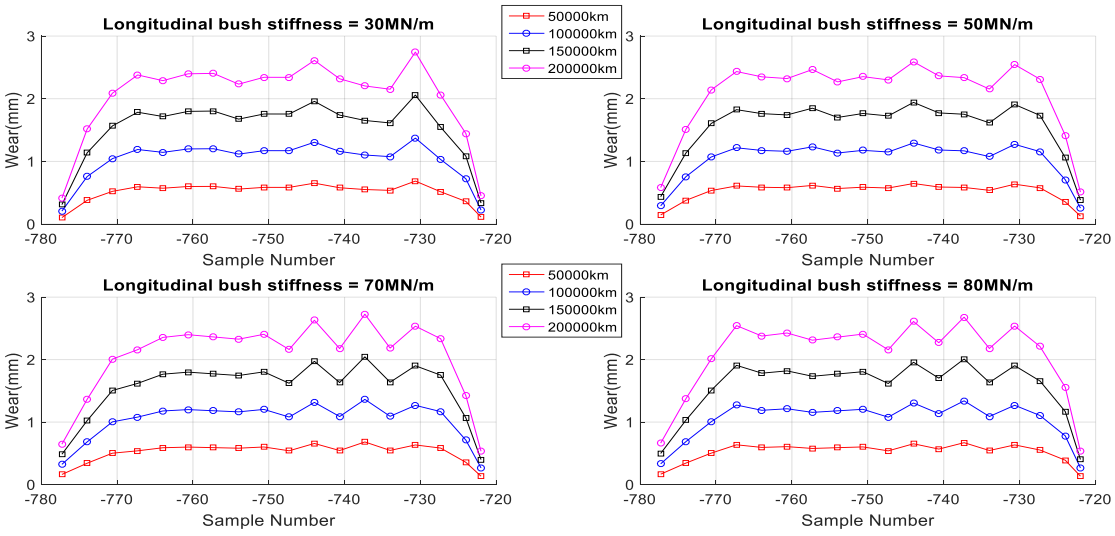

Figure 6. 12 Wheel wear at different longitudinal bush stiffness

1. Wheel wear prediction using the series-parallel NARXNN: The inputs to neural network are: longitudinal bush stiffness of 30MN/m, 50MN/m, and 70MN/m; running distance of 50000km, 100000km, and 150000km, wheel profiles $P_{11}, P_{12}, P_{13}, P_{14}, P_{21}, P_{22}, P_{23}, P_{24}, P_{31}, P_{32}, P_{33}$, and P_{34}; first derivative of wheel profile; and second derivative of wheel profile; while the output of the neural network was wheel wear. The wheel wear predicted using VAMPIRE and the NARXNN are given in Figure 6.13.

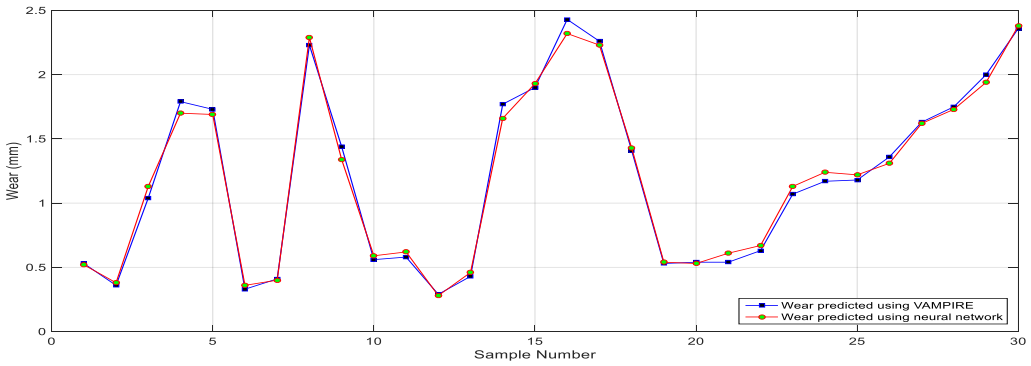

Figure 6. 13 Wheel wear predicted using VAMPIRE and series-parallel NARXNN

The simulation results show that the wheel wear predicted using neural netwrok was close to wheel wear predicted using VAMPIRE. The Mean absolute percentage error was 4.19%. Maximum predicted wear using VAMPIRE was 2.43mm.

2. Wheel wear prediction using parallel NARXNN: The inputs to the neural network were the longitudinal bush stiffness of 80MN/m, running distance of 200000km, wheel profile $P_{44}4$, first derivative of wheel profile, and second derivative of wheel profile; while the output of the neural network as wheel wear. The wheel wear predicted using VAMPIRE and the NARXNN are shown in Figure 6.14.

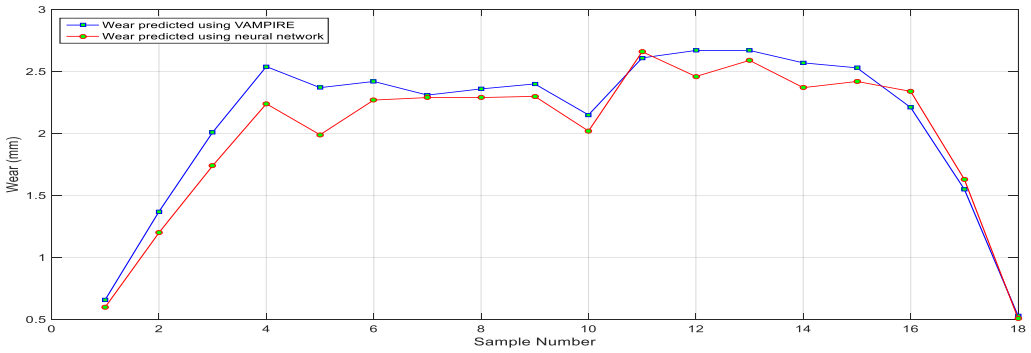

Figure 6. 14 Wheel wear predicted using VAMPIRE and parallel NARXNN (Unseen data)

The simulation results show that the predicted wheel wear using neural network was close to wheel wear predicted using VAMPIRE. The mean absolute percentage error was 7.46%. Maximum predicted wear using VAMPIRE was 2.67mm.

6.3.3 Change of lateral bush stiffness

The wheel profile with lateral bush stiffness of 2MN/m, 3MN/m, 4MN/m and 5MN/m; running distance of 50000km, 100000km, 150000km, and 200000km is shown in Figure 6.15 respectively.

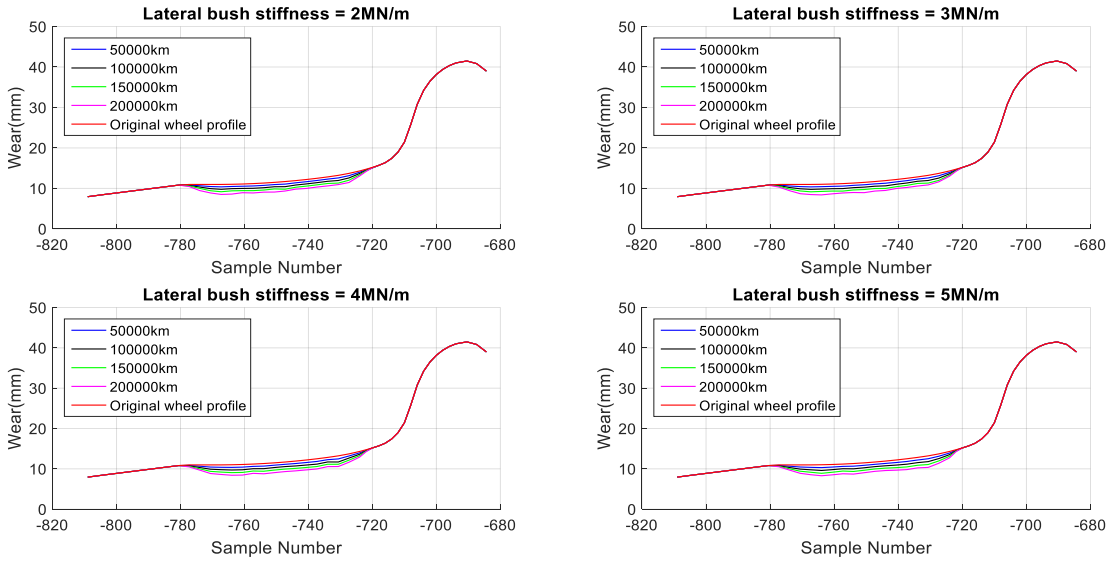

Figure 6. 15 Wheel profile evolution at different lateral bush stiffness

The wheel wear at different lateral bush stiffness are shown in Figure 6.16 respectively.

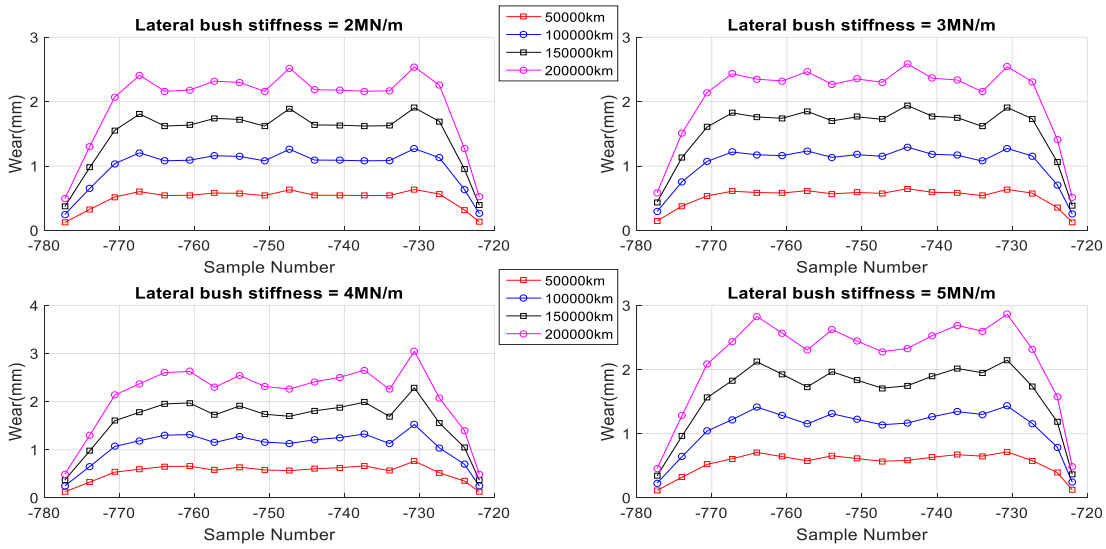

Figure 6. 16 Wheel wear at different lateral bush stiffness

1. Wheel wear prediction using series-parallel NARXNN: The inputs to the neural network are: lateral bush stiffness of 2MN/m, 3MN/m, and 4MN/m; running distance of 50000km, 100000km, and 150000km; wheel profiles $P_{11}, P_{12}, P_{13}, P_{14}, P_{21}, P_{22}, P_{23}, P_{24}, P_{31}, P_{32}, P_{33}$, and P_{34}; first derivative of wheel profile; and second derivative of wheel profile; while the output of the neural network was wheel wear. The wheel wear predicted using VAMPIRE and the NARXNN are shown in Figure 6.17.

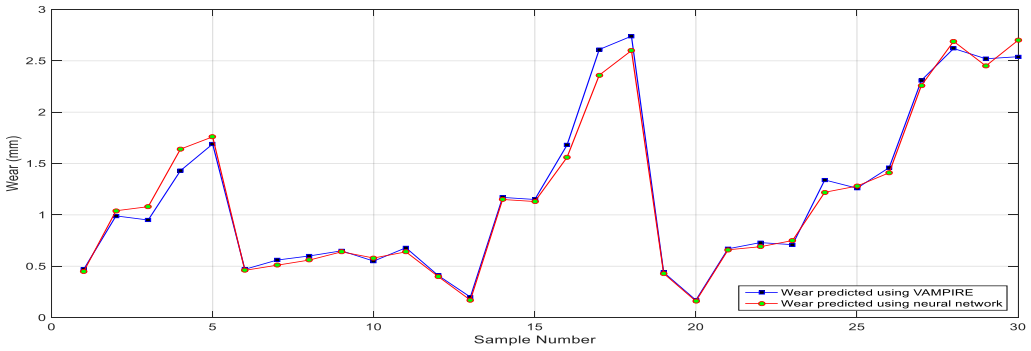

Figure 6. 17 Wheel wear predicted using VAMPIRE and series-parallel NARXNN

The simulation results show that the predicted wheel wear using neural network was close to wheel wear predicted using VAMPIRE. The mean absolute percentage error was 5.57%. Maximum predicted wear using VAMPIRE was 2.74mm.

2. Wheel wear prediction using parallel NARXNN: The inputs to the neural network were the lateral bush stiffness of 5MN/m, running distance of 200000km, wheel profile P_{44}, first derivative of wheel profile, and second derivative of wheel profile; while the output of the neural network was wheel wear. The wheel wear predicted using VAMPIRE and the NARXNN are shown in Figure 6.18.

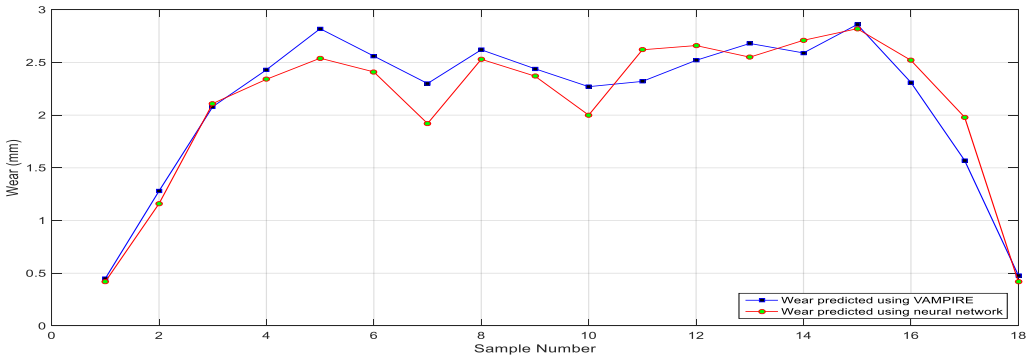

Figure 6. 18 Wheel wear predicted using VAMPIRE and parallel NARXNN

The simulation results show that the predicted wheel wear using neural network was close to wheel wear predicted using VAMPIRE. The mean absolute percentage error was 8.37%. Maximum predicted wear using VAMPIRE was 2.86mm.

6.3.4 Change of vertical bush stiffness

The wheel profile with vertical bush stiffness of 28MN/m, 30MN/m, 32MN/m and 34MN/m; running distance of 50000km, 100000km, 150000km, and 200000km is shown in Figure 6.19 respectively .

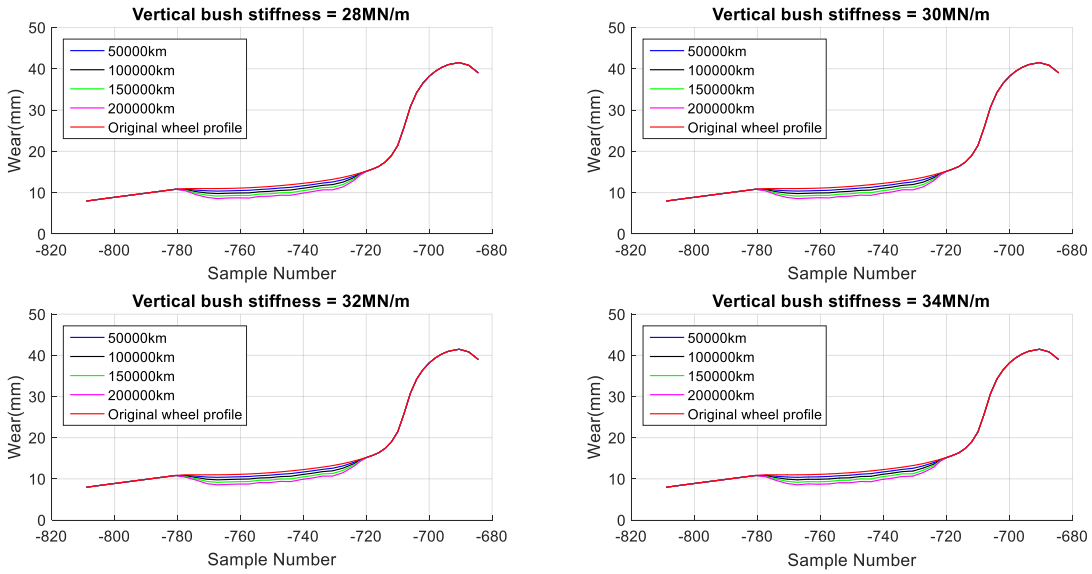

Figure 6. 19 Wheel profile evolution at different vertical bush stiffness

The wheel wear at different vertical bush stiffness are shown in Figure 6.20 respectively.

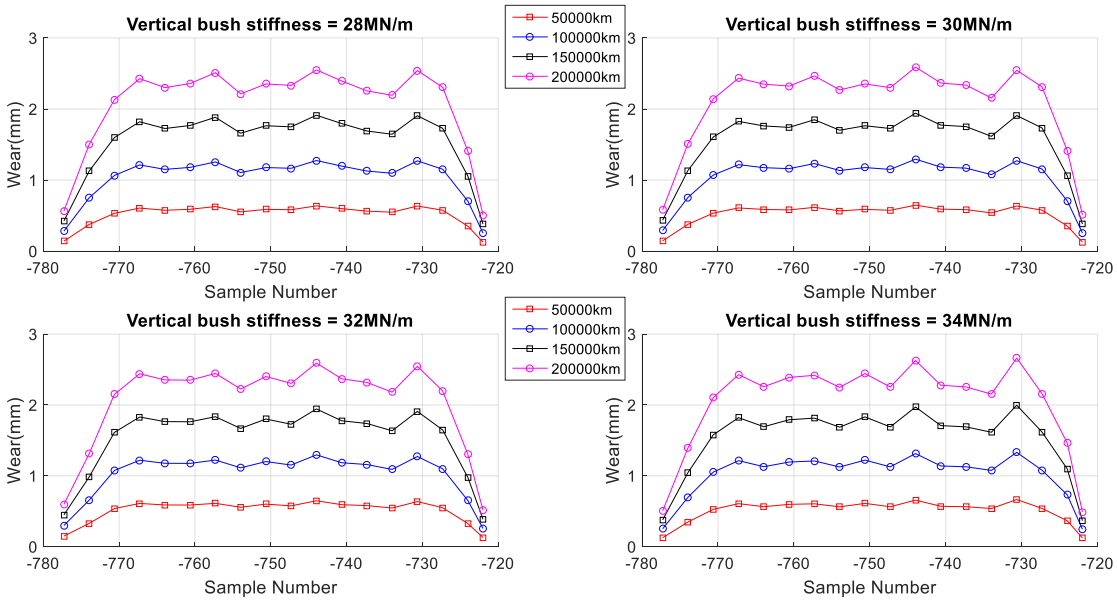

Figure 6. 20 Wheel wear at different vertical bush stiffness

1. Wheel wear prediction using series-parallel NARXNN: The inputs to the neural network are: vertical bush stiffness of 28MN/m, 30MN/m, and 32MN/m; running distance of 50000km, 100000km, and 150000km; wheel profiles $P_{11}, P_{12}, P_{13}, P_{14}, P_{21}, P_{22}, P_{23}, P_{24}, P_{31}, P_{32}, P_{33}$, and P_{34}; first derivative of wheel profile; and second derivative of wheel profile; while the output of the neural network was wheel wear. The wheel wear predicted using VAMPIRE and the NARXNN are shown in Figure 6.21.

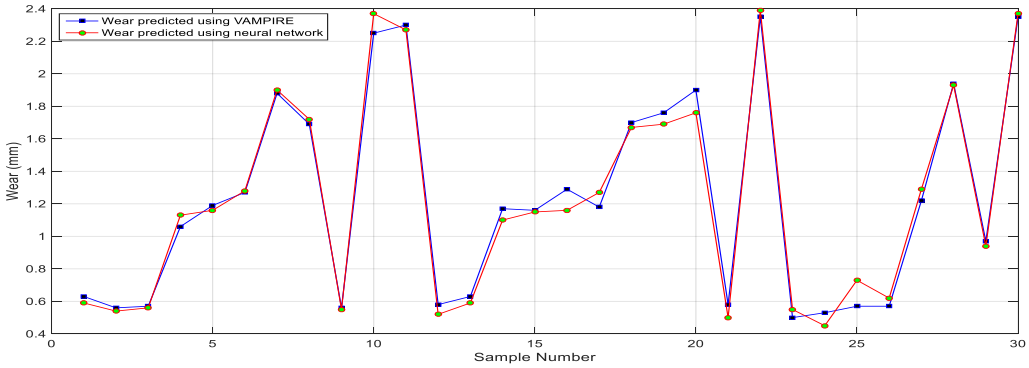

Figure 6. 21 Actual wheel wear and predicted using series-parallel NARXNN

The simulation results show that the predicted wheel wear using neural network was close to wheel wear predicted using VAMPIRE. The mean absolute percentage error was 5.83%. Maximum predicted wear using VAMPIRE was 2.35mm.

2. Wheel wear prediction using parallel NARXNN: The inputs to the neural network were the vertical bush stiffness of 34MN/m), running distance of 200000km, wheel profile P_{44}, first derivative of wheel profile, and second derivative of wheel profile; while the output of to the neural network was wheel wear. The wheel wear predicted using VAMPIRE and the NARXNN are shown in Figure 6.22.

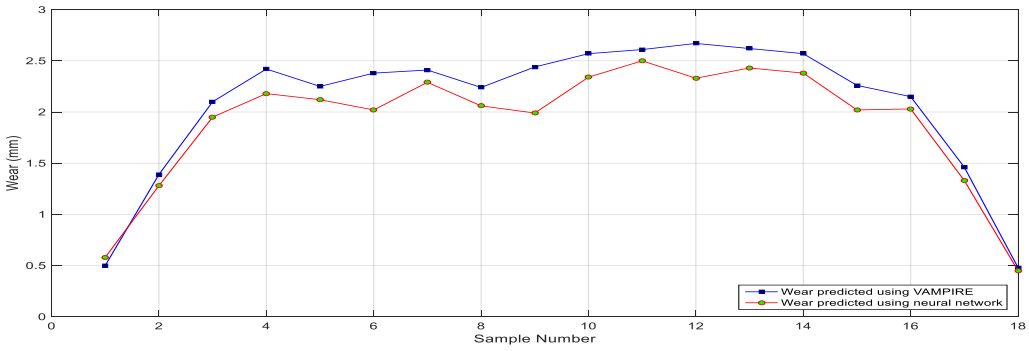

Figure 6. 22 Wheel wear predicted using VAMPIRE and parallel NARXNN

The simulation results show that the predicted wheel wear using neural network was close to wheel wear predicted using VAMPIRE. The mean absolute percentage error was 10.02%. Maximum predicted wear using VAMPIRE was 2.67mm.

6.3.5 Change of longitudinal shear stiffness

The wheel profile with longitudinal shear stiffness of 0.1MN/m, 0.3MN/m, 0.6MN/m and 0.8MN/m; running distance of 50000km, 100000km, 150000km, and 200000km is shown in Figre 6.23 respectively.

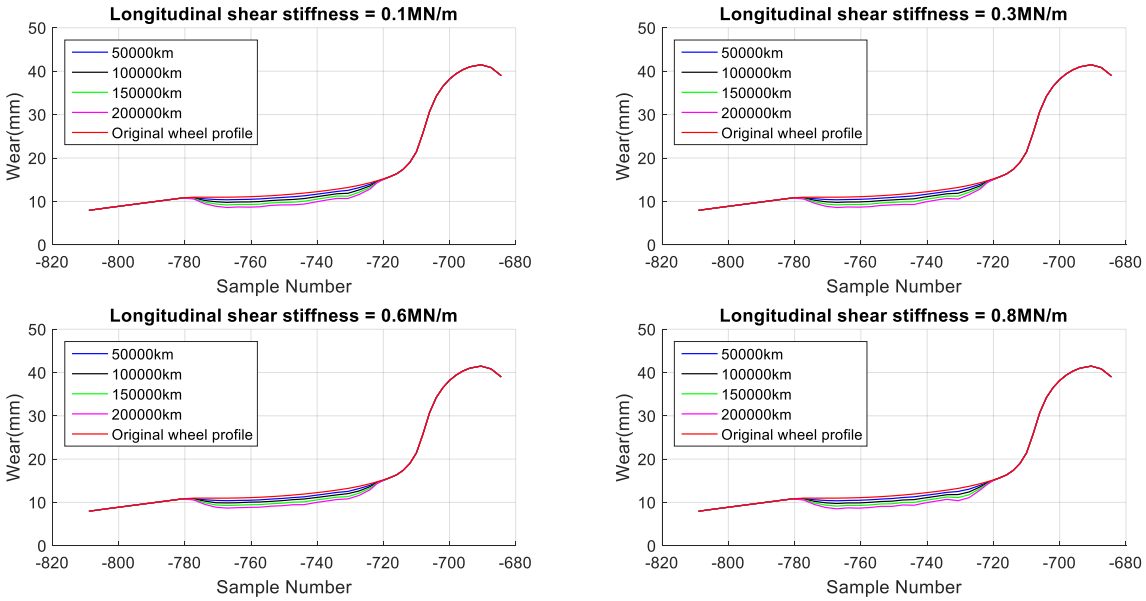

Figure 6. 23 Wheel profile evolution at different longitudinal shear stiffness

The wheel wear at different longitudinal shear stiffness are shown in Figure 6.24 respectively.

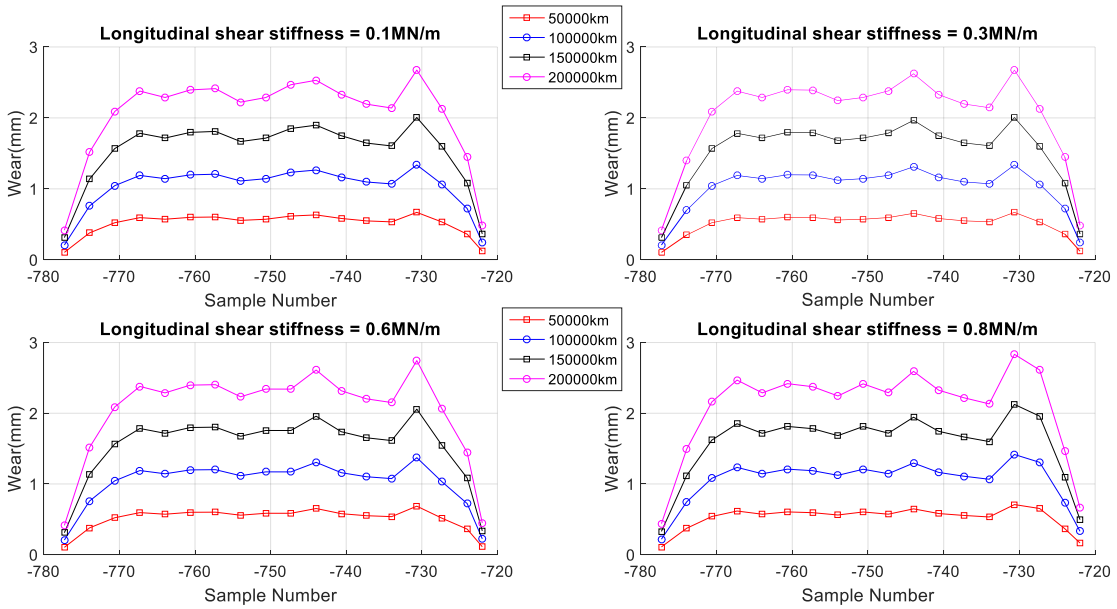

Figure 6. 24 Wheel wear at different longitudinal shear stiffness

1. Wheel wear prediction using series-parallel NARXNN: The inputs to the neural network: longitudinal shear stiffness of 0.1MN/m, 0.3MN/m, 0.6MN/m; running distance of 50000km, 100000km, and 150000km; wheel profiles $P_{11}, P_{12}, P_{13}, P_{14}, P_{21}, P_{22}, P_{23}, P_{24}, P_{31}, P_{32}, P_{33}$, and P_{34}; first derivative of wheel profile; and second derivative of wheel profile; while the output of to the neural network was wheel wear. The wheel wear predicted using VAMPIRE and the NARXNN are shown in Figure 6.25.

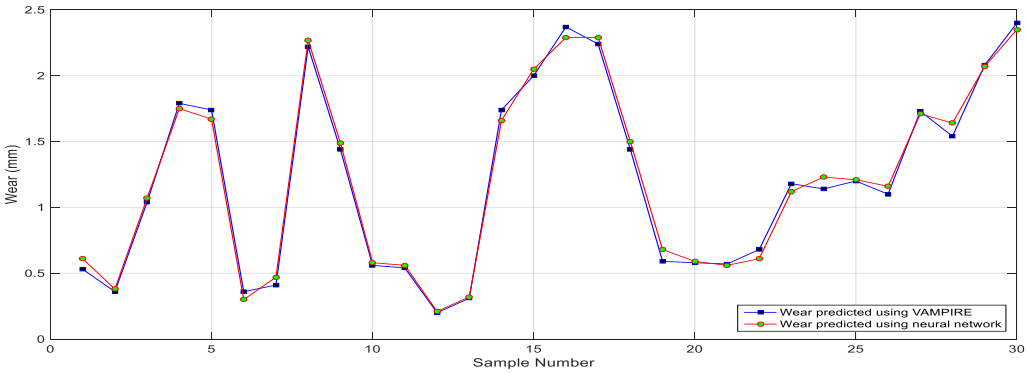

Figure 6. 25 Wheel wear predicted using VAMPIRE and series-parallel NARXNN

The simulation results show that the predicted wheel wear using neural network was close to wheel wear predicted using VAMPIRE. The mean absolute percentage error was 5.15%. Maximum predicted wear using VAMPIRE was 2.40mm.

2. Wheel wear prediction using parallel NARXNN: The inputs to the neural network were the longitudinal shear stiffness of 0.8MN/m, running distance of 200000km, wheel profile P_{44}, first derivative of wheel profile, and second derivative of wheel profile; while the output of the neural network was wheel wear. The wheel wear predicted using VAMPIRE and the NARXNN are shown in Figure 6.26.

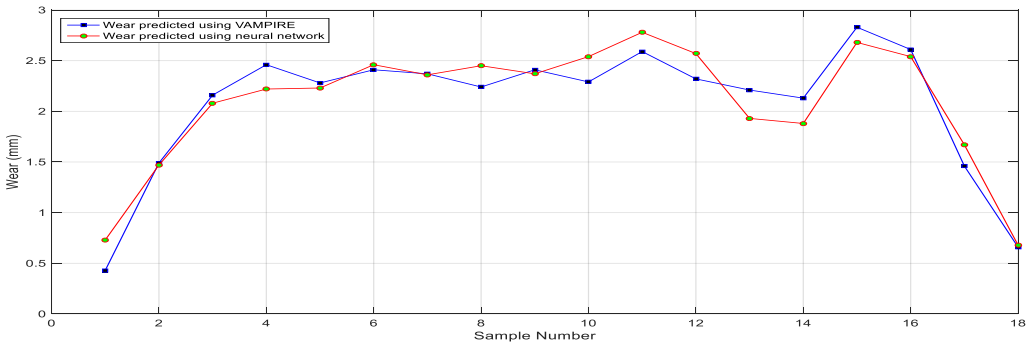

Figure 6. 26 Wheel wear predicted using VAMPIRE and parallel NARXNN

The simulation results show that the predicted wheel wear using neural network was close to wheel wear predicted using VAMPIRE. The mean absolute percentage error was 8.34%. Maximum predicted wear using VAMPIRE was 2.83mm.

6.3.6 Change of lateral shear stiffness

The wheel profile with lateral shear stiffness of 0.1MN/m, 0.3MN/m, 0.6MN/m and 0.8MN/m; running distance of 50000km, 100000km, 150000km, and 200000km is shown in Figure 6.27 respectively.

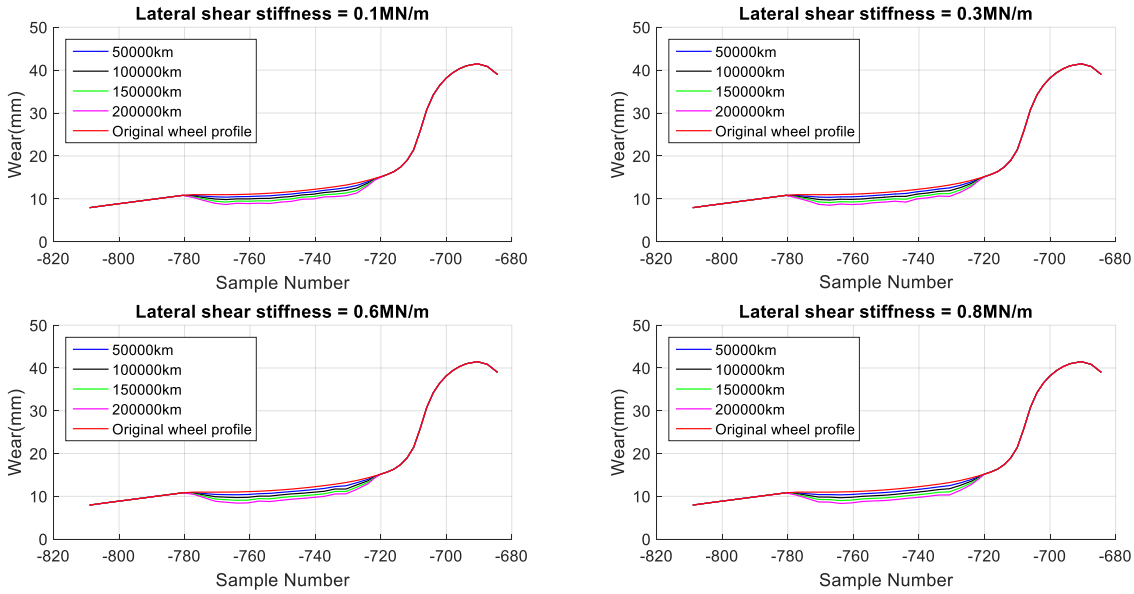

Figure 6. 27 Wheel profile evolution at different lateral shear stiffness

The wheel wear at at different lateral shear stiffness are shown in Figure 6.28 respectively.

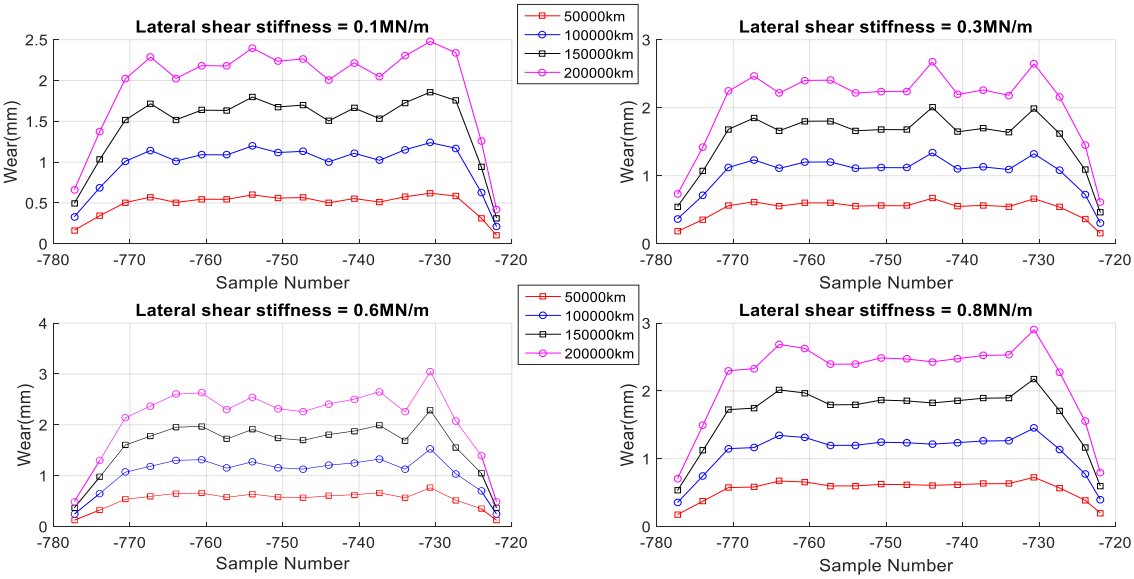

Figure 6. 28 Wheel wear at different lateral shear stiffness

1. Wheel wear prediction using series-parallel NARXNN: The inputs to the neural network are: lateral shear stiffness of 0.1MN/m, 0.3MN/m, and 0.6MN/m; running distance of 50000km, 100000km, and 150000km; wheel profiles $P_{11}, P_{12}, P_{13}, P_{14}, P_{21}, P_{22}, P_{23}, P_{24}, P_{31}, P_{32}, P_{33}$, and P_{34}; first derivative of wheel profile; and second derivative of wheel profile; while the output of to the neural network was wheel wear. The wheel wear predicted using VAMPIRE and the NARXNN are shown in Figure 6.29.

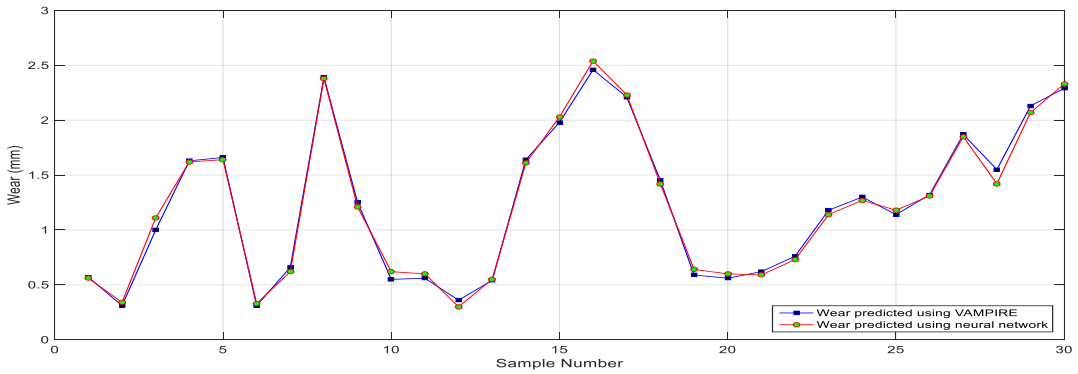

Figure 6. 29 Wheel wear predicted using VAMPIRE and series-parallel NARXNN

The simulation results show that the predicted wheel wear using neural network was close to wheel wear predicted using VAMPIRE. The mean absolute percentage error was 4.58 %. Maximum predicted wear using VAMPIRE was 2.46mm.

2. Wheel wear prediction using parallel NARXNN: The inputs to the neural network were the lateral shear stiffness of 0.8MN/m, running distance of 200000km, wheel profile P_{44}, first derivative of wheel profile; and second derivative of wheel profile; while the output of to the neural network was wheel wear. The wheel wear predicted using VAMPIRE and the NARXNN are shown in Figure 6.30.

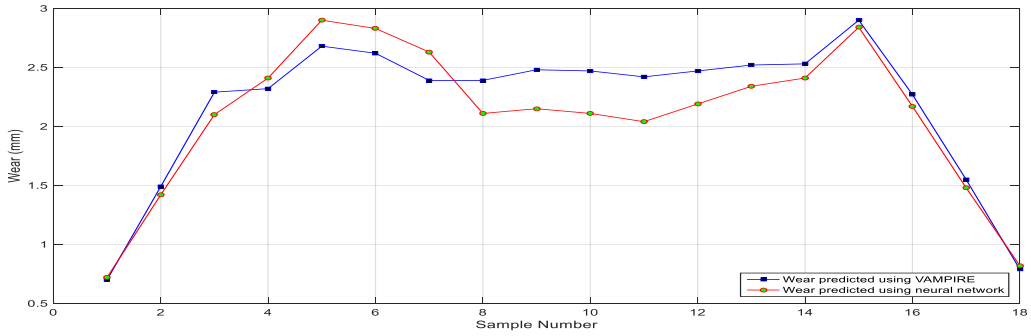

Figure 6. 30 Wheel wear predicted using VAMPIRE and parallel NARXNN

The simulation results show that the predicted wheel wear using neural network was close to wheel wear predicted using VAMPIRE. The mean absolute percentage error was 8.30%. Maximum predicted wear using VAMPIRE was 2.90mm.

6.3.7 Change of vertical shear stiffness

The wheel profile with vertical shear stiffness of 0.5MN/m, 0.6MN/m, 0.7MN/m and 0.8MN/m; running distance of 50000km, 100000km, 150000km, and 200000km is shown in Figure 6.31 respectively .

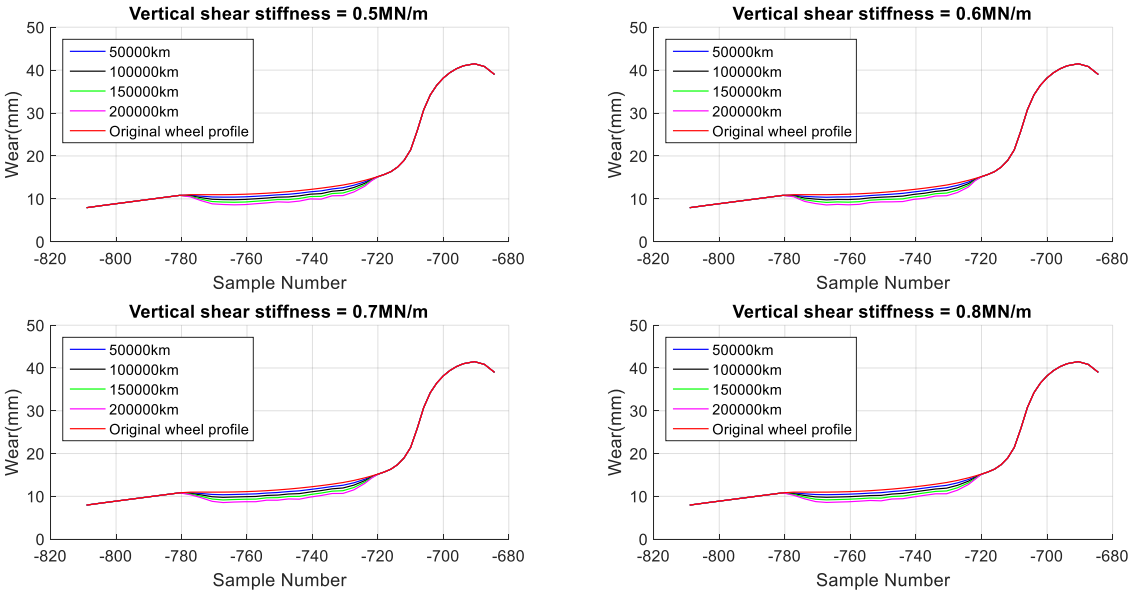

Figure 6. 31 Wheel profile evolution at different vertical shear stiffness

The wheel wear at at different vertical shear are shown in Figure 6.32 respectively.

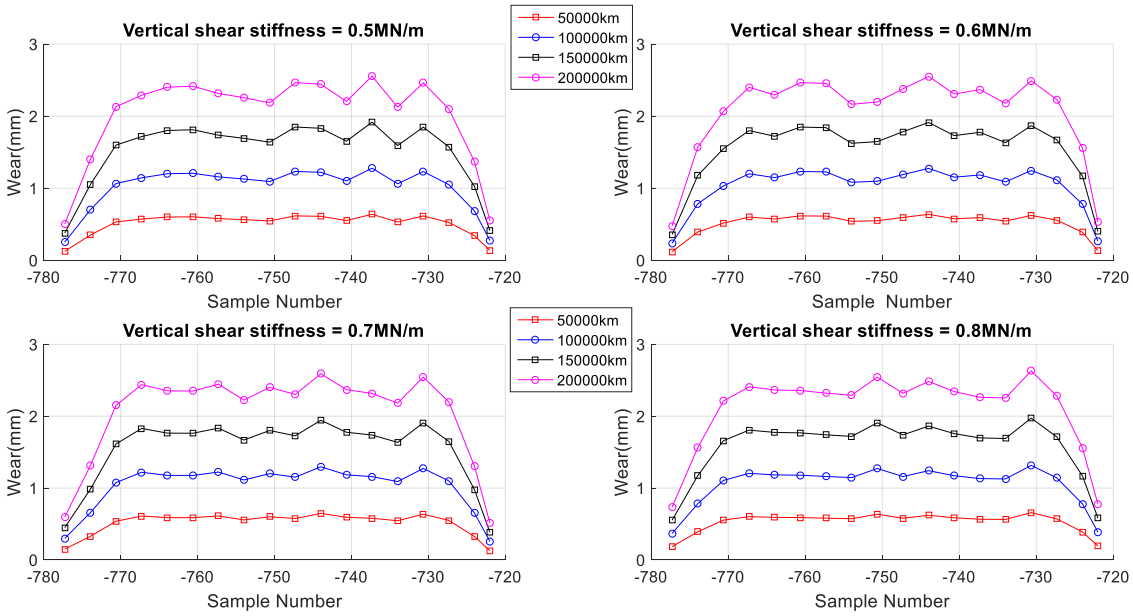

Figure 6. 32 Wheel wear at different vertical shear stiffness

1. Wheel wear prediction using series-parallel NARXNN: The inputs to the neural network are: vertical shear stiffness of 0.5MN/m, 0.6MN/m, and 0.7MN/m; running distance of 50000km, 100000km, and 150000km; wheel profiles $P_{11}, P_{12}, P_{13}, P_{14}, P_{21}, P_{22}, P_{23}, P_{24}, P_{31}, P_{32}, P_{33}$, and P_{34}; first derivative of wheel profile; and second derivative of wheel profile; while the output of to the neural network was wheel wear. The wheel wear predicted using VAMPIRE and the NARXNN are shown in Figure 6.33.

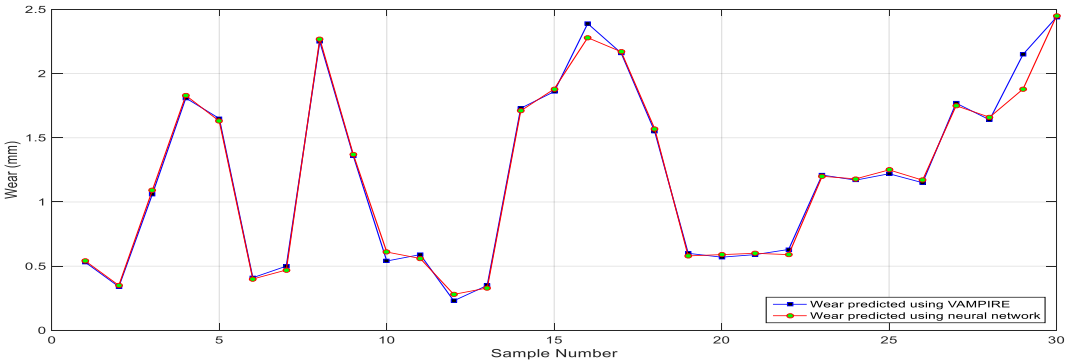

Figure 6. 33 Wheel wear predicted using VAMPIRE and series-parallel NARXNN

The simulation results show that the predicted wheel wear using neural network was close to wheel wear predicted using VAMPIRE. The mean absolute percentage error was was 3.60 %. Maximum predicted wear using VAMPIRE was 2.44mm.

2. Wheel wear prediction using parallel NARXNN: The inputs to the neural network were the vertical shear stiffness of 0.8MN/m, running distance of 200000km, wheel profile P_{44}, first derivative of wheel profile, and second derivative of wheel profile; while the output of to the neural network was wheel wear. The wheel wear predicted using VAMPIRE and the NARXNN are shown in Figure 6.34.

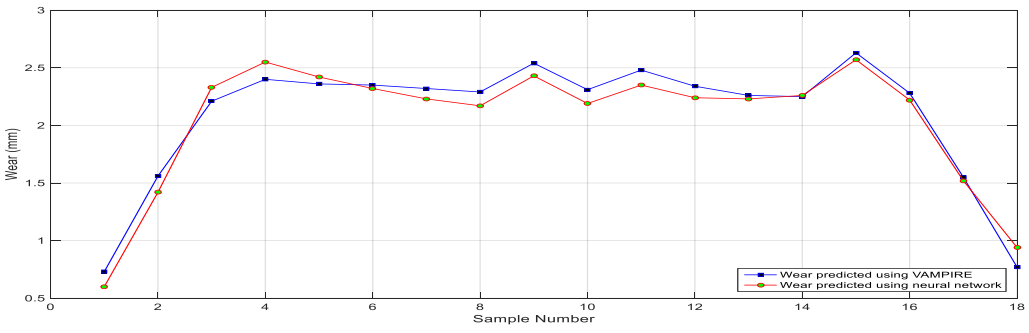

Figure 6. 34 Wheel wear predicted using VAMPIRE and parallel NARXNN

The simulation results show that the predicted wheel wear using neural network was close to wheel wear predicted using VAMPIRE. The mean absolute percentage error was 5.71%. Maximum predicted wear using VAMPIRE was 2.63mm.

6.3.8 Validation of wheel wear prediction

To additionally validate the wheel wear predicted using the neural network model, the results were compared with published results in some previous works [159]-[165], as shown in the following section and summarised in Table 6.2. In this section, seven previous works where the wheel tread wear was estimated were chosen. In the previous work different parameters were assessed for their effect on wear such as curvature, vehicle type, and route conditions. The range of wheel tread wear was between 1.5mm to 3mm after running distances of 200,000km as shown in Table 6.2. The wheel wear predicted using the neural network model after running distance of 200,000km was 2.5mm on average which is within of the previous published work. Several reasons such as the type of vehicle, and the type of simulation package which were used to estimate the wear can affect the wear predictions; in this project, Vampire software was used to generate the data which were used to train, validate, and test the neural network model and to predict the wheel wear.

After a running distance 200,000 km, the wheel wear was as shown in Figure 6.35.

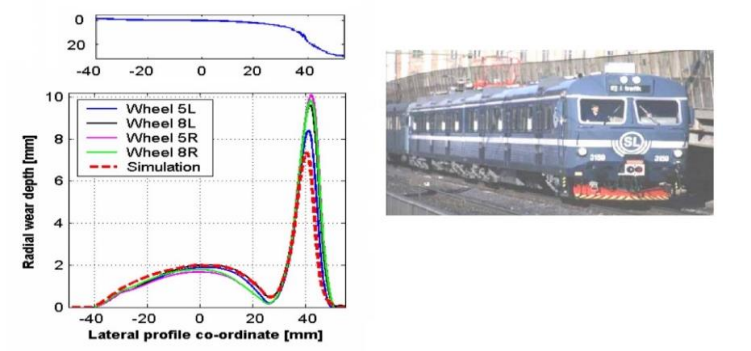

Figure 6. 35 Wheel wear comparison KTH wear [159]

After a running distance of 178000 mile, the wheel wear was as shown in Figure 6.36.

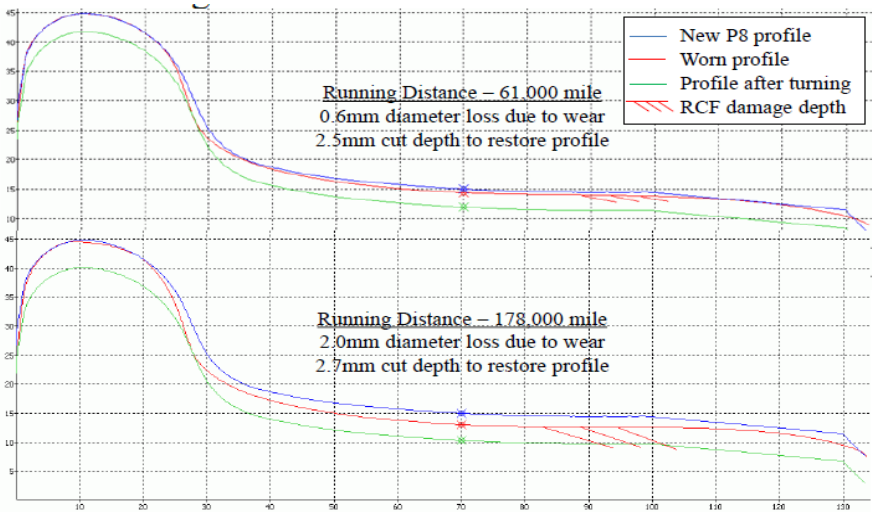

Figure 6. 36 Wheel wear [160]

After a running distance of 54,210km, the wheel wear was as shown in Figure 6.37.

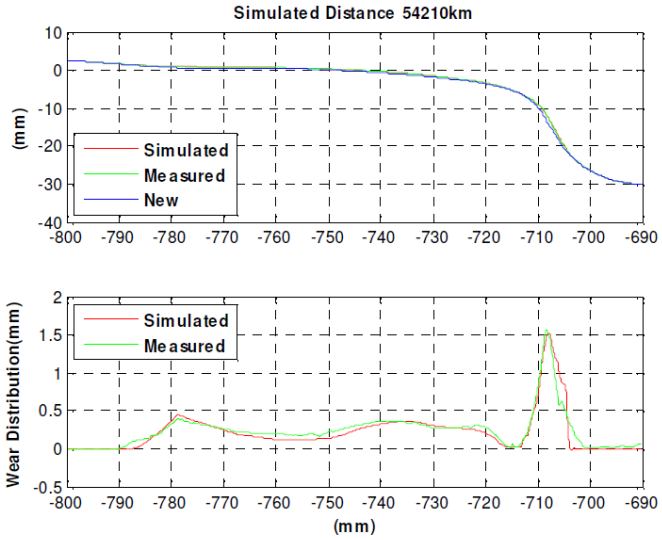

Figure 6. 37 Wheel tread wear [161]

The wheel tread profiles under 4 operation mileages 40000 km, 90000 km, 150000 km and 200000 km have been measured respectively as shown in Figure 6.38.

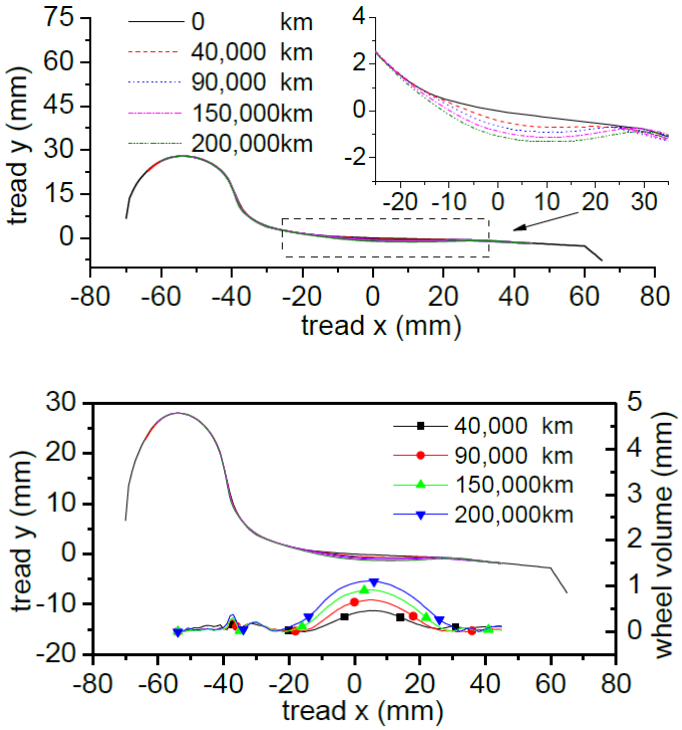

Figure 6. 38 Wheel wear [162]

After a running distance of 200,000km, the wheel wear was as shown in Figure 6.39.

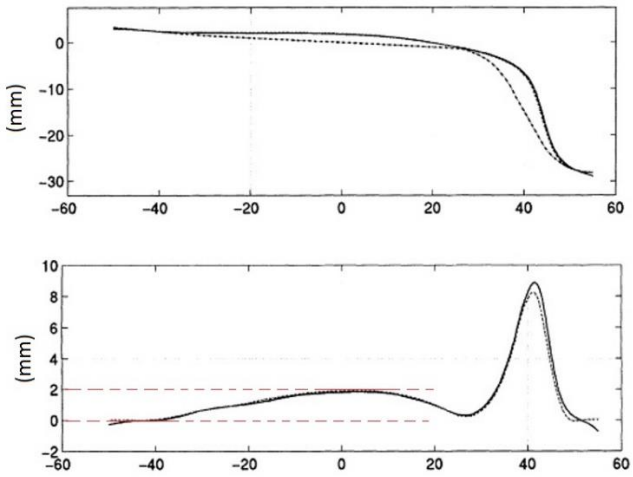

Figure 6. 39 Wheel wear [163], [164]

After a running distance of 200,000km, the wheel wear was as shown in Figure 6.40.

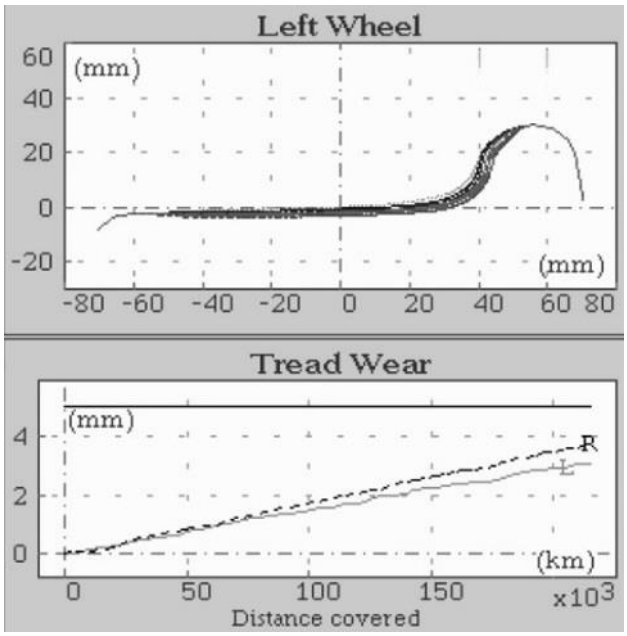

Figure 6. 40 Wheel wear of a vehicle type EV [165]

The wheel tread wear after a running distance of 200,000km was summarized as in Table 6.2.

Reference	Wheel wear after 200,000 km
[159]	1.9mm
[160]	1.5mm
[161]	1.84mm
[162]	1.2mm
[163], [164]	2mm
[165]	3mm

Table 6. 2 Wheel wear

Table 6.2 summarized the wheel wear after a running distance of 200,000 km which presented in different previous works was 1.9mm, 1.5mm, 1.2mm, 2mm, and 3mm. In this work, the wheel wear predicted using neural network after a running distance of 200,000 km was 2.5mm in average.

6.4 Chapter discussion

A nonlinear autoregressive model with exogenous input neural network (NARXNN) was developed to predict wheel wear for the case of changing parameters such as speed, longitudinal bush stiffness, lateral bush stiffness, vertical bush stiffness, longitudinal shear stiffness, lateral shear stiffness, and vertical shear stiffness.

The main findings are presented in the following sections are summarized in Table 6.3 and Table 6.4 respectively. Table 6.3 shows the mean absolute percentage error (MAPE) for railway wheel wear prediction using series-parallel NARXNN; while Table 6.4 shows the mean absolute percentage error (MAPE) railway wheel wear prediction using parallel NARXNN.

	Speed test	Change of longitudinal bush stiffness test	Change of lateral bush stiffness test	Change of vertical bush stiffness test	Change of longitudinal shear stiffness test	Change of lateral shear stiffness test	Change of vertical shear stiffness test
MAPE	4.32%	4.19%	5.57%	5.83%	5.15%	4.58%	3.60%

Table 6. 3 MAPE for wheel wear prediction using series-parallel NARXNN

	Speed test	Change of longitudinal bush stiffness test	Change of lateral bush stiffness test	Change of vertical bush stiffness test	Change of longitudinal shear stiffness test	Change of lateral shear stiffness test	Change of vertical shear stiffness test
MAPE	7.14%	7.46%	8.37%	10.02%	8.34%	8.30%	5.71%

Table 6. 4 MAPE for wheel wear prediction using parallel NARXNN

- The MAPE was between 3.60% and 5.83% for series-parallel NARXNN, meaning that the accuracy of NARXNN model was between 94.17% and 96.40%. The MAPE was between 5.71% and 10.02% for parallel NARXNN, meaning that the accuracy of NARXNN model was between 89.98% and 94.29%. Therefore, the accuracy of the NARXNN model was between 89.98% and 96.40%.
- The simulation results shown in Table 6.3 and Table 6.4 show that the wheel wear predicted using the neural network model was close to the wheel wear predicted using VAMPIRE, where the MAPE was less than 11%.
- The series-parallel NARXNN was more accurate than the parallel NARXNN for wheel wear prediction.
- The difference in the values of MAPE shown in Table 6.3 and Table 6.4 is due to the values of the input parameters used to train the neural network.

6.5 Chapter conclusion

Series-parallel NARXNN and parallel NARXNN were developed to predict the railway wheel where certain parameters have been changed such as speed, longitudinal bush stiffness, lateral bush stiffness, vertical bush stiffness, longitudinal shear stiffness, lateral shear stiffness, and vertical shear stiffness.

The optimal results during training and testing of the NARXNN obtained with input delays were 1:2, feedback delay 1:2, and 1 hidden layer with 10 neurons.

The inputs of the neural network model were: speed, running distance, longitudinal bush stiffness, lateral bush stiffness, vertical bush stiffness, longitudinal shear stiffness, lateral shear stiffness, vertical shear stiffness, wheel profile, first derivative of wheel profile, and second derivative of wheel profile. The output of the neural network was railway wheel wear.

The inputs and outputs which were used to train, validate, and test the neural network during wheel wear prediction were produced using VAMPIRE vehicle dynamics software simulations. These simulations were carried out using a passenger vehicle model, UK wheel profile type of P8, UK rail profile type of BS113a-20, and straight track with irregularities.

The main findings of this chapter are:

- The VAMPIRE vehicle dynamics software was used for vehicle-track simulations to generate the energy dissipated, and the contact position between wheel and rail. The energy dissipated and the contact position were used in this project to predict the railway wheel wear using neural network.
- The percentage error between wheel wear predicted using VAMPIRE and wheel wear predicted using neural network was calculated, the simulation results show that the predicted wheel wear using a neural network model was close to wheel wear predicted using VAMPIRE software.
- In view of mean absolute percentage error (MAPE), the simulation results reveal that the neural network model is able to predict the railway wheel wear efficiently. The results obtained using the proposed neural network approach show in overall, the MAPE was less than 11%; the neural network model achieved wheel prediction with accuracy up to 96.40%; this represents the accuracy of the neural network model for wheel wear prediction.
- Additionally, the wheel wear predicted using neural network model was validated with published results in some previous works after a running distance of 200,000 km. The results show that the predicted wheel wear using a neural network model was close to wheel wear predicted in the previous works. The wheel wear predicted using neural network after a running distance of 200,000 km was 2.5mm in average.

Chapter 7 Prediction of railway wheel wear using backpropagation and radial basis function neural networks for a railway vehicle

7.1 Introduction

In this chapter, a backpropagation neural network (BPNN) and a radial basis function neural network (RBFNN) were developed to predict the railway wheel wear. The aim of this chapter is to present how the wheel wear can be predicted using different types of neural networks. VAMPIRE vehicle dynamics software was used to collect data to train, validate, and test the neural network model.

The methodology of wheel wear prediction which was shown in Figure 6.2, and the neural network model which was shown in Figure 6.6 were used to predict wheel wear using BPNN and RBFNN. The inputs of the neural network model were: speed, running distance, longitudinal bush stiffness, lateral bush stiffness, vertical bush stiffness, longitudinal shear stiffness, lateral shear stiffness, vertical shear stiffness, wheel profile, first derivative of wheel profile, and second derivative for wheel profile; while the output of the neural network was railway wheel wear. The Matlab code which is shown in appendix 4 calculates the mean absolute percentage error (MAPE) and percentage error. The MAPE was calculated using equation 5.11, while the percentage error was calculated using equation 5.12.

The speed simulation which was shown in section 6.3.1, longitudinal bush stiffness simulation which was shown in section 6.3.2, and longitudinal shear stiffness simulation which was shown in section 6.3.5 were used for wheel prediction using BPNN and RBFNN. The simulation results were compared with wheel wear prediction using the nonlinear autoregressive model with exogenous input neural network (Parallel NARXNN), this to present that the railway wheel wear can be predicted using different types of neural network, and to investigate which type of these neural networks has a higher accuracy for wheel wear prediction.

The data obtained using VAMPIRE vehicle dynamics software after a running distance of 50000km, 100000km, and 150000km were used to train neural networks; while the data obtained after a running distance of 200000km were used to test the neural networks.

The Matlab code shown in appendix 10 was used to predict the wheel wear using BPNN [158]. The Levenberg-Marquardt algorithm to train the BPNN. An example of the BPNN architecture with architecture of 5-7-2-1 is shown in Figure 7.1.

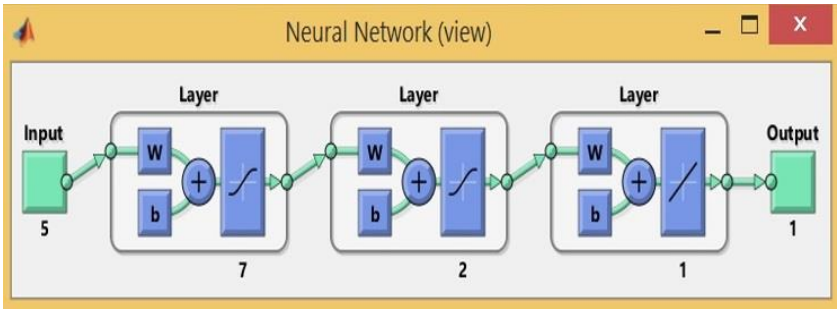

Figure 7. 1 BPNN architecture

The Matlab code shown in appendix 11 was used to predict the wheel wear using RBFNN. An example of the RBFNN architecture is shown in Figure 7.2. When the Matlab command "newrb" is used to design the RBFNN, there is no separation between the creation and training phases, therefore, once newrb created it, it trains itself, depending on the input parameters, the newrb automatically trains itself without the train/validate/test data division [166].

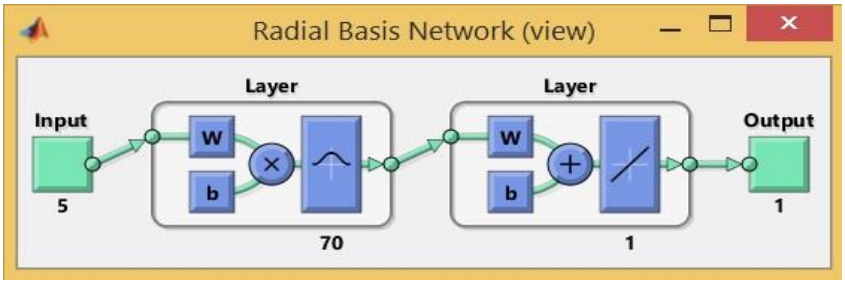

Figure 7. 2 RBFNN architecture

When the newrb command is used to create and train the RBFNN, the design of RBFNN takes six arguments: input vector, target vector, mean square error goal, spread, maximum number of neurons, and the number of neurons to add between displays. These parameters are explicitly set by the user using trial and error. In this work the parameters of newrb were set as: goal = 0.01, spread = 30, mn =500, and df =50 for wheel wear prediction using RBFNN. All results shown in this chapter are for unseen data.

7.2 Wheel wear prediction using neural networks with varying speed

The change of speed simulation which was shown in section 7.3.1was used to predict wheel wear using NARXNN, BPNN, and RBFNN. Wheel wear predicted using VAMPIRE and wheel wear predicted using NARXNN, BPNN, and RBFNN are shown in Figure 7.3.

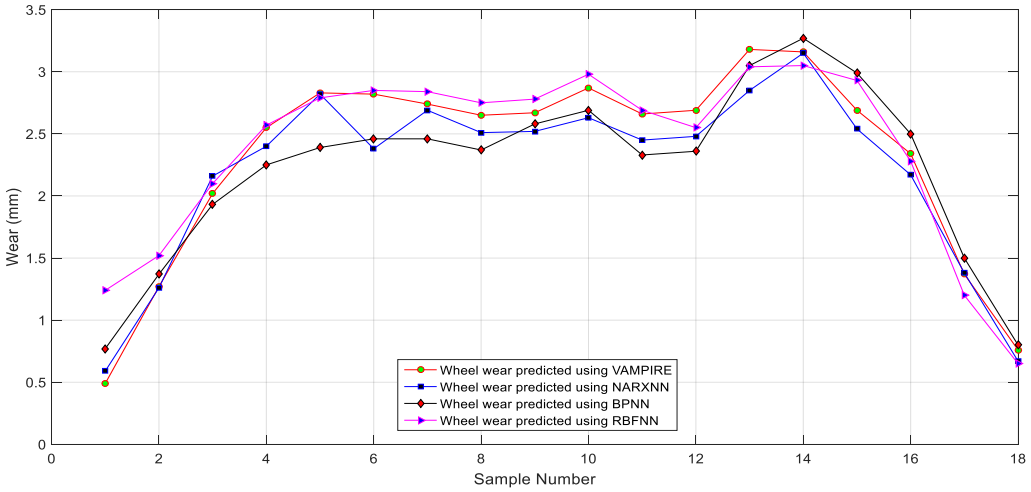

Figure 7. 3 Wheel wear predicted using VAMPIRE and predicted using neural networks

Wheel wear predictd using VAMPIRE and predicted using NARXNN, BPNN, and RBFNN; and the percentage error are shown in Table 7.1. The mean absolute percentage error was 7.14% for NARXNN, 8.63% for RBFN, and 10.70% for BPNN.

Sample Number	Wheel wear predicted using VAMPIRE	Wheel wear predicted using NARXNN	Error%	Wheel wear predicted using BPNN	Error%	Wheel wear predicted using RBFNN	Error%
1	0.49	0.59	16.94	0.77	36.46	1.24	60.57
2	1.27	1.26	0.79	1.37	7.36	1.52	16.88
3	2.02	2.16	6.48	1.932	4.52	2.10	3.84
4	2.55	2.40	6.25	2.25	13.02	2.57	0.98
5	2.83	2.82	0.35	2.39	17.93	2.79	1.08
6	2.82	2.38	18.48	2.46	14.21	2.85	1.17
7	2.74	2.69	1.85	2.46	11.11	2.84	3.65
8	2.65	2.51	5.57	2.37	11.64	2.75	3.77
9	2.67	2.52	5.95	2.58	3.25	2.78	4.18
10	2.87	2.63	9.12	2.69	6.64	2.98	3.94
11	2.66	2.45	8.57	2.33	13.78	2.69	1.19
12	2.69	2.48	8.46	2.36	13.50	2.55	5.09
13	3.18	2.85	11.57	3.05	4.11	3.04	4.52
14	3.16	3.15	0.31	3.27	3.47	3.05	3.41
15	2.69	2.54	5.90	2.99	10.07	2.93	8.47
16	2.34	2.17	7.83	2.50	6.53	2.28	2.62
17	1.37	1.38	0.72	1.50	9.08	1.20	13.86
18	0.76	0.67	13.43	0.80	5.90	0.65	16.05

Table 7. 1 Wheel wear predicted using VAMPIRE and predicted using neural networks; and error%

7.3 Wheel wear prediction using neural networks with varying longitudinal bush stiffness

The change of longitudinal bush stiffness simulation which was shown in section 6.3.2 was used to predict wheel wear using NARXNN, BPNN, and RBFNN. Wheel wear predicted using VAMPIRE and wheel wear predicted using NARXNN, BPNN, and RBFNN are shown in Figure 7.4.

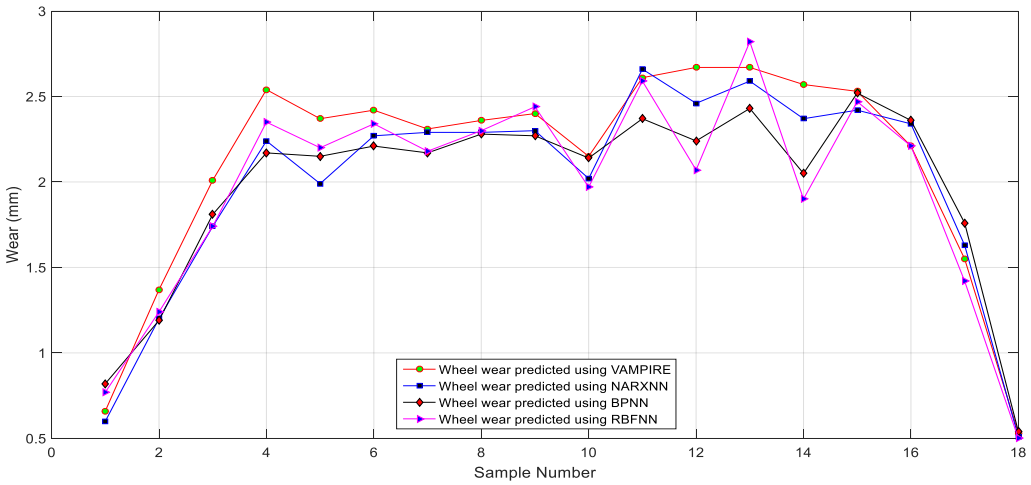

Figure 7. 4 Wheel wear predicted usingVAMPIRE and predicted using neural networks

Wheel wear predictd using VAMPIRE and predicted using NARXNN, BPNN, and RBFNN; and the percentage error are shown in Table 7.2. The mean absolute percentage error was 7.46% for NARXNN, 9.22% for RBFN, and 10.14% for BPNN.

Sample Number	Wheel wear predicted using VAMPIRE	Wheel wear predicted using NARXNN	Error%	Wheel wear predicted using BPNN	Error%	Wheel wear predicted using RBFNN	Error%
1	0.66	0.60	10.00	0.82	20.03	0.77	14.73
2	1.37	1.20	14.16	1.19	14.56	1.24	10.15
3	2.01	1.74	15.51	1.81	10.49	1.74	15.51
4	2.54	2.24	13.39	2.17	17.01	2.35	7.83
5	2.37	1.99	19.09	2.15	10.16	2.20	7.63
6	2.42	2.27	6.60	2.21	9.44	2.34	3.39
7	2.31	2.29	0.87	2.17	6.26	2.18	5.68
8	2.36	2.29	3.05	2.28	3.40	2.30	2.41
9	2.40	2.30	4.34	2.27	5.64	2.44	1.54
10	2.15	2.02	6.43	2.14	0.14	1.97	9.03
11	2.61	2.66	1.87	2.37	10.00	2.59	0.51
12	2.67	2.46	8.53	2.24	19.10	2.07	28.96
13	2.67	2.59	3.08	2.43	9.79	2.82	5.03
14	2.57	2.37	8.43	2.05	25.33	1.90	35.07
15	2.53	2.42	4.54	2.52	0.18	2.47	2.55
16	2.21	2.34	5.55	2.36	6.42	2.21	0.19
17	1.55	1.63	4.90	1.76	12.24	1.42	9.35
18	0.53	0.51	3.92	0.54	2.29	0.50	6.46

Table 7. 2 Wheel wear predicted using VAMPIRE and predicted using neural networks; and error%

7.4 Wheel wear prediction using neural networks with varying longitudinal shear stiffness

The change of longitudinal shear stiffness simulation which was shown in section 6.3.5 was used to predict wheel wear using NARXNN, BPNN, and RBFNN. Wheel wear predicted using VAMPIRE and wheel wear predicted using NARXNN, BPNN, and RBFNN are shown in Figure 7.5.

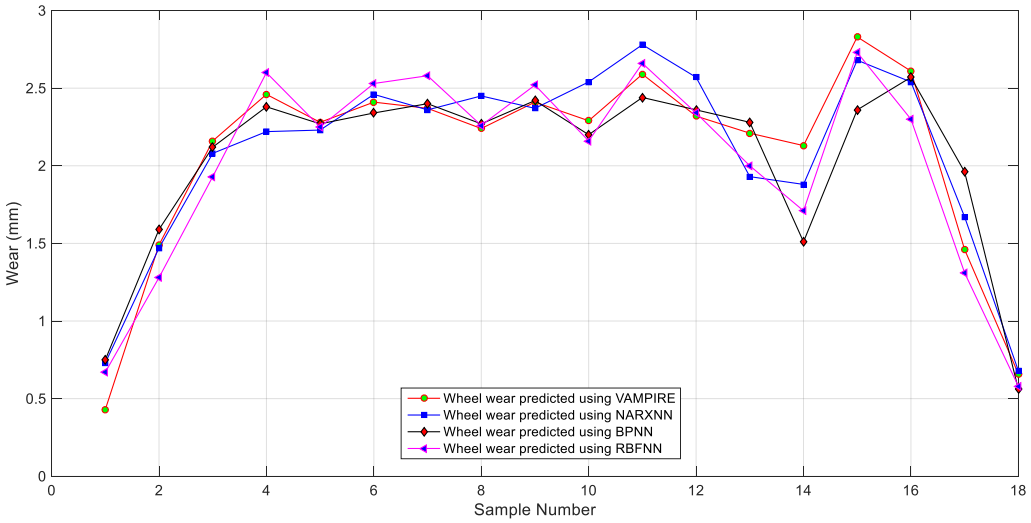

Figure 7. 5 Wheel wear predicted using VAMPIRE and predicted using neural networks

Wheel wear predictd using VAMPIRE, wheel wear predicted using NARXNN, BPNN, and RBFNN; and the percentage error is shown in Table 7.3. The mean absolute percentage error was 8.34% for NARXNN, 9.77% for RBFN, and 10.08% for BPNN.

Sample Number	Wheel wear predicted using VAMPIRE	Wheel wear predicted using NARXNN	Error %	Wheel wear predicted using BPNN	Error %	Wheel wear predicted using RBFNN	Error %
1	0.43	0.73	41.09	0.75	42.66	0.67	35.82
2	1.49	1.47	1.36	1.59	6.28	1.28	16.40
3	2.16	2.08	3.84	2.12	1.88	1.93	11.91
4	2.46	2.22	10.81	2.38	3.36	2.60	5.38
5	2.28	2.23	2.24	2.27	0.44	2.25	1.33
6	2.41	2.46	2.03	2.34	2.99	2.53	4.74
7	2.37	2.36	0.42	2.40	1.25	2.58	8.13
8	2.24	2.45	8.57	2.27	1.32	2.26	0.88
9	2.41	2.37	1.68	2.42	0.41	2.52	4.36
10	2.29	2.54	9.84	2.20	4.09	2.16	6.01
11	2.59	2.78	6.83	2.44	6.14	2.66	2.63
12	2.32	2.57	9.72	2.36	1.69	2.34	0.85
13	2.21	1.93	14.50	2.28	3.07	2.00	10.50
14	2.13	1.88	13.29	1.51	41.05	1.71	24.56
15	2.83	2.68	5.59	2.36	19.91	2.73	3.66
16	2.61	2.54	2.75	2.57	1.55	2.30	13.47
17	1.46	1.67	12.57	1.96	25.51	1.31	11.45
18	0.66	0.68	2.94	0.56	17.85	0.58	13.79

Table 7. 3 Wheel wear predicted using VAMPIRE and predicted using neural networks; and error%

7.5 Effects of RBFNN parameters (spread, mn, goal, and df) on wheel wear prediction

In this section the effects of the RBFNN parameters on wheel wear prediction were investigated. The Matlab code shown in appendix 11 was used to predict the wheel wear using RBFNN.

7.5.1 Effects of the spread parameter of RBFNN on wheel wear prediction

The vertical bush stiffness simulation which was shown in section 6.3.4 was used to investigate the effects of the spread parameter of RBFNN on wheel wear prediction. Wheel wear predicted using VAMPIRE, and wheel wear predicted using RBFNN with different values of spread are shown in Figure 7.6.

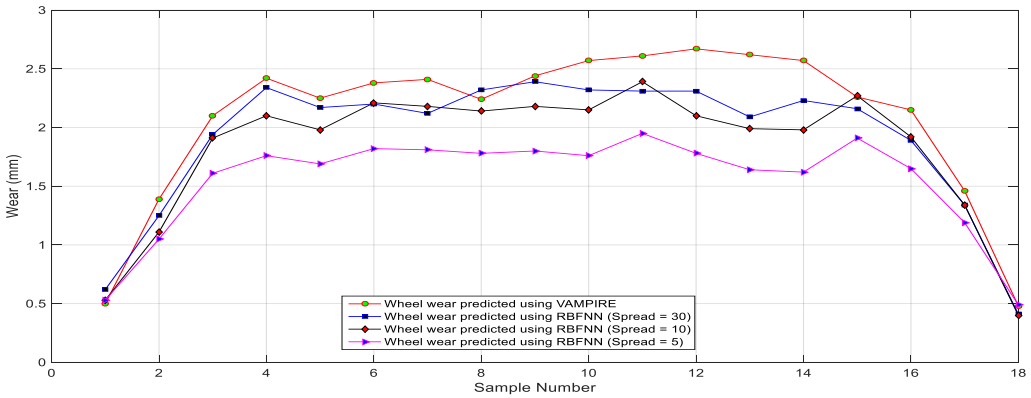

Figure 7. 6 Wheel wear predicted using VAMPIRE and predicted using RBFNN

Wheel wear predicted using VAMPIRE, wheel wear predicted using RBFNN, and the percentage error are shown in Table 7.4. The mean absolute percentage error (MAPE) was 10.98% at spread of 30, was 14.70% at spread of 10, and was 32.36% at spread of 5.

Sample Number	Wheel wear predicted using VAMPIRE	Wheel wear predicted using RBFNN spread = 30	Error %	Wheel wear predicted using RBFNN spread = 10	Error %	Wheel wear predicted using RBFNN spread = 5	Error %
1	0.50	0.62	19.35	0.53	5.13	0.53	5.45
2	1.39	1.25	11.20	1.11	25.23	1.05	31.72
3	2.10	1.94	8.24	1.91	9.96	1.61	30.56
4	2.42	2.34	3.41	2.10	15.54	1.76	37.50
5	2.25	2.17	3.68	1.98	13.80	1.69	33.27
6	2.38	2.20	8.18	2.21	7.79	1.82	31.07
7	2.41	2.12	13.67	2.18	10.78	1.81	33.27
8	2.24	2.32	3.44	2.14	4.63	1.78	26.03
9	2.44	2.39	2.09	2.18	11.54	1.80	35.09
10	2.57	2.32	10.77	2.15	19.19	1.76	45.74
11	2.61	2.31	12.98	2.39	9.32	1.95	33.65
12	2.67	2.31	15.58	2.10	27.40	1.78	49.74
13	2.62	2.09	25.35	1.99	31.51	1.64	59.86
14	2.57	2.23	15.24	1.98	29.88	1.62	58.24
15	2.26	2.16	4.62	2.27	0.52	1.91	17.99
16	2.15	1.89	13.75	1.92	11.85	1.65	30.79
17	1.46	1.34	8.95	1.34	8.84	1.19	21.96
18	0.48	0.41	17.07	0.40	21.71	0.49	0.63

Table 7. 4 Wheel wear predicted using VAMPIRE and predicted using RBFNN; and error%

7.5.2 Effects of the mn parameter of RBFNN on wheel wear prediction

The lateral bush stiffness simulation which was shown in section 6.3.3 was used to investigate the effects of the mn parameter of RBFNN on wheel wear prediction. Wheel wear predicted using VAMPIRE, and wheel wear predicted using RBFNN with different values of mn are shown in Figure 7.7. Where the mn is the maximum number of neurons of RBFNN.

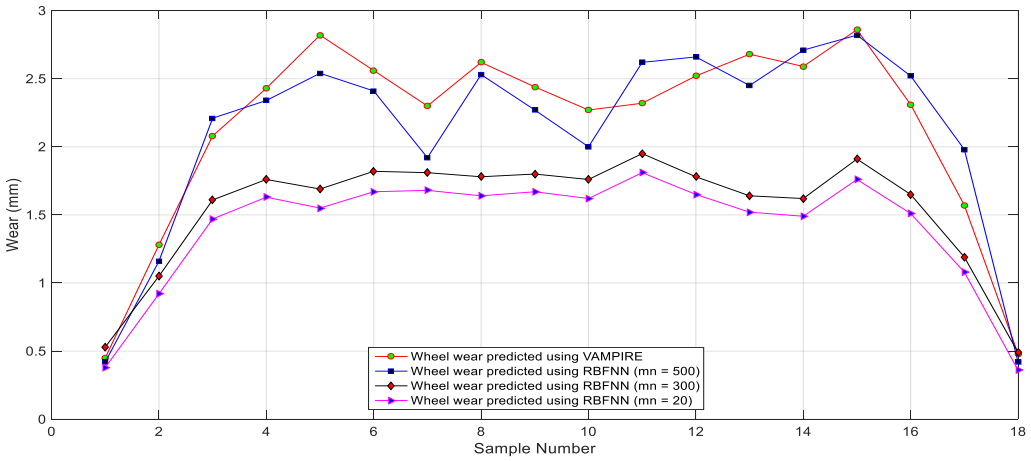

Figure 7. 7 Wheel wear predicted using VAMPIRE and predicted using RBFNN

Wheel wear predicted using VAMPIRE, and wheel wear predicted using RBFNN, and the percentage error are shown in Table 7.5. The mean absolute percentage error was 9.11% when mn was 500, was 36.39 % when mn was 300, and was 49.31% when mn was 20.

Sample Number	Wheel wear predicted using VAMPIRE	Wheel wear predicted using RBFNN mn =500	Error%	Wheel wear predicted using RBFNN mn =300	Error%	Wheel wear predicted using RBFNN mn =20	Error%
1	0.45	0.42	7.14	0.53	14.39	0.38	17.87
2	1.28	1.16	10.34	1.05	21.46	0.92	38.48
3	2.08	2.21	5.88	1.61	29.21	1.47	40.78
4	2.43	2.34	3.84	1.76	37.96	1.63	49.26
5	2.82	2.54	11.02	1.69	66.94	1.55	81.24
6	2.56	2.41	6.22	1.82	40.98	1.67	52.93
7	2.30	1.92	19.79	1.81	26.92	1.68	37.08
8	2.62	2.53	3.55	1.78	46.89	1.64	59.41
9	2.44	2.27	7.48	1.80	35.17	1.67	45.48
10	2.27	2.00	13.50	1.76	29.11	1.62	40.23
11	2.32	2.62	11.45	1.95	18.97	1.81	28.17
12	2.52	2.66	5.26	1.78	41.32	1.65	52.79
13	2.68	2.45	9.38	1.64	63.68	1.52	76.35
14	2.59	2.71	4.42	1.62	59.69	1.49	73.33
15	2.86	2.82	1.41	1.91	49.31	1.76	61.89
16	2.31	2.52	8.33	1.65	40.43	1.51	52.74
17	1.57	1.98	20.70	1.19	31.60	1.08	45.94
18	0.48	0.42	14.28	0.49	0.95	0.36	33.63

Table 7. 5 Wheel wear predicted using VAMPIRE and predicted using RBFNN; and error%

7.5.3 Effects of the goal parameter of RBFNN on wheel wear prediction

The lateral shear stiffness simulation which was shown in section 6.3.6 was used to investigate the effects of the goal parameter of RBFNN on wheel wear prediction. Wheel wear predicted using VAMPIRE, and wheel wear predicted using RBFNN with different values of goal are shown in Figure 7.8. Where the goal is denotes the mean squared error goal.

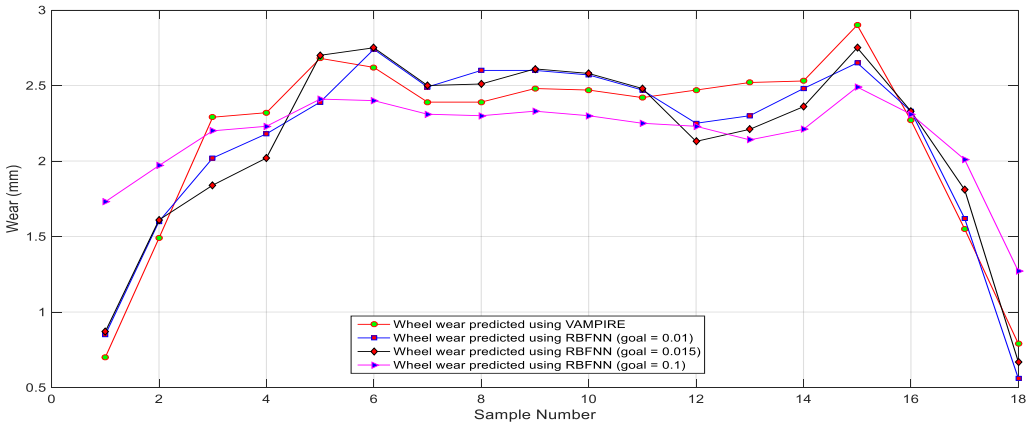

Figure 7. 8 Wheel wear predicted using VAMPIRE and predicted using RBFNN

Wheel wear predicted using VAMPIRE, and wheel wear predicted using RBFNN, and the percentage error are shown in Table 7.6. The mean absolute percentage error was 9.01% when goal was 0.01, was 9.45% when goal was 0.015, and was 14.55% when goal 0.1.

Sample Number	Wheel wear predicted using VAMPIRE	Wheel wear predicted using RBFNN Goal =0.01	Error %	Wheel wear predicted using RBFNN Goal = 0.015	Error %	Wheel wear predicted using RBFNN Goal = 0.1	Error %
1	0.70	0.85	7.64	0.87	7.45	1.73	59.26
2	1.49	1.60	6.87	1.61	24.45	1.97	24.46
3	2.29	2.02	13.36	1.84	14.85	2.20	4.01
4	2.32	2.18	6.42	2.02	0.74	2.23	4.33
5	2.68	2.39	12.13	2.70	4.72	2.41	11.30
6	2.62	2.74	4.37	2.75	4.40	2.40	9.09
7	2.39	2.49	4.01	2.50	4.78	2.31	3.55
8	2.39	2.60	8.07	2.51	4.98	2.30	3.90
9	2.48	2.60	4.61	2.61	4.26	2.33	6.52
10	2.47	2.57	3.89	2.58	2.41	2.30	7.22
11	2.42	2.47	2.02	2.48	15.96	2.25	7.76
12	2.47	2.25	9.77	2.13	14.02	2.23	10.69
13	2.52	2.30	9.56	2.21	7.20	2.14	17.43
14	2.53	2.48	2.01	2.36	5.45	2.21	13.99
15	2.90	2.65	9.43	2.75	2.57	2.49	16.45
16	2.27	2.33	2.57	2.33	14.36	2.31	1.44
17	1.55	1.62	4.32	1.81	17.91	2.01	23.02
18	0.79	0.56	41.07	0.67	7.45	1.27	37.45

Table 7. 6 Wheel wear predicted using VAMPIRE and predicted using RBFNN; and error%

7.5.4 Effects of the df parameter of RBFNN on wheel wear prediction

The vertical shear stiffness simulation which was shown in section 6.3.7 was used to investigate the effects of the df parameter of RBFNN on wheel wear prediction. Wheel wear predicted using VAMPIRE, and wheel wear predicted using RBFNN with different values of df are shown in Figure 7.9. Where df represents the number of neurons to add between displays.

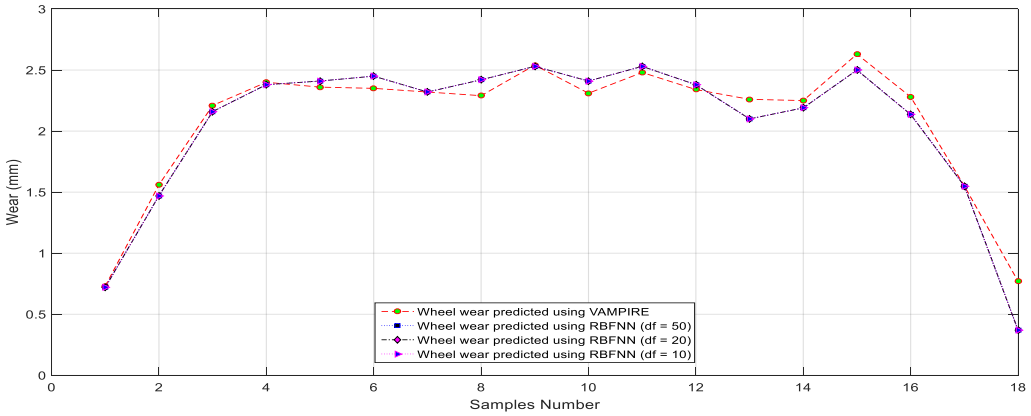

Figure 7. 9 Wheel wear predicted using VAMPIRE and predicted using RBFNN

Wheel wear predicted using VAMPIRE, wheel wear predicted using RBFNN, and the percentage error are shown in Table 7.7. The mean absolute percentage error was 6.65% when df was 50, was 6.65% when df was 20, and was 6.65% when df was 10. The simulation results show that the changing of df parameter had no effect on the accuracy of wheel wear prediciton.

Sample Number	Wheel wear predicted using VAMPIRE	Wheel wear predicted using RBFNN df = 50	Error %	Wheel wear predicted using RBFNN df = 20	Error %	Wheel wear predicted using RBFNN df = 10	Error %
1	0.73	0.72	1.07	0.72	1.07	0.72	1.07
2	1.56	1.47	5.88	1.47	5.88	1.47	5.88
3	2.21	2.16	2.14	2.16	2.14	2.16	2.14
4	2.40	2.38	1.15	2.38	1.15	2.38	1.15
5	2.36	2.41	1.93	2.41	1.93	2.41	1.93
6	2.35	2.45	4.05	2.45	4.05	2.45	4.05
7	2.32	2.32	0.29	2.32	0.29	2.32	0.29
8	2.29	2.42	5.49	2.42	5.49	2.42	5.49
9	2.54	2.53	0.24	2.53	0.24	2.53	0.24
10	2.31	2.41	3.87	2.41	3.87	2.41	3.87
11	2.48	2.53	2.07	2.53	2.07	2.53	2.07
12	2.34	2.38	1.85	2.38	1.85	2.38	1.85
13	2.26	2.10	7.65	2.10	7.65	2.10	7.65
14	2.25	2.19	2.80	2.19	2.80	2.19	2.80
15	2.63	2.50	5.05	2.50	5.05	2.50	5.05
16	2.28	2.136	6.76	2.13	6.76	2.13	6.76
17	1.55	1.55	0.01	1.55	0.01	1.55	0.01
18	0.77	0.46	67.40	0.46	67.40	0.46	67.40

Table 7. 7 Wheel wear predicted using VAMPIRE and predicted using RBFNN; and error%

The following section presents the training process of RBFNN during wheel wear prediction for the vertical shear stiffness simulation which was shown in section 6.3.7. The radial basis function neural network (RBFNN) was designed using newrb command such as shown in the following section: net = newrb (inputs, targets, goal, spread, mn, df); goal = 0.001, spread = 30, mn =50, and df =5. In this example, the mean squared error (MSE) is shown in Figure 7.10.

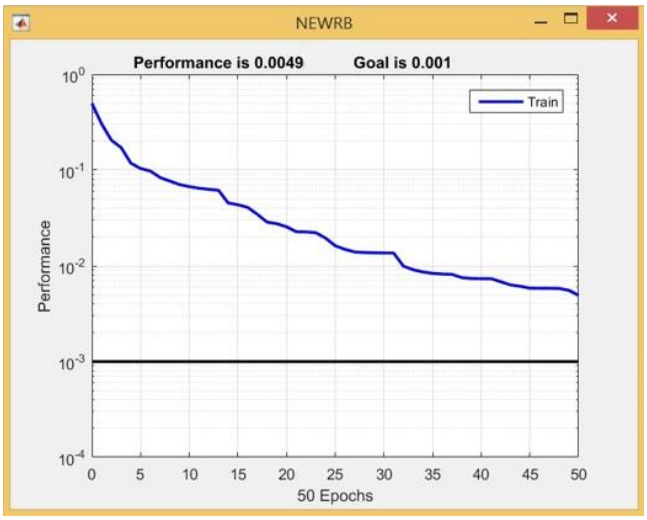

Figure 7. 10 The mean squared error (MSE) for RBFNN

Figure 7.10 shows the training process of RBFNN at wheel wear prediction in case of vertical shear stifness simulation, it shows that when the goal was 0.001, spread was 30, mn was 50, and df was 5; the MSE was 0.0049 and the training stopped at 50 epochs.

7.6 NARXNN and BPNN performance

To check the network performance of NARXNN and BPNN and determine if any changes need to be made to the training process; the performance function for training, validation and test subsets for all tests which were carried out in this thesis for wheel/rail wear prediction were checked. The result shows a good network performance because the test set error and the validation set error have very similar characteristics, and it does not appear that any significant over fitting has occurred. Moreover, the correlation coefficient (R) between the predicted and experimental/simulation values was checked as well. The value of R was close to 1 for all tests which were carried out in this thesis for wheel/rail wear prediction. It was greater than 0.9. It is a good sign for the neural network model to be accurate. It indicates a good matching between the experimental/simulation data and prediction of the neural network model.

An example of the performance plot and regression plot were illustrated in appendix 12 and appendix 13 respectively, it is for used the NARXNN and BPNN to predict railway wheel wear for vehicle dynamics simulations (for speed test).

7.7 Chapter discussion

The backpropagation neural network (BPNN), and the radial basis function neural network (RBFNN) were developed to predict wheel wear. The simulation results were compared with the wheel wear predicted using the Nonlinear Autoregressive model with eXogenous input neural network (NARXNN).

The simulation results show that the three types of neural networks achieved good wheel wear prediction. The percentage error was calculated, the results show that the wheel wear predicted using VAMPIRE was close to wheel wear predicted using the neural network model. The accuracy of the neural network model was assessed by mean absolute percentage error (MAPE), the accuracy of NARXNN was the best, followed respectively by the RBFNN and BPNN such as:

- In the change of speed test. MAPE was 7.14% for NARXNN, 8.63% for RBFN, and 10.70% for BPNN.
- In the change of longitudinal bush stiffness test. MAPE was 7.46% for NARXNN, 9.22% for RBFN, and 10.14% for BPNN.
- In the change of longitudinal shear stiffness test. MAPE was 8.34% for NARXNN, 9.77% for RBFN, and 10.08% for BPNN.

The simulation results show that the accuracy of a three type of neural network for wheel wear prediction was greater than 89.30%, it reached to 92.86%.

This chapter also investigated the effect of RBFNN parameters on wheel wear prediction; four parameters were examined: spread, mn, goal, and df; tests results were illustrated as:

- In the effects of spread parameter test: The MAPE was 10.98% when spread was 30, it was 14.70% when spread was 10, and it was 32.36% when spread was 5.
- In the effects of mn parameter test: The MAPE was 9.11% when mn was 500, it was 36.39 % when mn was 300, and it was 49.31% when mn was 20.
- In the effects of goal parameter test: The MAPE was 9.01% when goal was 0.01, it was 9.45% when goal was 0.015, and it was 14.55% when goal was 0.1.
- In the effects of df parameter test: The MAPE was 6.65% when df was 50, it was 6.65% when df was 20, and it was 6.65% when df was 10.

The simulation results show that the accuracy of neural network model for wheel wear prediction was affected by changing of spread, mn, and goal parameters.

7.8 Chapter conclusion

A nonlinear autoregressive model with exogenous input neural network (NARXNN), backpropagation neural network (BPNN), and the radial basis function neural network (RBFNN) were developed to predict railway wheel wear.

The inputs of the neural network model were: speed, running distance, longitudinal bush stiffness, lateral bush stiffness, vertical bush stiffness, longitudinal shear stiffness, lateral shear stiffness, vertical shear stiffness, wheel profile, first derivative of wheel profile, and second derivative for wheel profile; while the output of the neural network was railway wheel wear.

The simulation results show that the three types of neural network: NARXNN, BPNN, and RBFNN achieved good wear prediction in view of percentage error, where the wheel predicted using VAMPIRE software was close to the wheel wear predicted using the neural network model.

The accuracy of the three types of neural network for wheel wear prediction was calculated. The accuracy of neural network model was between 89.30% and 92.86%. It can therefore be concluded that the NARXNN, BPNN, and RBFNN are accurate models for wheel wear prediction.

The effects of the RBFNN parameters such as spread, goal, maximum number of neurons, and number of neurons to add between displays on wheel wear prediction was investigated. The simulation results show that the accuracy of wheel wear prediction was influenced by change of spread, mn, and goal; while the change of df parameter has no effect on the wheel wear prediction using RBFNN. Therfore, it can be concluded that the railway wheel wear prediction using neural network is dependent on the correct selection of the neural network parameters.

Finally, the VAMPIRE vehicle dynamic software can assist in using the neural network in railway wheel wear prediction; where several simulations were carried out in this work using VAMPIRE software to produce the data to train, validate, and test the neural network model.

Chapter 8 Discussion, conclusions, and future work

The discussion, and conclusions from the experimental and simulation results are presented in this chapter. Also, suggested future work is presented.

8.1 Discussion

Pin-on-disc experiments have been carried out to show how wear can be measured. Also, the effect of load on pin wear and disc wear under dry and sliding conditions was investigated. The experiments were conducted under loads of 6N, 10N, 16N, and 22N respectively, with a test time of one hour for each load, and sliding distance of 5mm in a forward and backward direction.

The pin wear and disc wear was measured using a 3D optical profilometer. Pin wear and disc wear were found to increase with an increase of applied load; a result of repeatedly sliding under applied load during time caused the temperature of pin and disc contact surface to rise and then the strength of pin and disc material was decreased, which led to an increase of pin wear and disc wear.

Test results show that the disc wear was greater than the pin wear, this was due to the pin being made of strong material (mild carbon steel EN8), while the disc was made of Aluminium 6082.

A new method was developed for measuring wheel wear and rail wear for a twin disc test rig. A replica material was used to make a copy of the surfaces of the two rollers before and after each test, then an Alicona profilometer was used to measure the wheel wear and rail wear. The wheel wear and rail wear were measured in term of volume loss per unit area ($\mathrm{mm}^3/\mathrm{mm}^2$).

The twin disc test rig experiments were carried out to investigate the effect of key parameters such as load, and yaw angle on wheel wear and rail wear for the twin disc test rig. The tests were conducted for a range of loads and the results show that the wheel/rail wear was increased by an increase of load, or yaw angle. Tests results also show that the load has an approximately linear relationship with wheel/rail wear; while the yaw angle has a nonlinear relationship with wheel/rail wear.

In addition, this project also investigated the effect of surface conditions such as wet, lubricated, and sanded conditions on wheel wear and rail wear for the twin disc test rig. As an example, with an applied load of 2200N, wet conditions decreased the wheel wear by a factor of 1.5, lubricated conditions decreased the wheel wear by a factor of 1.9, while sanded conditions increased the wheel wear by a factor of 1.3. Wet conditions decreased the rail wear by a factor of 1.2, lubricated conditions decreased the rail wear by a factor of 1.8, while sanded conditions increased the rail wear by a factor of 1.7.
On average; the wheel wear was decreased under wet conditions by a factor of 1.3, it was decreased under lubricated conditions by a factor of 1.8, while it increased by a factor of 1.2 under sanded conditions; the

rail wear was decreased under wet conditions by a factor of 1.1, it was decreased under lubricated conditions by a factor of 1.6, while it increased by a factor of 1.5 under sanded conditions. The test results show that the wheel wear and rail wear increased nonlinearly under dry, wet, lubricated, and sanded conditions with different loads.

For a twin disc test rig: The Nonlinear Autoregressive model with eXogenous input neural network (NARXNN) was developed in this project to predict the wheel and rail wear for the twin disc rig experiments. The inputs of the NARXNN were load, yaw angle, speed, wheel/rail profile, first derivative and second derivative of the wheel/rail profile; while the output of the NARXNN was the wheel/rail wear. A series-parallel NARXNN and a parallel NARXNN were developed to predict wheel/rail wear. The accuracy of the NARXNN model was evaluated using mean absolute percentage error (MAPE). The MAPE was between 6.63% and 11.37% for wear prediction using series-parallel NARXNN. The MAPE was between 14.46% and 18.63% for wear prediction using parallel NARXNN. The percentage error for wheel wear prediction was calculated; the simulation results exhibits good prediction of wheel and rail wear in view of percentage error; where the wheel wear and rail wear predicted using NARXNN wear was close to wheel/rail wear measured using Alicona profilometer for the twin disc rig experiemtns.

The accuracy of wheel/rail wear prediction using NARXNN was investigated and assessed in term of MAPE such as:

- The MAPE for series-parallel NARXNN (6-10-1) was 8.58%, it was smaller than the MAPE for the series-parallel NARXNN (6-7-1) and series-parallel NARXNN (6-13-1). Therefore, the series-parallel NARXNN (6-10-1) was more accurate than the series-parallel NARXNN (6-7-1) and series-parallel NARXNN (6-13-1) for wheel wear prediction.
- The MAPE for parallel NARXNN (6-10-1) was 7.17%, it was smaller than the MAPE for the parallel NARXNN (6-7-1) and parallel NARXNN (6-13-1). Therefore, the parallel NARXNN (6-10-1) was more accurate than the parallel NARXNN (6-7-1) and parallel NARXNN (6-13-1) for rail wear prediction.

Simulation results show that the wheel/rail wear depth after applied yaw angle of 0.5degree was greater than the wheel/rail wear depth after applied yaw angle of 0.2degree,0.3degree, and 0.4degree. Therefore, the wheel/rail wear depth increased with increase of yaw angle.

For vehicle dynamics simulations: The NARXNN was developed to predict the railway wheel wear in case of changing parameters such as speed, longitudinal bush stiffness, lateral bush stiffness, vertical bush stiffness, longitudinal shear stiffness, lateral shear stiffness, and vertical shear stiffness. The inputs of the NARXNN were running distance, speed, longitudinal bush stiffness, lateral bush stiffness, vertical bush stiffness, longitudinal shear stiffness, lateral shear stiffness, and vertical shear stiffness, wheel profile, first derivative and second derivative of the wheel profile; while the output of the NARXNN was the railway

wheel wear. VAMPIRE vehicle dynamic software was used to produce the data which were used to train, validate, and test the network. Results show that the NARXNN predicts the wheel wear within 89.98% to 96.40% accuracy.

A backpropagation neural network (BPNN), and a radial basis function neural network (RBFNN) were developed to predict railway wheel wear for vehicle dynamics simulations. The results were compared with wheel wear predicted using the NARXNN. The simulation results show that the three types of neural networks achieved good wheel wear prediction as can be seen bellow:

- The MAPE was 7.14% for NARXNN, 8.63% for RBFN, and 10.70% for BPNN during the change of speed parameter simulation.
- The MAPE was 7.46% for NARXNN, 9.22% for RBFN, and 10.14% for BPNN during the change of longitudinal bush stiffness simulation
- The MAPE was 8.34% for NARXNN, 9.77% for RBFN, and 10.08% for BPNN during the change of longitudinal shear stiffness simulation.

The NARXNN, the BPNN, and the RBFNN were developed to predict railway wheel wear. Results show that the wheel wear predicted using neural networks was close to wear predicted using simulation tests for unseen data. The findings obtained using the proposed neural approach yielded better results from the perspective of the mean absolute percentage error (MAPE) measure. Therefore, it can be concluded that an artificial neural network can be used efficiently as a predictor of railway wheel wear.

This project investigated the effect of RBFNN parameters on wheel wear. The effect of spread, mn, goal, and df parameters on wheel wear prediction were examined. The mean absolute percentage error (MAPE) was calculated as:

- The MAPE was 10.98% when spread was 30, it was 14.70% when spread was 10, and it was 32.36% when spread was 5 during the change of spread parameter test.
- The MAPE was 9.11% when mn was 500, it was 36.39 % when mn was 300, and it was 49.31% when mn was 20 during the change of mn parameter test.
- The MAPE was 9.01% when goal was 0.01, it was 9.45% when goal was 0.015, and it was 14.55% when goal was 0.1 during the change of goal parameter test.
- The MAPE was 6.65% when df was 50, it was 6.65% when df was 20, and it was 6.65% when df was 10 during the change of df parameter test.

The effect of neural network parameters selection such as spread, goal, maximum number of neurons, and number of neurons to add between displays on wheel wear prediction. Simulation results show that the accuracy of wheel wear prediction using neural network is dependent on the correct selection of neural network parameters.

8.2 Conclusions

The prediction of wheel and rail wear has previously been based on a classical models such as the Archard wear model or energy dissipated models. The work undertaken in this thesis attempts to build a neural network model to predict wheel wear and rail wear.

The conclusions from the experimental and simulation tests are presented in this section.

- The primary contribution of this project was the development of a neural network model to predict the wheel and rail wear for the twin disc rig experiments. The inputs of the neural network model for wheel and rail wear prediction for the twin disc rig experiments were load, yaw angle, speed, wheel/rail profile, and first and second derivative of wheel/rail profile. The output of the neural network model was wheel and rail wear.
- The second contribution of this work was the development three types of neural networks to predict railway wheel wear for vehicle dynamics simulations. The inputs of the neural network model for wheel and rail wear prediction for vehicle dynamics simulations were speed, running distance, longitudinal bush stiffness, lateral bush stiffness, vertical bush stiffness, longitudinal bush stiffness, lateral bush stiffness, vertical shear stiffness, wheel/rail profile, and first and second derivative of wheel profile. The output of the neural network model was railway wheel wear.
- A new method for wheel wear and rail wear measurements was applied during this work using replica material and an Alicona profilometer. This has been used in other fields but in this work it has been shown to be effective for measuring wheel and rail wear.

The conclusions are summarized as follows:
The test results for pin-on-disc experiments show that the pin wear and disc wear increased with increase of the load. The disc wear is bigger than the pin wear, because the disc is made of aluminium and the pin is made of steel.

The major finding in the pin-on-disc test is that the Alicona profilometer can be used for pin wear and disc wear measurements.

The University of Huddersfield twin disc test rig together with a replica technique and an Alicona profilometer were used for wheel wear and rail wear measurements. The replica material and Alicona profilometer are effective tools for the wheel wear and rail wear measurements. An advantage of using the replica method is that it is a permanent record of wheel and rail surface.

The effect of load, and yaw angle on wheel wear and rail wear were investigated. The test results show that the applied load, and yaw angle all influence the wheel/rail wear. Tests results show that the load has an approximately linear relationship with wheel/rail wear; while the yaw angle has a nonlinear relationship with wheel/rail wear.

This work investigated the effect of surface conditions such as wet, lubricated, and sanded conditions on wheel wear and rail wear for the twin disc rig experiments. The wet conditions decreased the wheel wear by an average factor of 1.3, the lubricated conditions decreased the wheel wear by a factor of 1.8, while the sanded conditions increased the wheel wear by a factor of 1.2. The wet conditions decreased the rail wear by a factor of 1.1, the lubricated conditions decreased the rail wear by a factor of 1.6, while the sanded conditions increased the rail wear by a factor of 1.5. The test results show that both water and oil reduced the wheel and rail wear; while the wheel and rail wear increased under sanded conditions. Test results show that the wheel/rail wear has nonlinear relationship with load under dry, wet, lubricated, and sanded conditions.

The Nonlinear Autoregressive model with eXogenous input neural network (NARXNN) was developed to predict the wheel and rail wear for the twin disc rig experiments under dry, wet, lubricated, and sanded conditions. NARXNN was predicted the wheel and rail wear successfully, and the accuracy of the model was calculated in view of mean absolute percentage error (MAPE). The accuracy of model was between 81.37% and 93.37%. The accuracy of the wheel/rail wear prediction using a neural network was influenced by the architecture of neural network. The wheel/rail wear depth was influenced by the yaw angle.

The NARXNN was developed to predict railway wheel wear in case of changing parameters such as speed, longitudinal bush stiffness, lateral bush stiffness, vertical bush stiffness, longitudinal bush stiffness, lateral bush stiffness, and vertical shear stiffness on wheel wear. VAMPIRE vehicle dynamics software was used to produce data to train, validate, and test the network. The mean absolute percentage error (MAPE) was calculated for unseen data and was between 3.60% and 10.02%; this reflects the degree of accuracy for the NARXNN for railway wheel wear prediction. The simulation results show that the NARXNN predicted the railway wheel wear within an accuracy of 89.98% to 96.40%. This indicates that the NARXNN is an accurate model for wheel wear prediction.

The backpropagation neural network (BPNN), and the radial basis function neural network (RBFNN) were developed to predict railway wheel wear, then, the results were compared with railway wheel wear prediction using the NARXNN. The simulation results show that the three types of neural network achieved good wear prediction in view of MAPE. The NARXNN was the best, followed by the RBFNN and BPNN respectively. Therefore, the three types of neural network are an effective tool for wheel wear prediction.
Additional investigations were carried out in this project to study the effects of change of the radial basis function neural network (RBFNN) parameters such as spread, mn, goal, and df on railway wheel wear prediction using neural network. The MAPE was calculated, results show that the MAPE was changed with change of neural network parameters. The simulation results show that the accuracy of railway wheel wear prediction using neural network was influenced by the changing of the neural netwrok parameters. Therefore, the accuracy of wheel wear prediction using neural network is dependent on the proper selection

of the neural network parameters. The accuracy of wheel wear and rail wear prediction using the neural network was investigated and assessed in term of mean absolute percentage error (MAPE). The MAPE was less than 11% using neural network for a twin disc rig tests; while the neural network model achieved wheel wear prediction with accuracy up to 96.40% for railway vehicle simulations. This represents the accuracy of the neural network model for wheel wear prediction. The results reveal that the neural network can be used efficiently to predict wheel wear and rail wear. This work introduced the replica material and Alicona profilometer which can assist to predict the wheel wear and rail wear. This work also demonstrated the neural network as a powerful tool for wheel wear and rail wear prediction.

The major conclusion in this thesis is that a properly designed neural network together with appropriately chosen inputs can predict wheel wear and rail wear successfully.

This work can be used to promote the use of predictive maintenance strategies by railway operators. It can for example help in understanding remaining life of wheels or rails and in planning of maintenance interventions.

8.3 Future work

The research work presented in this thesis points to several directions for future work. In this project, there are still a number of issues which have not been studied as follows:

- The use of replica material to measure the wheel wear and rail wear in real railway system.
- The use the replica material to study other characteristics of the wheel and rail surface, for example to investigate the relationship between wheel/rail wear and wheel/rail surface roughness.
- The development of a new technique to select the optimum number of hidden layers and neurons of neural networks to obtain the optimum wheel/rail wear prediction.
- This work studies the wheel wear and rail wear in terms of material removal; in future, wheel wear and rail wear could be investigated in terms of wear type such as abrasive, adhesive, and chemical wear.
- This work investigates the wheel wear on straight track. Wheel wear prediction using the neural network on the curved track could be investigated but the inputs of the neural network model will change and additional parameters included such as the track curve radii, and cant efficiency. It may be appropriate to consider different Neural Network architectures including possible variation between left and right wheels/rails in a curve. The methodology of wheel wear prediction using Vampire software shown in Figure 6.2 should be developed to predict forces and wear on the curved track.
- Investigate the effect of scaling method on wheel/rail wear, and compare the lab measurements of wheel/rail wear with the real system measurements.

Bibliography

[1] R. Lewis and U. Olofsson, *Wheel-rail interface handbook*: Elsevier, 2009.

[2] V. Reddy, "Development of an integrated model for assessment of operational risks in rail track," Queensland University of Technology, 2007.

[3] A. Khudhair and N. A. Talib, "Neural Network Analysis For Sliding Wear of 13% Cr Steel Coatings by Electric Arc Spraying," in *Diyala Journal of Engineering Sciences-First Engineering Scientific Conference, College of Engineering–University of Diyal*, 2010, pp. 157-169.

[4] K. Mehrotra, C. K. Mohan, and S. Ranka, *Elements of artificial neural networks*: MIT press, 1997.

[5] A. o. A. Railroads. TOTAL ANNUAL SPENDING,Association of American Railroads, 2015, https://www.aar.org/Fact%20Sheets/Safety/AAR%20Annual%20Spending_2016%20Update_7.15.16.pdf [Online].

[6] A. o. A. Railroads. Freight Railroad Capacity and Investment,Association of American Railroads, 2016, https://www.aar.org/BackgroundPapers/Freight%20Railroad%20Capacity%20and%20Investment.pdf [Online].

[7] N. A. Office. A Short Guide to Network Rail,National Audit Office, 2016, https://www.nao.org.uk/wp-content/uploads/2015/08/Network-rail-short-guide1.pdf [Online].

[8] O. g. o. transport. Accelerating innovation in rail, Official group of transport , 2016, https://connect.innovateuk.org/web/accelerating-innovation-in-rail1/article-view/-/blogs/rssb-opens-4-5-million-vehicle-dynamics-competition-for-innovations-to-address-rolling-contact-fatigue [Online].

[9] P. Molyneux-Berry and A. Bevan, "The Influence of Route Characteristics, Train Design and Maintenance Policy on Wheel Tread Damage, Wheel Life and Costs for Multiple-Unit Trains," 2013.

[10] R. Enblom, "On Simulation of uniform wear and prpfile evaluation in the wheel rail contact," Royal Institute of Technology KTH, KTH Engineering 2006

[11] B. Pugh, *Friction and wear*: Newnes-Butterworths, 1973.

[12] B. Bhushan, *Tribology: Friction, wear, and lubrication*: CRC Press LLC, 2000.

[13] A. Zmitrowicz, "Wear patterns and laws of wear–a review," *Journal of theoretical and applied mechanics*, vol. 44, pp. 219-253, 2006.

[14] A. Sethuramiah, *Lubricated wear: science and technology* vol. 42: Elsevier Science Limited, 2003.

[15] S. M. Nahvi, "Abrasive wear behaviour of steels and advanced HVOF-sprayed WC-M coatings," University of Nottingham, 2011.

[16] V. V. Sobolev, J. M. Guilemany, J. Nutting, and S. Joshi, *High velocity oxy-fuel spraying: theory, structure-property relationships and applications*: Maney, 2004.

[17] B. Bhushan, *Principles and applications of tribology*: John Wiley & Sons, 2013.

[18] V. Sarin, *Comprehensive hard materials*: Newnes, 2014.

[19] B. Bhushan, *Modern Tribology Handbook, Two Volume Set*: Crc Press, 2000.

[20] J. Stokes, "The Theory and Application of the HVOF (High Velocity Oxy-Fuel)," ed, 2011.

[21] A. Khamis and S. N. S. B. Abdullah, "Forecasting Wheat Price Using Backpropagation And NARX Neural Network," *The International Journal Of Engineering And Science (IJES)*, vol. Vol. 3, pp. 19-26, 2014.

[22] G. Stachowiak and A. W. Batchelor, *Engineering tribology*: Butterworth-Heinemann, 2013.

[23] S. Iwnicki, *Handbook of railway vehicle dynamics*: CRC press, 2006.

[24] J. Thompson, *Vehicle dynamics and vehicl/track interaction* Interface technology 2011.

[25] Railway. BOGIE PARTS & DESCRIPTION, Railway , 2016, http://www.railway-technical.com/bogie1.shtml [Online].

[26] M. Spiryagin, C. Cole, Y. Q. Sun, M. McClanachan, V. Spiryagin, and T. McSweeney, *Design and simulation of rail vehicles*: CRC Press, 2014.

[27] S. Kaewunruen and A. Remennikov, "Dynamic properties of railway track and its components: a state-of-the-art review," *Faculty of Engineering-Papers*, p. 493, 2008.

[28] I. Povilaitiene and A. Laurinavičius, "Reduction of external rail wearing on road curves," *Journal of civil engineering and management*, vol. 10, pp. 123-130, 2004.

[29] J. Mundrey, *Railway track engineering*: Tata McGraw-Hill Education, 2009.

[30] O. Polach, "Characteristic parameters of nonlinear wheel/rail contact geometry," *Vehicle System Dynamics*, vol. 48, pp. 19-36, 2010.

[31] A. TUDOR and N. S. E. TOUNTAS, "Wheel/rail friction power in curved track," *U.P.B. Sci. Bull* 2009.

[32] S. Jon, "On wear transitions in the wheel-rail contact," phD thesis Royal Institute of Technology Stockholm 2009.

[33] C. E. Pit, "Wear and microstructure relationships in Carbide-Free Bainitic rail steels " phD, Cambridge University, UK, UK, 1999.

[34] H. A. Ahmad, "Dynamic Braking Control for Accurate Train Braking Distance Estimation under Different Operating Conditions," 2013.

[35] P. Waara, "Lubricant influence on flange wear in sharp railroad curves," *Industrial lubrication and tribology*, vol. 53, pp. 161-168, 2001.

[36] P. Waara, "Lubricants influence on wear in sharp rail curves," Division of Machine Elements, Luleå University of Technology, 2006.
[37] L. J. Wilson, "Performance measurements of rail curve lubricants," 2006.
[38] J. Zhang, *Detection and monitoring of wear using imaging methods*: University of Twente, 2006.
[39] ASTM, "Standard Test Method for Wear Testing with a Pin-on-Disk Apparatus," *Annual Book of ASTM Standards, G99-05*, vol. 3, 2000.
[40] M. Hadfield, C. Brebbia, and J. Seabra, *Tribology & Design*. WIT Press, 2010.
[41] R. G. Bayer, *Mechanical Wear Fundamentals and Testing, revised and expanded*: CRC Press, 2004.
[42] M. Windarta and F. Khairul, "Influence of applied load on wear characterizations of rail material," *Journal of Applied Science*, vol. 11, pp. 1636-1641, 2011.
[43] M. Chowdhury, M. Khalil, D. Nuruzzaman, and M. Rahaman, "The effect of sliding speed and normal load on friction and wear property of aluminum," *Int. J. Mech. Mechatron. Eng*, vol. 11, pp. 53-57, 2011.
[44] H. A. Ameen, K. S. Hassan, E. M. M. Mubarak, H. Ameen, K. Hassan, and E. Mubarak, "Effect of loads, sliding speeds and times on the wear rate for different materials," *American journal of scientific and industrial research*, vol. 2, pp. 99-106, 2011.
[45] V. Lakshminarayana and V. Balu, "INFLUENCE OF VARYING LOAD ON WEAR RATE AND FRICTIONAL RESISTANCE OF EN-8 STEEL SLIDING AGAINST EN-31 STEEL " *ARPN Journal of Engineering and Applied Sciences*, vol. VOL. 10, NO. 13, 2015.
[46] D. Singla and S. Mediratta, "Effect of load and speed on wear properties of al 7075-fly ash composite material," *International Journal of Innovative Research in Science, Engineering and Technology*, vol. 2, pp. 1-9, 2013.
[47] E. Gallardo-Hernandez and R. Lewis, "Twin disc assessment of wheel/rail adhesion," *Wear*, vol. 265, pp. 1309-1316, 2008.
[48] N. Tassini, X. Quost, R. Lewis, R. Dwyer-Joyce, C. Ariaudo, and N. Kuka, "A numerical model of twin disc test arrangement for the evaluation of railway wheel wear prediction methods," *Wear*, vol. 268, pp. 660-667, 2010.
[49] N. Bosso and N. Zampieri, "Experimental and numerical simulation of wheel-rail adhesion and wear using a scaled roller rig and a real-time contact code," *Shock and Vibration*, vol. 2014, 2014.
[50] F. Braghin, R. Lewis, R. Dwyer-Joyce, and S. Bruni, "A mathematical model to predict railway wheel profile evolution due to wear," *Wear*, vol. 261, pp. 1253-1264, 2006.
[51] R. Lewis, R. Dwyer-Joyce, U. Olofsson, and R. Hallam, "Wear mechanisms and transitions in railway wheel steels," *Proceedings of the Institution of Mechanical Engineers, Part J: Journal of Engineering Tribology*, vol. 218, pp. 467-478, 2004.
[52] R. Lewis, F. Braghin, A. Ward, S. Bruni, R. Dwyer-Joyce, K. Bel Knani, *et al.*, "Integrating dynamics and wear modelling to predict railway wheel profile evolution," 2003.
[53] P. Allen, "Error quantification of a scaled railway roller rig," phD, Manchester Metropolitan University, 2001.
[54] S. Montgomery, D. Kennedy, and N. O'Dowd, "Analysis of wear models for advanced coated materials," 2009.
[55] H. Meng and K. Ludema, "Wear models and predictive equations: their form and content," *Wear*, vol. 181, pp. 443-457, 1995.
[56] E. Mönch, "Zur elementaren Theorie der Zapfenreibung," *ZAMM-Journal of Applied Mathematics and Mechanics/Zeitschrift für Angewandte Mathematik und Mechanik*, vol. 31, pp. 94-94, 1951.
[57] A. Carpinteri and N. Pugno, "Evolutionary fractal theory of erosion and experimental assessment on MIR space station," *Wear*, vol. 257, pp. 408-413, 2004.
[58] B. Majumdar, *Introduction to tribology of bearings*: S. Chand Limited, 2008.
[59] C. R. Á. da Silva and G. Pintaude, "Uncertainty analysis on the wear coefficient of Archard model," *Tribology International*, vol. 41, pp. 473-481, 2008.
[60] M. Braunovic, N. Myshkin, and V. Konchits, *Electrical contacts: fundamentals, applications and technology*: CRC press, 2010.
[61] K. Corp., "Digital Microscope VHX-500 Series " in *http://www.keyence.com/*, ed. Japan, 2016.
[62] A. Azushima, *Tribology in Sheet Rolling Technology*: Springer, 2016.
[63] A. A. Tseng, *Tip-Based Nanofabrication: Fundamentals and Applications*. USA Springer, 2011.
[64] G. E. Totten, *Handbook of Lubrication and Tribology: Volume I Application and Maintenance* vol. 1: CRC Press, 2006.
[65] J. Williams, "Wear modelling: analytical, computational and mapping: a continuum mechanics approach," *Wear*, vol. 225, pp. 1-17, 1999.
[66] E. R. Booser, "CRC handbook of lubrication. Theory and practice of tribology: Volume II: Theory and design," 1984.
[67] A. Orvnäs, "Simulation of rail wear on the swedish light rail line Tvärbanan," 2005.

[68] J. Pombo, J. Ambrosio, M. Pereira, R. Lewis, R. Dwyer-Joyce, C. Ariaudo, *et al.*, "Development of a wear prediction tool for steel railway wheels using three alternative wear functions," *Wear*, vol. 271, pp. 238-245, 2011.
[69] J. Tunna, J. Sinclair, and J. Perez, "The development of a wheel wear and rolling contact fatigue model," 2007.
[70] R. Narayan, "Tribological Characterization of Biomaterials," 2012.
[71] S. Kucharski and Z. Mróz, "Identification of wear process parameters in reciprocating ball-on-disc tests," *Tribology International*, vol. 44, pp. 154-164, 2011.
[72] J. Pombo, J. Ambrósio, M. Pereira, R. Lewis, R. Dwyer-Joyce, C. Ariaudo, *et al.*, "A study on wear evaluation of railway wheels based on multibody dynamics and wear computation," *Multibody System Dynamics*, vol. 24, pp. 347-366, 2010.
[73] T. Pearce and N. Sherratt, "Prediction of wheel profile wear," *Wear*, vol. 144, pp. 343-351, 1991.
[74] X. Shu, M. Dembosky, C. Urban, and N. Wilson, "Rail Wear Simulation and Validation," in *2010 Joint Rail Conference*, 2010, pp. 313-322.
[75] A. Ward, R. Lewis, and R. Dwyer-Joyce, "Incorporating a railway wheel wear model into multi-body simulations of wheelset dynamics," *Tribology Series*, vol. 41, pp. 367-376, 2003.
[76] R. Enblom, "Simulation of Wheel and Rail Profile Evolution: Wear Modelling and Validation," 2004.
[77] J. Pombo, J. Ambrósio, M. Pereira, R. Lewis, R. Dwyer-Joyce, C. Ariaudo, *et al.*, "A railway wheel wear prediction tool based on a multibody software," *Journal of theoretical and applied mechanics*, vol. 48, pp. 751-770, 2010.
[78] A. Bevan, P. Molyneux-Berry, B. Eickhoff, and M. Burstow, "Development and validation of a wheel wear and rolling contact fatigue damage model," *Wear*, vol. 307, pp. 100-111, 2013.
[79] A. Sánchez Arandojo, "On validation of a wheel-rail wear prediction code," 2013.
[80] K. Tanifuji, "A Study on Prediction of Wear Progress of Railway Wheel," Niigata University, Japan. 2015.
[81] C. Ramesh and R. Kumar, "Mathematical and neural network models for prediction of wear of mild steel coated with inconel 718—A comparative study," *International Journal of Scientific and Research Publications*, vol. 2, pp. 1-8, 2012.
[82] A. Singh, S. Panda, D. Chakraborty, and S. Pal, "Predicting drill wear using an artificial neural network," *The International Journal of Advanced Manufacturing Technology*, vol. 28, pp. 456-462, 2006.
[83] J. Huang, H. Jin, X. Xie, and Q. Zhang, "Using NARX neural network based load prediction to improve scheduling decision in grid environments," in *Natural Computation, 2007. ICNC 2007. Third International Conference on*, 2007, pp. 718-724.
[84] A. J. P. Kumar and D. K. J. Singh, "Artificial neural network-based wear loss prediction for a390 aluminium alloy," *J. Theor. Appl. Inf. Technol*, pp. 961-964, 2008.
[85] M. H. Al Shamisi, A. H. Assi, and H. A. Hejase, *Using MATLAB to Develop Artificial Neural Network Models for Predicting Global Solar Radiation in Al Ain City-UAE*: INTECH Open Access Publisher, 2011.
[86] A. Fathy and A. Megahed, "Prediction of abrasive wear rate of in situ Cu–Al2O3 nanocomposite using artificial neural networks," *The International Journal of Advanced Manufacturing Technology*, vol. 62, pp. 953-963, 2012.
[87] H. Zhang and J. Li, "Prediction of tourist quantity based on RBF neural network," *Journal of Computers*, vol. 7, pp. 965-970, 2012.
[88] A. Nagaraj, Shivalingappa, D., Halesh Koti and Channankaiah, "Modelling and predicting adhesive wear behaviour of Aluminium-Silicon Alloy using neural network " *International Journal of Recent Scientific Research*, vol. 3, pp. 378 -381, 2012.
[89] K. R. Kumar, K. Mohanasundaram, G. Arumaikkannu, and R. Subramanian, "Artificial neural networks based prediction of wear and frictional behaviour of aluminium (A380)-fly ash composites," *Tribology-Materials, Surfaces & Interfaces*, vol. 6, pp. 15-19, 2012.
[90] C. Cătălina-Lucia and G. Hakob, "An Artificial Neural Network for Data Forecasting Purposes," *Informatica Economica*, vol. 19, 2015.
[91] D. A. Macdonald, "The application of focus variation microscopy for lithic use-wear quantification," *Journal of Archaeological Science*, vol. 48, pp. 26-33, 2014.
[92] Alicona. Alicona InfiniteFocus Specification, Alicona, 2016, http://www.alicona.com/home/fileadmin/alicona/pdfs/InfiniteFocusG5_System_and_technical_specification_E.pdf [Online].
[93] M. Tailor, "Automatic surface defect quantification in 3D," © Mitulkumar J. Tailor, 2013.
[94] R. Danzl, F. Helmli, and S. Scherer, "Focus variation–a new technology for high resolution optical 3D surface metrology," in *Proceedings of the 10th international conference of the Slovenian society for non-destructive testing*, 2009.
[95] T. Yingzhong, W. Albert, H. Tino, S. Alexander, and H. Bin, "MEASUREMENT STRATEGIES IN OPTICAL 3-D SURFACE MEASUREMENT WITH FOCUS VARIATION," *The 11th International Symposium on Measurement and Quality Control - 11th ISMQC, Krakau - Kielce, Polen*, 2011.

[96] R. Lewis, R. Dwyer-Joyce, U. Olofsson, and R. Hallam, "Wheel material wear mechanisms and transitions," 2004.
[97] S. S. Hsu, Z. Huang, S. D. Iwnicki, D. J. Thompson, C. J. Jones, G. Xie, *et al.*, "Experimental and theoretical investigation of railway wheel squeal," *Proceedings of the Institution of Mechanical Engineers, Part F: Journal of Rail and Rapid Transit*, vol. 221, pp. 59-73, 2007.
[98] S. Gasparin, H. N. Hansen, L. De Chiffre, and G. Tosello, "Verification of tolerance chains in micro manufacturing," Technical University of DenmarkDanmarks Tekniske Universitet, Department of Management EngineeringInstitut for Systemer, Produktion og Ledelse, 2012.
[99] Alicona, *Optical 3D micro coordiate measurement from & roughness* vol. Version 3.9.1 EN 2011.
[100] A. Broquetas, A. Comerón, A. Gelonch, J. M. Fuertes, J. A. Castro, D. Felip, *et al.*, "Track detection in railway sidings based on MEMS gyroscope sensors," *Sensors*, vol. 12, pp. 16228-16249, 2012.
[101] P. d. Milano, "RAILWAY BOGIE STABILITY CONTROL FROM SECONDARY YAW ACTUATORS Relatore:," Corso di Laurea MAGISTRALE in Ingegneria dell'Automazione, 2014.
[102] S. o. Kraft, "Identification des parametres d'un modele TGV," 2012.
[103] J. Leao, V. Bouillon, L. Muntada, C. Johnson, P. Wilson, O. Vergnes, *et al.*, "New formulations of sunflower based bio-lubricants with high oleic acid content–VOSOLUB project," *OCL*, vol. 23, p. D509, 2016.
[104] F. A. M.Pau, F. Ginesu, M. Ishida, H. Chen "EVALUATION OF THE INFLUENCE OF SURFACE CONDITIONS ON WHEEL-RAIL CONTACT PERFORMANCES."
[105] A. C. Rosander, *Applications of quality control in the service industries*: CRC Press, 1985.
[106] W. S. McCulloch and W. Pitts, "A logical calculus of the ideas immanent in nervous activity," *The bulletin of mathematical biophysics*, vol. 5, pp. 115-133, 1943.
[107] M. Minsky and S. Papert, "Perceptrons," 1969.
[108] D. Rumelhart, G. Hinton, and R. Williams, "Learning Internal Representation by Error Propagation. D. Rumelhart and J. McClelland, Eds., Parallel Distributed Processing," ed: MIT Press, Cambridge, Mass, 1986.
[109] B. Kröse, B. Krose, P. van der Smagt, and P. Smagt, "An introduction to neural networks," 1993.
[110] B. Yegnanarayana, *Artificial neural networks*: PHI Learning Pvt. Ltd., 2009.
[111] E. R. Jones, *An Introduction to Neural Networks* USA: Visual Numerics, 2004.
[112] S. Sivanandam and S. Deepa, *Introduction to neural networks using Matlab 6.0*: Tata McGraw-Hill Education, 2006.
[113] N. Nedjah and L. de Macedo Mourelle, *Evolvable machines: theory & practice* vol. 161: Springer Science & Business Media, 2005.
[114] K. L. Priddy and P. E. Keller, *Artificial neural networks: an introduction* vol. 68: SPIE Press, 2005.
[115] J. Heaton, *Introduction to neural networks with Java*: Heaton Research, Inc., 2008.
[116] S. Sumathi and S. Paneerselvam, *Computational intelligence paradigms: theory & applications using MATLAB*: CRC Press, 2010.
[117] R. Matignon, *Neural network modeling using SAS enterprise miner*: AuthorHouse, 2005.
[118] A. Ukil, *Intelligent systems and signal processing in power engineering*: Springer Science & Business Media, 2007.
[119] A. Zalzala and X. Liu, "Neural Networks for Identification, Prediction and Control," ed: Great Britain: Springer-Verlag London Limited, 1995.
[120] C. R. Tosh and G. D. Ruxton, *Modelling perception with artificial neural networks*: Cambridge University Press, 2010.
[121] G. Mihalakakou, M. Santamouris, and D. Asimakopoulos, "Modeling ambient air temperature time series using neural networks," *Journal of Geophysical Research: Atmospheres (1984–2012)*, vol. 103, pp. 19509-19517, 1998.
[122] E. Diaconescu, "The use of NARX neural networks to predict chaotic time series," *WSEAS Transactions on Computer Research*, vol. 3, pp. 182-191, 2008.
[123] Mathworks, "Design Time Series NARX Feedback Neural Networks " in *Matlab help*, ed, 2015.
[124] A. Di Piazza, M. Di Piazza, and G. Vitale, "Estimation and forecast of wind power generation by FTDNN and NARX-net based models for energy management purpose in smart grids," *algorithms*, vol. 8, p. 10, 2014.
[125] Mathworks, "Multistep Neural Network Prediction," in *Matlab help* ed, 2015.
[126] Mathworks, "Modeling and Prediction with NARX and Time-Delay Networks," in *Matlab help*, ed, 2015.
[127] Mathworks, "Neural Network Time Series Prediction and Modeling," in *Matlab help*, ed, 2015.
[128] T. J. Griinke, "Development of an artificial neural network (ANN) for predicting tribological properties of kenaf fibre reinforced epoxy composites (KFRE)," 2013.
[129] D. W. Patterson, *Artificial neural networks: theory and applications*: Prentice Hall PTR, 1998.
[130] Mathworks, "Train and Apply Multilayer Neural Networks," in *Matlab help*, ed, 2015.
[131] K. G. Sheela and S. Deepa, "Review on methods to fix number of hidden neurons in neural networks," *Mathematical Problems in Engineering*, vol. 2013, 2013.
[132] H. H. W. Yu, and N. Zhang, Ed., *Advances in Neural Networks* China: Springer publishing 2009.
[133] S. Haykin and N. Network, "A comprehensive foundation," *Neural Networks*, vol. 2, 2004.

[134] R. J. Howlett and L. C. Jain, *Radial basis function networks 2: new advances in design* vol. 67: Springer Science & Business Media, 2001.
[135] M. K. Kundu, Ed., *Advanced Computing, Networking and Informatics*. Switzerland Springer publishing, 2014.
[136] M. Patel, V. Honavar, and K. Balakrishnan, *Advances in the evolutionary synthesis of intelligent agents*: MIT press, 2001.
[137] S. Sabnam, D. Kunal, and K. Gitosree, *Emerging Trends in Computing and Communication*: Springer 2014.
[138] G. M. Fathalla, "Analysis and implementation of radial basis function neural network for controlling non-linear dynamic systems," phD thesis Faculty of Engineering University of Newcastle UK, 1998.
[139] S. Fosseng, "Learning Distance Functions in k-Nearest," Norwegian University of Science and Technology, Department of Computer and Information Science 2013.
[140] S. S. A. Ali, M. Moinuddin, K. Raza, and S. H. Adil, "An adaptive learning rate for RBFNN using time-domain feedback analysis," *The Scientific World Journal*, vol. 2014, 2014.
[141] L. D. Fredendall and E. Hill, *Basics of supply chain management*: CRC Press, 2000.
[142] Mathworks, "Design radial basis network - newrb " in *Mathlab help*, ed, 2015.
[143] D. Li and Y. Chen, *Computer and Computing Technologies in Agriculture VII: 7th IFIP WG 5.14 International Conference, CCTA 2013, Beijing, China, September 18-20, 2013, Revised Selected Papers* vol. 419: Springer, 2014.
[144] M. Iskander, V. Kapila, and M. A. Karim, *Technological Developments in Education and Automation*: Springer Science & Business Media, 2010.
[145] H. Demuth and M. Beale, *Neural Network Toolbox*. Mathworks 2002
[146] N. Networks. Lab 4: Radial Basis Functions (RBF) Networks. Regression and prediction, Neural Networks, 2016, http://web.info.uvt.ro/~dzaharie/nn2009_lab4.pdf [Online].
[147] J. M. F. Jose Mira, Jose-Ramon Alvarez Sanchez, Felix Paz, Javier Toledo *Bioinspired Applications in Artificial and Natural Computation Part 2*: Springer 2009.
[148] L. Rutkowski, *Computational intelligence: methods and techniques*: Springer Science & Business Media, 2008.
[149] K. Arya and V. P. Vishwakarma, "Performance Comparison on Face Recognition System Using Different Variants of Back-Propagation Algorithm with Radial Basis Function Neural Networks," *network*, vol. 3, pp. 1588-1595, 2013.
[150] S. Z. Xiaodong Chai, Song Geng, Lei Zhang "The Prediction of Railway Vehicle Vibration Based on Neural Network," *Journal of Information & Computational Science* vol. 12:16 (2015), pp. 5889–5899, 2015.
[151] B. Mahadevan, *Operations management: Theory and practice*: Pearson Education India, 2010.
[152] C. W. Chase Jr, *Demand-driven forecasting: a structured approach to forecasting*: John Wiley & Sons, 2013.
[153] R. A. Yaffee and M. McGee, *An introduction to time series analysis and forecasting: with applications of SAS® and SPSS®*: Academic Press, 2000.
[154] R. E. Klosterman, *Community analysis and planning techniques*: Rowman & Littlefield Publishers, 1990.
[155] P. Kennedy, *A guide to econometrics*: MIT press, 2003.
[156] DeltaRail, *VAMPIRE help manual V5.60* UK, 2012.
[157] DeltaRail, *VAMPIRE help manual V6.30* UK, 2012.
[158] "RAILWAY BOGIE STABILITY CONTROL FROM SECONDARY YAW ACTUATORS Relatore:," Corso di Laurea MAGISTRALE in Ingegneria dell'Automazione, 2014.
[159] R. Enblom, "Simulation of railway wheel profile evolution due to wear," in *Proceedings of the SIMPACK User'Meeting*, 2006.
[160] A. Bevan, P. Molyneux-Berry, S. Mills, A. Rhodes, and D. Ling, "Optimisation of wheelset maintenance using whole-system cost modelling," *Proceedings of the Institution of Mechanical Engineers, Part F: Journal of Rail and Rapid Transit*, vol. 227, pp. 594-608, 2013.
[161] S. Iwnicki, "The effect of profiles on wheel and rail damage," *International Journal of Vehicle Structures & Systems*, vol. 1, pp. 99-104, 2009.
[162] F. GAN, H.-Y. DAI, H. GAO, and M.-R. CHI, "Wheel-Rail Contact Relationship Calculation of Worn LMA Tread," in *2014 International Conference on Mechanics and Civil Engineering (icmce-14)*, 2014.
[163] T. Jendel and M. Berg, "Prediction of Wheel Wear for Rail Vehicles—Methodology and Verification," in *Contact Mechanics*, ed: Springer, 2002, pp. 229-236.
[164] J. A. C. Martins and M. D. M. Marques, *Contact Mechanics: Proceedings of the 3rd Contact Mechanics International Symposium, Praia da Consolação, Peniche, Portugal, 17–21 June 2001* vol. 103: Springer Science & Business Media, 2013.
[165] A. Szabó and I. Zobory, "On simulation of wheel/rail wear in metro operation," *Transportation Engineering*, vol. 30, pp. 3-19, 2003.
[166] Mathworks. How to train the neural network using RBF?, Mathworks , 2016, http://uk.mathworks.com/matlabcentral/answers/74999-how-to-train-the-neural-network-using-rbf [Online].

Appendices

Appendix 1 Wheel/rail profiles of the University of Huddersfield twin disc rig

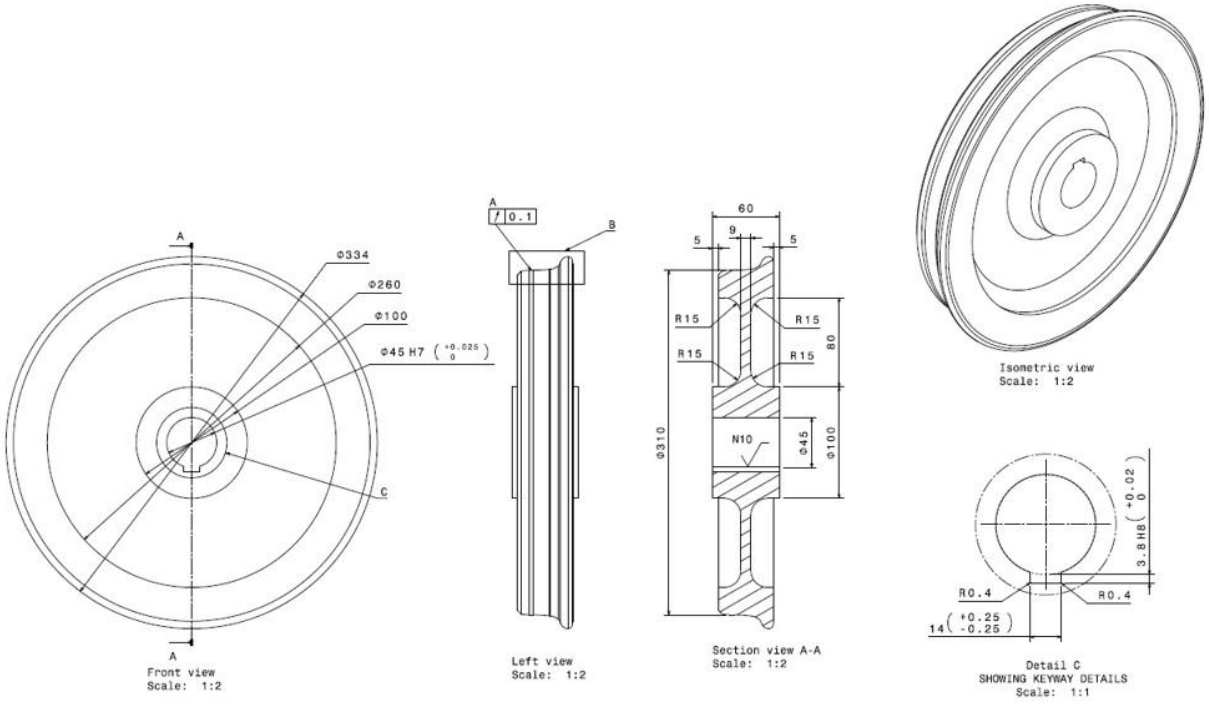

Wheel of the University of Huddersfield twin disc rig

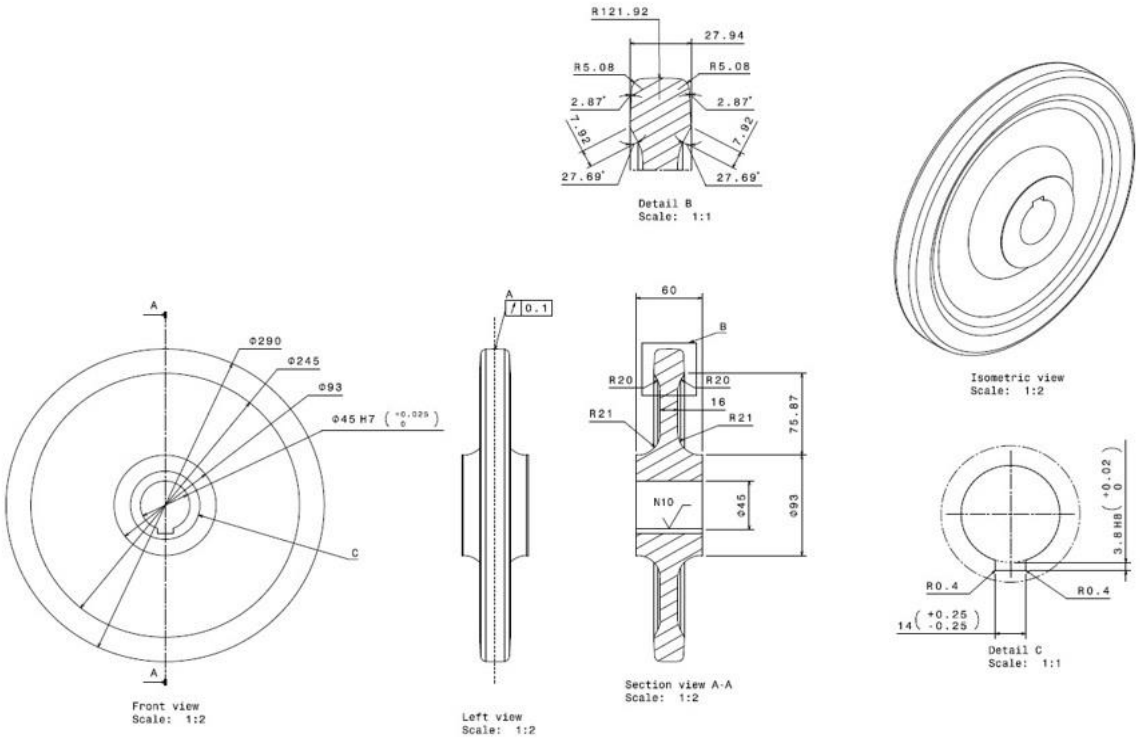

Rail of University of the Huddersfield twin disc rig

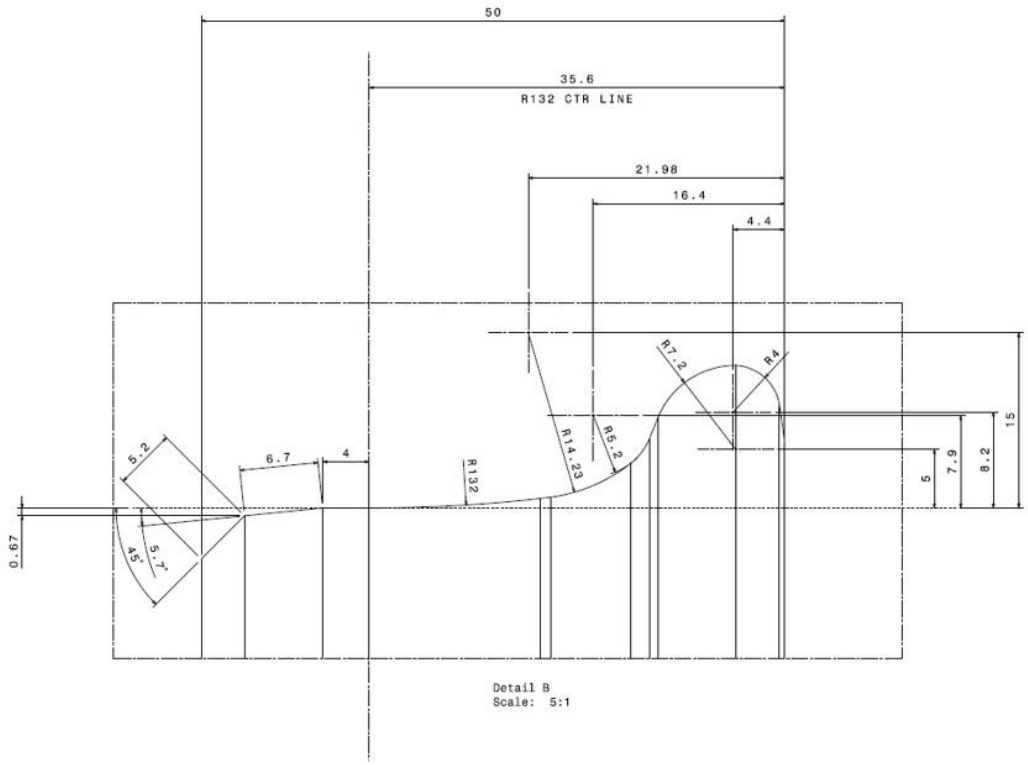

Wheel profile of the Huddersfield University twin disc rig

Appendix 2 Wheel/rail wear measurements using an Alicona profilometer

The following steps illustrates the process of wheel/rail wear measurements using an Alicona profilometer:

1. Alicona software was switched on.
2. A new project was opened.
3. The magnification setting was selected in Alicona-If-LaboratoryMeasurmentModule, it was 5X in this work.
4. A replica sample was put under an Alicona lens (new sample).
5. The lens was moved up/down/left/right until a clear image of the replica surface was appeared on the screen.
6. To ensure the image surface was clear, the histogram drawing was put in the middle of its window.
7. The exposure (Brightness) setting and the contrast setting between the min and max settings were changed until a suitable colour was obtained for the replica surface.
8. A sensor setting was selected: Gain equal 1, light source equal one and ring light equal zero.
9. A measurement range was selected: start position for x, y, and z; and end position for x, y, and z.
   For example for wheel sample:
   Start position: $x = 0\mu m,\ y = 0\mu m, and\ z = 200\mu m.$
   End position: $x = 35000\mu m,\ y = -5000\mu m, and\ z = -3000\mu m.$
10. Polarize was Deactivated, and Imagefield was General Imagefield.
11. The start measurement switch was pressed.

12. Alicona lens started flushing, and scanned the selected replica surface area.
13. After the scanning finished, the image was saved (sample before wear).
14. Set all to zero button was pressed.
15. The replica sample (worn sample) was changed.
16. A steps 5 to 13 were repeated.
17. The image was saved (sample after wear).
18. Final wear measurement steps:
    - Alicona-If-MeasurmentSuite was selected.
    - Database was selected.
    - Sample before wear image was selected.
    - DefferenceMeausrement was pressed.
    - Sample after wear image was selected.
    - Alignment-sample alignment-apply-automatic alignment setting-apply was selected.
    - The Difference button was pressed.
    - The volume loss was measured (wheel/rail wear).

Figure below shows the software window of an Alicona profilometer, which was used to select the setting for wear measurements.

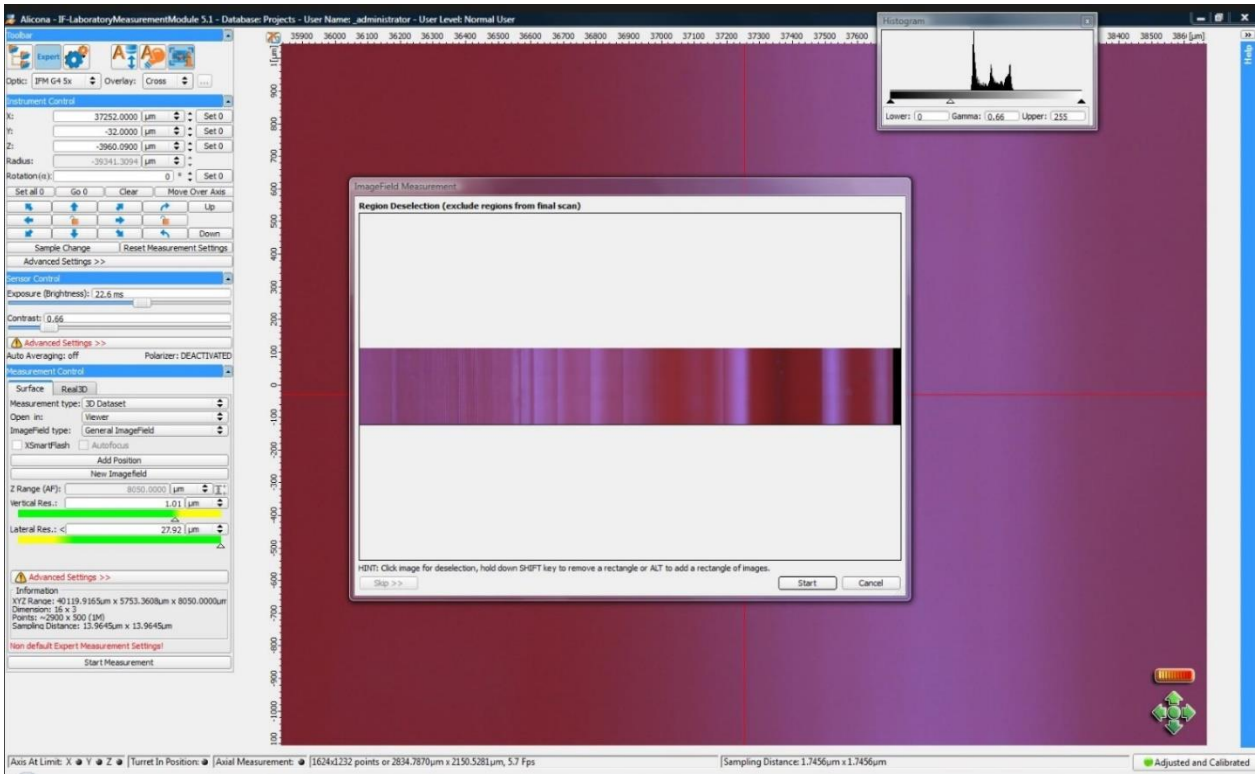

Wheel/rail Wear measuring using Alicona profilometer

Appendix 3 NARXNN for wheel/rail wear prediction

```
% The nonlinear autoregressive network with exogenous inputs (NARX) model
% This model used for wheel/rail wear prediction using series-parallel NARXNN and parallel NARXNN
.....
inputs1 = importdata('RI1.xlsx'); % upload data (input) to train, validate, and test the model
targets1 = importdata('RO1.xlsx'); % upload data (target)
aa1=inputs1';
aa2=targets1';
.....
inputs2 = importdata('RI2.xlsx'); % upload data (input) to test the model (in case of a new samples)
targets2 = importdata('RO2.xlsx'); % upload data (target)
bb1=inputs2';
bb2=targets2';
.....
out1=num2cell(aa1,1);   % to convert aa1 to cell
out2=num2cell(bb1,1);   % to convert bb1 to cell
aaa2=num2cell(aa2,1);   % to convert aa2 to cell
.....
[x] = [out1];
[t]= [aaa2];
inputSeries = x;
targetSeries = t;
.....
% Create a Nonlinear Autoregressive Network with External Input Neural Netwrok (NARXNN)
inputDelays = 1:2;
feedbackDelays = 1:2;
hiddenLayerSize = 10;
net = narxnet(inputDelays,feedbackDelays,hiddenLayerSize);
.....
% Wear prediction using series-parallel NARXNN
% Set up Division of Data for Training, Validation, Testing
net.divideParam.trainRatio = 70/100;
net.divideParam.valRatio = 15/100;
net.divideParam.testRatio = 15/100;
.....
% Prepare the Data for Training and Simulation using PREPARETS function
[Xs,Xi,Ai,Ts] = preparets(net,x,{},t);
.....
% Train the Network
[net,tr] = train(net,Xs,Ts,Xi,Ai);
.....
% Test the Network
Y = net(Xs,Xi,Ai);
perf = mse(net,Ts,Y);  % performance
E = gsubtract(Ts,Y);  %  error
.....
% View the Network
view(net)
.....

% Plots (wear predcited using series-parallel NARXNN):
figure(1);
```

```
hold on;
plotperform(tr);
plotresponse(Ts,Y);
ploterrcorr(E);
plotinerrcorr(Xs,E);
.....
% Closed Loop Network, use this network to do multi-step prediction.
% The function CLOSELOOP replaces the feedback input with a direct connection from the outout layer.
netc = closeloop(net);
netc.name = [net.name ' - Closed Loop'];
view(netc)
[Xs,Xi,Ai,Ts] = preparets(netc,x,{},t);
yc = netc(Xs,Xi,Ai);
.....
% Wear prediction using parallel NARXNN (in case of a new samples)
figure(2);
hold on;
q=netc(out2,Xi,Ai); % q is the wear predicted
w=cell2mat(q); % convert q from cell to numeric matrix
t=[1:87]';
plot(t,w,'r',t,bb2,'b')
legend('Wear predicted using parallel NARXNN','Actual Wear','Location','NorthEast');
xlabel('Samples');
ylabel('Wear (Micrometer)');
hold off;
grid on;
.....
```

Appendix 4 Error percentage and mean absolute percentage error (MAPE)

```
% The error percentage and the mean absolute percentage error (MAPE)


Errors = y - x;  % relative error , y is the actual wear, and x is the predicted wear

Error_Percentage = (abs(Errors)./x) * 100  % error percentage

MAPE = mean(Error_Percentage(~isinf(Error_Percentage)))  % (MAPE)
```

Appendix 5 How the data is used to train, validate, and test the neural network model during prediction of wheel and rail wear using neural network (an example).

Samples	Load	Yaw angle	Speed	Wheel/rail profile	1st derivative of wheel/rail profile	2nd derivative of wheel/rail pfofile
1	1200	0.2	420	-0.037	-0.0810	-0.0105
.	.	.	.	.	.	.
.	.	.	.	.	.	.
.	.	.	.	.	.	.
87	1200	0.2	420	-0.3583	0.25624	-0.1711
1	1400	0.3	540	-0.0523	-0.0674	-0.1732
.	.	.	.	.	.	.
.	.	.	.	.	.	.
.	.	.	.	.	.	.
87	1400	0.3	540	-0.42547	0.1966	0.0044
1	1600	0.4	660	-0.07567	-0.2261	0.0769
.	.	.	.	.	.	.
.	.	.	.	.	.	.
.	.	.	.	.	.	.
87	1600	0.4	660	-0.7205	0.3987	-0.1155
1	1800	0.5	780	-0.0839	-0.4359	0.3904
.	.	.	.	.	.	.
.	.	.	.	.	.	.
.	.	.	.	.	.	.
87	1800	0.5	780	-0.83489	0.4213	-0.0563

The data randomly divided into three sets as follows:

15% for training (seen data)

15% for validation

15% for testing (unseen data) → **Wear prediction using series-parallel NARXNN**

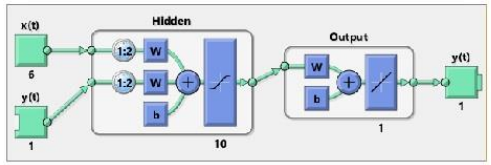

series-parallel NARXNN

Use the network saved to perform additional test

100% for testing (unseen data) → **Wear prediction using parallel NARXNN**

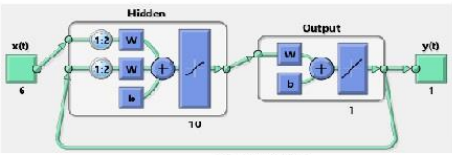

parallel NARXNN

Appendix 6 Wheel/rail wear prediction under wet, lubricated, and sanded conditions

1. Wheel/rail wear prediction using NARXNN under dry conditions

i. The actual wheel wear, the wheel wear predicted using series-parallel NARXNN, and percentage error.

Sample No	Actual wheel wear (μm)	Wheel wear predicted using NARXNN (μm)	Error %
1	-0.28	-0.25	-10.71
2	-0.48	-0.53	-10.41
3	-0.42	-0.37	-11.90
4	-0.39	-0.38	-2.56
5	-1.95	-1.35	-30.76
6	-2.56	-2.11	-17.57
7	-2.67	-2.45	-8.23
8	-2.20	-1.83	-16.81
9	-2.41	-2.37	-1.65
10	-2.58	-2.13	-17.44
11	-1.28	-1.24	-3.12
12	-0.42	-0.43	-2.38
13	-0.15	-0.16	-6.66
14	-0.22	-0.24	-9.09
15	-0.27	-0.21	-22.22
16	-1.27	-1.21	-4.72
17	-0.49	-0.45	-8.16
18	-5.49	-5.90	-7.46
19	-4.96	-5.55	-11.89
20	-4.50	-5.52	-22.66
21	-6.17	-6.30	-2.10
22	-5.81	-6.33	-8.95
23	-6.53	-6.47	-0.91
24	-6.54	-6.73	-2.90
25	-6.70	-6.12	-8.65
26	-5.94	-5.57	-6.22
27	-1.06	-1.04	-1.88
28	-1.29	-1.28	-0.77
29	-1.11	-1.11	0.00
30	-0.12	-0.12	0.00
31	-0.03	-0.03	0.00
32	-7.89	-7.07	-10.39
33	-9.95	-9.47	-4.82
34	-8.15	-8.75	-7.36
35	-7.75	-8.32	-7.35
36	-6.27	-4.92	-21.53
37	-1.00	-1.01	-1.00
38	-1.06	-0.83	-21.69
39	-0.60	-0.61	-1.66

ii.The actual wheel wear, the wheel wear predicted using parallel NARXNN, and percentage error.

Sample No	Actual wheel wear (μm)	Wheel wear predicted using NARXNN (μm)	Error %		Sample No	Actual wheel wear (μm)	Wheel wear predicted using NARXNN (μm)	Error %
1	-0.01	-0.01	0.00		45	-5.43	-5.41	-0.36
2	-0.24	-0.17	-41.17		46	-6.50	-4.51	-44.12
3	-0.23	-0.21	-9.52		47	-6.51	-4.96	-31.25
4	-0.28	-0.25	-12.00		48	-7.61	-6.62	-14.95
5	-0.63	-0.94	-32.97		49	-8.76	-7.17	-22.17
6	-0.79	-0.69	-14.49		50	-9.81	-8.12	-20.81
7	-0.52	-0.51	-1.96		51	-10.77	-9.14	-17.83
8	-1.76	-1.18	-49.15		52	-10.83	-9.83	-10.17
9	-2.11	-2.05	-2.92		53	-10.76	-10.31	-4.36
10	-2.62	-2.78	-5.75		54	-10.72	-9.54	-12.36
11	-4.08	-3.78	-7.93		55	-10.60	-10.69	-0.84
12	-3.97	-3.75	-5.86		56	-8.58	-8.59	-0.11
13	-5.15	-4.10	-25.60		57	-9.52	-8.05	-18.26
14	-4.19	-3.81	-9.97		58	-7.56	-6.39	-18.30
15	-3.20	-3.73	-14.20		59	-8.43	-7.68	-9.76
16	-3.40	-3.57	-4.76		60	-8.30	-7.16	-15.92
17	-3.15	-3.93	-19.84		61	-7.48	-5.64	-32.62
18	-2.80	-1.90	-47.36		62	-6.36	-5.40	-17.77
19	-1.99	-1.52	-30.92		63	-6.26	-5.48	-14.23
20	-4.28	-3.80	-12.63		64	-5.11	-5.10	-0.19
21	-5.47	-4.69	-16.63		65	-4.04	-4.01	-0.74
22	-6.68	-5.30	-26.03		66	-3.93	-3.42	-14.91
23	-5.75	-4.55	-26.37		67	-3.80	-3.37	-12.75
24	-5.74	-4.44	-29.27		68	-2.73	-2.67	-2.24
25	-5.86	-4.95	-18.38		69	-3.59	-2.53	-41.89
26	-4.74	-3.93	-20.61		70	-3.62	-3.31	-9.36
27	-5.91	-4.29	-37.76		71	-4.43	-4.78	-7.32
28	-8.13	-8.02	-1.37		72	-3.33	-2.88	-15.62
29	-7.16	-6.46	-10.83		73	-3.12	-3.10	-0.64
30	-6.04	-5.23	-15.48		74	-2.96	-2.67	-10.86
31	-6.11	-5.48	-11.49		75	-2.70	-2.94	-8.16
32	-5.29	-5.23	-1.14		76	-2.61	-2.46	-6.09
33	-5.27	-4.18	-26.07		77	-1.54	-1.91	-19.37
34	-6.17	-6.01	-2.66		78	-2.31	-2.63	-12.16
35	-6.15	-5.17	-98.81		79	-2.06	-2.07	-0.48
36	-6.11	-4.74	-28.90		80	-1.06	-1.16	-8.62
37	-6.25	-4.25	-47.05		81	-0.99	-0.88	-12.50
38	-4.29	-4.12	-4.12		82	-1.10	-0.99	-11.11
39	-6.20	-5.45	-13.76		83	-0.09	-0.06	-50.00
40	-6.22	-6.16	-0.97		84	-0.61	-0.97	-37.11
41	-5.24	-5.09	-2.94		85	-1.13	-1.69	-33.13
42	-5.21	-3.55	-46.76		86	-0.68	-0.74	-8.10
43	-5.33	-5.24	-1.71		87	-0.01	-0.01	0.00
44	-4.39	-4.18	-5.02					

iii. The actual rail wear, the rail wear predicted using series-parallel NARXNN, and percentage error.

Sample No	Actual rail wear (μm)	Rail wear predicted using NARXNN (μm)	Error %
1	-0.15	-0.15	0.00
2	-1.40	-1.32	-6.06
3	-1.65	-1.57	-5.09
4	-3.91	-3.06	-27.77
5	-1.83	-2.11	-13.27
6	-2.52	-1.93	-30.56
7	-2.62	-2.73	-4.02
8	-1.99	-2.67	-25.46
9	-1.86	-1.61	-15.52
10	-1.53	-1.52	-0.65
11	-1.70	-1.75	-2.85
12	-1.47	-1.67	-11.97
13	-0.25	-0.26	-3.84
14	-0.18	-0.17	-5.88
15	-0.11	-0.11	0.00
16	-3.69	-3.80	-2.89
17	-3.78	-3.58	-5.58
18	-6.13	-5.86	-4.60
19	-5.87	-5.22	-12.45
20	-5.64	-5.47	-3.10
21	-5.55	-5.45	-1.83
22	-4.09	-4.08	-0.24
23	-6.27	-5.72	-9.61
24	-2.40	-2.46	-2.43
25	-4.12	-3.97	-3.77
26	-2.29	-2.64	-13.25
27	-1.66	-1.82	-8.79
28	-0.67	-0.56	-19.64
29	-1.40	-1.31	-6.87
30	-0.19	-0.18	-5.55
31	-0.01	-0.01	0.00
32	-8.11	-8.03	-0.99
33	-7.21	-7.24	-0.41
34	-7.31	-7.33	-0.27
35	-6.09	-6.02	-1.16
36	-7.11	-6.88	-3.34
37	-4.66	-4.92	-5.28
38	-4.40	-4.31	-2.08
39	-0.09	-0.08	-12.50

iv. The actual rail wear, the rail wear predicted using parallel NARXNN, and percentage error.

Sample No	Actual rail wear (μm)	Rail wear predicted using NARXNN (μm)	Error %		Sample No	Actual rail wear (μm)	Rail wear predicted using NARXNN (μm)	Error %
1	-0.01	-0.01	0.00		45	-6.91	-6.48	-6.63
2	-0.30	-0.20	-50.00		46	-7.31	-6.83	-7.02
3	-1.05	-1.57	-33.12		47	-7.32	-7.78	-5.91
4	-1.72	-2.69	-36.05		48	-3.49	-3.72	-6.18
5	-2.87	-1.74	-64.94		49	-4.15	-4.32	-3.93
6	-3.08	-2.02	-52.47		50	-4.80	-4.29	-11.88
7	-2.95	-2.58	-14.34		51	-4.50	-3.83	-17.49
8	-4.19	-3.30	-26.96		52	-3.83	-4.22	-9.24
9	-3.99	-3.49	-14.32		53	-3.54	-3.75	-5.60
10	-3.79	-2.37	-59.91		54	-3.75	-3.59	-4.45
11	-3.90	-3.55	-9.85		55	-3.09	-2.56	-20.70
12	-8.93	-7.21	-23.85		56	-3.05	-3.03	-0.66
13	-8.75	-7.16	-22.20		57	-3.65	-2.56	-42.57
14	-10.37	-9.79	-5.92		58	-2.47	-1.83	-34.97
15	-9.09	-8.51	-6.81		59	-2.73	-2.06	-32.52
16	-7.80	-6.12	-27.45		60	-3.33	-2.71	-22.87
17	-8.42	-7.39	-13.93		61	-2.67	-2.54	-5.11
18	-7.75	-6.46	-19.96		62	-2.80	-1.87	-49.73
19	-7.37	-6.63	-11.16		63	-2.24	-4.22	-46.91
20	-7.04	-6.34	-11.04		64	-1.94	-1.78	-8.98
21	-7.95	-7.34	-8.310		65	-1.90	-1.45	-31.03
22	-7.57	-6.11	-23.89		66	-1.19	-1.30	-8.46
23	-8.11	-7.82	-3.70		67	-0.99	-0.94	-5.31
24	-8.80	-7.07	-24.46		68	-0.99	-0.89	-11.23
25	-10.10	-9.69	-4.23		69	-0.98	-0.95	-3.15
26	-10.68	-9.82	-8.75		70	-0.99	-0.97	-2.06
27	-10.69	-10.36	-3.18		71	-0.98	-0.80	-22.50
28	-10.66	-10.16	-4.92		72	-1.36	-1.12	-21.42
29	-10.57	-9.01	-17.31		73	-1.33	-1.73	-23.12
30	-10.34	-10.62	-2.63		74	-1.33	-1.38	-3.62
31	-9.88	-9.54	-3.56		75	-1.33	-1.49	-10.73
32	-9.15	-9.33	-1.92		76	-1.32	-1.05	-25.71
33	-8.14	-7.97	-2.13		77	-1.30	-1.27	-2.36
34	-7.20	-6.62	-8.76		78	-0.28	-0.25	-12.00
35	-7.15	-6.89	-3.77		79	-1.22	-1.19	-2.52
36	-6.70	-6.85	-2.18		80	-1.16	-1.12	-3.57
37	-7.30	-7.44	-1.88		81	-0.10	-0.12	-16.66
38	-7.05	-7.57	-6.86		82	-0.02	-0.02	0.00
39	-6.54	-6.15	-6.34		83	-0.11	-0.12	-8.33
40	-6.33	-5.87	-7.83		84	-0.11	-0.07	-57.14
41	-6.49	-6.01	-7.98		85	-0.05	-0.08	-37.50
42	-7.39	-6.24	-18.31		86	-0.09	-0.12	-25.00
43	-7.20	-7.53	-4.49		87	-0.09	-0.07	-28.57
44	-7.33	-7.78	-5.83					

2. Wheel/rail wear prediction using NARXNN under wet conditions

i. The actual wheel wear, the wheel wear predicted using series-parallel NARXNN, and percentage error.

Sample No	Actual wheel wear (μm)	Wheel wear predicted using NARXNN (μm)	Error %
1	-0.05	-0.05	0.00
2	-0.11	-0.11	0.00
3	-2.06	-1.82	-13.18
4	-2.62	-2.08	-25.96
5	-0.75	-0.85	-11.76
6	-1.41	-1.42	-0.70
7	-1.75	-1.66	-5.42
8	-2.19	-2.29	-4.36
9	-2.10	-2.19	-4.10
10	-2.38	-2.33	-2.14
11	-0.72	-0.58	-24.13
12	-1.13	-0.92	-22.82
13	-1.08	-1.03	-4.85
14	-0.39	-0.38	-2.63
15	-0.21	-0.21	0.00
16	-0.27	-0.34	-20.58
17	-0.22	-0.32	-31.25
18	-3.79	-3.79	0.00
19	-5.08	-4.07	-24.81
20	-3.45	-3.76	-8.24
21	-3.06	-2.70	-13.33
22	-1.15	-1.09	-5.50
23	-0.28	-0.24	-16.66
24	-0.09	-0.09	0.00
25	-0.02	-0.02	0.00
26	-0.60	-0.60	0.00
27	-0.41	-0.42	-2.38
28	-1.51	-1.64	-7.92
29	-1.24	-1.35	-8.14
30	-3.53	-3.86	-8.54
31	-2.12	-2.11	-0.47
32	-1.43	-1.55	-7.74
33	-3.03	-2.87	-5.57
34	-4.43	-4.74	-6.54
35	-4.32	-3.99	-8.27
36	-2.27	-2.62	-13.35
37	-0.26	-0.25	-4.00
38	-1.82	-1.81	-0.55
39	-0.68	-0.82	-17.07

ii. The actual wheel wear, the wheel wear predicted using parallel NARXNN, and percentage error.

Sample No	Actual wheel wear (μm)	Wheel wear predicted using NARXNN (μm)	Error %		Sample No	Actual wheel wear (μm)	Wheel wear predicted using NARXNN (μm)	Error %
1	-0.01	-0.01	0.00		45	-3.07	-3.01	-1.99
2	-0.16	-0.18	-11.11		46	-3.63	-3.31	-9.66
3	-0.34	-0.44	-22.72		47	-4.43	-6.14	-27.85
4	-0.10	-0.11	-9.09		48	-4.66	-5.79	-19.51
5	-0.38	-0.27	-40.74		49	-5.13	-6.01	-14.64
6	-0.57	-0.54	-5.55		50	-5.46	-5.77	-5.37
7	-1.06	-1.22	-13.11		51	-4.20	-5.17	-18.76
8	-2.09	-2.01	-3.98		52	-5.37	-5.38	-0.18
9	-2.58	-2.42	-6.61		53	-6.57	-6.21	-5.79
10	-4.03	-3.43	-17.49		54	-5.24	-5.34	-1.87
11	-3.19	-3.78	-15.60		55	-4.48	-4.63	-3.23
12	-3.51	-3.14	-11.78		56	-3.83	-4.93	-22.31
13	-4.90	-4.24	-15.56		57	-3.39	-5.17	-34.42
14	-5.40	-4.80	-12.50		58	-3.33	-4.95	-32.72
15	-6.54	-5.67	-15.34		59	-3.75	-4.90	-23.46
16	-6.47	-5.75	-12.52		60	-3.47	-3.70	-6.21
17	-5.80	-4.72	-22.88		61	-2.89	-3.00	-3.66
18	-4.77	-5.92	-19.42		62	-2.77	-2.88	-3.81
19	-5.78	-4.48	-29.01		63	-3.26	-3.03	-7.59
20	-4.85	-4.41	-9.97		64	-3.29	-3.88	-15.20
21	-5.19	-4.46	-16.36		65	-2.54	-3.74	-32.08
22	-4.84	-3.97	-21.91		66	-2.38	-2.48	-4.03
23	-5.21	-3.96	-31.56		67	-2.40	-2.23	-7.62
24	-5.77	-4.65	-24.08		68	-2.26	-2.26	0.00
25	-5.95	-5.85	-1.70		69	-1.74	-1.64	-6.09
26	-5.49	-5.68	-3.34		70	-3.54	-3.55	-0.28
27	-5.87	-6.23	-5.77		71	-3.56	-4.51	-21.06
28	-6.20	-6.28	-1.27		72	-4.86	-5.22	-6.89
29	-6.86	-6.38	-7.52		73	-5.25	-3.94	-33.24
30	-5.54	-5.58	-0.71		74	-5.93	-4.49	-32.07
31	-6.10	-6.13	-0.48		75	-4.04	-4.64	-12.931
32	-5.32	-5.73	-7.15		76	-3.18	-3.13	-1.59
33	-5.34	-5.57	-4.12		77	-2.52	-2.48	-1.61
34	-4.86	-5.78	-15.91		78	-2.96	-2.54	-16.53
35	-3.91	-5.67	-31.04		79	-3.42	-3.16	-8.22
36	-4.57	-5.79	-21.07		80	-1.62	-1.79	-9.49
37	-3.38	-3.62	-6.62		81	-3.27	-2.05	-59.51
38	-3.13	-3.85	-18.70		82	-0.53	-0.63	-15.87
39	-3.30	-3.81	-13.38		83	-0.71	-0.80	-11.25
40	-4.57	-4.03	-13.39		84	-0.54	-0.41	-31.70
41	-4.49	-4.91	-8.55		85	-0.48	-0.41	-17.07
42	-3.84	-2.44	-57.37		86	-0.21	-0.25	-16.00
43	-3.05	-2.86	-6.64		87	-0.23	-0.35	-34.28
44	-3.10	-2.91	-6.52					

iii. The actual rail wear, the rail wear predicted using series-parallel NARXNN, and percentage error.

Sample No	Actual rail wear (μm)	Rail wear predicted using NARXNN (μm)	Error %
1	-0.30	-0.41	-26.82
2	-0.34	-0.38	-10.52
3	-1.08	-0.92	-17.39
4	-1.39	-1.57	-11.46
5	-1.70	-1.55	-9.67
6	-2.61	-2.55	-2.35
7	-1.01	-1.07	-5.60
8	-1.52	-1.59	-4.40
9	-0.01	-0.01	0.00
10	-0.07	-0.08	-12.50
11	-0.01	-0.01	0.00
12	-0.03	-0.04	-25.00
13	-0.01	-0.01	0.00
14	-0.08	-0.06	-33.33
15	-0.10	-0.11	-9.09
16	-3.41	-3.42	-0.29
17	-2.66	-2.79	-4.65
18	-1.99	-2.00	-0.50
19	-3.27	-2.34	-39.74
20	-2.92	-3.34	-12.57
21	-1.29	-1.69	-23.66
22	-1.37	-1.40	-2.14
23	-1.72	-1.34	-28.35
24	-1.43	-1.45	-1.37
25	-1.14	-1.48	-22.97
26	-0.99	-0.91	-8.79
27	-0.95	-0.88	-7.95
28	-0.81	-0.71	-14.08
29	-0.48	-0.54	-11.11
30	-0.42	-0.43	-2.32
31	-0.58	-0.55	-5.45
32	-3.76	-3.55	-5.91
33	-2.98	-2.53	-17.78
34	-2.99	-3.49	-14.32
35	-1.85	-2.14	-13.55
36	-0.40	-0.40	0.00
37	-0.55	-0.50	-10.00
38	-0.42	-0.37	-13.51
39	-0.08	-0.07	-14.28

iv. The actual rail wear, the rail wear predicted using parallel NARXNN, and percentage error.

Sample No	Actual rail wear (μm)	Rail wear predicted using NARXNN (μm)	Error %		Sample No	Actual rail wear (μm)	Rail wear predicted using NARXNN (μm)	Error %
1	-0.01	-0.01	0.00		45	-8.76	-8.23	-6.43
2	-0.13	-0.14	-7.14		46	-8.93	-9.35	-4.49
3	-0.06	-0.05	-20.00		47	-5.43	-8.38	-35.20
4	-0.05	-0.08	-37.50		48	-4.23	-4.28	-1.16
5	-0.08	-0.07	-14.28		49	-4.70	-7.57	-37.91
6	-0.13	-0.11	-18.18		50	-6.09	-7.99	-23.77
7	-0.05	-0.08	-37.50		51	-8.21	-9.07	-9.48
8	-0.17	-0.15	-13.33		52	-8.60	-9.61	-10.50
9	-0.62	-0.44	-40.90		53	-7.08	-7.40	-4.32
10	-0.87	-0.77	-12.98		54	-7.86	-7.56	-3.96
11	-0.96	-1.09	-11.92		55	-7.10	-8.44	-15.87
12	-1.13	-1.21	-6.61		56	-6.85	-7.02	-2.42
13	-1.07	-0.80	-33.75		57	-5.57	-5.85	-4.78
14	-0.59	-0.55	-7.27		58	-5.65	-5.91	-4.39
15	-1.99	-2.12	-6.13		59	-5.00	-5.38	-7.06
16	-1.81	-2.28	-20.61		60	-4.34	-5.45	-20.36
17	-1.58	-2.04	-22.54		61	-4.61	-3.78	-21.95
18	-1.96	-2.37	-17.29		62	-4.67	-4.67	0.00
19	-3.52	-4.00	-12.00		63	-4.22	-3.59	-17.54
20	-3.34	-4.36	-23.39		64	-4.13	-4.13	0.00
21	-3.31	-3.73	-11.26		65	-4.49	-5.10	-11.96
22	-4.03	-4.79	-15.86		66	-3.02	-4.06	-25.61
23	-4.43	-5.15	-13.98		67	-4.71	-5.06	-6.91
24	-4.28	-5.78	-25.95		68	-3.85	-4.01	-3.99
25	-7.56	-7.80	-3.07		69	-1.16	-1.10	-5.45
26	-5.69	-6.11	-6.87		70	-1.72	-2.14	-19.62
27	-5.36	-6.09	-11.98		71	-2.44	-2.13	-14.55
28	-6.75	-7.97	-15.30		72	-1.63	-2.11	-22.74
29	-7.13	-8.26	-13.68		73	-2.74	-2.06	-33.00
30	-5.16	-6.18	-16.50		74	-1.50	-1.14	-31.57
31	-4.55	-5.04	-9.72		75	-2.55	-2.00	-27.50
32	-2.66	-2.90	-8.27		76	-1.80	-1.71	-5.26
33	-2.76	-2.50	-10.40		77	-1.47	-1.14	-28.94
34	-5.75	-6.10	-5.73		78	-1.50	-1.19	-26.05
35	-5.14	-5.17	-0.58		79	-1.55	-1.14	-35.96
36	-5.71	-5.36	-6.52		80	-0.55	-0.71	-22.53
37	-4.16	-5.36	-22.38		81	-0.45	-0.45	0.00
38	-3.79	-3.45	-9.85		82	-0.47	-0.46	-2.17
39	-4.75	-4.85	-2.06		83	-0.49	-0.47	-4.25
40	-5.87	-5.64	-4.07		84	-0.12	-0.15	-20.00
41	-5.57	-7.44	-25.13		85	-0.07	-0.05	-40.00
42	-5.44	-7.19	-24.33		86	-0.03	-0.02	-50.00
43	-5.47	-7.90	-30.75		87	-0.03	-0.03	0.00
44	-7.73	-8.15	-5.15					

3. Wheel/rail wear prediction using NARXNN under lubricated conditions

i. The actual wheel wear, the wheel wear predicted using series-parallel NARXNN, and percentage error.

Sample No	Actual wheel wear (μm)	Wheel wear predicted using NARXNN (μm)	Error %
1	-0.21	-0.19	-10.52
2	-1.16	-1.26	-7.93
3	-0.91	-1.07	-14.95
4	-1.50	-1.31	-14.50
5	-0.94	-0.92	-2.17
6	-1.06	-1.22	-13.11
7	-0.91	-1.05	-13.33
8	-1.17	-1.11	-5.40
9	-2.13	-2.11	-0.94
10	-1.91	-2.34	-18.37
11	-1.19	-1.33	-10.52
12	-0.97	-0.88	-10.22
13	-0.64	-0.63	-1.58
14	-0.24	-0.28	-14.28
15	-0.30	-0.31	-3.22
16	-0.04	-0.04	0.00
17	-0.01	-0.01	0.00
18	-0.11	-0.11	0.00
19	-1.91	-1.76	-8.52
20	-1.42	-1.93	-26.42
21	-2.15	-1.98	-8.58
22	-0.71	-0.73	-2.73
23	-0.83	-0.95	-12.63
24	-0.80	-0.88	-9.09
25	-0.07	-0.063	-11.11
26	-0.11	-0.09	-22.22
27	-0.11	-0.14	-21.42
28	-1.27	-1.19	-6.72
29	-1.23	-1.01	-21.78
30	-2.53	-2.32	-9.05
31	-2.55	-2.46	-3.65
32	-2.31	-2.51	-7.96
33	-3.11	-3.10	-0.32
34	-2.18	-2.02	-7.92
35	-2.45	-2.37	-3.37
36	-1.11	-1.01	-9.90
37	-0.42	-0.43	-2.32
38	-0.48	-0.44	-9.09
39	-0.34	-0.33	-3.03

ii. The actual wheel wear, the wheel wear predicted using parallel NARXNN, and percentage error.

Sample No	Actual wheel wear (μm)	Wheel wear predicted using NARXNN (μm)	Error %		Sample No	Actual wheel wear (μm)	Wheel wear predicted using NARXNN (μm)	Error %
1	-0.01	-0.01	0.00		45	-4.36	-2.64	-65.15
2	-0.09	-0.08	-12.50		46	-4.37	-4.32	-1.15
3	-0.08	-0.08	0.00		47	-4.42	-4.23	-4.49
4	-0.20	-0.21	-4.76		48	-4.71	-2.73	-72.52
5	-0.25	-0.36	-30.55		49	-2.90	-2.89	-0.34
6	-0.35	-0.50	-30.00		50	-2.26	-2.83	-20.14
7	-0.37	-0.46	-19.56		51	-2.88	-2.60	-10.76
8	-0.13	-0.24	-45.83		52	-3.59	-2.54	-41.33
9	-0.28	-0.39	-28.20		53	-2.62	-1.54	-70.12
10	-0.19	-0.16	-18.75		54	-1.78	-1.54	-15.58
11	-0.38	-0.20	-90.00		55	-0.80	-0.75	-6.66
12	-1.28	-1.48	-13.51		56	-1.76	-2.55	-30.98
13	-1.31	-1.22	-7.37		57	-2.57	-1.85	-38.91
14	-1.76	-1.59	-10.69		58	-2.21	-2.19	-0.91
15	-1.82	-1.74	-4.59		59	-1.48	-1.43	-3.49
16	-1.69	-1.58	-6.96		60	-1.12	-1.89	-40.74
17	-1.74	-1.70	-2.35		61	-1.64	-2.20	-25.45
18	-1.40	-1.90	-26.31		62	-1.29	-1.42	-9.15
19	-1.30	-1.82	-28.57		63	-0.91	-0.86	-5.81
20	-1.53	-1.97	-22.33		64	-0.86	-0.70	-22.85
21	-1.42	-2.18	-34.86		65	-0.69	-0.53	-30.18
22	-1.59	-2.46	-35.36		66	-0.66	-0.51	-29.41
23	-0.92	-0.89	-3.37		67	-0.76	-0.69	-10.14
24	-1.80	-1.73	-4.04		68	-0.93	-0.80	-16.25
25	-1.72	-1.61	-6.83		69	-1.20	-1.14	-5.26
26	-1.82	-1.64	-10.97		70	-1.12	-1.25	-10.40
27	-1.76	-1.41	-24.82		71	-0.94	-0.72	-30.55
28	-2.20	-2.55	-13.72		72	-0.84	-0.72	-16.66
29	-2.33	-2.43	-4.11		73	-0.87	-0.81	-7.40
30	-2.26	-2.62	-13.74		74	-0.91	-0.90	-1.11
31	-2.11	-2.67	-20.97		75	-0.91	-0.80	-13.75
32	-2.57	-2.80	-8.21		76	-0.98	-1.15	-14.78
33	-2.61	-2.66	-1.87		77	-0.67	-0.50	-34.00
34	-2.88	-2.62	-9.92		78	-0.44	-0.34	-29.41
35	-2.51	-2.55	-1.56		79	-0.20	-0.23	-13.04
36	-3.01	-2.51	-19.92		80	-0.45	-0.31	-45.16
37	-2.71	-2.41	-12.44		81	-0.29	-0.39	-25.64
38	-2.49	-2.25	-10.66		82	-0.37	-0.31	-19.35
39	-2.35	-2.68	-12.31		83	-0.30	-0.28	-7.14
40	-2.47	-2.74	-9.85		84	-0.14	-0.10	-40.00
41	-2.40	-2.83	-15.19		85	-0.19	-0.18	-5.55
42	-2.49	-2.84	-12.32		86	-0.22	-0.18	-22.22
43	-2.97	-2.97	0.00		87	-0.23	-0.22	-4.54
44	-3.31	-2.93	-12.96					

iii. The actual rail wear, the rail wear predicted using series-parallel NARXNN, and percentage error.

Sample No	Actual rail wear (μm)	Rail wear predicted using NARXNN (μm)	Error %
1	-0.03	-0.03	0.00
2	-0.16	-0.15	-6.66
3	-0.76	-0.76	0.00
4	-1.75	-1.62	-8.02
5	-1.99	-1.97	-1.01
6	-2.03	-2.05	-0.97
7	-0.52	-0.53	-1.88
8	-0.46	-0.43	-6.97
9	-1.67	-1.64	-1.82
10	-1.23	-1.21	-1.65
11	-0.84	-0.76	-10.52
12	-0.27	-0.25	-8.00
13	-0.23	-0.27	-14.81
14	-0.27	-0.27	0.00
15	-1.37	-1.53	-10.45
16	-1.42	-1.70	-16.47
17	-1.03	-1.07	-3.73
18	-2.22	-2.50	-11.20
19	-2.38	-2.23	-6.72
20	-1.06	-1.29	-17.82
21	-1.03	-1.02	-0.98
22	-1.38	-1.07	-28.97
23	-0.10	-0.10	0.00
24	-0.14	-0.13	-7.69
25	-0.09	-0.09	0.00
26	-0.10	-0.12	-16.66
27	-0.52	-0.49	-6.12
28	-1.09	-0.97	-12.37
29	-0.96	-0.91	-5.49
30	-1.05	-0.97	-8.24
31	-1.09	-1.20	-9.16
32	-1.61	-1.43	-12.58
33	-3.01	-3.00	-0.33
34	-1.91	-1.73	-10.40
35	-2.09	-1.7176	-21.68
36	-0.91	-0.90	-1.11
37	-0.89	-0.88	-1.13
38	-0.55	-0.68	-19.11
39	-0.28	-0.29	-3.44

iv. The actual rail wear, the rail wear predicted using parallel NARXNN, and percentage error.

Sample No	Actual rail wear (μm)	Rail wear predicted using NARXNN (μm)	Error %		Sample No	Actual rail wear (μm)	Rail wear predicted using NARXNN (μm)	Error %
1	-0.01	-0.01	0.00		45	-2.54	-2.33	-9.01
2	-0.03	-0.04	-25.00		46	-2.56	-2.32	-10.34
3	-0.03	-0.04	-25.00		47	-2.55	-2.60	-1.92
4	-0.12	-0.12	0.00		48	-1.54	-1.32	-16.66
5	-0.21	-0.21	0.00		49	-2.47	-3.60	-31.38
6	-0.10	-0.10	0.00		50	-2.30	-2.46	-6.50
7	-0.26	-0.35	-25.71		51	-2.30	-2.37	-2.95
8	-0.11	-0.12	-8.33		52	-2.50	-2.37	-5.48
9	-0.13	-0.11	-18.18		53	-2.50	-2.58	-3.10
10	-0.77	-0.76	-1.31		54	-2.59	-2.58	-0.38
11	-0.66	-0.90	-26.66		55	-2.10	-2.21	-4.97
12	-1.00	-1.06	-5.66		56	-2.33	-2.44	-4.50
13	-0.92	-1.13	-18.58		57	-2.32	-3.50	-33.71
14	-0.43	-0.33	-30.30		58	-2.68	-2.31	-16.01
15	-0.66	-0.76	-13.15		59	-3.58	-3.41	-4.98
16	-1.33	-1.35	-1.48		60	-3.73	-4.42	-15.61
17	-0.73	-0.75	-2.66		61	-4.36	-4.24	-2.83
18	-0.97	-0.91	-6.59		62	-4.44	-4.30	-3.25
19	-0.69	-0.51	-35.29		63	-3.75	-5.70	-34.21
20	-0.25	-0.24	-4.16		64	-4.69	-4.06	-15.51
21	-0.62	-0.46	-34.78		65	-3.27	-3.54	-7.62
22	-1.66	-1.51	-9.93		66	-2.27	-3.91	-41.94
23	-1.09	-0.92	-18.47		67	-0.87	-0.87	0.00
24	-0.60	-0.95	-36.84		68	-1.21	-1.99	-39.19
25	-1.11	-1.00	-11.00		69	-0.74	-1.07	-30.84
26	-1.18	-1.20	-1.66		70	-0.48	-0.46	-4.34
27	-1.01	-1.17	-13.67		71	-1.13	-0.98	-15.30
28	-0.73	-0.62	-17.74		72	-1.16	-0.88	-31.81
29	-0.61	-0.57	-7.01		73	-0.72	-0.72	0.00
30	-0.61	-0.53	-15.09		74	-0.95	-0.86	-10.46
31	-0.63	-0.55	-14.54		75	-1.33	-1.13	-17.69
32	-0.72	-0.63	-14.28		76	-0.86	-0.49	-75.51
33	-0.75	-0.56	-33.92		77	-1.73	-1.41	-22.69
34	-1.88	-1.64	-14.63		78	-2.18	-2.06	-5.82
35	-2.03	-2.74	-25.91		79	-2.24	-2.21	-1.35
36	-1.90	-1.87	-1.60		80	-1.79	-1.47	-21.76
37	-2.02	-2.83	-28.62		81	-0.96	-0.59	-62.71
38	-2.20	-1.84	-19.56		82	-0.87	-0.61	-42.62
39	-2.12	-2.27	-6.60		83	-0.83	-0.65	-27.69
40	-2.11	-2.00	-5.50		84	-0.92	-0.73	-26.02
41	-2.14	-2.8	-23.57		85	-0.94	-0.73	-28.76
42	-2.26	-2.12	-6.60		86	-0.62	-0.64	-3.12
43	-2.50	-2.91	-14.08		87	-0.55	-0.55	0.00
44	-2.70	-2.32	-16.37					

4. Wheel/rail wear prediction using NARXNN under sanded conditions

i. The actual wheel wear, the wheel wear predicted using series-parallel NARXNN, and percentage error.

Sample No	Actual wheel wear (μm)	Wheel wear predicted using NARXNN (μm)	Error %
1	-0.19	-0.19	0.00
2	-0.07	-0.07	0.00
3	-2.80	-2.72	-2.94
4	-2.96	-2.72	-8.82
5	-3.42	-3.65	-6.30
6	-6.84	-7.46	-8.31
7	-5.93	-5.99	-1.00
8	-6.40	-6.30	-1.58
9	-4.96	-4.82	-2.90
10	-4.45	-4.69	-5.11
11	-0.17	-0.17	0.00
12	-0.13	-0.13	0.00
13	-0.01	-0.01	0.00
14	-0.14	-0.14	0.00
15	-0.07	-0.07	0.00
16	-2.76	-2.50	-10.40
17	-1.57	-1.45	-8.27
18	-4.13	-3.20	-29.06
19	-7.31	-8.00	-8.62
20	-6.42	-7.13	-9.95
21	-4.63	-5.45	-15.04
22	-4.11	-4.84	-15.08
23	-4.17	-4.49	-7.12
24	-5.57	-5.52	-0.90
25	-5.38	-5.33	-0.93
26	-3.88	-3.79	-2.37
27	-2.23	-3.07	-27.36
28	-0.59	-0.57	-3.50
29	-1.14	-1.14	0.00
30	-0.74	-0.70	-5.71
31	-1.03	-1.02	-0.98
32	-6.82	-6.71	-1.63
33	-6.88	-8.44	-18.48
34	-6.16	-7.17	-14.08
35	-6.30	-7.18	-12.25
36	-3.32	-2.93	-13.31
37	-1.17	-1.14	-2.63
38	-1.03	-1.02	-0.98
39	-0.26	-0.23	-13.04

ii. The actual wheel wear, the wheel wear predicted using parallel NARXNN, and percentage error.

Sample No	Actual wheel wear (μm)	Wheel wear predicted using NARXNN (μm)	Error %		Sample No	Actual wheel wear (μm)	Wheel wear predicted using NARXNN (μm)	Error %
1	-0.01	-0.01	0.00		45	-10.03	-9.98	-0.50
2	-0.15	-0.25	-40.00		46	-10.93	-9.33	-17.14
3	-0.18	-0.15	-20.00		47	-11.46	-10.29	-11.37
4	-0.70	-0.95	-26.31		48	-14.79	-13.32	-11.03
5	-1.05	-1.19	-11.76		49	-15.30	-13.05	-17.24
6	-2.41	-2.35	-2.55		50	-11.99	-10.29	-16.52
7	-3.12	-2.86	-9.09		51	-11.88	-10.54	-12.71
8	-3.00	-2.44	-22.95		52	-12.95	-11.64	-11.25
9	-4.06	-3.98	-2.01		53	-12.04	-12.15	-0.90
10	-4.15	-2.44	-70.08		54	-12.12	-13.57	-10.68
11	-4.07	-3.36	-21.13		55	-12.14	-12.66	-4.10
12	-4.03	-3.89	-3.59		56	-12.15	-10.96	-10.85
13	-4.46	-3.27	-36.39		57	-11.19	-10.63	-5.26
14	-6.85	-5.99	-14.35		58	-10.21	-9.81	-4.07
15	-7.84	-6.31	-24.24		59	-10.17	-9.39	-8.30
16	-6.03	-5.95	-1.34		60	-9.28	-8.48	-9.43
17	-6.43	-4.42	-45.47		61	-10.37	-9.65	-7.46
18	-7.06	-6.62	-6.64		62	-8.34	-7.53	-10.75
19	-9.21	-8.31	-10.83		63	-7.98	-6.41	-24.49
20	-6.57	-5.91	-11.16		64	-8.71	-7.33	-18.82
21	-7.39	-6.68	-10.62		65	-6.73	-5.28	-27.46
22	-4.78	-5.59	-14.49		66	-5.12	-5.35	-4.29
23	-5.34	-4.45	-20.00		67	-5.36	-4.67	-14.77
24	-4.03	-4.49	-10.24		68	-6.19	-5.99	-3.33
25	-2.76	-2.98	-7.38		69	-4.92	-5.84	-15.75
26	-6.38	-5.07	-25.83		70	-3.45	-5.44	-36.58
27	-6.76	-5.90	-14.57		71	-4.50	-5.28	-14.77
28	-7.09	-7.04	-0.71		72	-3.73	-5.28	-29.35
29	-6.96	-5.27	-32.06		73	-2.81	-4.73	-40.59
30	-6.93	-5.04	-37.50		74	-1.72	-2.15	-20.00
31	-6.89	-5.63	-22.38		75	-2.15	-3.54	-39.26
32	-6.81	-5.39	-26.34		76	-5.16	-5.95	-13.27
33	-6.81	-4.67	-45.82		77	-3.19	-2.73	-16.84
34	-7.00	-7.49	-6.54		78	-4.24	-5.68	-25.35
35	-7.26	-7.42	-2.15		79	-2.17	-2.57	-15.56
36	-7.44	-6.45	-15.34		80	-1.03	-1.42	-27.46
37	-7.35	-6.02	-22.09		81	-1.03	-1.59	-35.22
38	-7.28	-6.94	-4.89		82	-1.03	-1.25	-17.60
39	-7.28	-6.63	-9.80		83	-1.02	-1.55	-34.19
40	-5.39	-7.01	-23.10		84	-0.74	-0.47	-57.44
41	-5.29	-5.93	-10.79		85	-0.18	-0.14	-28.57
42	-5.21	-5.01	-3.99		86	-0.02	-0.02	0.00
43	-6.26	-5.46	-14.65		87	-0.13	-0.15	-13.33
44	-7.79	-6.66	-16.96					

iii. The actual rail wear, the rail wear predicted using series-parallel NARXNN, and percentage error.

Sample No	Actual rail wear (μm)	Rail wear predicted using NARXNN (μm)	Error %
1	-0.06	-0.06	0.00
2	-0.23	-0.21	-9.52
3	-1.26	-1.44	-12.50
4	-1.26	-1.01	-24.75
5	-0.62	-0.63	-1.58
6	-4.28	-4.51	-5.09
7	-0.36	-0.36	0.00
8	-1.86	-1.88	-1.06
9	-1.43	-1.21	-18.18
10	-1.04	-1.04	0.00
11	-0.21	-0.28	-25.00
12	-0.36	-0.36	0.00
13	-0.04	-0.04	0.00
14	-0.21	-0.20	-5.00
15	-0.29	-0.29	0.00
16	-1.31	-1.37	-4.37
17	-0.29	-0.28	-3.57
18	-4.55	-4.55	0.00
19	-3.36	-3.89	-13.62
20	-3.05	-3.45	-11.59
21	-5.72	-4.57	-25.16
22	-9.82	-8.29	-18.45
23	-7.51	-9.39	-20.02
24	-4.95	-4.59	-7.84
25	-3.12	-2.90	-7.58
26	-1.09	-1.06	-2.83
27	-1.42	-1.52	-6.57
28	-1.13	-0.99	-14.14
29	-0.56	-0.56	0.00
30	-0.45	-0.34	-32.35
31	-0.33	-0.33	0.00
32	-2.47	-2.24	-10.26
33	-9.75	-8.65	-12.71
34	-8.26	-8.32	-0.72
35	-11.00	-10.65	-3.28
36	-1.61	-1.20	-34.16
37	-0.22	-0.22	0.00
38	-0.74	-0.58	-27.58
39	-0.09	-0.08	-12.50

iv. The actual rail wear, the rail wear predicted using parallel NARXNN, and percentage error.

Sample No	Actual rail wear (μm)	Rail wear predicted using NARXNN (μm)	Error %		Sample No	Actual rail wear (μm)	Rail wear predicted using NARXNN (μm)	Error %
1	-0.01	-0.01	0.00		45	-6.93	-6.44	-7.60
2	-0.03	-0.03	0.00		46	-7.19	-6.56	-9.60
3	-0.32	-0.31	-3.22		47	-6.85	-7.32	-6.42
4	-0.78	-0.69	-13.04		48	-7.51	-6.80	-10.44
5	-0.71	-0.65	-9.23		49	-7.07	-5.45	-29.72
6	-0.76	-0.68	-11.76		50	-7.79	-7.32	-6.42
7	-0.51	-0.48	-6.25		51	-8.96	-5.98	-49.83
8	-0.38	-0.32	-18.75		52	-8.64	-6.47	-33.53
9	-0.30	-0.47	-36.17		53	-7.91	-7.82	-1.15
10	-0.26	-0.37	-29.72		54	-7.74	-7.32	-5.73
11	-0.34	-0.35	-2.85		55	-7.37	-6.44	-14.44
12	-0.15	-0.28	-46.42		56	-8.40	-9.19	-8.59
13	-1.13	-1.70	-33.52		57	-8.63	-7.32	-17.89
14	-2.22	-2.67	-16.85		58	-8.91	-9.16	-2.72
15	-2.15	-2.08	-3.36		59	-7.19	-6.44	-11.64
16	-3.20	-2.61	-22.60		60	-10.13	-9.57	-5.85
17	-2.23	-3.85	-42.07		61	-8.97	-9.16	-2.07
18	-4.24	-5.70	-25.61		62	-10.69	-10.47	-2.10
19	-4.37	-5.04	-13.29		63	-12.44	-11.60	-7.24
20	-5.35	-6.58	-18.69		64	-12.41	-11.57	-7.26
21	-5.34	-6.58	-18.84		65	-10.61	-9.68	-9.60
22	-5.44	-6.58	-17.32		66	-11.31	-9.72	-16.35
23	-8.47	-7.55	-12.18		67	-11.62	-9.68	-20.04
24	-7.57	-6.21	-21.90		68	-12.88	-10.21	-26.15
25	-11.14	-10.22	-9.00		69	-14.24	-13.57	-4.93
26	-8.25	-7.85	-5.09		70	-14.50	-12.55	-15.53
27	-7.87	-6.98	-12.75		71	-13.73	-12.55	-9.40
28	-7.85	-7.56	-3.83		72	-11.81	-10.70	-10.37
29	-6.15	-4.39	-40.09		73	-9.72	-7.70	-26.23
30	-4.00	-3.85	-3.89		74	-7.15	-6.70	-6.71
31	-5.08	-4.67	-8.77		75	-5.16	-6.55	-21.22
32	-5.49	-5.72	-4.02		76	-3.19	-3.85	-17.14
33	-7.15	-6.23	-14.76		77	-4.24	-6.04	-29.80
34	-5.14	-6.33	-18.79		78	-3.17	-4.73	-32.98
35	-5.70	-7.32	-22.13		79	-2.07	-2.70	-23.33
36	-6.66	-5.45	-22.20		80	-0.46	-0.57	-19.29
37	-6.71	-7.57	-11.36		81	-1.06	-1.70	-37.64
38	-6.04	-7.32	-17.48		82	-1.02	-1.32	-22.72
39	-8.62	-7.57	-13.87		83	-0.56	-0.66	-15.15
40	-8.57	-6.30	-36.03		84	-0.43	-0.42	-2.38
41	-8.83	-7.21	-22.46		85	-0.31	-0.23	-34.78
42	-7.42	-6.45	-15.03		86	-0.33	-0.32	-3.12
43	-8.05	-7.21	-11.65		87	-0.14	-0.13	-7.69
44	-6.43	-5.45	-17.98					

Appendix 7 Passenger vehicle model using VAMPIRE software

```
Coach Inflated
        UNITS VAMPIRE
**
** Parameter List
*PARAMETER
**
        BogSemiSpac = 9.5
        SemiWhlBase = 1.28
        WhlRad = 0.46
        PriSemiLat = 1.0
        SecSemiLat = 1.0
        DS = 0.2
**
*MASS
** Car Body
        INERTIA   32.000   56.800   1970.000   1970.000
 M1     POSITION   0.000   0.000     1.800
        NAME      Car_Body
** Leading Bogie
        INERTIA    2.615    1.722     1.476     3.067
 M2     POSITION   BogSemiSpac   0.000   0.600
        NAME      Ldg_Bogie
** Trailing Bogie
 M3     POSITION  -BogSemiSpac   0.000   0.600
        NAME      Tlg_Bogie
**
*WHEELSET
** Wheelsets
        INERTIA    1.813   1.120   0.112
 M4/W1  POSITION   BogSemiSpac+SemiWhlBase   0.000   WhlRad
        NAME      Wheelset1
 M5/W2  POSITION   BogSemiSpac-SemiWhlBase   0.000   WhlRad
        NAME      Wheelset2
 M6/W3  POSITION  -BogSemiSpac+SemiWhlBase   0.000   WhlRad
        NAME      Wheelset3
 M7/W4  POSITION  -BogSemiSpac-SemiWhlBase   0.000   WhlRad
**
*SHEAR
** Primary Springs
        STIFFNESS  0.617   0.617   0.732   0.008   0.008   0.000
        POSITION   BogSemiSpac+SemiWhlBase   PriSemiLat   0.940   0.680  Ldg_Bogie   Wheelset1
        POSITION   BogSemiSpac+SemiWhlBase  -PriSemiLat   0.940   0.680  Ldg_Bogie   Wheelset1
        POSITION   BogSemiSpac-SemiWhlBase   PriSemiLat   0.940   0.680  Ldg_Bogie   Wheelset2
        POSITION   BogSemiSpac-SemiWhlBase  -PriSemiLat   0.940   0.680  Ldg_Bogie   Wheelset2
**
        POSITION  -BogSemiSpac+SemiWhlBase   PriSemiLat   0.940   0.680  Tlg_Bogie   Wheelset3
        POSITION  -BogSemiSpac+SemiWhlBase  -PriSemiLat   0.940   0.680  Tlg_Bogie   Wheelset3
        POSITION  -BogSemiSpac-SemiWhlBase   PriSemiLat   0.940   0.680  Tlg_Bogie   Wheelset4
        POSITION  -BogSemiSpac-SemiWhlBase  -PriSemiLat   0.940   0.680  Tlg_Bogie   Wheelset4
**
*DAMPER
```

```
** Primary Dampers
      DAMPING    0.004
      SERIES     1.000
      POSITION   BogSemiSpac+SemiWhlBase+0.27  PriSemiLat  0.880  Ldg_Bogie
             BogSemiSpac+SemiWhlBase+0.27  PriSemiLat  0.460  Wheelset1
      POSITION   BogSemiSpac+SemiWhlBase+0.27 -PriSemiLat  0.880  Ldg_Bogie
             BogSemiSpac+SemiWhlBase+0.27 -PriSemiLat  0.460  Wheelset1
      POSITION   BogSemiSpac-SemiWhlBase-0.27  PriSemiLat  0.880  Ldg_Bogie
             BogSemiSpac-SemiWhlBase-0.27  PriSemiLat  0.460  Wheelset2
      POSITION   BogSemiSpac-SemiWhlBase-0.27 -PriSemiLat  0.880  Ldg_Bogie
             BogSemiSpac-SemiWhlBase-0.27 -PriSemiLat  0.460  Wheelset2
**
      POSITION  -BogSemiSpac+SemiWhlBase+0.27  PriSemiLat  0.880  Tlg_Bogie
            -BogSemiSpac+SemiWhlBase+0.27  PriSemiLat  0.460  Wheelset3
      POSITION  -BogSemiSpac+SemiWhlBase+0.27 -PriSemiLat  0.880  Tlg_Bogie
            -BogSemiSpac+SemiWhlBase+0.27 -PriSemiLat  0.460  Wheelset3
      POSITION  -BogSemiSpac-SemiWhlBase-0.27  PriSemiLat  0.880  Tlg_Bogie
            -BogSemiSpac-SemiWhlBase-0.27  PriSemiLat  0.460  Wheelset4
      POSITION  -BogSemiSpac-SemiWhlBase-0.27 -PriSemiLat  0.880  Tlg_Bogie
            -BogSemiSpac-SemiWhlBase-0.27 -PriSemiLat  0.460  Wheelset4
**
*BUSH
** Trailing Arm Bushes
      STIFFNESS  30.774  3.267  30.774  0.000  0.000  0.000
      DAMPING     0.015  0.002  0.015  0.000  0.000  0.000
      SERIES     60.000  7.500  60.000  0.000  0.000  0.000
      POSITION   BogSemiSpac+SemiWhlBase-0.45  PriSemiLat  0.880  Ldg_Bogie  Wheelset1
      POSITION   BogSemiSpac+SemiWhlBase-0.45 -PriSemiLat  0.880  Ldg_Bogie  Wheelset1
      POSITION   BogSemiSpac-SemiWhlBase+0.45  PriSemiLat  0.880  Ldg_Bogie  Wheelset2
      POSITION   BogSemiSpac-SemiWhlBase+0.45 -PriSemiLat  0.880  Ldg_Bogie  Wheelset2
**
      POSITION  -BogSemiSpac+SemiWhlBase-0.45  PriSemiLat  0.880  Tlg_Bogie  Wheelset3
      POSITION  -BogSemiSpac+SemiWhlBase-0.45 -PriSemiLat  0.880  Tlg_Bogie  Wheelset3
      POSITION  -BogSemiSpac-SemiWhlBase+0.45  PriSemiLat  0.880  Tlg_Bogie  Wheelset4
      POSITION  -BogSemiSpac-SemiWhlBase+0.45 -PriSemiLat  0.880  Tlg_Bogie  Wheelset4
**
*AIRSPRING
**
      VERTICAL
       AIRSPRING 0.8
       RESERVOIR 0.9
       DAMPING SQUARE  1.1
       DAMPING LINEAR  0.05
       INERTIA   0.3
       AUXILIARY 4.0
      LATERAL
       STIFFNESS 0.1
       MOMENTS   0.8
       DAMPING   0.014  0.009
       HYSTER    0.3    100.0
       LINEAR    0.019  0.02
      POSITION   BogSemiSpac   SecSemiLat  1.13  0.83   Car_Body  Ldg_Bogie
      POSITION   BogSemiSpac  -SecSemiLat  1.13  0.83   Car_Body  Ldg_Bogie
      POSITION  -BogSemiSpac   SecSemiLat  1.13  0.83   Car_Body  Tlg_Bogie
      POSITION  -BogSemiSpac  -SecSemiLat  1.13  0.83   Car_Body  Tlg_Bogie
```

```
**
*BUSH
** Anti-Roll Bar and Traction Link
      STIFFNESS  5.00  0.100  0.00  0.940  0.000  0.000
      DAMPING    0.025 0.005  0.00  0.000  0.000  0.000
      SERIES     10.000 0.200  0.00  0.000  0.000  0.000
      POSITION   BogSemiSpac   0.00  0.600  Car_Body  Ldg_Bogie
      POSITION  -BogSemiSpac   0.00  0.600  Car_Body  Tlg_Bogie
**
*DAMPER
** Secondary lateral dampers
      DAMPING    0.032
      SERIES     6.000
      POSITION   BogSemiSpac  0.665   0.7000 Car_Body
             BogSemiSpac  0.230   0.7000 Ldg_Bogie
      POSITION   BogSemiSpac -0.665   0.7000 Car_Body
             BogSemiSpac -0.230   0.7000 Ldg_Bogie
      POSITION  -BogSemiSpac  0.665   0.7000 Car_Body
            -BogSemiSpac  0.230   0.7000 Tlg_Bogie
      POSITION  -BogSemiSpac -0.665   0.7000 Car_Body
            -BogSemiSpac -0.230   0.7000 Tlg_Bogie
**
*PINLINK
**
      DAMPING    0.200
      SERIES     4.000
      POSITION   BogSemiSpac-0.300  1.300   0.6100 Car_Body
             BogSemiSpac+0.500  1.300   0.5300 Ldg_Bogie
      POSITION   BogSemiSpac-0.300 -1.300   0.6100 Car_Body
             BogSemiSpac+0.500 -1.300   0.5300 Ldg_Bogie
      POSITION  -BogSemiSpac-0.300  1.300   0.6100 Car_Body
            -BogSemiSpac+0.500  1.300   0.5300 Tlg_Bogie
      POSITION  -BogSemiSpac-0.300 -1.300   0.6100 Car_Body
            -BogSemiSpac+0.500 -1.300   0.5300 Tlg_Bogie
**
*BUMPSTOP
**
      DISPLACEMENT   0.00 5.00 10.00 15.00 20.00 25.00 30.00 35.00 40.00
      FORCE          0.00 0.60  1.76  3.73  6.87 11.58 17.17 29.20 230.00
      CLEARANCE      25.00
      POSITION   BogSemiSpac  DS  0.600  Car_Body
             BogSemiSpac -DS  0.600  Ldg_Bogie
      POSITION  -BogSemiSpac  DS  0.600  Car_Body
            -BogSemiSpac -DS  0.600  Tlg_Bogie
**
*STIFFNESS
** Grounding
      STIFFNESS  0.01
      POSITION   0.00   0.00   1.80  Car_Body
             2*DS   0.00   1.80  0
*
```

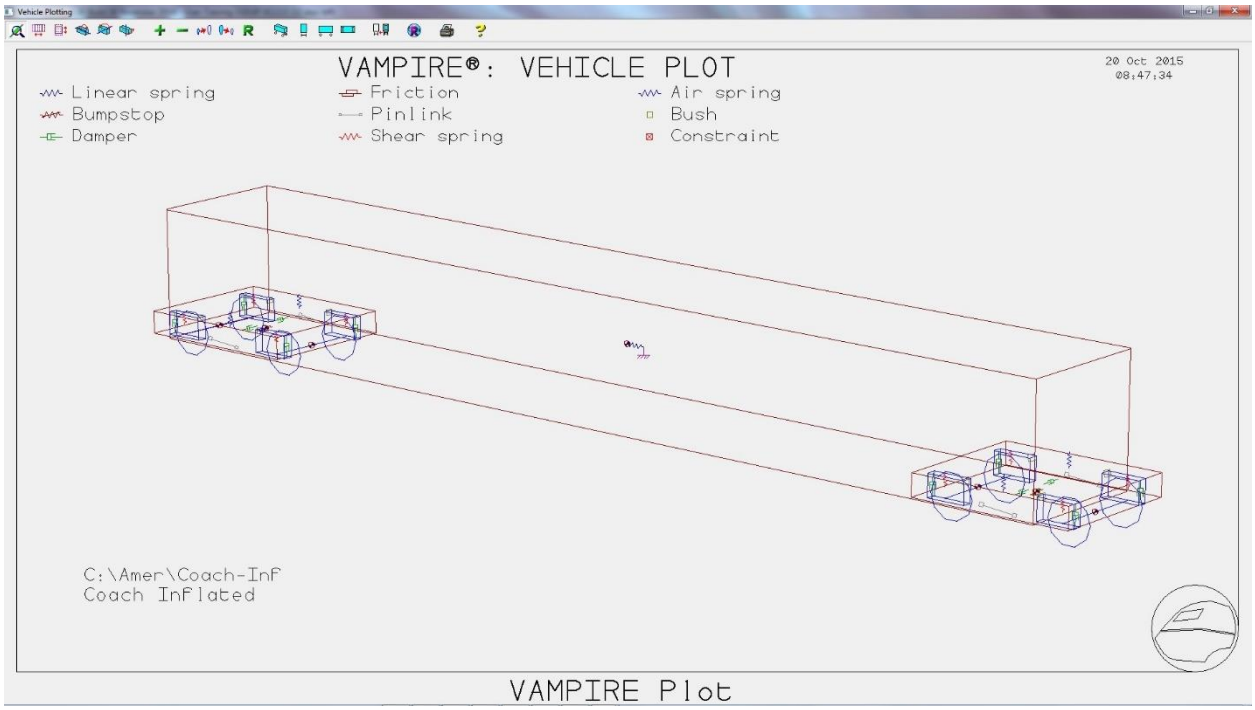

VAMPIRE Plot

Suspension Elements

Stiffness or Bumpstop element

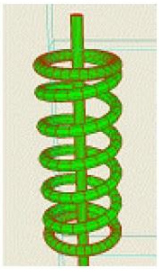

Damper element

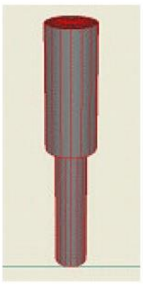

Shear Spring element

Airspring element

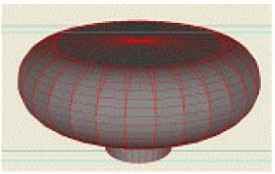

Friction element

Bush element

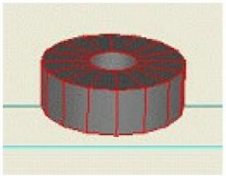

Constraint element

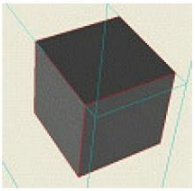

Pinlink element

Appendix 8 Estimate wheel wear using energy dissipated and contact position

```
% This program to calculate the wheel wear after differnt running distances (50000km,
100000km, 150000km, and 200000km).
Position = [upload the data of position]; % the data is the position of contact point which
are calculated using vampire.
TG = [upload the data of TG (TGamma)]; % the data is the TGamma on the wheel which are
calculated using vampire.
% For distance of 50000km.
WI = 0.005 * TG * 10^-4; % WI is the wear index
Data = [position, WI]
sortrows(Data,1); % to rearrange the data of contact position from minus to plus; Where the
first column of data is contact position and the second column is the wear index(w)
.....
w= [upload the data of wear index, wear index is the second column resulting from
“sortrows(data,1), “just upload the first 990 values”]
.....
% This program to calculate the wear on the wheel tread (w1 to w18)
n1=1
n2=((length(w)/18))
 for i = n1 : n2 : 990
      a(i)=sum(w(n1:n2));
      n1=n2+1
n2=n2+((length(w)/18))
if n1 > length(w)
    break
end
 end
a(a==0) = []; % to delete zero components in vector a.
ee=a'; % ee is the wheel tread wear
.....

% To calculate the wear after 50000km
b = ee(end:-1:1)
Wi = b * 10000 % to get the w1 to w18 wheel wear tread after 50000km.
.....
.....
%Note: To obtain the worn wheel profile, subtract the w1 to w18 from the wheel profile values
which are lies from -777 to -722.
.....
% After calculate the wear after running distance of 50000km, and worn profile obtained.
% Upload the worn wheel profile to vampire, and run program, and calculate the wear after
running distance of 100000km.
.....
 % Repeat the previous steps to calculate the wear after running distance of 150000km and
200000km.
.....
```

Appendix 9 Wheel wear predicted using VAMPIRE and neural network

1. Change of speed

The wheel wear predicted using VAMPIRE and series-parallel NARXNN, and percentage error.

Sample Number	Wheel wear predicted using VAMPIRE (mm)	Wheel wear predicted using NARXNN (mm)	Error %
1	0.49	0.53	7.54
2	0.54	0.59	8.47
3	0.55	0.54	1.85
4	1.07	1.12	4.46
5	1.05	1.07	1.86
6	1.02	1.10	7.27
7	1.48	1.54	3.89
8	1.64	1.62	1.23
9	0.56	0.60	6.66
10	2.11	2.16	2.31
11	2.19	2.18	0.45
12	2.23	2.11	5.68
13	0.58	0.57	1.75
14	0.68	0.66	3.03
15	1.14	1.12	1.78
16	1.19	1.25	4.80
17	1.30	1.29	0.77
18	1.15	1.19	3.36
19	1.67	1.77	5.64
20	1.75	1.81	3.31
21	2.05	1.97	4.06
22	0.41	0.40	2.50
23	2.34	2.33	0.42
24	0.44	0.43	2.32
25	0.58	0.56	3.57
26	0.56	0.54	3.70
27	0.70	0.67	4.47
28	1.26	1.62	22.22
29	2.19	2.21	0.90
30	0.93	0.85	9.41

The wheel wear predicted using VAMPIRE and parallel NARXNN, and percentage error.

Sample Number	Wheel wear predicted using VAMPIRE (mm)	Wheel wear predicted using NARXNN (mm)	Error %
1	0.49	0.59	16.94
2	1.27	1.26	0.79
3	2.02	2.16	6.48
4	2.55	2.40	6.25
5	2.83	2.82	0.35
6	2.82	2.38	18.48
7	2.74	2.69	1.85
8	2.65	2.51	5.57
9	2.67	2.52	5.95
10	2.87	2.63	9.12
11	2.66	2.45	8.57
12	2.69	2.48	8.46
13	3.18	2.85	11.57
14	3.16	3.15	0.31
15	2.69	2.54	5.90
16	2.34	2.17	7.83
17	1.37	1.38	0.72
18	0.76	0.67	13.43

2. Change of longitudinal bush stiffness

The wheel wear predicted using VAMPIRE and series-parallel NARXNN, and percentage error.

Sample Number	Wheel wear predicted using VAMPIRE (mm)	Wheel wear predicted using NARXNN (mm)	Error %
1	0.53	0.52	1.92
2	0.36	0.38	5.26
3	1.04	1.13	7.96
4	1.79	1.70	5.29
5	1.73	1.69	2.36
6	0.33	0.36	8.33
7	0.41	0.40	2.50
8	2.23	2.29	2.62
9	1.44	1.34	7.46
10	0.56	0.59	5.08
11	0.58	0.62	6.45
12	0.29	0.28	3.57
13	0.43	0.46	6.52
14	1.77	1.66	6.62
15	1.90	1.93	1.55
16	2.43	2.32	4.74
17	2.26	2.23	1.34
18	1.41	1.43	1.39
19	0.53	0.54	1.85
20	0.54	0.53	1.88
21	0.54	0.61	11.47
22	0.63	0.67	5.97
23	1.07	1.13	5.30
24	1.17	1.24	5.64
25	1.18	1.22	3.27
26	1.36	1.31	3.81
27	1.63	1.62	0.61
28	1.75	1.73	1.15
29	2.00	1.94	3.09
30	2.36	2.38	0.84

The wheel wear predicted using VAMPIRE and parallel NARXNN, and percentage error.

Sample Number	Wheel wear predicted using VAMPIRE (mm)	Wheel wear predicted using NARXNN (mm)	Error %
1	0.66	0.60	10.00
2	1.37	1.20	14.16
3	2.01	1.74	15.51
4	2.54	2.24	13.39
5	2.37	1.99	19.09
6	2.42	2.27	6.60
7	2.31	2.29	0.87
8	2.36	2.29	3.05
9	2.40	2.30	4.34
10	2.15	2.02	6.43
11	2.61	2.66	1.87
12	2.67	2.46	8.53
13	2.67	2.59	3.08
14	2.57	2.37	8.43
15	2.53	2.42	4.54
16	2.21	2.34	5.55
17	1.55	1.63	4.90
18	0.53	0.51	3.92

3. Change of lateral bush stiffness

The wheel wear predicted using VAMPIRE and series-parallel NARXNN, and percentage error.

Sample Number	Wheel wear predicted using VAMPIRE (mm)	Wheel wear predicted using NARXNN (mm)	Error %
1	0.47	0.45	4.44
2	0.99	1.04	4.80
3	0.95	1.08	12.03
4	1.43	1.64	12.80
5	1.69	1.76	3.97
6	0.47	0.46	2.17
7	0.56	0.51	9.80
8	0.60	0.56	7.14
9	0.65	0.64	1.56
10	0.55	0.58	5.17
11	0.68	0.64	6.25
12	0.41	0.40	2.50
13	0.20	0.17	17.64
14	1.17	1.15	1.73
15	1.15	1.13	1.76
16	1.68	1.56	7.69
17	2.61	2.36	10.59
18	2.74	2.60	5.38
19	0.44	0.43	2.32
20	0.17	0.16	6.25
21	0.67	0.66	1.51
22	0.73	0.69	5.79
23	0.71	0.75	5.33
24	1.34	1.22	9.83
25	1.26	1.28	1.56
26	1.46	1.41	3.54
27	2.31	2.26	2.21
28	2.62	2.69	2.60
29	2.52	2.45	2.85
30	2.54	2.70	5.92

The wheel wear predicted using VAMPIRE and parallel NARXNN, and percentage error.

Sample Number	Wheel wear predicted using VAMPIRE (mm)	Wheel wear predicted using NARXNN (mm)	Error %
1	0.45	0.42	7.14
2	1.28	1.16	10.34
3	2.08	2.11	1.42
4	2.43	2.34	3.84
5	2.82	2.54	11.02
6	2.56	2.41	6.22
7	2.30	1.92	19.79
8	2.62	2.53	3.55
9	2.44	2.37	2.95
10	2.27	2.00	13.50
11	2.32	2.62	11.45
12	2.52	2.66	5.26
13	2.68	2.55	5.09
14	2.59	2.71	4.42
15	2.86	2.82	1.41
16	2.31	2.52	8.33
17	1.57	1.98	20.70
18	0.48	0.42	14.28

4. Change of vertical bush stiffness

The wheel wear predicted using VAMPIRE and series-parallel NARXNN, and percentage error.

Sample Number	Wheel wear predicted using VAMPIRE (mm)	Wheel wear predicted using NARXNN (mm)	Error %
1	0.63	0.59	6.77
2	0.56	0.54	3.70
3	0.57	0.56	1.78
4	1.06	1.13	6.19
5	1.19	1.16	2.58
6	1.27	1.28	0.78
7	1.88	1.90	1.05
8	1.69	1.72	1.74
9	0.56	0.55	1.81
10	2.25	2.37	5.06
11	2.30	2.27	1.32
12	0.58	0.52	11.53
13	0.63	0.59	6.77
14	1.17	1.10	6.36
15	1.16	1.15	0.86
16	1.29	1.16	11.20
17	1.18	1.27	7.08
18	1.70	1.67	1.79
19	1.76	1.69	4.14
20	1.90	1.76	7.95
21	0.58	0.50	16.00
22	2.35	2.39	1.67
23	0.50	0.55	9.09
24	0.53	0.45	17.77
25	0.57	0.73	21.91
26	0.57	0.62	8.06
27	1.22	1.29	5.42
28	1.94	1.93	0.51
29	0.97	0.94	3.19
30	2.35	2.37	0.84

The wheel wear predicted using VAMPIRE and parallel NARXNN, and percentage error.

Sample Number	Wheel wear predicted using VAMPIRE (mm)	Wheel wear predicted using NARXNN (mm)	Error %
1	0.50	0.58	13.79
2	1.39	1.28	8.59
3	2.10	1.95	7.69
4	2.42	2.18	11.00
5	2.25	2.12	6.13
6	2.38	2.02	17.82
7	2.41	2.29	5.24
8	2.24	2.06	8.73
9	2.44	1.99	22.61
10	2.57	2.34	9.82
11	2.61	2.50	4.40
12	2.67	2.33	14.59
13	2.62	2.43	7.81
14	2.57	2.38	7.98
15	2.26	2.02	11.88
16	2.15	2.03	5.91
17	1.46	1.33	9.77
18	0.48	0.45	6.66

5. Change of longitudinal shear stiffness

The wheel wear predicted using VAMPIRE and series-parallel NARXNN, and percentage error.

Sample Number	Wheel wear predicted using VAMPIRE (mm)	Wheel wear predicted using NARXNN (mm)	Error %
1	0.53	0.61	13.11
2	0.36	0.38	5.26
3	1.04	1.07	2.80
4	1.79	1.75	2.28
5	1.74	1.67	4.19
6	0.36	0.30	20.00
7	0.41	0.47	12.76
8	2.22	2.27	2.20
9	1.44	1.49	3.35
10	0.56	0.58	3.44
11	0.54	0.56	3.57
12	0.20	0.21	4.76
13	0.31	0.32	3.12
14	1.74	1.66	4.81
15	2.00	2.05	2.43
16	2.37	2.29	3.49
17	2.24	2.29	2.18
18	1.44	1.50	4.00
19	0.59	0.68	13.23
20	0.58	0.59	1.69
21	0.57	0.56	1.78
22	0.68	0.61	11.47
23	1.18	1.12	5.35
24	1.14	1.23	7.31
25	1.20	1.21	0.82
26	1.10	1.16	5.17
27	1.73	1.71	1.16
28	1.54	1.64	6.09
29	2.08	2.07	0.48
30	2.40	2.35	2.12

The wheel wear predicted using VAMPIRE and parallel NARXNN, and percentage error.

Sample Number	Wheel wear predicted using VAMPIRE (mm)	Wheel wear predicted using NARXNN (mm)	Error %
1	0.43	0.73	41.33
2	1.49	1.47	0.93
3	2.16	2.08	3.35
4	2.46	2.22	10.46
5	2.28	2.23	2.05
6	2.41	2.46	2.05
7	2.37	2.36	0.20
8	2.24	2.45	8.80
9	2.41	2.37	1.63
10	2.29	2.54	10.12
11	2.59	2.78	7.09
12	2.32	2.57	9.94
13	2.21	1.93	14.38
14	2.13	1.88	13.01
15	2.83	3.28	13.78
16	2.61	2.54	2.36
17	1.46	1.67	12.77
18	0.66	0.68	3.71

6. Change of lateral shear stiffness

The wheel wear predicted using VAMPIRE and series-parallel NARXNN, and percentage error.

Sample Number	Wheel wear predicted using VAMPIRE (mm)	Wheel wear predicted using NARXNN (mm)	Error %
1	0.57	0.56	1.78
2	0.31	0.34	8.82
3	1.00	1.11	9.90
4	1.63	1.62	0.61
5	1.66	1.64	1.21
6	0.31	0.33	6.06
7	0.66	0.62	6.45
8	2.39	2.38	0.42
9	1.25	1.21	3.30
10	0.55	0.62	11.29
11	0.56	0.60	6.66
12	0.36	0.30	20.00
13	0.54	0.55	1.81
14	1.64	1.61	1.86
15	1.98	2.03	2.46
16	2.46	2.54	3.14
17	2.21	2.23	0.89
18	1.45	1.42	2.11
19	0.59	0.64	7.81
20	0.56	0.60	6.66
21	0.62	0.59	5.08
22	0.76	0.73	4.10
23	1.18	1.14	3.50
24	1.30	1.27	2.36
25	1.14	1.18	3.38
26	1.32	1.31	0.76
27	1.87	1.85	1.08
28	1.55	1.42	9.15
29	2.13	2.07	2.89
30	2.29	2.33	1.71

The wheel wear predicted using VAMPIRE and parallel NARXNN, and percentage error.

Sample Number	Wheel wear predicted using VAMPIRE (mm)	Wheel wear predicted using NARXNN (mm)	Error %
1	0.70	0.72	2.77
2	1.49	1.42	4.92
3	2.29	2.10	9.04
4	2.32	2.41	3.73
5	2.68	2.90	7.58
6	2.62	2.83	7.42
7	2.39	2.63	9.12
8	2.39	2.11	13.27
9	2.48	2.15	15.34
10	2.47	2.11	17.06
11	2.42	2.04	18.62
12	2.47	2.19	12.78
13	2.52	2.34	7.69
14	2.53	2.41	4.97
15	2.90	2.84	2.11
16	2.27	2.17	4.60
17	1.55	1.48	4.72
18	0.79	0.82	3.65

7. Change of vertical shear stiffness

The wheel wear predicted using VAMPIRE and series-parallel NARXNN, and percentage error.

Sample Number	Wheel wear predicted using VAMPIRE (mm)	Wheel wear predicted using NARXNN (mm)	Error %
1	0.53	0.54	1.85
2	0.34	0.35	2.85
3	1.06	1.09	2.75
4	1.81	1.83	1.09
5	1.65	1.63	1.22
6	0.41	0.40	2.50
7	0.50	0.47	6.38
8	2.25	2.27	0.88
9	1.36	1.37	0.72
10	0.54	0.61	11.47
11	0.59	0.56	5.35
12	0.23	0.28	17.85
13	0.35	0.33	6.06
14	1.73	1.71	1.16
15	1.86	1.88	1.06
16	2.39	2.28	4.82
17	2.16	2.17	0.46
18	1.55	1.57	1.27
19	0.60	0.58	3.44
20	0.57	0.59	3.38
21	0.59	0.60	1.66
22	0.63	0.59	6.77
23	1.21	1.20	0.83
24	1.17	1.18	0.84
25	1.22	1.25	2.40
26	1.15	1.17	1.70
27	1.77	1.75	1.14
28	1.64	1.66	1.20
29	2.15	1.88	14.36
30	2.44	2.45	0.40

The wheel wear predicted using VAMPIRE and parallel NARXNN, and percentage error.

Sample Number	Wheel wear predicted using VAMPIRE (mm)	Wheel wear predicted using NARXNN (mm)	Error %
1	0.73	0.60	21.66
2	1.56	1.42	9.85
3	2.21	2.33	5.15
4	2.40	2.55	5.88
5	2.36	2.42	2.47
6	2.35	2.32	1.29
7	2.32	2.23	4.03
8	2.29	2.17	5.53
9	2.54	2.43	4.52
10	2.31	2.19	5.47
11	2.48	2.35	5.53
12	2.34	2.24	4.46
13	2.26	2.23	1.34
14	2.25	2.26	0.44
15	2.63	2.57	2.33
16	2.28	2.22	2.70
17	1.55	1.52	1.97
18	0.77	0.94	18.08

Appendix 10 BPNN for wheel wear prediction

```
inputs = importdata('Ri121.xlsx'); % upload the input data
targets = importdata('Ro121.xlsx'); %upload the target data
inputs = inputs';
targets = targets';
% Create a network
net = network;
net.numInputs = 1;
net.numLayers = 3;
net.biasConnect = [1; 1; 1];
net.inputConnect = [1; 0; 0 ];
net.layerConnect = [0 0 0 ; 1 0 0 ; 0 1 0 ];
net.outputConnect = [0 0 1];
net.layers{1}.size = 7;
net.layers{1}.transferFcn = 'tansig';
net.layers{1}.initFcn = 'initnw';
net.layers[32].size = 2;
net.layers[32].transferFcn = 'tansig';
net.layers[32].initFcn = 'initnw';
% Choose Input and Output Pre/Post-Processing Functions
net.inputs{1}.processFcns = {'removeconstantrows','mapminmax'};
net.outputs{1}.processFcns = {'removeconstantrows','mapminmax'};
% Setup Division of Data for Training, Validation, Testing
net.divideFcn = 'dividerand'; % Divide data randomly
net.divideMode = 'sample'; % Divide up every sample
net.divideParam.trainRatio = 70/100; % train the network
net.divideParam.valRatio = 15/100;  % validate the network
Net.divideParam.testRatio = 15/100; % test the netwrok
% Training function 'trainlm'
net.trainFcn = 'trainlm'; % Levenberg-Marquardt algorithm
%Choose a Performance Function
net.performFcn = 'mse'; % Mean squared error
%Set training stopping criteria
net.trainParam.min_grad = 1e-4;
net.trainParam.epochs = 10;
net.trainParam.max_fail = 6;
% Choose Plot Functions
net.plotFcns = {'plotperform','plottrainstate','ploterrhist', ...
'plotregression', 'plotfit'};
```

```
% Train the Network
[net,tr] = train(net,inputs,targets);
% Test the Network
outputs = net(inputs);
errors = gsubtract(targets,outputs);
performance = perform(net,targets,outputs);
% Recalculate Training, Validation and Test Performance
trainTargets = targets .* tr.trainMask{1};
%valTargets = targets .* tr.valMask{1};
testTargets = targets .* tr.testMask{1};
trainPerformance = perform(net,trainTargets,outputs);
%valPerformance = perform(net,valTargets,outputs);
testPerformance = perform(net,testTargets,outputs);
%Find indice values of targets and extract train,val and test outputs
trainOutputs = outputs(:,tr.trainInd');
%valOutputs = outputs(:, tr.valInd');
testOutputs = outputs(:, tr.testInd');
.....
figure(2)
hold on
% Regression plot
plotregression(trainTargets(1,tr.trainInd'),trainOutputs(1,:),'Train',testTargets(1,tr.testInd'),testOutputs(1,:)
,'Testing')
hold off
.....
% Use the network
inputs = importdata('Ri122.xlsx'); % upload the input data
Testdata=inputs';
grid on
Predicted=sim(net,Testdata)
figure(3);
hold on
L = 1:18;
targets = importdata('Ro122.xlsx'); % upload the target data
Measured=targets'
plot(L,Predicted,'.r-', L,Measured,'.b-')
legend('Wheel wear predicted using BPNN','Wheel wear predcited using
VAMPIRE','Location','NorthWest');
xlabel('Sample Number)');
ylabel('Wear(mm)');
hold off
grid on
```

Appendix 11 RBFNN for wheel wear prediction

```
inputs = importdata('Ri121.xlsx'); % upload the input data to train the RBFNN
targets = importdata('Ro121.xlsx'); % upload the target data to train the RBFNN
inputs = inputs';
targets = targets';
%   Create and train the RBFNN:
%  The function "newrb" is used for iteratively creating an RBFNN by including one neuraon at a time.
% neurons are added to the network until the sum squared error is found to be very small or the maximum
% numbers of neurons are reached.
%   net= newrb(input, target,goal,spread, mn, df)
%   "goal" denotes the mean squared error goal
%   "spread" represents the spread of radial basis functions
%   "mn" is the maximum number of neurons
%   "df" represents the number of neurons to add between displays
goal = 0.01;
spread = 35;
mn =200;
df = 50;
net = newrb(inputs,targets,goal,spread, mn, df); % create and train the RBFNN
.....
inputs = importdata('Ri122.xlsx'); % upload the input data to test the RBFNN
Testdata=inputs';
grid on
Predicted=sim(net,Testdata); % test the RBFNN
.....
L = 1:18; % L is the samples numbers
targets1 = importdata('Ro122.xlsx'); % upload the target data (wheel predicted using VAMPIRE)
Measured=targets1'
.....
figure(1)
plot(L,Predicted,'.r-', L,Measured,'.b-')
legend('Wear predicted using RBFNN', 'Wheel wear predcited using VAMPIRE','Location','NorthWest');
xlabel('Sample Number');
ylabel('Wear(mm)');
hold off
grid on
```

Appendix 12 Performance plot, and regression plot respectively (NARXNN)

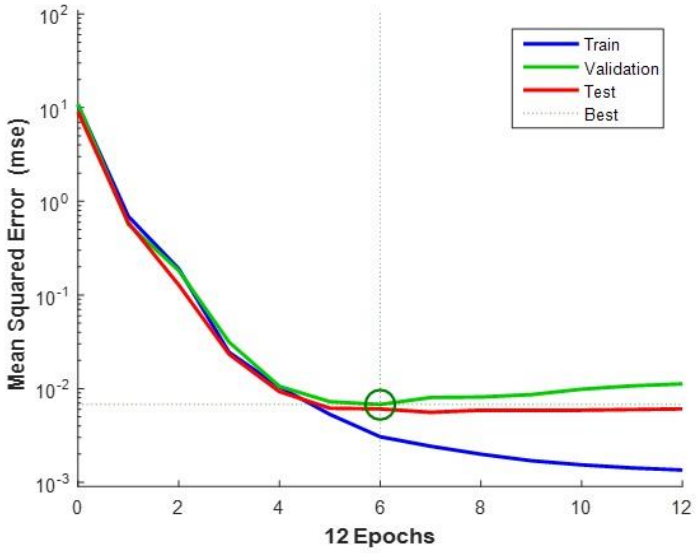

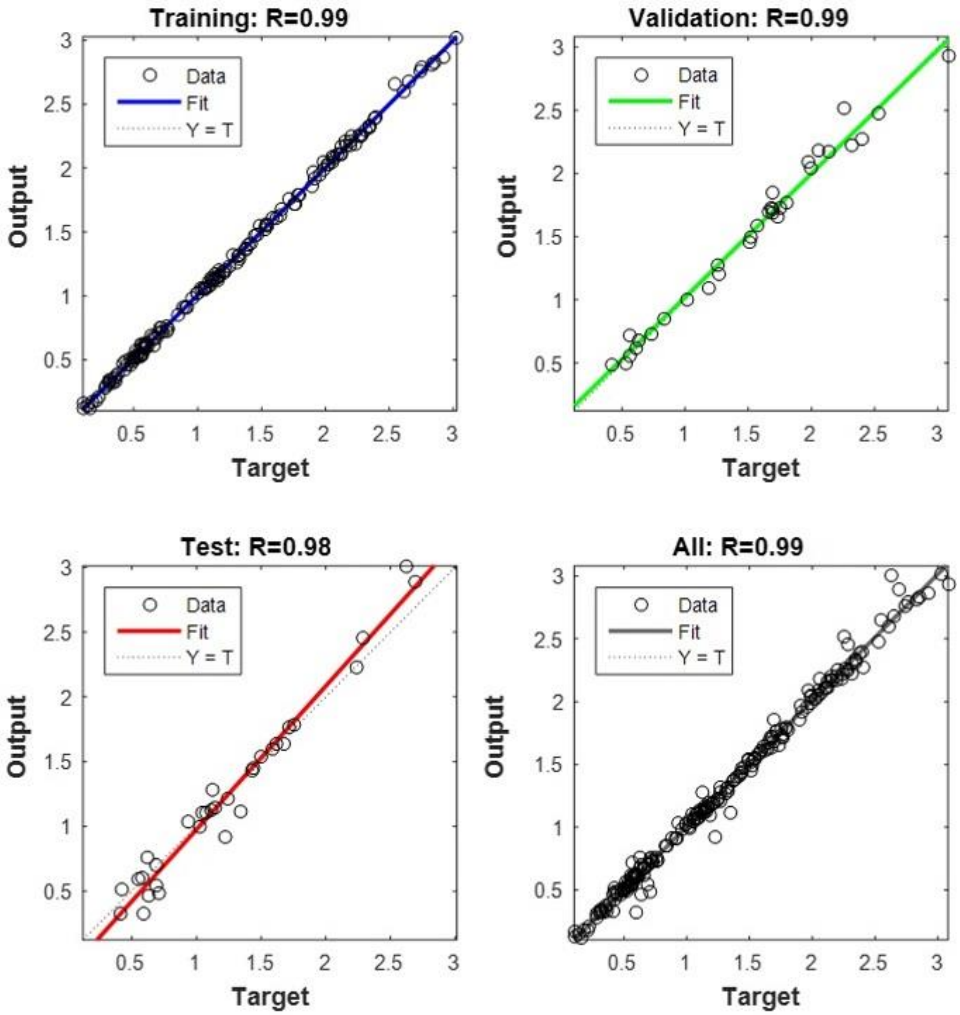

Appendix 13 Performance plot, and regression plot respectively (BPNN)